EVALUATION OF LATERAL BEHAVIOR OF PILE-SUPPORTED BRIDGES UNDER SCOUR CONDITIONS

By

Cheng Lin

Submitted to the graduate degree program in Civil, Environmental, and Architectural Engineering and the Graduate Faculty of the University of Kansas in partial fulfillment of the requirements for the degree of Doctor of Philosophy.

_____

Co-chairperson Dr. Jie Han

_____

Co-chairperson Dr. Caroline R. Bennett

_____

Dr. Alfred D. Parr

_____

Dr. Robert L. Parsons

_____

Dr. Samuel P. Perkins

Date Defended: 02/28/2012

The Dissertation Committee for Cheng Lin

certifies that this is the approved version of the following dissertation:

EVALUATION OF LATERAL BEHAVIOR OF PILE-SUPPORTED BRIDGES UNDER SCOUR CONDITIONS

_____

Co-chairperson Dr. Jie Han

_____

Co-chairperson Dr. Caroline R. Bennett

Date approved: 04/09/2012

ABSTRACT

Scour is the removal of soils in the vicinity of bridge foundations, resulting in a reduced capacity of the foundations, which may lead to a bridge failure. Scour causes 60% of bridge failures in the United States. To minimize bridge failures, the Federal Highway Administration (FHWA) has established a requirement that all state highway agencies should evaluate whether bridges in their inventory are scour susceptible. Therefore, it is critical that state Departments of Transportation (DOTs) are able to determine quickly and effectively which bridges in their inventories are scour-critical, enabling responsible management of those bridges during and after scour events. It is of importance to identify and explore analytical methods for determining bridge system susceptibility to scour events. However, most research so far has mainly focused on the prediction of scour depth, and limited knowledge is available for the evaluation of bridge performance under scour conditions. In addition, scour by removing soils around bridge foundations changes the stress history of the remaining soils. The change of the stress history however is often ignored in the analysis or design. The objective of this study was to understand potential scour effects on the behavior of laterally loaded piles by considering the stress history of the remaining soils and the scour-hole dimensions. Furthermore, a comprehensive study was conducted to evaluate the lateral behavior of an entire bridge under a scour condition by considering soil, pile foundation, and superstructure interactions.

To consider the effects of the stress history change by scour on the behavior of laterally loaded piles, the conventional *p-y* curves for clays and sands were modified. To examine the effects of the scour-hole dimensions on the behavior of laterally loaded piles, 3D finite difference analysis run in $FLAC^{3D}$ was performed to evaluate the responses of laterally loaded piles under different scour-hole dimensions including scour depth, scour width, and scour-hole slope angle.

And one-dimensional simplified methods were developed to address the effects of scour-hole dimensions of the behavior of laterally loaded piles in clays and sands by modifying the *p-y* curve method based on wedge failure. Finally, analysis of the bridge structures as a whole system was conducted using the integrated analysis program that was developed by integrating Soil Spring Module (*SSM*) into the structure software, *STAAD.Pro*. With the integrated analysis program, the analysis of soil-pile foundation-structure interactions was accomplished and the lateral behavior of the bridge was evaluated at different scour depths by considering the change of the stress history of the remaining soils. The analytical results show that scour substantially affected the behavior of laterally loaded piles; however, the scour effects on the lateral behavior of the entire bridge were considerably reduced due to the interactive effects of bridge components within the bridge structure.

TABLE OF CONTENTS

LIST OF FIGURES

LIST OF TABLES

ACKNOWLEDGEMENTS

I wish to express my great gratitude to my research advisors Drs. Jie Han and Caroline Bennett for giving me the opportunity to complete a Ph.D. at University of Kansas under their direction. Without their guidance, support, and encouragement, this dissertation would not be possible. Their wealth of knowledge and commitment to excellence are admirable. I appreciate they afford me the time for discussing my research and giving suggestions besides research. I am also deeply grateful that they create opportunities for me to develop different skills for my future career. For example, they generously sponsored me attending more than ten conferences. Therefore, I really enjoy the time that I spend with them, and their excellence in both academics and personality is admirable.

This research is supported by Kansas Department of Transportation (KDOT), through the KTRANS program. Mr. John Jones at KDOT is the project monitor. I would like to thank them for sponsoring this study and making this dissertation possible. The results and opinions presented in this dissertation do not reflect the policy and recommendation of KDOT.

I would like to thank my Ph.D. committee members, Dr. Samuel P. Perkins, Dr. Robert L. Parsons, and Dr. Alfred D. Parr for reviewing my dissertation and serving on my comprehensive exam. I appreciate Dr. Steven L. McCabe for serving on my comprehensive exam. I would also like to thank Mr. John Delphia at Texas Department of Transportation for his suggestion on my research when I just started my research in this area.

I am honored to be a part of Kansas University Geotechnical Society (KUGS) and I am grateful to its members including former and current visiting scholars and graduate students for their help. I also appreciate the incredible friendship with my colleagues at KU. Their kindness to me means a lot to me.

Finally, I would like to express my love and gratitude to my family, especially my wife and my 11-month daughter. Their support and sacrifice for me make the dissertation and many other things possible and are inspiring me to pursuit excellence at all times.

CHAPTER 1

INTRODUCTION

1.1 Background

Scour is the removal of soils around bridge foundations by flowing water, which may result in not only the loss of soil supports to bridge foundations, but also the deterioration of the foundation elements. Consequently, scour reduces the capacity of bridge foundations, which in turn may result in bridge instability, posing a potential threat to public safety. According to Lagasse et al. (2007), 60% of bridge failures in the United States resulted from scour.

Wardhana and Hadipriono (2003) conducted a survey of bridge failures in the United States and found that flood and scour were responsible for 165 and 78 failures from a total of 503 bridge failures occurring from 1989 to 2000; if the failures from flood and scour were considered together, they accounted for nearly 50% of the total bridge failures in that time period. In the 1993 flood, 23 bridge failures occurred in the upper Mississippi basin, which caused estimated damage of $15 million (Richardson and Davis 2001). Scour damaged over 500 bridges on the Georgia highway system in 1994 flood, claiming a financial loss of $130 million (Richardson and Davis 2001).

To minimize bridge failures, the Federal Highway Administration (FHWA) has established a requirement that all state highway agencies should evaluate whether bridges in their inventory are scour-susceptible. Accordingly, it is critical that state Departments of Transportation (DOTs) are able to determine quickly and effectively which bridges in their inventories are scour-critical, enabling responsible management of those bridges during and after scour events. As this is an important issue facing all state DOTs, it is of clear benefit to identify

and explore analytical methods for determining bridge system susceptibility to scour events. However, current research has mainly focused on the prediction of scour depth, and limited knowledge is available on the evaluation of overall bridge system performance under scour.

Some studies have examined bridge systems under scour (Daniels et al. 2007; Hughes et al. 2007a; Hughes et al. 2007b); however, there are significant areas of this field that remain unexplored. From a geotechnical perspective, scour creates stress history effects as overburden soils are removed by scour, resulting in the remaining soils being overconsoliated. The overconsolidated remaining soils may have higher strength than normally consolidated soils. The stress history effects may become significant as the scour depth increases, because the remaining soils would be further overconsolidated when more overburden soils are removed during the scour process. However, the current evaluation of existing bridge performance or design of a new bridge is usually simplified by neglecting stress history of the remaining soils. In addition, other design simplifications are also employed when examining scour susceptibility of bridges; for example, the existence of a scour hole is accounted in most analyses and designs by simply removing the whole soil layer to the scour depth. While such simplifications of the soils and scour-hole properties create a convenient method for assessing bridge performance under scour conditions, they may lead to non-realistic solutions.

In addition to simplifications that are often made concerning the soil and scour-hole properties, there are over-simplifications in modeling that are often made from a structural engineering perspective. For example, evaluation of bridge behavior is often accomplished either by analyzing only one component of a bridge while ignoring the other components, or by analyzing an entire bridge using simplified boundary conditions for the foundations. Since a bridge always behaves as a system, neither of these approaches captures the bridge behavior from an analysis standpoint, nor do they provide a suitable design approach for a bridge subjected to scour. As a result, realistic consideration of scour effects on bridges should consider the bridge

structure as an integrated system including complex contributions to behavior arising from soil, foundation, and superstructure interactions.

1.2 Objective and Scope of This Study

The objective of this study was to evaluate lateral behavior of pile-supported bridges under scour conditions. Scour effects on lateral bridge behavior were analyzed in an integrated system involving soil, foundation, and superstructure interactions. The integrated analysis of bridges under scour conditions was achieved by addressing the following sub-objectives:

1. Soil-foundation interaction under scour conditions considering stress history effects was addressed using the modified *p-y* method.
2. Soil-foundation interaction under scour conditions considering scour-hole dimensions was studied using the 3D finite difference method ($FLAC^{3D}$ modeling) and the 1D simplified methods that were developed from the wedge failure based *p-y* methods..
3. The integrated analysis program was developed by programming the Soil Spring Module (*SSM*) considering soil-foundation interaction into the structure model in the commercially-available software package *STAAD.Pro*.
4. Scour effects on the lateral behavior of an entire bridge involving soil, pile, and superstructure interactions, were evaluated using the integrated analysis program.

This study limited to the analysis of pile-supported bridges as they are more representative than shallow-foundation supported bridges in rivers. Limit states defined by lateral bridge behavior were focused upon because they are generally more critical to bridge stability under the flood and scour conditions than vertical and torsional behavior. Furthermore, the study focused on a system involving soil, pile, and bridge superstructure with known hydraulic factors such as flood velocity and scour-hole dimensions. Prediction of scour depths or scour widths was

not the purpose of this investigation and hydraulic factors were only considered as input parameters for evaluation of lateral bridge behavior.

1.3 Organization of the Dissertation

Following this Introduction, Chapter 2 presents a literature review of basic scour conceptions, a study of 36 cases of bridge failures due to scour, a discussion of research on laterally loaded piles, and a review of scour effects on lateral behavior of bridge systems. Chapter 3 discusses methods for considering soil stress history effects in the soil-foundation interaction under scour conditions by modifying the *p-y* curves. Chapters 4 to 6 continue the discussion of soil-foundation interaction under scour conditions by accounting for the effects of scour-hole dimensions in which the 3D finite difference analysis, Fast Lagrangian Analysis of Continua ($FLAC^{3D}$) was used; additionally, the 1D *p-y* based simplified methods were developed and verified from results of the 3D finite difference analysis. Chapters 7 presents development of the integrated analysis program by seamlessly linking soil model in *SSM* to structure model in *STAAD.Pro*, and analysis of lateral bridge behavior in an integrated system was accomplished using the integrated analysis program. The final chapter of this dissertation provides conclusions and recommends the future work that may be done in this area of study.

CHAPTER 2

LITERATURE REVIEW

2.1 Introduction

In this chapter, a literature review is conducted to synthesize the research on the effects of scour on lateral bridge behavior under scour conditions. To this end, four parts of the literature review are presented. The first part (Section 2.2) introduces bridge scour in terms of origins, composition, and scour-hole parameters. The second part (Section 2.3) discusses the case studies of 36 bridge failures due to scour based on failure cases reported in the literature. The third part (Section 2.4) discusses research on laterally loaded pile foundations. The fourth part (Section 2.5) discusses state-of-the-art studies on scour effects on lateral behavior of bridge structures and foundations. A brief summary (Section 2.6) discusses the limitations of the studies presented in the literature and concludes the literature review.

2.2 Review of Bridge Scour

Bridge scour is reviewed by presenting scour definition, scour types, and scour-hole parameters.

2.2.1 Scour definition

Bridge scour occurs when flowing water washes away materials from bed and banks of streams and from around foundations, piers, and abutments of bridges. It results when the erosive power of stream flow exceeds erosion resistance of the bed materials. The rate of scour depends

on a wide variety of factors, such as flow rates, flow orientations, properties of streambed materials, and the shape and dimensions of the bridge piers (Richardson and Davis 2001).

2.2.2 Scour types

Bridge scour is generally divided into three components according to Melville and Coleman (2000) as depicted in Figure 2-1: general scour, contraction scour, and local scour. These three components generally correspond to, respectively, long-term aggradation and degradation, general scour, and local scour as defined by Richardson and Davis (2001). In addition to these components, Richardson and Davis (2001) also included channel migration as a scour component.

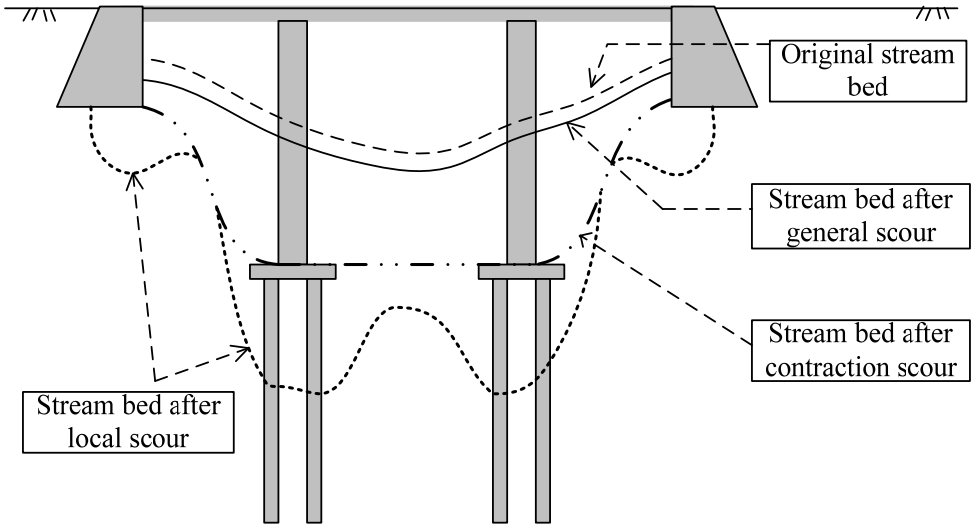

Figure 2-1. Scour types that occur at a bridge

General scour is the result of long-term natural or man-made change of streambed elevation, which occurs even without any obstructions in the river channel.

Contraction scour occurs in a streambed where bridges are placed or a natural contraction occurs. The lowering of streambed can be caused by the contraction of flow area which causes an increase of the average flow velocity and bed shear stress through the contraction. Contraction scour removes materials from streambed across the whole channel section. This mode of scour can reach equilibrium in riverine areas because scour increases flow area, which in turn decreases average flow velocity; however, in coastal area contraction scour may not reach equilibrium as a result of tidal effects, thus causing a continual removal of streambed materials. Consequently, contraction scour is generally a short-term scour effect in riverine environments but a long-term action in coastal areas.

Local scour can be described as the type of scour that occurs around bridge piers and abutments. The presence of piers and abutments causes vortices which result in the removal of bed materials at the bases of submerged structural elements. These vortices include both horseshoe vortices and wake vortices as show in Figure 2-2. A horseshoe vortex is caused by the pileup of flow on the upstream surface of piers or abutments, which leads to the acceleration of stream and removal of soils around the piers or abutments. A wake vortex is a vertical erosion that occurs downstream of an obstruction and gradually diminishes as the distance downstream from the obstruction increases. The vortices tend to develop a scour hole when their transport rate is greater than the deposit rate in live-bed scour, or their scouring strength exceeds the resistance of soils in clear-water scour. Live-bed scour occurs when the bed materials upstream are transported to the scour hole; while clear water scour occurs when there is no transport of bed materials upstream to the scour hole. However, local scour ceases once equilibrium is attained between erosion strength arising from vortices and resistance from bed materials.

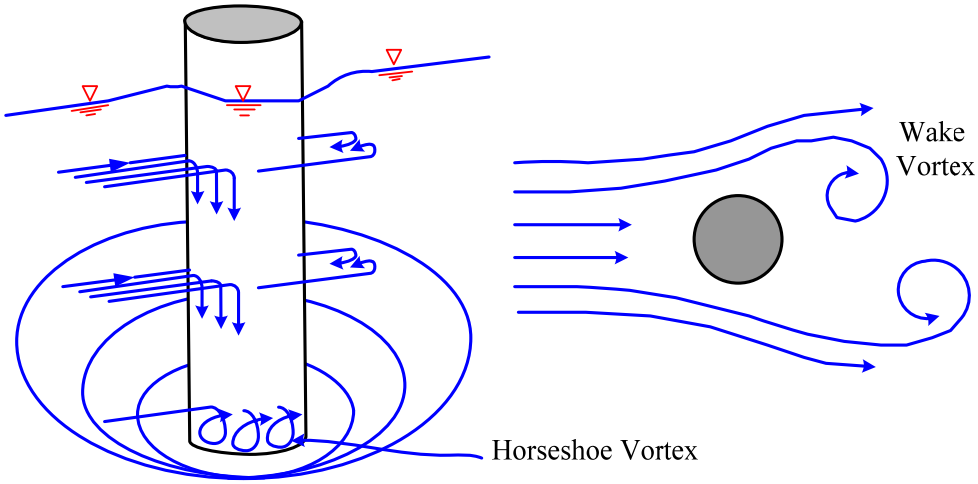

Figure 2-2. Schematic of local scour at a cylindrical pier (Richardson and Davis 2001)

Channel migration may occur as a consequence of dynamic stream flow, which may concentrate the flow area and continually shift banklines. Meadering streams lead to the channel moving both laterally and downstream. When meandering streams move into the reach of a bridge, local and contraction scour will be affected and approach embankment may be eroded as well. Channel migration is difficult to predict and thus not easily incorporated into the evaluation on the bridge stability.

2.2.3 Scour-hole parameters

2.2.3.1 Scour depth

Depth of a scour hole may be produced by general scour, contraction scour, and local scour contributions. Richardson and Davis (2001) illustrated the procedure for calculating the total scour-hole depth. Melville and Coleman (2000) also presented the detail on the calculation

of the total scour depth. However, local scour depth has received more attentions in this regard than general and contraction scour because it usually has a greater effect on the total scour depth.

Extensive research has been conducted on the prediction of local scour depth, and a number of predictive methods have been proposed (Laursen 1963; Shen et al. 1969; Raudkivi 1986; Melville 1997; Briaud et al. 1999; Richardson and Davis 2001; Briaud et al. 2004). Among those methods, the HEC-18 equation (Richardson and Davis 2001) is the most widely used, which considers local scour as a function of characteristics of riverbed materials, bed configuration, flow characteristics, fluid properties, and the geometry of the pier and footing, as shown in the equation below.

$$\frac{y_s}{y_1} = 2.0 K_1 K_2 K_3 K_4 \left(\frac{a}{y_1}\right)^{0.65} Fr_1^{0.43} \qquad 2.1$$

where, y_s = scour depth, m; y_1 = flow depth directly upstream of the pier, m; K_1 = correction factor for pier nose shape; K_2 = correction factor for angle of attack of flow; K_3 = correction factor for bed condition; K_4 = correction factor for armoring by bed material size; a = pier width, m; L = pier Length, m; Fr_1 = Froude number directly upstream of the pier = $V_1/(gy_1)^{1/2}$; V_1 = Mean velocity of flow directly upstream of the pier, m/s; g = acceleration of gravity (9.81 m/s^2)

As the HEC-18 equation was developed based on the laboratory tests performed in sands, it appears to be overly conservative and therefore is an expensive approach for scour design in clays. For that reason, Briaud et al. (1999) proposed a method termed SRICOS to predict local scour depth in clays, given by:

$$z = \frac{t}{\frac{1}{\dot{z}_i} + \frac{t}{z_{\max}}} \qquad 2.2$$

where, z = scour depth at pier, mm; t = scour time, hour; $\dot{z}_i$ = initial slope of the z versus t curve, mm/h; z_{max} = maximum scour depth, mm.

The initial scour rate, $\dot{z}_i$ can be obtained from an erosion curve of $\dot{z}$ versus τ which is generated with an erosion function apparatus (EFA) on samples obtained from the field site. The value for $\dot{z}_i$ is determined from that curve when τ is equal to the maximum shear stress, τ_{max}. The maximum shear stress is calculated in Equation 2.3 which is obtained based on numerical simulation results.

$$\tau_{\max} = 0.094\rho V^2 \left(\frac{1}{\log R} - \frac{1}{10}\right) \qquad 2.3$$

where, ρ = density of water, kg/m^3; V = mean velocity of flow, m/s; R= Reynolds number, equal to VD/υ ; D = pier diameter, m; υ = kinematic viscosity of the water, equal to 10^{-6} m^2/s at 20˚C ;

The maximum scour depth is:

$$z_{\max}(mm) = 0.18(R)^{0.635} \qquad 2.4$$

2.2.3.2 Other scour-hole parameters

Other scour-hole parameters of interests include width, length, and slope of the scour hole. For example, the scour-hole size is required to calculate the extent of riprap that is needed for scour countermeasure, and to identify whether local scour regions overlap. Scour width is needed for determining the scour zone size near abutments where the main hydraulic flow interacts with the flow around the abutments (Richardson and Abed 1993). In addition, scour-hole width, length, and slope are also important in characterizing the scour-hole geometry in the numerical modeling of the soil-foundation interaction under scour conditions.

Richardson and Davis (2001) used Equation 2.5 to estimate the top width of a scour hole in cohesionless materials from one side of a pier or footing. The top width of scour-hole depends on the scour depth, slope, and bottom width of the scour hole.

$$W = S_d(b + \cot\theta) \qquad 2.5$$

where, W = top width of the scour hole from each side of the pier or footing, m; S_d = scour depth, m; b = bottom width of the scour hole from each side of the pier, m; θ = angle of repose of the bed materials in air ranging from 30^o to 44^o.

However, for practical applications it is recommended that the top width of a scour hole be twice the scour depth (Richardson and Davis 2001), as shown in Figure 2-3.

Based on laboratory tests performed on pea-sized gravels (3.2 mm diameter) in clear water, Richardson and Abed (1993) proposed a series of empirical calculation equations for top and bottom scour-hole widths in free and pressure flows, as presented in Equations 2.6 to 2.9. These calculations are only valid for the flow that is not skewed with respect to the pier.

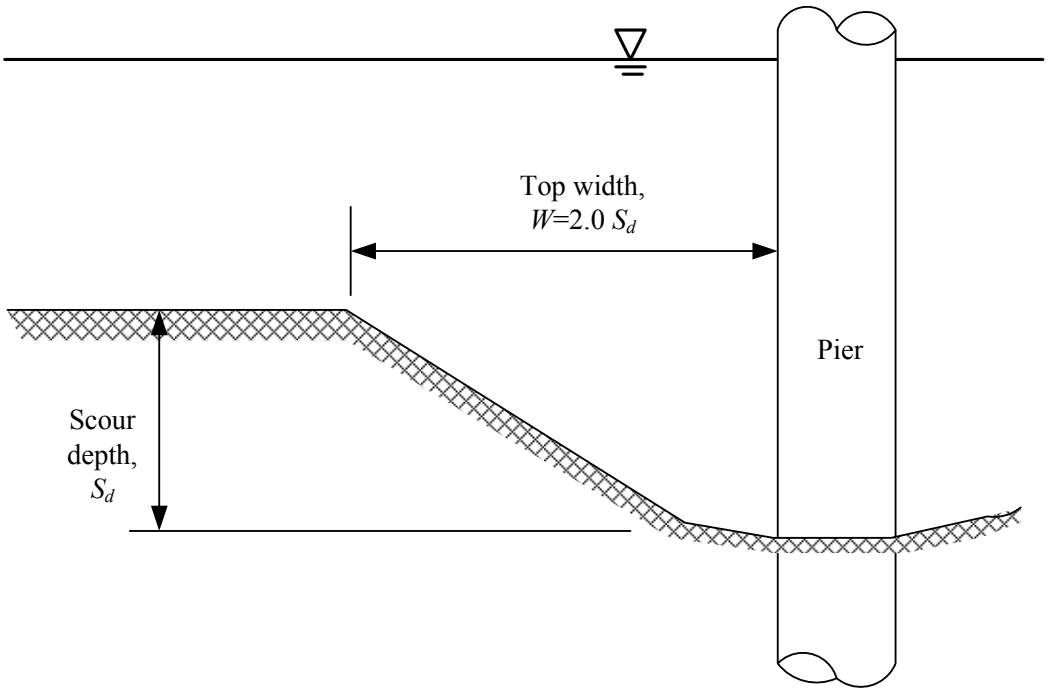

Figure 2-3. Top width of local scour hole (Richardson and Davis 2001)

In free flow conditions,

$$W_f = S_d(0.44 + 1.36\cot\theta) + 0.10 \quad (2.6)$$

$$b_f = 0.323S_d - 0.016 \quad (2.7)$$

In pressure flow condition,

$$W_p = S_d(0.53 + 0.89\cot\theta) + 0.12 \quad (2.8)$$

$$b_p = 0.6S_d + 0.062 \quad (2.9)$$

where, W_f = top width of the scour hole from each side of the pier for free flow, ft; b_f = bottom width of the scour hole for free flow, ft; W_p = top width of the scour hole for pressure flow, ft;

B_p = bottom width of the scour hole for pressure flow, ft; S_d = scour depth, ft; θ = angle of repose of the bed materials in air, at#34˚± 3˚.

In addition to observations in laboratory tests, field investigations have also been reported by Butch (1996) who observed scour-hole widths at 128 bridge piers, and scour-hole lengths at 40 bridge piers in New York State streams. The average pier width investigated was 1.5 m and 75% of the scour hole studied had widths less than 2.1 m. The mean value and maximum value of scour depths were 0.8 m and 2.3 m respectively. It was found that ratio of the scour-hole top width to scour depth was 4.7 on average and minimum at -0.8. The negative sign reflects scour had not protruded beyond the edge of the pier or footing. Streambed slope anlge in scour holes was found to have a mean value of 14.6˚, which was less than the repose angle in air (30˚ - 44˚) as suggested by Richardson and Davis (2001); however, the maximum slope angle was found to reach 57˚. The maximum slope that exceeded the repose angle might be due to the cohesive soils, cobble, or debris in the streambed.

The ratio of the upstream scour-hole length to scour depth was found to be 5.2 on average and the lower bound was found to be 1.8. In contrast, downstream scour-hole lengths were generally greater than upstream scour-hole lengths. The average slope angle in a scour hole upstream from a pier was 9.8˚ and the maximum was found to be 45˚, while the average slope anlge at the downstream side was found to be 7.1˚.

2.3 Case Studies of Bridge Failures due to Scour

Case studies provide insight into scour-induced bridge failures, and help to highlight key factors responsible for the failures. It is expected that the studies will be beneficial in the bridge analysis and design under scour conditions. In the case studies examined, 36 cases of bridge failures pertaining to scour were collected and analyzed in terms of hydraulic, structural, and

geotechnical aspects. The 36 cases of bridge failures include 20 cases from New Zealand, 14 cases from USA, and 2 cases from Canada. The failure modes and remediation measures are discussed is this section. Prior to the analysis and discussion, two classic cases are reviewed.

2.3.1 Review of the failures of Schoharie creek and Hatchie river bridges

Failure of the Schoharie Creek Bridge in New York State and the Hatchie River Bridge in Tennessee are two classic examples of catastrophic bridge failures attributed to scour. Specifics of both case studies are presented herein.

2.3.1.1 Failure of Schoharie creek bridge

Two spans of the New York State Thruway Bridge over the Schoharie Creek near Amsterdam, New York collapsed in 1987, claiming 10 lives. This tragedy was triggered by the collapse of Pier 3 and then Spans 3 and 4 of the bridge, after it sustained severe scour damage after a spring flood (Storey and Delatte 2003). The flood was estimated to be 50-year flood with a velocity of 4.6 m/s, caused by a combination of heavy rainfall and snowmelt [Wiss, Janney, Elstner Associates, Inc. and Mueser Rutledge Consulting Engineers (WJE and MR) 1987]. The high flood rate created a scour hole approximately 3-m deep around Pier 3. The Schoharie Creek Bridge was supported by shallow footing foundations with limited embedment depth into the riverbed. The shallow footing of Pier 3 rested on erodible soils (i.e. layers of gravel, sand, and silt) making the bridge highly susceptible to scour (Thornton-Tomasetti 1987).

Causes of the bridge failure were investigated after the bridge collapse (Thornton-Tomasetti 1987; WJE and MR 1987). It was found that the collapse was attributable to a number of design and maintenance deficiencies which included limited embedment of the shallow

footing, shallow footing bearing on erodible soils, use of erodible backfill for the footing excavation, and inadequate riprap protection, inspection, and maintenance. The scour was aggravated by a combination of other factors. For example, the flood velocity was higher than anticipated in the original design; debris accelerated downward scour; berms increased the floodwater under the bridge; and a high hydraulic gradient formed between upstream and downstream in the spring. Failure was also accelerated as a consequence of insufficient design of the bridge structure for scour conditions. For example, the superstructure bearings allowed for the uplift and slide of the superstructure from the piers; simple spans were utilitzed, which have no redundancy; the lightly reinforced concrete piers had limited ductility; and deficient plinth reinforcement resulted in sudden cracking of the plinth instead of a hinging failure.

2.3.1.2 Failure of Hatchie river bridge

The Hatchie River Bridge near Covington, Tennessee failed in 1989, and this failure killed nine vehicle occupants. The bridge collapsed during a flood stage; the failure was characterized by the collapse of two adjacent pile-supported southbound column bents. Scour exposed friction piles under one column bent to water for a depth of 3 meters, resulting in the piles losing capacity to support the bent. Failure of the bridge progressed from settlement to complete span collapse within a time span of 45 minutes. As vehicles passed over the spans supported by one of the distressed column bents (Column bent 70), the bent began to settle and leaned northward. Along with the forces induced by the sliding of the heavy superstructure elements (up to 78 tons), additional lateral and vertical loads were added to column bent 70, resulting in continuous settlement and buckling of the friction piles. The piles were found as part of this forensic investigation to have deteriorated after being exposed to water over prolonged periods of time, with a 25% decrease of pile diameter noted; this was hypothesized to be another

primary reason for buckling failure that occured (NTSB 1990; Thompson 1990; Jackson et al. 1991).

It was determined that a combination of channel migration and local scour directly contributed to the collapse of the Hatchie River Bridge. However, insufficient inspection was a contributing human factor responsible for the bridge failure. Scour inspection had not reached the lowest level of riverbed at the time before the collapse. In addition, evaluators failed to recognize the importance of the exposure of the friction piles. This was a key piece of information because friction piles are dependent on the surrounding soils to attain vertical capacity, and thus exposure of the friction piles would significantly reduce foundation capacity to carry bridge loads. Furthermore, a variety of overweight trucks permitted to travel across the bridge might also have aggravated the collapse of the Hatchie River Bridge.

2.3.2 Analysis of bridge failures due to scour

Bridge failures in this section will be analyzed by relating them to the various influence factors including hydraulic, geotechnical, and structural aspects. Note that the current case studies were limited to 36 cases from New Zealand, United State, and Canada. Errors that may arise due to the geological and climatical differences were not considered in these case studies. Therefore, the results herein are interimand should be used with cautions. The results will be used with confidence when a database for bridge failures due to scour is enriched by inputing more case studies that consider geological and climatical diversity.

2.3.2.1 Hydraulic factors

Hydraulic factors such as scour types, scour depths, and miscellaneous factors are related to the bridge failures.

As stated previously, scour to a bridge may include contributions from local scour, contraction scour, general scour, and channel migration. In the case studies, each type of scour is related to number of bridge failures, presented in Table 2-1. In the table, five cases of bridge failures were not associated with any type of scour as they were not reported in the literature. It should be noted that if a bridge failure was induced by several scour types at the same time, only dominant scour type was counted; this is why the summation of bridge failures associated with scour types is equal to the total number of cases. Considering the dominant contributing factor and neglecting the secondary factor(s) also applies to the analysis of other factors pertaining to bridge failures in the later sections. Table 2-1 shows local scour to be the predominant scour type occurring in the bridge case studies examined, occupying 64% of bridge failures. It is followed by channel migration which accounted for 14% of bridge failures. In contrast, contraction and general scour occurred much less frequently.

Table 2-2 illustrates the range of scour depth observed in the various bridges at failure in the literature review. Scour depth was not always measured during or after bridge failures, or was not presented in the source of cases collected. As a result, only 22 cases of bridge failures were available for this type of analysis. Table 2-2 shows that scour depth ranged from 0.5 to 15 m for these 22 cases. A shallow scour depth of 0.5 to 2.0 m accounted for 16% of the bridge failures. This may be because these amounts of bridges were supported by shallow foundations. However, most of bridge failures (25% of total 36 cases) occurred at the scour depth ranging between 2.0 to 5.0 m. Bridge failures also occurred at greater scour depths, although these were found to occur less frequently.

Table 2-1. Scour types and number of bridge failures

Types of scour	Number	Percentage
Local scour	23	64%
Contraction scour	2	5%
General scour	1	3%
Channel migration	5	14%
Not Available	5	14%
Total	36	100%

Although scour can happen any time, scour effects are most significant during flood events. This is because flood generally results in higher stream flow velocity than normal flow. High stream velocity tends to increase scour depth around bridge foundations. In addition, flood events are often accompanied by debris, since large hydraulic forces of flood can easily transport drifts, logs, and other debris along the river. As a result, AASHTO (2007) requires that bridge scour should be investigated for flood conditions, i.e. design flood (100-year flood) and check flood (500-year flood). Accumulations of debris around the bridge tend to direct water downward and thus increase the scour depth. Also, debris accumulation increases lateral loads to bridges, and therefore increases the possibility of bridge failures. Figure 2-4 shows that 75% of scour-induced bridge failures were related to flood. Half of the bridge failures examined were bound up with debris. Flow with an angle of attack to the bridge also influenced bridge scour and stability. For example, skewed flows could lead to a higher rate of scour around the bridge, and also could exert a torsional force to bridges. A bridge may start with no angle of attack at the

beginning; however, flow can become skewed to the bridge if channel migration occurs. Figure 2-4 shows 44% of bridge failures were associated with skewed flows.

Table 2-2. Scour depth and number of bridge failures

Scour depth (m)	Number	Percentage
0.5-2.0	6	16%
2.0-5.0	9	25%
5.0-7.0	2	6%
7.0-10.0	3	8%
10.0-15.0	2	6%
Not Available	14	39%
Total	36	100%

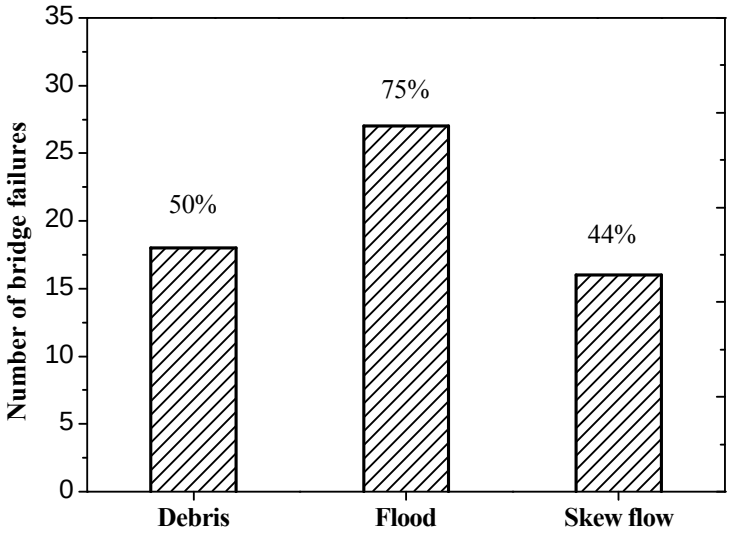

Figure 2-4. Occurrence of debris, flood, and skew flow during bridge failures

2.3.2.2 Geotechnical factors

As illustrated previously, different soils have different resistances to scour. A riverbed containing erodible soils (e.g. gravel, sand, and silt) will make a bridge susceptible to scour. As shown in Table 2-3, most of bridge failures occured in the erodible riverbed materials, such as cobble/gravel and sand, while silt and clay contributed to 14% of total failures. Failure could also occur in mudstone/siltstone and earth loam but fewer cases were noted for these soil types. The armored layers of gravels/cobbles are always deemed as non-erodible; however they may overlie erodible soils such as silt. In this case, scour can progress onto the underlying silt.

Table 2-3. Soil types and number of bridge failures

Soil types	Number	Percentage
Boulders	2	5%
Cobbles / gravels	8	22%
Armored gravels / cobbles	4	11%
Sand or fine Sand with gravel or clay	5	14%
Mudstone/siltstone	1	3%
Silt/clay	5	14%
Others (earth loam, gravel with sands)	1	3%
Not Available	10	28%
Total	36	100%

Foundation types also contribute greatly to the level of bridge stability that may be expected under scour conditions. Shallow foundations can easily lose capacity as compared with deep foundations. Timber piles may be more susceptible to deterioration under scour than concrete and steel piles. Table 2-4 shows reinforced concrete piles have claimed the highest percentage of bridge failures. Most of the reinforced concrete piles were installed in groups to support a pier or abutment. In contrast, spread footings were much less commonly used for bridge foundations than deep foundations. However, the number of bridge failures associated with the use of spread footings was found to be the second highest. This may be because compared with deep foundations, spread footings may be more susceptible to scour, resulting in a reduced vertical and lateral capacity. Timber piles were also commonly encountered in the failed bridges, with the number of failures behind that of spread footing. This may be associated with the fact that timbers were susceptible to deterioration in harsh environments. Steel HP piles and unknown foundations were the least commonly occurring type of foundation connected to bridge failures under scour conditions for the case studies examined.

Table 2-4. Foundation types and number of bridge failures

Foundation types	Number	Percentage
Spread footing	8	22%
Concrete reinforced piles	15	42%
HP Steel Piles	2	5%
Timber piles	5	14%
Unknown foundation	1	3%
Not Available	5	14%
Total	36	100%

2.3.2.3 Structure factors

Bridge types that suffered scour-induced failures were summarized in Table 2-5. This collection of data was limited because superstructure information was not available for 14 out of 36 cases. However, data still showed rough distribution of bridge types when bridge failed under scour. From Table 2-5, the slab-on-girder bridge was found to be the superstructure system most susceptible to scour failures. This result may correspond to the fact that girder bridges are the most prevalent highway bridges; for example girder bridges are the most numerous of the bridges in the United States (Barker and Puckett 2007); therefore they have more statistical representation in the bridge inventory. Girder bridges with simply supported spans were more susceptible to failure due to scour than those with continuous spans. In contrast to girder bridges, arch and truss bridges were considerably less represented in the data.

Table 2-5. Bridge types and number of bridge failures

Bridge types	materials	Number	Percentage
Arch	concrete	1	3%
---	steel	1	3%
Beam/Girder	concrete	7	19%
---	steel	11	30%
Box girder	concrete	1	3%
Truss	steel	1	3%
Not Available	-	14	39%
Total		36	100%

Bridge failures due to scour may occur at bridge deck, abutments, piers, and bridge foundations (including spread footings and pile foundations). In most cases, failures of bridge foundations were the trigger of pier or abutment failures. Thus, failures of foundations were not counted separately but were included into pier and abutment failures in Figure 2-5. The figure shows that failures mostly resulted from the pier failure, accounting for 61% of the total failures. It is followed by abutment failures which comprised 19% of the total failures. Abutment failures were found to be influenced by channel migration, and slide of slope at the abutment. Others failure modes in Figure 2-5 refer to washout of bridge deck, or an unsafe bridge with a tendency to failure as deep scour was observed.

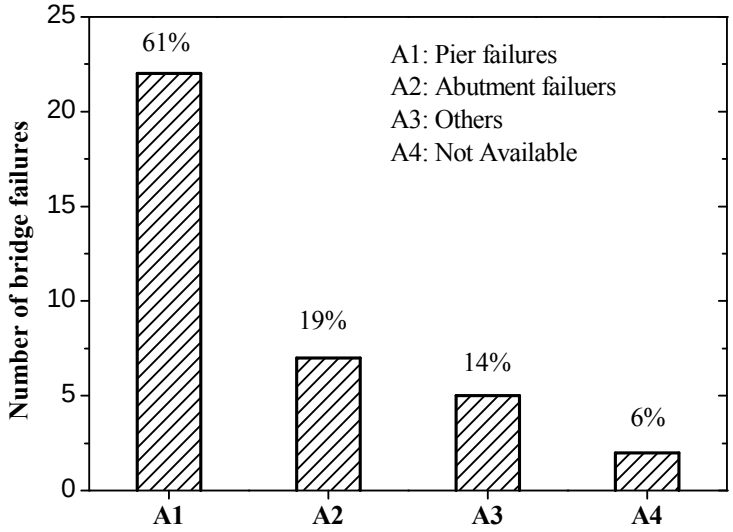

Figure 2-5. Failures of bridge components due to scour

2.3.3 Bridge failure modes due to scour

Based on the case studies, failure modes have been classified into four types: vertical failure, lateral failure, torsional failure, and bridge deck failure. Failures due to each of these modes are discussed in the following sections.

2.3.3.1 Vertical failure

Vertical failure refers to the bridge failure in vertical direction, which can be caused by inadequate soil support or pile instability. Shallow foundations have a high tendency to fail in this mode because scour easily reaches the base of shallow foundations when compared with deep foundations, causing inadequate vertical bearing capacity as shown in (a). Collapse of the Schoharie Creek Bridge is an example of a case in which a shallow footing collapsed into a scour hole as scour reached below the footing base.

Deep foundations may also be subject to failure as a result of inadequate vertical bearing capacity. Friction piles which obtain vertical bearing capacity by the friction between piles and their surrounding soils are susceptible to scour, as illustrated in (b). The failure of the Hatchie River Bridge is an example of a case in which insufficient friction was sustained by the friction piles after scour. In contrast, end bearing piles whose pile tips rest on a hard layer or bedrock are relatively vertically stable under scoured conditions; however pile tips may also be undermined when scour goes deep enough to the hard layer or bedrock, as seen in (c).

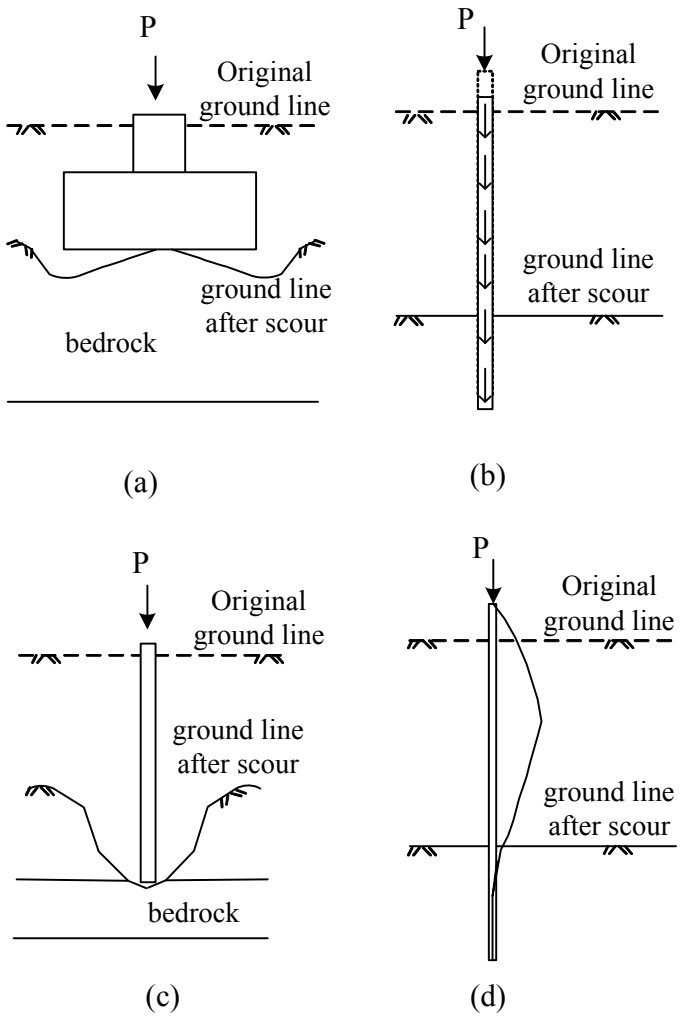

Figure 2-6. Vertical failure modes of bridge foundations (a) undermine of footing base, (b) penetration of friction pile, (c) undermine of pile tip, (d) buckling of pile

Piles may also fail as a consequence of instability when scour increasingly removes the surrounding soils from around the piles, resulting in an increase of the unsupported pile length, as seen in (d). As piles become increasingly slender, the pile tendency towards buckling increases; instability can be produced through the vertical load from the bridge superstructure or a combination of vertical and lateral loads. Furthermore, piles may be deteriorated by corrosion,

resulting in a reduced cross-section. For example, in the Hatchie River Bridge, corrosion reduced the cross-section of timber piles by approximately 44% (Thompson 1990), and by 50% for steel HP piles in the I-10 Bridge over the Jourdan River in Mississippi (Avent and Alawady 2005). Corrosion tends to exacerbate the buckling susceptibility of piles through reduction of the cross-sectional area. In terms of steel HP shapes, buckling can occur globally (flexural buckling) or locally (local buckling).

Table 2-6 indicates that approximate 30% of the total failures included in the series of case studies examined were vertical failures. Most of vertical failures were due to insufficient soil support, while two of the 36 failures were due to buckling.

Table 2-6. Failure modes and number of bridge failures

Failure modes	Number	Percentage
Vertical failure	11	30%
Buckling	2	5%
Lateral failure	14	39%
Structural hinge	5	14%
Pushover failure	4	11%
Torsional failure	1	3%
Bridge deck failure	1	3%
Others	5	14%
Not Identified	4	11%
Total	36	100%

#

2.3.3.2 Lateral failure

The term *lateral failure* is used herein to refer to pushover failures of piers, structural hinging of piles, kick-out failures of foundations, and excessive lateral movement of piers or foundations.

Pushover failures occur when transverse flood and debris loads push bridge piers incrementally until bridge piers fail. Pushover analysis is a static and nonlinear analysis to determine the lateral load versus displacement relationship and the pushover capacity of the structure, as shown in Figure 2-7 (a). Pushover failures become a significant concern when a bridge continuously accumulates debris in the flood conditions. In addition, accumulation of debris tends to push the hydraulic flow downward, resulting in an even deeper scour-hole. The greater scour depth results in further decrease of lateral capacity from the soils, thereby reducing the pushover capacity of the bridge structure.

Structural hinging failures occur when transverse loads produce sufficiently large bending moments to the structural elements when their boundaries are full or partial fixed, as seen in Figure 2-7 (b). In the case studies examined, this failure mode was observed with the pier cap rotating towards the upstream direction (Melville and Coleman 2000). Structural hinging failures occur when transverse loads produce sufficiently large bending moments to the structural elements when their boundaries are full or partial fixed, as seen in Figure 2-7 (b). Piles with limited embedment into a pile cap may fail in a hinging mode due to limited bending resistance. Furthermore, floods carrying large and heavy debris such as stones may attack the pier or piles, resulting in a potential structural hinging (Melville and Coleman 2000).

Kick-out failure of foundations tends to occur when scour develops deeply enough to wash out the piles from the location of pile tips, as depicted in Figure 2-7 (c). This failure mode happens at the bridge that has relatively high lateral resistance from superstructures but loses

lateral bearing capacity at the foundations. Shallow foundations are exceptionally susceptible to kick-out failures; however, piles also fail in kicking out once scour moves deeper than the embedment of piles into the soils.

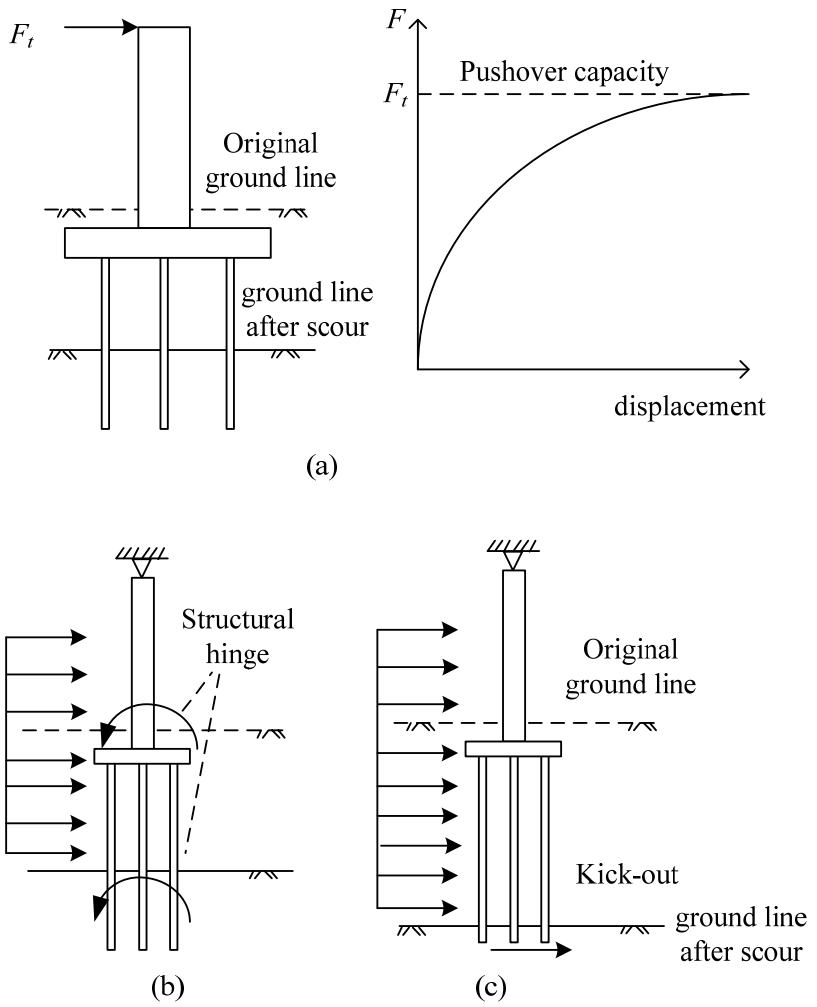

Figure 2-7. Lateral failure modes of the bridge (a) pushover failure, (b) structural hinging, (c) kick out of foundations

Table 2-6 shows that lateral failures were responsible for most of the bridge failures in the case studies examined, accounting for 39% of total failures. Hinging and kick-out failures accounted for 14%, and pushover failures for 11% of the total failures. Lateral failures in Table 2-6 also include excessive lateral movements.

2.3.3.3 Torsional failure

The term *torsional failure* refers to piers and foundations subjected to skewed flows which result in a torsional (twisting) failure mode of the structure or structural component. Flows with an angle of attack give arise to eccentric lateral loads, and thus piers and piles are subjected to torsion as shown in Figure 2-8. In Table 2-6, only one case was found to be dominated by a torsional mode by observing that piles in the bridge foundation twisted (Melville and Coleman 2000). However, rotational failure modes may exist in conjunction with other lateral failure modes under skew flow conditions even in cases where they may not be predominant.

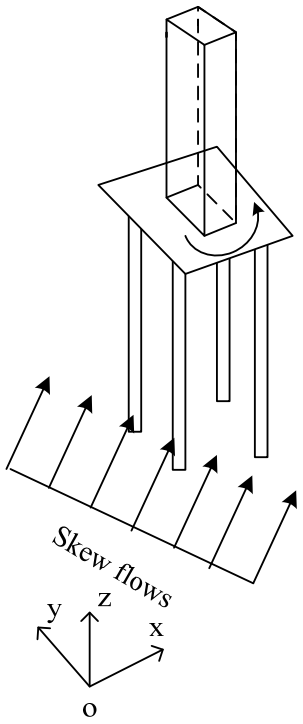

Figure 2-8. Torsion of bridge structures under skew flows

2.3.3.4 Bridge deck failure and others

Bridge deck failures may occur when bridge deck is outflanked by floods. Debris loads contribute to the washout of bridge deck in flood events. In addition, simply supported spans are susceptible to the removal of bridge deck by the flood if the deck is not structurally attached to the superstructure elements. One case of the 36 examined was found to be related to bridge deck failure and is presented in Table 2-6.

The term *others* in Table 2-6 refers to a non-structural failure of a bridge, such as a slope failure at an abutment or washout of an approach to an abutment. Five of the 36 cases studied were classified as *others,* as channel migration produced intense scour to the approaches of the abutments.

2.3.4 Remedial work

Remedial work performed in the case studies included repairing damaged superstructure and foundation elements of bridges, and performing scour countermeasures. Temporary Bailey bridges were often built for those bridges with their spans washed out or collapsed. Alternatively, some damaged bridges were forced to close and new bridges were constructed. Foundation rehabilitation included underpinning the damaged pile foundation with steel HP or pipe piles embedded to the desired soil layer. Deteriorated piles were replaced with sound piles, and in some cases, battered piles were constructed for the foundations to resist lateral loads. Grouting techniques were also used as remedial work to fill the scour-holes under spread footings.

Scour protection and channel stabilization were considered important in the remedial works. Scour protection included placing rock riprap and filter cloth on the riverbed under bridges. Channel stabilization included stabilization of dikes to prevent the development of meander and to realign channels to establish smooth flows to the bridges.

2.4 Research on Laterally Loaded Piles

Methods for analyzing laterally-loaded piles are discussed in the following sections, covering ready-to-use equations (Broms method), and numerical solutions ranging from a simple, one-dimensional method (elastic solution and *p-y* method), to more sophisticated 3D continuum numerical modeling.

2.4.1 Broms's method

Broms (1964a; 1964b) presented ready-to-use equations for calculating the ultimate lateral resistance and lateral deflection of piles in cohesive and cohesionless soils. Two boundary

conditions for pile head (i.e. free pile head and fixed pile head) were considered for the calculation. The ultimate lateral resistance was determined for short and long piles based on different failure modes. These failures were assumed to take place when soil strength was exceeded or when the yield moment of the structure occurred. In terms of clay, ultimate lateral resistance was related to the undrained shear strength of clay. In terms of sands, ultimate lateral resistance was assumed to be three times Rankine passive pressure. Equations to calculate the lateral deflection of piles were also provided based on a subgrade reaction concept in which modulus of subgrade reactionwas assumed to be constant with depth in clays and to linearly increase with depth in sands.

2.4.2 Elastic solution

3±°¶±¹ë(1971) used elastic theory to calculate lateral deflection of laterally loaded piles. In his approach, a single pile was divided into a number of elements with uniform loading. Lateral displacement compatibility between pile elements and soil elements was imposed to obtain a solution for lateral deflection. Lateral displacements of soils were determined based on the Mindlin's solution and lateral displacements for the pile were calculated based on the governing beam equation. This approach was developed within the elastic framework, and thus was not capable of considering nonlinear problems. In addition, shearing forces between the soil and pile were ignored. However, this approach was capable of considering continuum interdependency between soil elements.

2.4.3 The *p-y* method

In the *p-y* method, lateral soil resistance to a pile is treated as a series nonlinear Winkler springs which are independent to each other, as illustrated in . The solution for responses of laterally loaded piles is obtained in the governing beam equation which has incorporated the Winkler springs. The governing beam equation in elastic soil mass was developed by Hetenyi (1946) and widely used in calculation of laterally loaded piles (Reese and Van Impe 2001), given by:

$$\frac{d^2}{dx^2}(R_h \frac{d^2y}{dx^2}) + P_t \frac{d^2y}{dx^2} + p - W = 0 \qquad 2.10$$

where, $R_h = EI$, Flexural stiffness of the pile, kN/m^{2}x m^4; P_t = Vertical load on the pile, kN; p = Lateral soil resistance per unit length of the pile, kN/m; W = Distributed load along the length of the pile, kN/m; y = Lateral deflection of the pile, m.

If relationship between p and y is known, a solution to Equation 2.10 can be obtained. If the *p-y* relationship is assumed to be linear, the closed-form solution is readily available (Hetényi 1946). If the *p-y* relationship is nonlinear, numerical techniques are often employed to achieve a solution. Numerical techniques such as finite difference method (FDM) and finite element method (FEM) have been used to solve for nonlinear problems, which leads to development of the widely-used commercial softwares such as *LPILE* (an FDM code) and *FB-Multipier* (an FEM code). In addition, different types of soils present different *p-y* relationships. Hence, a series of *p-y* curves have been developed based on the full scale tests for different soils such as sands, soft clays, stiff clays, and rock. The *p-y* family for each type of soils has been included in *LPILE* and *FB-Multipier*.

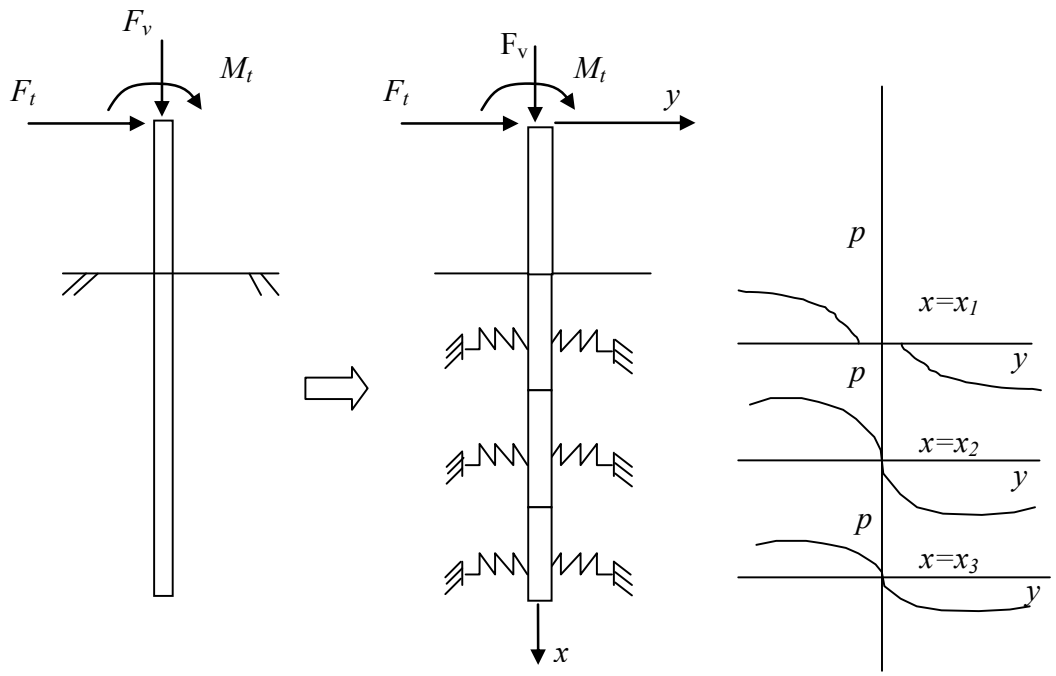

Figure 2-9. Illustration of *p-y* curves used in a pile analysis (Reese and Van Impe 2001)

The ultimate lateral soil resistance is vital to the determination of the nonlinear *p-y* curves. The ultimate lateral soil resistance is calculated by assuming the wedge failure near the ground surface and plain strain failure well below the ground line (Reese and Van Impe 2001). The ultimate lateral resistance is reached when the lateral deflection of soil reaches a certain magnitude. For example, the mobilizing deflection is 3/80 times the pile diameter in sand (Reese et al. 1974) while it is eitht times y_{50} in soft clay, where y_{50} is lateral deflection at one-half the ultimate soil resistance (Matlock 1970).

In terms of a pile group with relatively close spacing between piles, group effects should be considered because close spacing of piles results in a reduced soil resistance to the pile within the pile group when compared to the resistance provided to a single pile. Thus, a reduction factor for the soil resistance, termed as a p-multiplier (f_m), has been introduced to account for the group

effects (Brown et al. 1988), as shown in Figure 2-10. The f_m varies with pile locations and spacing in Figure 2-11. It can be seen from the figure that the f_m becomes smaller when the pile group has tigher spacing and the pile is located closer to the applied load.

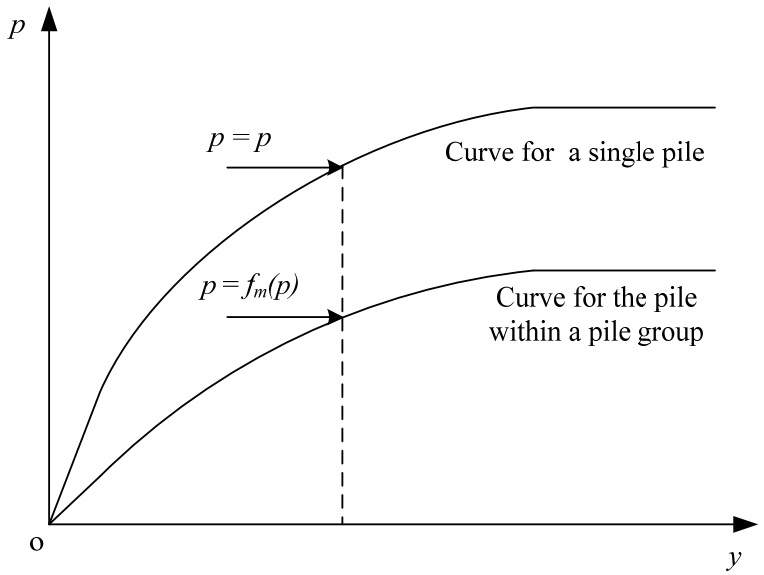

Figure 2-10. Concept of p-multiplier, f_m,for considering group effects

The *p-y* method adopts independent Winker springs to represent the lateral soil resistance to a pile, and therefore is not able to consider interactions between soil elements. The shearing forces at the interface between the pile and soil are also neglected, as is the case in the method of Poulos (1971). However, as the *p-y* method has been developed based on full-scale test results and is easily operated using the software, it is the most widely-used method for designing and analyzing piles under lateral loading.

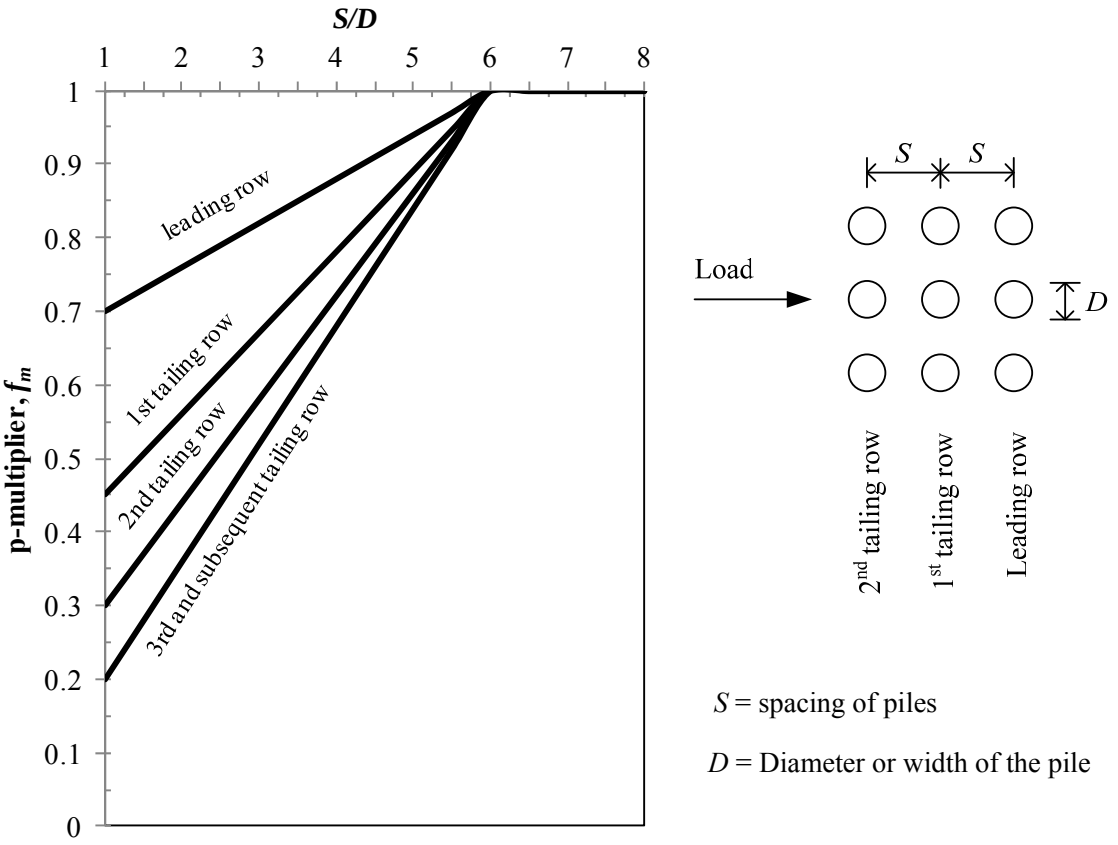

Figure 2-11. Determination of p-multiplier, f_m, in a pile group (Mokwa et al. 2000)

2.4.4 3D finite difference modeling

The 3D finite difference modeling (FDM) using Fast Lagrangian Analysis of Continua in 3 Dimensions ($FLAC^{3D}$) has been widely adopted for modeling soil-structure interaction (Dodds 2005; Martin and Chen 2005; Ng and Zhang 2001; Zhang et al. 2004). $FLAC^{3D}$ is an explicit finite difference code which has been designed preferably for solving for nonlinear and large displacement problems. However, for explicit finite difference method, a sufficiently small step should be guaranteed for a better computation result. $FLAC^{3D}$ achieves static solutions by

iterating through motion and constitutive equations supplemented with damping equations. In addition to the numerical technique itself, accuracy of numerical modeling results are heavily dependent on the appropriate selection of constitutive models, soil parameters, boundary conditions, and mesh density. Discussion herein is extended to finite element modeling (FEM) because FDM and FEM have similar sensitivities in selecting the abovementioned parameters.

2.4.4.1 Constitutive models

The Mohr-Coulomn (M-C) model, modified M-C model, von Mises model, and modified Cam-Clay (MCC) model have been used in the modeling of laterally loaded piles. Dodds (2005) calibrated field tests of laterally loaded piles in sands and clays using $FLAC^{3D}$ and then investigated the responses of pile groups under lateral loading. In his FDM, an elasto-plastic M-C model was adopted for the simulation. The elasto-plastic M-C model has also been used in FDM for simulating pile effects on sloping ground (Ng and Zhang 2001; Zhang et al. 2004) and pile responses due to lateral slope movement (Martin and Chen 2005). Wakai et al. (1999) employed an elasto-plastic modified M-C model for a laterally loaded pile group in dense sands using FEM and compared the numerical results with the measured, showing a good agreement. The modified M-C model actually utilitzed the yielding equation from Mohr-Coulomn model and the potential equation from Drucker-Prager model because the combination could improve the convergence of the finite element calculation (Wakai et al. 1999). The von Mises model has been used in FEM to simulate laterally loaded piles in undrained clay conditions (Brown and Shie 1990); results from FEM did not compare well with those from the *p-y* method. Brown and Shie (1990) attributed the discrepancy partly to incapability of von Mises model to consider the influence of loading paths on the mobilized shear strength; Ahmadi and Ahmari (2009) believed anisotropy and soil secondary structure effects were the fundamental causes and thus back-

calculated soil parameters were more reasonable for use than those from experiments. The MCC model has been used in FEM for parametric study of laterally loaded piles in clays but no experimental verification was provided (Budiman and Ahn 2005; Sanjaya Kumar et al. 2007). Dodds (2005) attempted to include MCC in the simulation of laterally loaded piles in clays using $FLAC^{3D}$ but failed to achieve satisfactory results. He attributed the failure to errors arising from the computation of the plastic multiplier associated with plastic flow.

2.4.4.2 Soil parameters

Soil parameters of interest in numerical modeling usually include soil modulus and strength, which are commonly determined based on laboratory or in-situ tests. However, back-calculated soil parameters are also used. Empirical estimations between soil parameters are necessary sometimes when insufficient data exists.

Soils surrounding a pile may experience different stress paths under lateral loading. Near the surface, soils in front of the pile experience a stress path in which horizontal stress gradually increases but vertical stress is unchanged. Soils behind the pile experience another stress path where horizontal stress gradually decreases and vertical stress does not change. Both stress paths can be simulated in a triaxial extension test. Thus, if a triaxial compression test was used for determining the shear strength, the determined value cannot represent the shear stress in the soil at failure (Brown and Shie 1990). Ahmadi and Ahmari (2009) compared the back-calculated undrained shear strength used in the modeling with those measured under vane shear and unconfined undrained (UU) compression triaxial tests. He found that to achieve a satisfactory modeling result, for normally consolidated high plasticity clays (CH), vane shear measured undrained shear strength could be used directly, but UU test measured undrained shear strength should be reduced by 20% to be used in the modeling. For overconsolidated clays, due to

anisotropy and secondary structure, the measured undrained shear strength should be reduced by an approximate 80% for the use in the numerical modeling.

Empirical relationships between elastic modulus and soil strength (cohesion and friction angle) have been studied extensively. For clays, ratio of elastic modulus to undrained shear strength could range from 100-1500 (Duncan and Buchignani 1976); Coduto (2001) suggested the ratio be taken as 300. However, Poulos (1971) suggested a range of 20 to95 based on the back-calculated data from field tests provided by Broms (1964a; 1964b). For sands, Kulhawy and Mayne (1990) tabulated various estimations of elastic modulus based on friction angle and relative density.

2.4.4.3 Boundary conditions

Dodds (2005) constructed a model in $FLAC^{3D}$ having the horizontal boundary a distance 24D (D represents pile diameter) away from the pile center in dense sands and vertical boundary a distance 0.35L (L denotes the pile length) below the pile tip. In the case of soft clays, the FEM mesh was considered to be sufficiently accurate when horizontal boundary was at a distance of 11D from the pile center and vertical boundary at 0.58L from the pile tip in soft clays. Ahmadi and Ahmari (2009) conducted a FEM sensitivity study on the horizontal boundary effects on laterally loaded piles in soft clays. He found that horizontal boundary effects could be neglectable when the distance of horizontal boundary from the pile center was greater than 40D. Trochins et al. (1988) built a FEM mesh in which the horizontal boundary was placed at a distance of 12D from the pile center and vertical boundary placed at a distance of 0.6 to 0.7L below the pile tip.

2.4.4.4 Mesh density

Mesh density plays an important role in the accuracy of numerical results when lateral soil-pile modeling is performed. When a pile's mesh density was increased from 10 to 30 elements along the pile length, the maximum lateral displacement and bending moment could increase as many as two and four times respectively (Dodds 2005). In terms of meshing technique for soils, a coarse mesh is often utilized for elements that undergo small deformation (Brown and Shie 1990; Dodds 2005; Martin and Chen 2005). In addition, Budiman and Ahn (2005) used a linear elastic soil model (substituted for nonlinear soil model) for the less deformed soil zone in order to improve computation efficiency. They built a soil model consisting of inner and outer soil zones by assigning nonlinear modified cam-clay for the inner (more deformed) zone and linear elastic models for the outer (less deformed) zone.

Proper pile mesh density may be estimated based on a simple 3D pile model that excluds soil materials. The calculated lateral responses using different mesh density can be compared with the theoretical beam solution to determine mesh sensitivity and convergence. Martin and Chen (2005) estimated a sufficient pile-mesh density based on a comparison of shear force from an elastic cantilever pile model and from the theoretical beam solution. An alternate approach was taken by Dodds (2005) who adopted a model of a simply supported pile with triangular loading to estimate the pile discretization by comparing the bending moment and lateral displacement calculated from numerical model and theoretical beam solution.

2.5 Scour Effects on Bridge Structures Concerning Lateral Behavior

Studies concerning with scour effects on lateral behavior of bridge structures have generally focused on bridge pile bents, bridge foundations, and bridge superstructures. Most of

these studies were based on theoretical and numerical analyses but very few studies were experimental.

Performance of bridge pile bents under scour effects has been closely investigated using numerical analysis (Daniels et al. 2007; Hughes et al. 2007a; Hughes et al. 2007b). A screening procedure was proposed by Ramey et al. (2007) to protect bridge pile pents from scour damage by checking failure modes of pile settlement, pile buckling, pile kick out, and pile bent pushover. Hughes et al. (2007a) researched the effects of subgrade reaction modulus on the buckling of bridge pile bents without bracing at different scour depths. *FB-MultiPier* was used to analyze the effects of subgrade reaction modulus on the lateral movement of pile bents and pile buckling. Hughes et al. (2007a) concluded that the subgrade reaction modulus had little influence on the buckling capacity of the bridge pile bent and the piles may be assumed to be fixed at a depth of 1.5 m below the ground surface. Related studies by Hughes et al. (2007b) and Daniels et al. (2007) discussed the pushover failure of bridge pile bent under scour conditions. They assumed the bridge pile bent to be fixed or pinned at the ground surface and investigated the effects of the number of pile and presence of X-brace on the lateral stiffness of bridge. They found that the presence of X-brace was beneficial to the improvement of bridge pile bent's lateral resistance to scour. The addition of a horizontal strut at the bottom of pile bent significantly increased the pushover capacity of two-story X-braced pile bents at different scour depths; however it had a limited effect on the increase of the pushover capacity of one-story X-braced pile bent.

Scour effects on lateral behavior of bridge foundations have been investigated (Diamantidis and Arnesen 1986; Achmus et al. 2010). Diamantidis and Arnesen (1986) conducted a sensitivity analysis of scour effects on the response of laterally loaded piles. The *p-y* method was adopted for the analysis, and the sensitivity analysis investigated the parameters such as pile length and diameter, scour depth, scour width, and soil friction angle and subgrade reaction modulus. They concluded that increase of bending stress with scour depth was lower for

pile with higher stiffness but higher for sand with higher strength. As the *p*-y method cannot consider scour-hole dimensions, the scour width effects were considered in an approximate way based on the estimation of soil effective stress around the pile. In the approximation, the total scour depth (S_d) of the scour hole was reduced by multiplying with a reduction factor (f_s) which was a function of scour width as shown in Figure 2-12. As seen in Figure 2-12, when scour width greater than 6.5 times of pile diameter, the scour width has no effects on the behavior of laterally loaded piles.

Achmus et al. (2010) performed a finite element analysis of scour effects on windfarm monopiles under cyclic lateral loading. Scour-hole dimensions were considered by using the slope angle of the scour hole of $\frac{1}{2}\phi$, with ϕ being the effective friction angle. As anticipated, scour significantly increased the deflection and rotation of the monopile. However, the pile diameter had limited influence on the increase of rotation of the pile due to scour.

Few studies have focused on field tests because monitoring bridge is a long-term process and the measured bridge responses are systematic reactions due to a combination of different factors other than mere scour. McConnell and Cann (2010) monitored the lateral movement of Indian River Inlet Bridge (IRIB), located in Sussex County, Delaware using D-Series Dual Axis Inclinometers mounted at the interior piers. However, since the installation in 2007, the inclinometers have showed little movement. Recently, dynamic measurement was applied to qualitatively estimate effects of foundation scour (Foti and Sabia 2011), by monitoring traffic induced vibration of the bridge. Modal identification of vibration of bridge spans and dynamic responses of bridge piers were the two methods employed for the measurement. Even though they did not quantify the extent of scour, they were able to provide insights into relative bridge integrity before and after retrofitting (Foti and Sabia 2011).

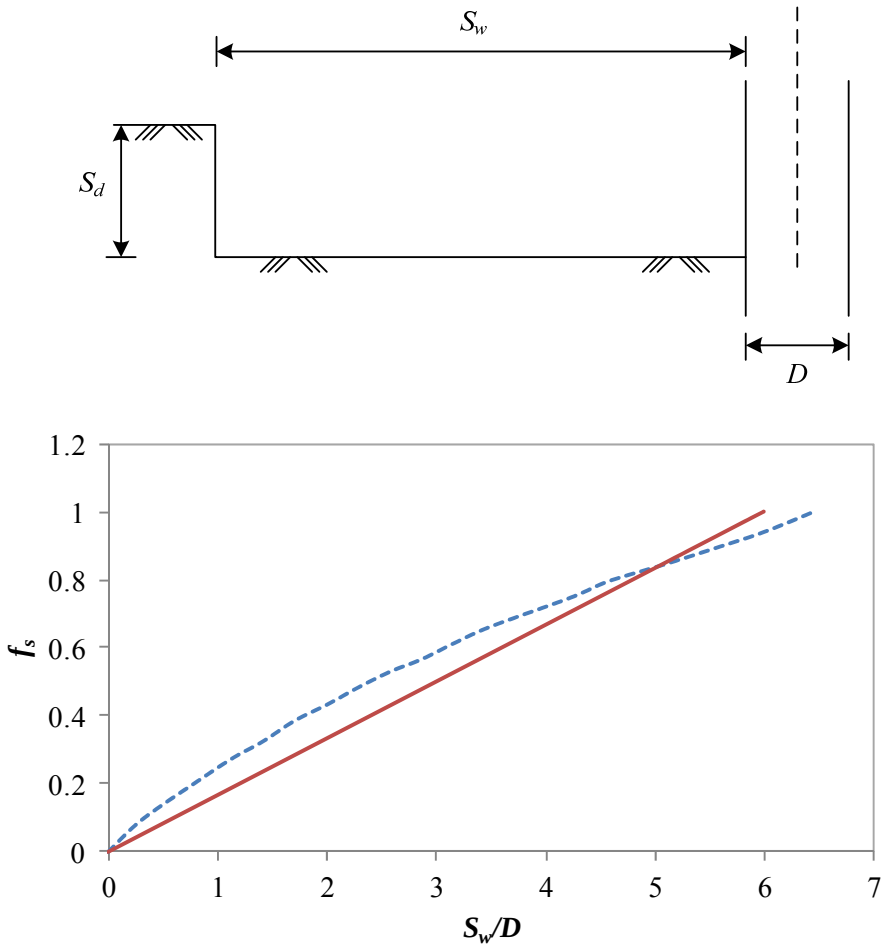

Figure 2-12. Equivalent general scour depth as a function of scour width (Diamantidis and Arnesen 1986)

2.6 Summary

A comprehensive literature review of the various key factors influencing the susceptibility of bridges to scour presented in Chapter 2. Scour-induced bridge failures were discussed in terms of hydraulic, structural, and geotechnical aspects, based on 36 case studies found in the literature. Lateral failure was found to be the most prominent failure mode.

Additionally, different techniques for determining lateral soil-pile interaction were examined, of which *p-y* method is the most widely used method in practice. 3D numerical modeling techniques were also discussed, but it was noted that while finite element and finite difference techniques are capable of representing real conditions more closely than less-sophisticated techniques, accuracy of these may be heavily influenced by a number of factors.

The limitations of current research based on the literature review presented are summarized as follows:

(1) The conventional one-dimensional *p-y* method cannot address the effects of scour-hole dimensions. An approximate approach for considering scour width by Diamantidis and Arnesen (1986) has been proposed without verification. Additionally, this method is not capable of characterizing scour-hole shape because scour-hole slope angle was not considered in the model.

(2) Stress history effects of the remaining soils after scour has occured have not been addressed in the literature.

(3) 3D numerical modeling of scour effects on pile foundations in current research is limited, and many parameters of interest, including different soil types and scour-hole dimensions, have not been adequately studied.

(4) Study of lateral performance of bridges under scour conditions in an integrated system has not been adequately studied.

CHAPTER 3

SCOUR EFFECTS ON LATERALLY LOADED PILES CONSIDERING STRESS HISTORY EFFECTS

Geological loading and unloading due to glacial ice or erosion and deposit of sediments have been known to produce overconsolidated soils. The maximum stress the soil experiences in history is termed as preconsolidation stress at which major changes in soil structures take place (Terzaghi et al. 1996). Scour by removing the soils around bridge foundations also creates stress history, thereby altering properties of the remaining soils. This chapter is to incorporate scour induced stress history of soils into the analysis of laterally loaded piles. The conventional *p-y* curves for analyzing laterally loaded piles are modified to accommodate the stress history of soils. Soft and stiff clays and sandy soils are investigated separately because of the different *p-y* characteristics for each of them. Comparisons are made of response of laterally loaded single piles resulting from considering and ignoring stress history effects due to scour.

3.1 Stress History Effects in Soft Clay

Soft clay which has a low strength is usually under normally consolidated or lightly overconsolidated conditions. For simplicity, soft clay before scour is approximately considered as a normally consolidated soil in this study but after scour it becomes an overconsolidated soil. In the analysis of laterally loaded piles in soft clay, the *p-y* curves proposed by Matlock (1970) have been widely used in practice and are adopted herein. The *p-y* curves for soft clay are formulated as follows:

$$\frac{p}{p_{ult}} = 0.5(\frac{y}{y_{50}})^{1/3} \quad 3.1$$

where, p = lateral soil resistance per unit length of pile, kN/m^3; y = lateral soil displacement, m; y_{50} = the lateral displacement at half the maximum soil stress, m, and is determined by Equation 3.2; p_{ult} = ultimate soil resistance per unit length of pile, kN/m^3, using the smaller value computed by Equations 3.3 and 3.4 . In Equation 3.1, when y is greater than $8y_{50}$, p remains constant at p_{ult}.

$$y_{50} = 2.5\varepsilon_{50}D \quad 3.2$$

$$p_{ult1} = (3 + \frac{\gamma'}{C_u}z + \frac{J}{D}z)C_uD \quad 3.3$$

$$p_{ult2} = 9C_uD \quad 3.4$$

where, D = width of pile, m; z = soil depth measured from the ground surface, m; ε_{50} = strain at one-half the maximum stress, typically between 0.01 and 0.02; C_u = undrained shear strength, kPa; J = a constant value, typically using 0.5; γ' = effective unit weight of soil.

Equations 3.1 to 3.4 indicate that the key soil parameters for the *p-y* curve of soft clay are effective unit weight and undrained shear strength. To address the stress history effects of soft clay on response of laterally loaded piles, these two parameters before and after scour should be examined (Delphia 2009).

In this section, effective unit weight before and after scour is related to each other by including the changes of void ratio and overburden stress during scour. The relationship of

undrained shear strength before and after scour is established based on critical state soil mechanics and expressed as a function of overconsolidation ratio (*OCR*). Once soil effective unit weight and undrained shear strength are determined after scour, the *p-y* curve is thus modified to consider stress history effects. In the end of this section, an example is presented to compare lateral pile response under scour conditions by considering and ignoring stress history of soft clay.

3.1.1 Effective unit weight after scour

The effective unit weight of soil before scour can be correlated to void ratio:

$$\gamma_{\text{int}}' = \frac{G_s - 1}{1 + e_{\text{int}}}\gamma_w \qquad 3.5$$

where, γ_{int}' = the soil effective unit weight before scour, kN/m^3; G_s = the soil specific gravity; e_{int} = the soil void ratio before scour; and γ_w = unit weight of water, kN/m^3.

The effective unit weight of soil after scour can be also correlated to void ratio after scour:

$$\gamma_{sc}' = \frac{G_s - 1}{1 + e_{sc}}\gamma_w \qquad 3.6$$

where, γ_{sc}' = the effective unit weight after scour, kN/m^3 and e_{sc} = the void ratio of soil after scour.

By dividing Equation 3.6 by 3.5, relationship of effective unit weight before and after scour is:

$$\gamma_{sc}' = \frac{1+e_{\text{int}}}{1+e_{sc}}\gamma_{\text{int}}' \qquad 3.7$$

In the saturated soil condition, the void ratio is expressed as follows:

$$e = G_s w \qquad 3.8$$

where, e = soil void ratio and w = soil moisture content.

By substituting Equation 3.8 into 3.7 , the effective unit weight after scour can be rewritten as:

$$\gamma_{sc}' = \frac{1+Gw_{\text{int}}}{1+e_{sc}}\gamma_{\text{int}}' \qquad 3.9$$

The void ratio after scour can be expressed by Equation 3.10 based on soil consolidation curve (Figure 3-1) and overburden stresses before and after scour are presented in Equations 3.11 and 3.12.

$$e_{sc} = e_{\text{int}} + C_{ur}\log(\sigma_{v\text{int}}/\sigma_{vsc}) \qquad 3.10$$

$$\sigma_{v\text{int}} = (\gamma_{\text{int}}')(z + s_d) \tag{3.11}$$

$$\sigma_{vsc} = (\gamma_{sc}')z \tag{3.12}$$

In Equations 3.10 to 3.12, σ_{vsc} = vertical stress after scour at the point of interest, kN/m^2; σ_{vint} = vertical stress before scour at the point of interest, kN/m^2; z = the depth of point of interest measured from mudline after scour, m; s_d = scour depth, m. In Figure 3-1, C_c and C_{ur} represent the compression and swelling indices obtained from oedometer test.

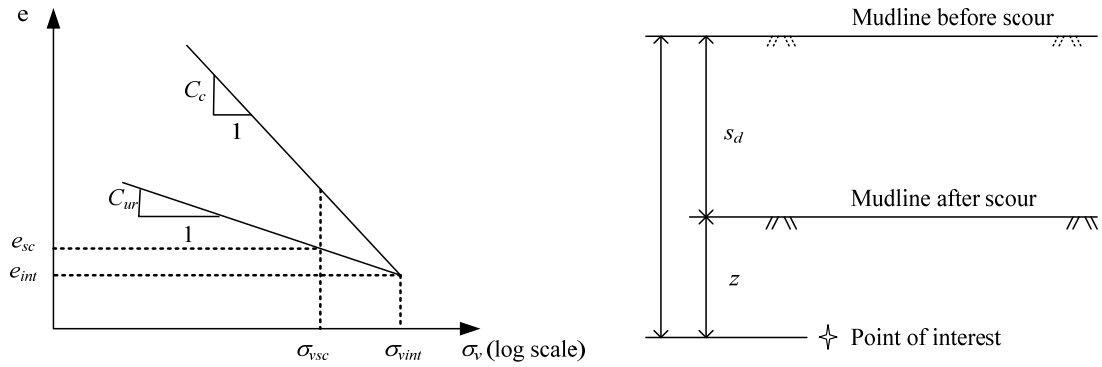

Figure 3-1. (a) *e*-log *p* curve (b) profile of soft clay under scour

Combining Equations 3.9 and 3.12 , the effective unit weight after scour can be determined by the following equation.

$$\gamma_{sc}' = \frac{1 + G_s w_{\text{int}}}{1 + G_s w_{\text{int}} + C_{ur} \log\left(\dfrac{(\gamma_{\text{int}}')(z + s_d)}{(\gamma_{sc}')z}\right)} \gamma_{\text{int}}' \tag{3.13}$$

In Equation 3.13, G_s and w_{int} are dependent on each other, and their relationship can be derived from Equations 3.5 and 3.8. For example, G_s can be expressed a function of w_{int}:

$$G_s = \frac{\gamma_{\text{int}}' + \gamma_{\text{w}}}{\gamma_{\text{w}} - w_{\text{int}}\gamma_{\text{int}}'} \qquad 3.14$$

3.1.2 Undrained shear strength after scour

Soils after scour becomes overconsolidated from normally consolidated soils. Undrained shear strength of the overconsolidated soils can be evaluated based on the following equations which have been derived based on the modified Cam-Clay model (Kulhawy and Mayne 1990; Muir Wood 1990).

$$\frac{(C_u/\sigma_v)_{sc}}{(C_u/\sigma_v)_{\text{int}}} = \frac{(C_u/\sigma_v)_{OC}}{(C_u/\sigma_v)_{NC}} = OCR^{\Lambda} \qquad 3.15$$

$$\Lambda = \frac{\lambda - \kappa}{\lambda} = 1 - \frac{C_{ur}}{C_c} \qquad \text{(typically} \approx 0.8\text{)} \qquad 3.16$$

In Equations 3.15 and 3.16, σ_v = the vertical stress, kN/m^2; λ and κ are compression and swelling indices from the isotropic consolidation test.

3.1.3 Modified *p-y* curve

The *p-y* curve for considering stress history of soft clay is obtained essentially by modifying the ultimate soil resistance, p_{ult}. The modification of p_{ult} fundamentally depends on the change of effective unit weight (Equation 3.13) and undrained shear strength (Equation 3.15). By substituting Equations 3.15 into Equations 3.4 and 3.5, the p_{ult} equations for soft clay after scour can be rewritten:

$$p_{ult1} = (OCR)^{\Lambda}(\sigma_{vsc}')(3D + Jz)\left[\frac{(c_u)_{\text{int}}}{\sigma_{v\text{int}}'}\right] + (\sigma_{vsc}')D \qquad 3.17$$

$$p_{ult2} = 9D(OCR)^{\Lambda}(\sigma_{vsc}')\left[\frac{(c_u)_{\text{int}}}{\sigma_{v\text{int}}'}\right] \qquad 3.18$$

By incorporating Equations 3.11 and 3.12, the above two equations become:

$$p_{ult1} = (OCR)^{\Lambda}\gamma_{sc}'z(3D + Jz)\left[\frac{(c_u)_{\text{int}}}{(z + s_d)\gamma_{\text{int}}'}\right] + \gamma_{sc}'zD \qquad 3.19$$

$$p_{ult2} = 9D(OCR)^{\Lambda}\gamma_{sc}'z\left[\frac{(c_u)_{\text{int}}}{(z + s_d)\gamma_{\text{int}}'}\right] \qquad 3.20$$

In Equations 3.19 and 3.20, γ_{sc}' can be obtained by solving Equation 3.13 through iterations. Once soil parameters before scour (e.g. moisture content or specific gravity, effective unit weight, and undrained shear strength) and scour depth are provided, The ultimate soil

resistance after scour can be determined by Equations 3.13, 3.19, and 3.20. The ultimate soil resistance after scour is then substituted into Equation 3.1 and the *p-y* curve is thus modified.

3.1.4 A case study

A laterally loaded pile test in soft clay near the Lake Austin, Texas (Matlock 1970) was used herein as a case study. However, it was only used as an initial condition (before scour), since the test did not involve any scour processes. Therefore, scour was assumed to take place along the pile in order to analyze stress history effects on behavior of laterally loaded piles under scour conditions. Soil properties before scour are summarized in Table 3-1, where compression index, C_c, was estimated based on moisture content (Djoenaidi 1985) and swelling index, C_{ur}, is taken as $1/5C_c$ (Kulhawy and Mayne 1990). The undrained shear strength was measured with a field vane and was an average value along the soil depth from ground surface to pile tip as presented in Table 3-1. The initial void ratio, e_{int}, was 1.60 and the specific gravity, G_s, was 3.6; both parameters were computed by Equations 3.8 and 3.14. The pipe pile was used in the test with its parameters tabulated in Table 3-2.

Table 3-1. Properties of soft clay

Undrained shear strength, C_u (kPa)	Effective unit weight, γ_{int}' (kN/m^3)	Strain at half maximum stress, ε_{50}	Water content, w_{int} (%)	Compression index, C_c	Swelling index, C_{ur}
32.3	10	0.012	44.5	0.38	0.076

Table 3-2. Pile parameters (Matlock 1970)

Length, L(m)	Outer diameter, D (m)	Thickness, t (m)	Moment of inertia, I_p (m^4)	Elastic modulus, E_p (kN/m^2)	Yielding moment, M_y (kN-m)
12.8	0.319	0.0127	1.44×10^{-4}	2.18×10^{8}	231

The water table was kept above ground surface and two scour depths (i.e. 1.6 and 3.2 m approximately equal to 5D and 10D with D being pile diameter) were investigated as shown in Figure 3-2.

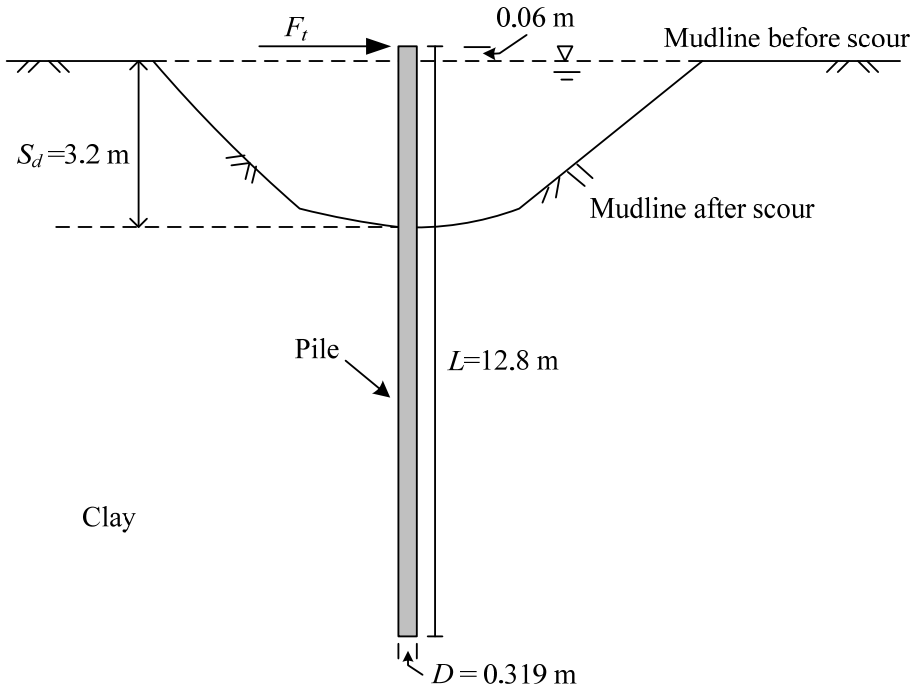

Figure 3-2. Profile of soil and pile before and after scour

The most direct way to evaluate lateral behavior of piles considering stress history effects is using numerical methods to solve for the governing beam equation (Equation 2.10) that incorporates the modified *p-y* curve (Equations 3.1, 3.13, 3.19, and 3.20). The initial soil

parameter (before scour) can be used directly to compute the modified *p-y* curve based on the listed equations. The widely used finite difference code, *LPILE*, is fundamentally to solve for the governing beam equation incorporating nonlinear *p-y* curves; however, *LPILE* cannot directly take initial soil parameters to generate the modified *p-y* curves. Alternatively, the modified *p-y* curves can be computed first in *LPILE* using modified effective unit weight and undrained shear strength (i.e. after scour) (Equations 3.13 and 3.15). Then lateral behavior of piles considering stress history of soft clay can be evaluated in *LPILE*. As such,this study adopted the second option. The influence depth, within which the average shear strengths were averaged, could be determined based on mobilized soil reaction distribution along the pile length. The influence depth was 12 m because the soil resistance at the depth below was negligent. Hence, soil properties within the soil depth of 12 m were averaged. By using initial average input soil properties, the computed result (i.e. lateral pile-head displacement before scour) showed a general good agreement with that of field test, as shown in Figures 3-3 and 3-4.

Tables 3-3 and 3-4 present the calculated soil properties at different soil depths when the scour depth is 5 and 10 *D* respectively. The results show that changes of effective unit weight and void ratio were negligent during scour, with minor decrease for the former and small increase for the latter. The undrained shear strengths after scour slightly decreased comparing that before scour (Table 3-1) and appeared to decrease more with increase of the scour depth. Overconsolidation ratio (OCR) also increased slightly from 1.5 to 2.0 when the scour depth increased from 5 to 10 *D*. In general, the soil properties were altered insignificantly during scour process but the changes appeared to be more apparent as scour depth became larger.

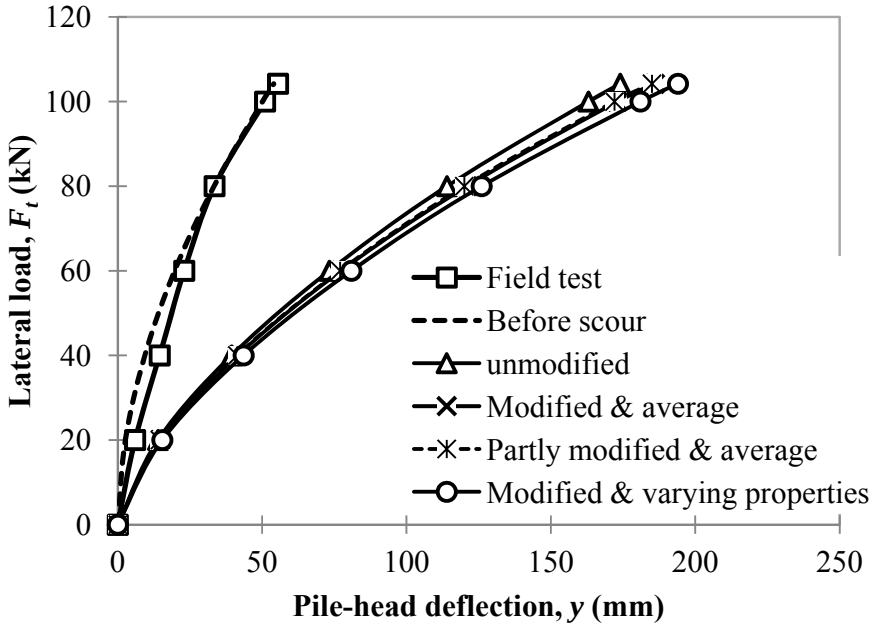

Figure 3-3. Lateral pile-head displacement (S_d = 5 D)

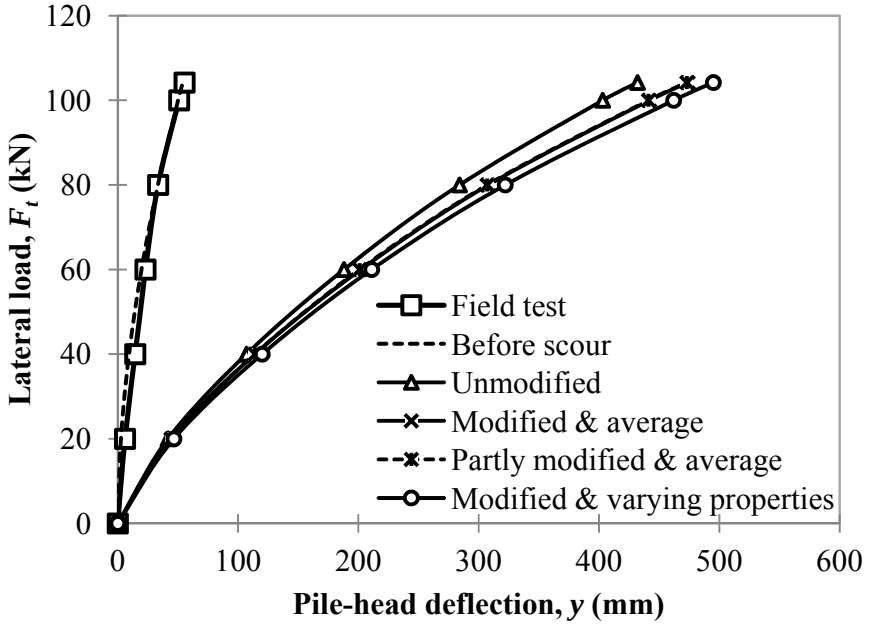

Figure 3-4**. Lateral pile-head displacement (S_d = 10 D)**

Table 3-3. Calculated soil properties after considering stress history effects (S_d = 5 D)

Soil depth from mudline after scour(m)	γ_{sc}' (kN/m^3)	e_{sc}	$(C_u)_{sc}$ (kN/m^2)	*OCR*
1.14	9.74	1.67	27.0	2.5
3.39	9.88	1.63	29.8	1.5
3.70	9.89	1.63	30.0	1.5
4.30	9.90	1.63	30.2	1.4
5.69	9.92	1.62	30.7	1.3
7.25	9.94	1.62	31.0	1.2
9.47	9.95	1.61	31.2	1.2
11	9.97	1.61	31.4	1.2
Average value	9.90	1.63	30.1	1.5

Table 3-4. Calculated soil properties after considering stress history effects (S_d = 10 D)

Soil depth from mudline after scour(m)	γ_{sc}' (kN/m^3)	e_{sc}	$(C_u)_{sc}$ (kN/m^2)	*OCR*
1.14	9.61	1.71	24.5	4.0
3.39	9.80	1.65	28.1	2.0
3.70	9.81	1.65	28.4	1.9
4.30	9.83	1.65	28.8	1.8
5.69	9.87	1.64	29.4	1.6
7.25	9.89	1.63	29.9	1.5
9.47	9.91	1.63	30.4	1.4
Average value	9.82	1.65	28.5	2.0

Two approaches for inputting effective unit weight and undrained shear strength after scour within the influence depth were considered in *LPILE*. One approach was to select average values while another was to use varying values along the soil depth.

The *p-y* curve after scour was termed unmodified *p-y* curve if generated using the initial soil parameters (before scour), modified *p-y* curve using the modified soil parameters (after scour), and partly modified *p-y* curve using modified undrained shear strength but initial effective unit weight. Both modified and partly modified *p-y* curves were generated based on the input of average values of soil properties and were able to address stress history of soft clay but unmodified *p-y* curves did not consider stress history. Partly modified *p-y* curve was computed to evaluate effects of effective unit weight on the result of response of laterally loaded piles. The varying properties along the soil depth were also considered during the input of soil properties for *LPILE*. The *p-y* curves were calculated as shown in Figures 3-5 and 3-6. In the figures, modified and partly modified *p-y* curves were the same but both had lower soil resistance (p) than unmodified *p-y* curves at the same lateral displacement (y). As the scour depth increased, the gap of soil resistance between modified and unmodified *p-y* curves increased slightly. Furthermore, soil resistance became smaller using the varying properties than using the average properties.

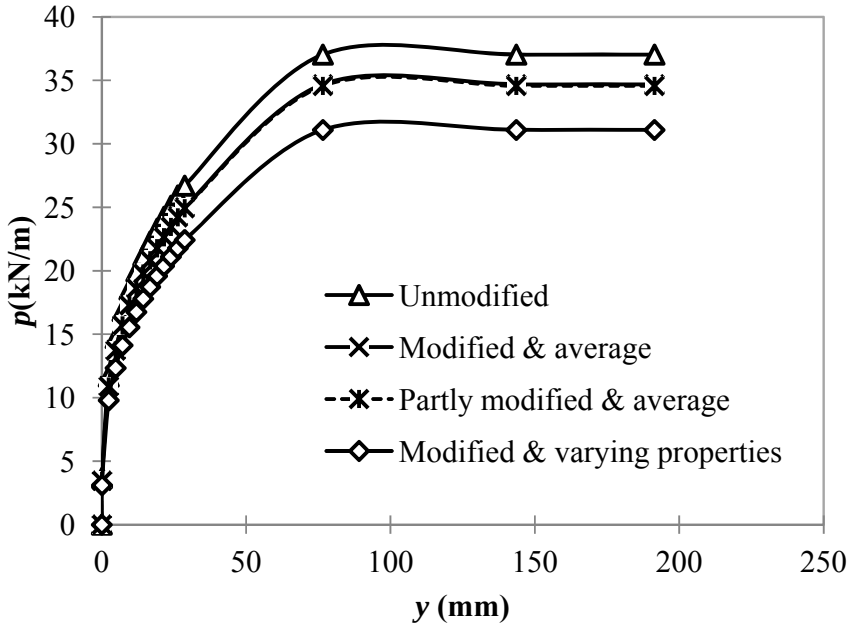

Figure 3-5. The *p-y* curves at soil depth of 1 *D* considering and ignoring stress history effects (S_d = 5 *D*)

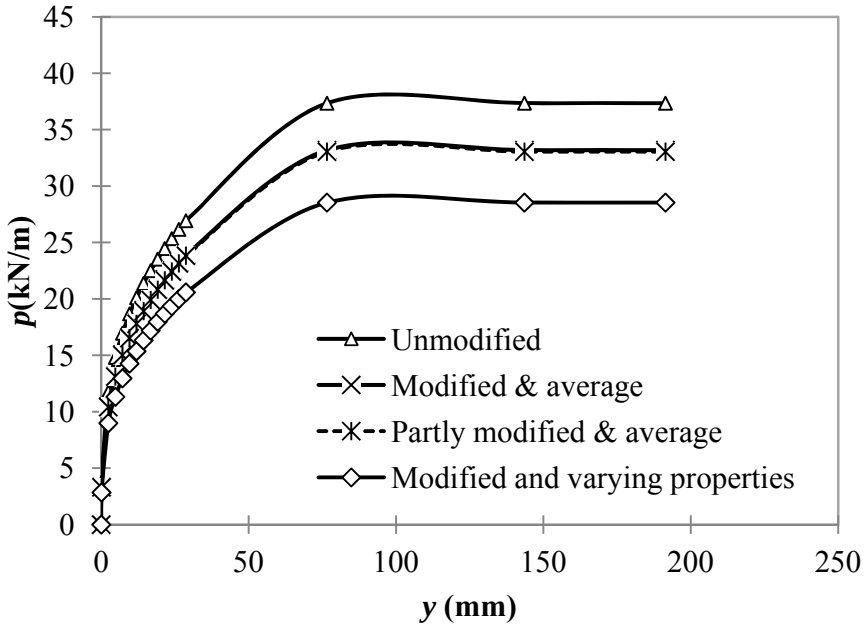

Figure 3-6. The *p-y* curves at soil depth of 1 *D* considering and ignoring stress history effects (S_d = 10 *D*)

As shown in Figures 3-3 and 3-4, lateral pile-head displacement calculated using modified *p-y* curves was slightly larger than that calculated using unmodified *p-y* curves and the disparity of the displacement slightly increased as scour depth increased. In addition, by using the soil properties varied along the soil depth, the lateral pile-head displacement increased compared with that by using the average values. For example, at 100 kN lateral load, the difference of the displacement relative to the displacement computed using unmodified *p-y* curves was 6% (average properties) and 11% (varying properties) at scour depth of 5 *D*, and marginally increased to 9% (average properties) and 15% (varying properties) at scour depth of 10 *D*. Furthermore, modified and partly modified *p-y* curves produced the same pile-head displacement, which indicated the change of effective unit weight due to scour had no effect on lateral behavior of pile, and thus could be neglected.

In general, scour effects on the reposne of laterally loaded piles in soft clay were investigated by considering stress history effects. The analysis showed the change of effective unit weight due to scour could be ignored; hence the minor difference of pile-head displacement calculated by considering and ignoring stress history effects was only caused by the change of undrained shear strength. By using the varying soil properties along the soil depth, the lateral displacement increased compared with that using the average values. Increase of scour depth enhanced the stress history effects on the lateral behavior of the pile in soft clay but the effects were still limited. So, stress history of soft clay might be insignificant to be considered in analysis of scour effects on the response of laterally loaded piles.

3.2 Stress History Effects in Stiff Clay

Similar to soft clay, analysis of laterally loaded piles in stiff clay using *p-y* method also requires effective unit weight and undrained shear strength. But the analysis in stiff clay involves

an additional input parameter that is coefficient of subgrade reaction, K_{py}. Empirical estimation of K_{py} is given in Table 3-5 based on undrained shear strength. Because K_{py} depends on undrained shear strength, the parameters for considering stress history of stiff clay also reduce to effective unit weight and undrained shear strength are the chief. Additionaly, stiff clay is usually overconsolidated or highly overconsolidated and has much higher undrained shear strength than soft clay. As a result, before scour stiff clay needs to be considered as an overconsolidated soil and after scour it becomes a further overconsolidated soil.

In this section, the conventional *p-y* curve for stiff clays proposed by Reese et al. (1975) is modified by modifying effective unit weight and undrained shear strength to addresses the stress history effects in stiff clay due to scour. A case study that follows is presented. Similarly defined in soft clay, the *p-y* curve which addresses stress history of stiff clay is referred to as "modified *p-y* curve", whereas that ignoring stress history effects is termed as "unmodified *p-y* curve".

Table 3-5. Representative values of coefficient of subgrade reaction K_{py} for overconsolidated clays (Reese and Van Impe 2001)

Average undrained shear strength, C_u (kN/m^2)	Coefficient of subgrade reaction, K_{py} (MN/m^3)
50-100	135
100-200	270
300-400	540

3.2.1 Effective unit weight after scour

Effective unit weight after scour can also be computed in Equation 3.13 as used in soft clay. However, by using the equation, assumption is involved that soil before and after scour has the same preconsolidation stress. The same preconsolidation stress ensures the soil stress path at the same rebound line and thus Equation 3.13 is still valid. However, if soil preconsolidation stress before and after scour is different, then Figure 3-1 is redrawn to Figure 3-7. In Figure 3-7, soil stress of point of interest before scour has preconsolidation stress, $(\sigma_p)_{int}$ and is at the upper rebound line whereas soil stress of the same point after scour has a different preconsolidation stress, $(\sigma_p)_{sc}$ and is at a different (lower) but parallel rebound line.

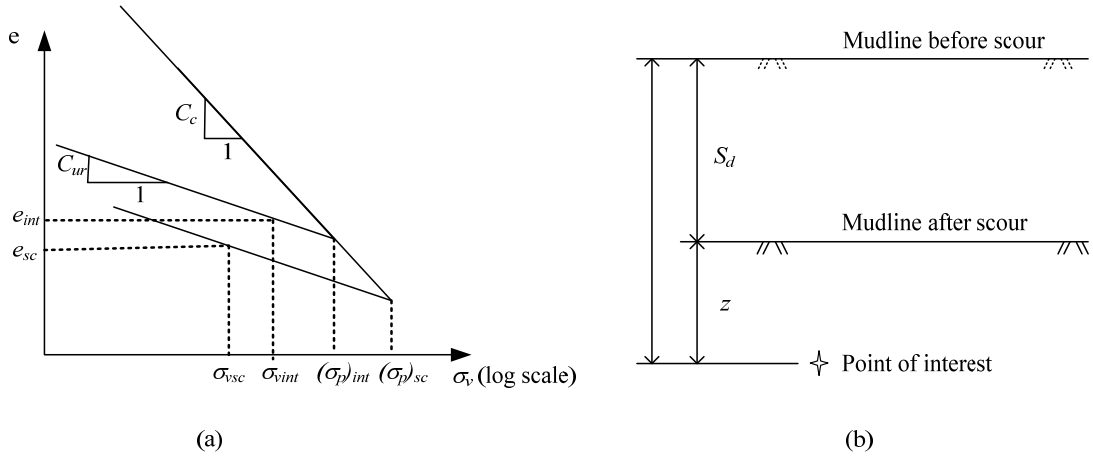

Figure 3-7. (a) *e*-log *p* curve from odeometer test (b) profile of stiff clay under scour

The void ratio after scour, e_{sc}, may be written as follows:

$$e_{sc} = e_{\text{int}} + C_{ur} \log\left(\frac{\sigma_{v\text{int}}}{\sigma_{vsc}}\right) + (C_c - C_{ur}) \log\left(\frac{(\sigma_p)_{\text{int}}}{(\sigma_p)_{sc}}\right) \qquad 3.21$$

The effective unit weight, γ_{sc}', may be rewritten below:

$$\gamma_{sc}' = \frac{1+G_s w_{\text{int}}}{1+G_s w_{\text{int}} + C_{ur}\log\left(\frac{(\gamma_{\text{int}}')(z+S_d)}{(\gamma_{sc}')z}\right) + (C_c - C_{ur})\log\left(\frac{(\sigma_p)_{\text{int}}}{(\sigma_p)_{sc}}\right)}\gamma_{\text{int}}' \qquad 3.22$$

3.2.2 Undrained shear strength after scour

As initial soil (before scour) is overconsolidated, to compute undrained shear strength after scour, Equation 3.15 may be revised as follows:

$$\frac{(C_u/\sigma_v)_{sc}}{(C_u/\sigma_v)_{\text{int}}} = \left(\frac{OCR_{sc}}{OCR_{\text{int}}}\right)^{\Lambda} \qquad 3.23$$

where, OCR_{int} = overconsolidation ratio before scour, equal to $(\sigma_p)_{int}/\sigma_{vint}$; and OCR_{sc} =overconsolidation ratio after scour, equal to $(\sigma_p)_{sc}/\sigma_{vsc}$.

After rearranging the above equation, the undrained shear strength after scour is:

$$(C_u)_{sc} = (C_u)_{\text{int}}\left[\frac{(\sigma_p)_{sc}}{(\sigma_p)_{\text{int}}}\right]^{\Lambda}\left(\frac{\sigma_{v\text{int}}}{\sigma_{vsc}}\right)^{\Lambda-1} \qquad 3.24$$

3.2.3 Modified *p-y* curve

The *p-y* curve after scour is changed fundamentally by the changes of ultimate soil resistance and initial soil modulus (represented by K_{py}). Because ultimate soil resistance is dependent on soil effective unit weight, γ', and undrained shear strength, C_u, the γ', C_u, and K_{py} determine the *p-y* curve of stiff clay. Once C_u after scour is determined (Equation 3.23), K_{py} can be estimated in Table 3-5. The ultimate soil resistance per unit length is the smaller value given by the following two equations (Reese et al. 1975):

$$p_{ult1} = 2C_u D + \sigma_v' D + 2.83 C_u z \tag{3.25}$$

$$p_{ult2} = 9C_u D \tag{3.26}$$

After scour, the ultimate soil resistance per unit length may be rewritten below (using the smaller value):

$$p_{ult1} = (2D + 2.83z)(C_u)_{\text{int}} \left[\frac{(\sigma_p)_{sc}}{(\sigma_p)_{\text{int}}}\right]^{\Lambda} \left[\frac{(\gamma_{\text{int}}')(S_d + z)}{(\gamma_{sc}')z}\right]^{\Lambda-1} + (\gamma_{sc}')zD \tag{3.27}$$

$$p_{ult2} = 9D(C_u)_{\text{int}} \left[\frac{(\sigma_p)_{sc}}{(\sigma_p)_{\text{int}}}\right]^{\Lambda} \left[\frac{(\gamma_{\text{int}}')(S_d + z)}{(\gamma_{sc}')z}\right]^{\Lambda-1} \tag{3.28}$$

If soil has the same preconsolidation stress before and after scour [i.e. $(\sigma_p)_{int} = (\sigma_p)_{sc}$], and change of effective unit weight is ignored ($\gamma_{int}' = \gamma_{sc}'$), then Equations 3.27 and 3.28 can be rewritten below (using the smaller value):

$$p_{ult1} = (2D + 2.83z)(C_u)_{\text{int}} \left(\frac{S_d + z}{z} \right)^{\Lambda - 1} + (\gamma_{\text{int}}')zD \qquad 3.29$$

$$p_{ult2} = 9D(C_u)_{\text{int}}(C_u)_{\text{int}} \left(\frac{S_d + z}{z} \right)^{\Lambda - 1} \qquad 3.30$$

After ultimate soil resistance per unit length of pile and coefficient of subgrade reaction are modified for stiff clays after scour, the *p-y* curve is modified and thus can be used to address the stress history of stiff clay due to scour.

3.2.4 A case study

The purpose was to investigate scour effects on response of laterally loaded single pile by considering and ignoring stress history of stiff clay. The soil properties in the initial condition, as shown in Table 3-6 , were common values of stiff clay. The pile parameters were presented in Table 3-2.

Table 3-6. Properties of stiff clay

Undrained shear strength, C_u (kPa)	Effective unit weight, γ_{int}' (kN/m^3)	Water content, w_{int} (%)	Compression index, C_c	Swelling index, C_{ur}	OCR_{int}
150	10	30	0.26	0.052	2

Overconsolidation Ratio, *OCR* of 2 was used and preconsolidation stress in the pre-scour condition could be computed by multiplying *OCR* with the overburdened stress. However, for simplicity, soil preconsolidation stress before and after scour was assumed the same, that is $(\sigma_p)_{int} = (\sigma_p)_{sc}$. As a result, Equation 3.13 could be used to calculate effective unit weight after scour, γ_{sc}'. Undrained shear strength after scour in Equation 3.24 was revised and given by:

$$(C_u)_{sc} = (C_u)_{\text{int}} \left[\frac{\gamma_{\text{int}}'(S_d + z)}{\gamma_{sc}' z} \right]^{\Lambda - 1} \qquad 3.31$$

The above equation indicates that if preconsolidation stress before and after scour is the same, then *OCR* is cancelled from the calculation of undrained shear strength after scour. Hence, although soil preconsolidation stress before scour is not measured, the effective unit weight and undrained shear strength after scour can still be determined once the preconsolidtion stress before and after scour is the same.

In this study, only a scour depth of 10 pile diameter (i.e. S_d =10 D or 3.2 m) was investigated and the profile is the same as shown in Figure 3-2. The specific gravity, G_s

(Equation 3.14) and initial void ratio, e_{int} (Equation 3.8), were computed to be 2.86 and 0.858 respectively. By using Equation 3.13, 3.21, and 3.31, soil parameters after scour [e.g. γ_{sc}', e_{sc}, and $(C_u)_{sc}$] were determined as presented in Table 3-7. OCR_{sc} in the table was calculated by Equation 3.32. K_{py} was estimated to be 270 MN/m^3 for the C_u between 100 and 200 kN.

Table 3-7. Calculated soil properties after considering stress history effects (S_d = 10 D)

Soil depth from mudline after scour(m)	γ_{sc}' (kN/m^3)	e_{sc}	$(C_u)_{sc}$ (kN/m^2)	OCR_{sc}
1.14	9.63	0.93	114	7.9
3.39	9.81	0.89	131	4.0
3.70	9.82	0.89	132	3.8
4.30	9.84	0.89	134	3.6
5.69	9.87	0.89	137	3.2
7.25	9.89	0.88	139	2.9
9.47	9.91	0.87	141	2.7
Average value (1.14 to 5.69)	9.79	0.90	130	4.5

$$OCR_{sc} = OCR_{\text{int}} \frac{\gamma_{\text{int}}'(S_d + z)}{\gamma_{sc}' z} \qquad 3.32$$

The influence depth was found to be 6 m below which soil reaction was negligent. Hence, average values of the soil properties were limited to the soil depth less than 6 m as presented in Table 3-7. The table shows that scour slightly reduced soil effective unit weight and

increased void ratio; moderately reduced undrained shear strength; and significantly increased *OCR*. Change of soil parameters near the ground surface was more noteworthy than that at depth.

Similar to soft clay, average values of soil parameters after scour were used to compute behavior of laterally loaded pile considering stress history effects. However, soil parameters with varying values at different soil depths were also used herein to explore their influence on computation results, since behavior of laterally loaded piles might be significantly affected by soil properties at low depths. The computed *p-y* curves, as illustrated in Figure 3-8, reveal that modified *p-y* curves had smaller soil resistance than unmodified *p-y* curve and modified *p-y* curve computed using the average soil properties had a higher soil resistance that using the varying soil properties at depth. For example, the peak resistances computed using modified *p-y* curves with average and varying values were 13% and 23% less respectively than that computed using the unmodified *p-y* curve.

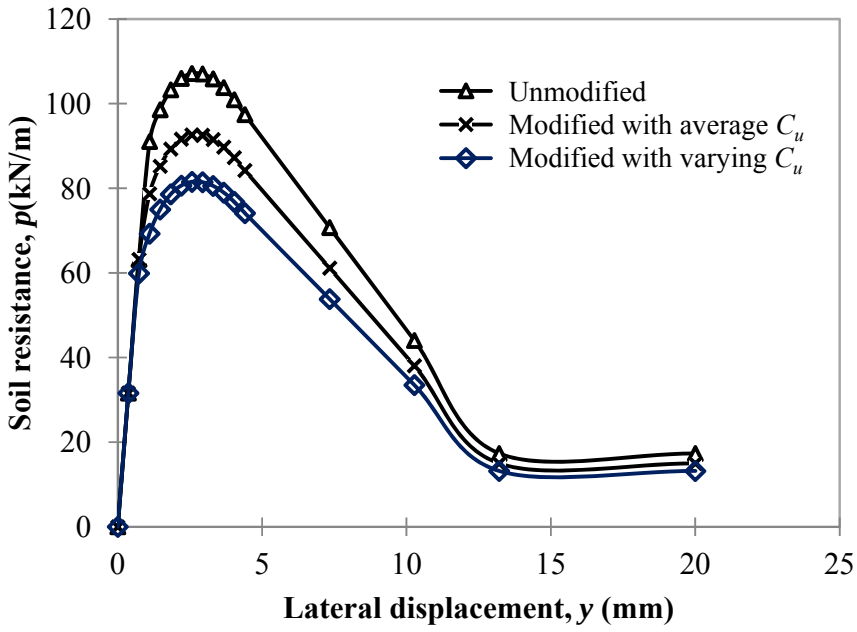

Figure 3-8. The *p-y* curves for soil depth of 1 *D* below ground surface after scour (S_d = 10 *D*)

Lateral pile-head displacement under lateral loading was calculated and plotted in Figure 3-9. The figure shows the significant increase of lateral pile-head displacement when scour depth of 10 *D* (3.2 m) was occurred, comparing dash line to solid lines. However, for all scour cases, stress history effects seemed limited on lateral pile-head displacement because modified *p-y* curves only produced a marginally larger displacement than unmodified *p-y* curve. At F_t =70 kN, the pile reached yielding bending strength. At F_t = 50 kN, lateral pile-head displacement was 55 mm, 58 mm, and 61 mm respectively computed using unmodified, modified *p-y* curve with average values of soil parameters, and modified *p-y* curve with varying values. By comparing these numbers in percentage, considering stress history of stiff clay only caused 5.5% (using average values) and 11% (using varying values) increase of the displacement than ignoring stress history.

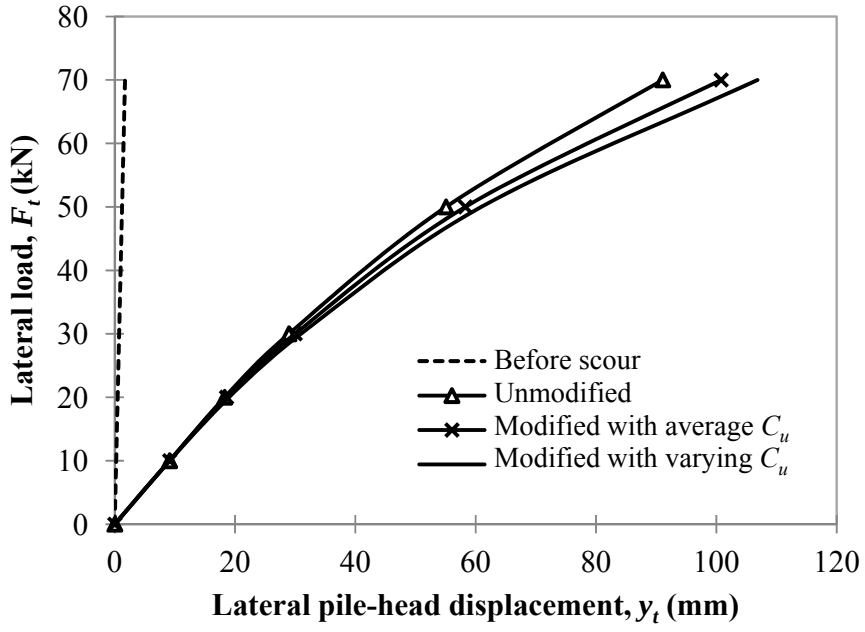

Figure 3-9. Lateral pile-head displacement considering and ignoring stress history effects (S_d = 10 *D*)

In total, similar to soft clay, scour induced stress history of stiff clay had a limited effect on the lateral behavior of the pile. Laterally loaded pile was significantly influenced by the soil near the ground surface, so that employing varying values of soil parameters at different depths was more reasonable and also produced a conservative analysis.

3.3 Stress History Effects in Sand

Stress history of sand can be also reflected by a loading and unloading process, in which deposition of soils can be considered as a process of loading, while removal of soils by scour can be considered as a process of unloading. Scouring also leads to the changes of remaining cohesionless soil from normally consolidated (NC) to overconsolidated (OC). Unlike clay, cohesionless soils are commonly analyzed and designed in drained conditions and therefore vertical and lateral effective soil stress may be different. Furthermore, unloading tends to reduce soil stresses in the vertical direction more than those in the lateral direction (Mayne and Kulhawy 1982). The lateral effective soil stress is decisive to the lateral soil resistance to the laterally loaded piles. It can be determined by multiplying vertical effective stress with the ratio of the lateral to vertical effective stress. The ratio is defined as the coefficient of lateral earth pressure at rest.

For a normally consolidated (NC) soil, the coefficient of lateral earth pressure at rest is given (Jaky 1944):

$$K_{on} = 1 - \sin \phi' \qquad 3.33$$

where K_{on} = coefficient of lateral earth pressure at rest for a normally consolidated soil and ϕ' = friction angle of the soil, °.

For an over-consolidated (OC) soil, the coefficient of lateral earth pressure at rest is given (Mayne and Kulhawy 1982):

$$K_{oc} = (1 - \sin\phi')OCR^{\sin\phi'} \qquad 3.34$$

where K_{oc} = coefficient of earth pressure at rest for an over-consolidated soil.

In terms of sand, relative density is an essential parameter needed to evaluate soil properties under scour. Delphia (2009) proposed the estimation of relative density at different scour conditions, relating it to basic parameters, such as the effective unit weight, the effective friction angle, and the modulus of subgrade reaction. The effective unit weight, the effective friction angle, and the modulus of subgrade reaction, K_{py}, are required input parameters for the analysis of laterally loaded piles in sand using *p-y* method.

In this study of stress history of sand, the effects of scour on soil resistance were considered for analyzing the response of laterally loaded piles in sand. The relative density and other soil properties (γ', ϕ', and K_{py}) of the remaining soils were then re-examined under a stress history due to scour. The coefficients of lateral earth pressure at rest under OC and NC conditions, K_{nc} and K_{oc}, respectively, were accounted for when the ultimate soil resistance for sand was calculated. A modified *p-y* curve was used to represent the remaining soils post-scour in which the laterally loaded pile was embedded. A field test reported in Cox et al. (1974) was used as a case-study example. A comparison was made between the calculated results considering scour effects and those determined without consideration of the effects of scour on the remaining soils.

3.3.1 Soil stresses and relative density after scour

The relative density of sand before scour can be determined based on a laboratory or field test results, which is considered as the initial state herein. However, the change of the relative density after scour can be estimated based on the scour depth as described below.

The change of the relative density is essentially equal to the change of the void ratio. The change of the void ratio, *e*, with the mean effective stress, *p'*, after scour can be characterized, as shown in Figure 3-10.

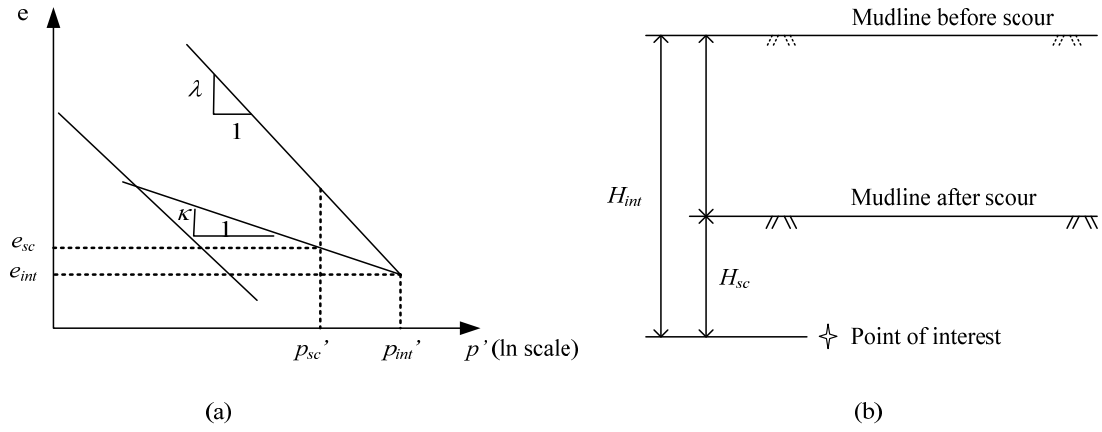

Figure 3-10. (a) Isotropic consolidation of soil and (b) Corresponding profile of sand under scour

The remaining soils after scour are subjected to unloading from the initial state corresponding to the state before scour, which can be expressed as (Budhu 2007):

$$\Delta e = e_{sc} - e_{\text{int}} = -\kappa \ln(p_{sc}'/\ p_{\text{int}}') \tag{3.35}$$

where κ = unloading index (equal to $0.434C_{ur}$); p_{int}' = mean effective stress before scour, kN/m^2; and p_{sc}' = mean effective stress after scour, kN/m^2. The mean effective stresses before and after scour can be calculated as follows:

Before scour:

The major principle effective stress is:

$$\sigma_1' = \sigma_v' = \gamma_{\text{int}}' H_{\text{int}} \tag{3.36}$$

where σ_1' = major principal effective stress, kN/m^2; σ_v' = vertical effective stress, kN/m^2; γ_{int}' = effective unit weight of soil before scour, kN/m^3; and H_{int} = depth of point interest before scour, m (Figure 3-10).

The minor principle effective stress is:

$$\sigma'_3 = \sigma'_h = K_{on}\sigma'_v = (1-\sin\phi')\gamma'_{\text{int}} H_{\text{int}} \tag{3.37}$$

where σ_3' = minor principal effective stress, kN/m^2 and σ_h' = horizontal effective stress, kN/m^2.

The mean effective stress is:

$$p'_{\text{int}} = (\sigma'_1 + 2\sigma'_3)/3 = \gamma'_{\text{int}} H_{\text{int}} (3-2\sin\phi')/3 \tag{3.38}$$

After scour:

The major principal effective stress is:

$$\sigma'_1 = \sigma'_v = \gamma_{sc}' H_{sc} \tag{3.39}$$

where H_{sc} = depth of point interest after scour, m (Figure 3-10).

The minor principal effective stress is

$$\sigma'_3 = \sigma'_h = K_{oc}\sigma'_v = [(1-\sin\phi')OCR^{\sin\varphi'}]\gamma_{sc}' H_{sc} \tag{3.40}$$

The overconsolidation ratio is defined as follows:

$$OCR = \gamma'_{\text{int}} H_{\text{int}} / (\gamma'_{sc} H_{sc}) \tag{3.41}$$

The mean effective stress can be calculated:

$$p'_{sc} = (\sigma'_1 + 2\sigma'_3)/3 = \gamma'_{sc} H_{sc}[1 + 2(1-\sin\varphi')OCR^{\sin\varphi'}]/3 \tag{3.42}$$

The change of the void ratio of the sand is determined after substituting Equations 3.38 and 3.42 into Equation 3.35.

$$\Delta e = -\kappa \ln[\frac{1 + 2(1-\sin\phi')OCR^{\sin\phi'}}{(3-2\sin\phi')OCR}] \tag{3.43}$$

The change of the relative density of the sand is:

$$\Delta D_r = \Delta e / (e_{\max} - e_{\min}) = \kappa \ln[\frac{(3-2\sin\phi')OCR}{1+2(1-\sin\phi')OCR^{\sin\phi'}}] / (e_{\max} - e_{\min}) \quad 3.44$$

where e_{max} = maximum void ratio; and e_{min} = minimum void ratio.

Relative density after scour is:

$$D_{rsc} = D_{r\,int} - \Delta D_r \quad 3.45$$

where D_{rint} = relative density before scour and D_{rsc} = relative density after scour.

It should be pointed out that the effective friction angle, ϕ', in Equation 3.44 is the peak effective friction angle, which is determined in the state of NC before scour. However, there is a discrepancy in the literature concerning the usage of the friction angle for K_{on} and K_{oc}. Hau (2003) and Terzaghi et al. (1996) used the critical friction angle for both coefficients of lateral earth pressure. Kulhawy and Mayne (1990) used the peak friction angle at a NC state to calculate the coefficients. Delphia (2009) recommended the peak friction angle determined under an NC state for K_{on} and the peak friction angle determined under an OC state for K_{oc}. In this study, Kulhawy and Mayne's approach (Kulhawy and Mayne 1990) was adopted because the equations for lateral earth pressure coefficients based on their approach were verified through an extensive literature review (Mayne and Kulhawy 1982).

If change of effective unit weight during scour is ignored (i.e. $\gamma_{sc}' = \gamma_{int}'$), relative density after scour, $D_{rsc,}$ after scour can be easily determined once soil parameters before scour (e_{max}, e_{min}, κ, ϕ', and D_{int}) and scour depth, s_d, are given. However, if change of effective unit weight due to scour is considered, then relationship between γ_{sc}' and D_{rsc} should be established, which will be described in the following section.

3.3.2 Relationship between relative density and soil parameters

Effective unit weight, effective friction angle, and modulus of subgrade reaction are three parameters needed for determining the soil resistance to laterally loaded piles. Each of these parameters can be related to the relative density of sand, D_r.

First, the effective unit weight can be determined below:

$$\gamma' = \frac{(G_s - 1)\gamma_w}{1 + e_{\max} - D_r(e_{\max} - e_{\min})} \tag{3.46}$$

Second, the effective friction angle of sand can be estimated based on relative density and initial mean effective stress below:

$$\phi' = \phi'_{cs} + 3D_r\left(10 - \ln\left(p'_o \Big/ \left(1 - \frac{2\sin\phi'}{3 - \sin\phi'}\right)\right)\right) - 3 \tag{3.47}$$

where, ϕ'_{cs} = critical effective friction angle and p'_o = initial mean effective stress which is p_{int}' in the pre-scour condition but is p_{cs}' in the post-scour condition.

Equation 3.47 was initially developed by Bolton (1986) using the mean effective stress at failure, and then modified by Yang and Mu (2008) based on the initial mean effective stress.

Lastly, the modulus of subgrade reaction can be estimated based on relative density in Table 3-8.

Table 3-8. Relative density and representative values of K_{py} for submerged sand

Relative Density	D_r (%)[a]	Recommended K_{py} (MN/m^3) [b]
Very loose to loose	0 to 35	5.4
Medium	35 to 65	16.3
Dense to very dense	65 to 100	34

[a] Source: (Lambe and Whitman 1969); [b] Source: (Reese and Van Impe 2001).

In the above correlations, the estimated soil parameters (γ', ϕ', and K_{py}) and relative density, D_r, are represented by γ_{int}', ϕ_{int}', $(K_{py})_{int}$, and D_{rint} in the pre-scour condition and γ_{sc}, ϕ_{sc}', $(K_{py})_{sc}$, and D_{rsc} in the post-scour condition. As Equation 3.46 gives the relationship between γ_{sc} and D_{rsc}, the abovementioned change of relative density, ΔD_r, can be obtained by solving for the Equations 3.41, 3.44, 3.45, and 3.46. Once ΔD_r is known, soil parameters after scour [γ_{sc}, ϕ_{sc}', $(K_{py})_{sc}$] can be readily solved based on the correlations above.

3.3.3 Modified *p-y* curve

A *p-y* curve for sand proposed by Reese et al. (1974) is adopted herein for unmodified *p-y* curve which does not address stress history of sand. The *p-y* curve is modified to address stress history effect, referred as modified *p-y* curve, by modifying the ultimate soil resistance. Ultimate soil resistance for sand was derived by considering a wedge failure near the ground surface and a plane strain failure well below the ground surface as presented in Equations

$$p_{st} = \gamma' z\left[\frac{K_o z \tan\phi' \sin\beta}{\tan(\beta-\phi')\cos\alpha} + \frac{\tan\beta}{\tan(\beta-\phi')}(b + z\tan\beta\tan\partial) + K_o z\tan\beta(\tan\phi'\sin\beta - \tan\alpha) - K_a b\right] \quad 3.48$$

where p_{st} = ultimate soil resistance near the ground surface; z = depth of soil; β = passive failure angle, using $45^\circ+\phi'/2$; α = angle defining the shape of the wedge, typically $\phi'/2$; and K_a = minimum coefficient of active lateral earth pressure, equal to $\tan^2(45^\circ - \phi'/2)$; and b =diameter of pile.

$$p_{sd} = K_a b\gamma' z(\tan^8 \beta - 1) + K_o b\gamma z \tan\phi' \tan^4 \beta \qquad 3.49$$

In Equations 3.48 and 3.49, Reese et al. (1974) used K_o of 0.4 for loose sand and 0.5 for dense sand, which were based on the suggestion by Terzaghi and Peck (1948). In a later study, Reese and Van Impe (2001) suggested the use of K_o = 0.4 for all sands. To consider the effect of stress history, K_o can be set as K_{on} (Equation 3.33) for the soil condition without scour but as K_{oc} (Equation 3.34) for the soil condition after scour instead of a constant value (i.e., 0.4).

Before scour, or after scour but ignoring the effect of the stress history for the remaining soils, the soil properties can be expressed as $\gamma' = \gamma_{int}'$; $\phi' = \phi_{int}'$; $K_{py} = (K_{py})_{int}$; and $K_o = K_{on}$. If the effects of stress history are considered for the remaining soils after scour, however, the soil properties become $\gamma = \gamma_{sc}'$; $\phi' = \phi_{sc}'$; $K_{py} = (K_{py})_{sc}$; and $K_o = K_{oc}$, which are representative of an OC soil. Therefore, the *p-y* curve of the pile in the remaining soils after scour can be modified accordingly to account for the effect of soil stress history. These *p-y* curves were used in the computer software *LPILE* for the deflections of piles under different lateral loads.

3.3.4 A case study

3.3.4.1 Site conditions

To investigate the effect of soil stress history on the *p-y* curve of a laterally loaded pile in the remaining soils, a field test on laterally loaded piles in sand conducted at Mustang Island, Texas (Cox et al. 1974) has been cited herein for the initial conditions of the soil. However, it should be noted that a scour depth of 3 m (approximately 5 *D*) was assumed in the current study for the analyses. The unmodified *p-y* curves of a single pile in sand at static loads were obtained using the *LPILE* software but modified *p-y* curves were generated in spreadsheet then input into *LPILE*. Four soil depths in the remaining soils (d_1 = 1.5 m, d_2 = 3 m, d_3 = 6 m, and d_4 = 12 m, measured from the mudline after scour) were used to compute the ultimate soil resistance as shown in Figure 3-11. The influence of soil-stress behavior on pile response for embedment lengths greater than 12 m from the mudline after scour was considered negligible.

Uniformly-graded fine sand was found at the Mustang Island site. Properties of the sand are provided in Table 3-9. The relative density was 70% for the sand at depths smaller than 3 m measured from the mudline before scour, and 90 % for sand at depths greater than 3 m. The critical friction angle was not determined in the referenced test. It was estimated to be 28.5^o in this study based on the fact that the soil ranged from a silty fine sand to fine sand and on the results of Standard Penetration Test at the test site reported by Cox et al. (1974). According to Bolton's research (Bolton 1986), critical friction angles for most natural sand deposits are rarely greater than 30° to 33°, and may be as low as 27° when the silt content is high. The peak friction angles before and after scour at different depths would be calculated using Equation 3.47 based on the critical friction angle of 28.5°, and p_o' equal to p_{int}' for a pre-scour condition and to p_{sc}' for a post-scour condition, as shown in Table 3-10. In the referenced test, the groundwater table was

maintained at 0.15 m above the mudline for the unscoured site conditions, and a lateral load was applied on the pile head at an elevation of 0.31 m above the mudline (Figure 3-11). The properties of the test single pile are summarized in Table 3-9.

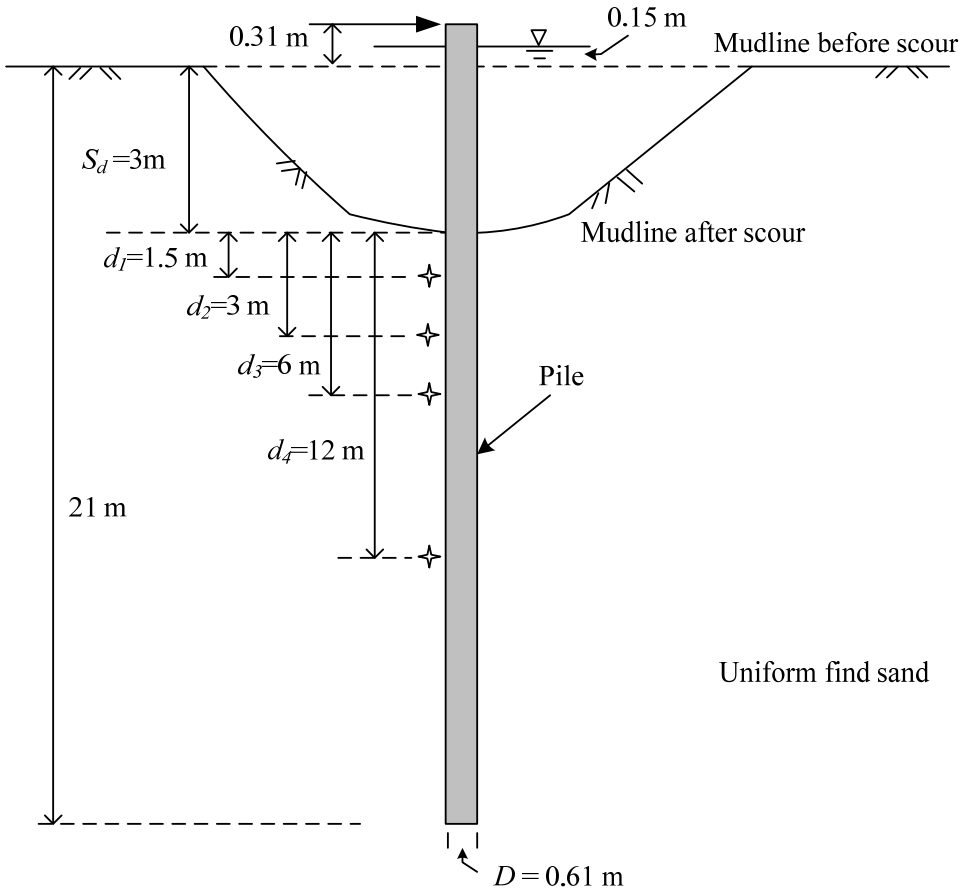

Figure 3-11. Illustration of a laterally loaded single pile in the field of the Mustang Island and the investigated scoured conditions

Table 3-9. Soil and pile properties in Mustang Island (Cox et al. 1974)

	Critical friction angle, ϕ_{cs}' (deg)	Effective unit weight, γ_{int}' (kN/m^3)	Relative density, D_{rint} (%)	Maximum void ratio, e_{max}	Minimum void ratio, e_{min}	Specific gravity, G_s
Soil	28.5	10.4	70 (depth ≤3m) 90 (depth ≥3m)	1.0	0.598	2.65
	Length, L(m)	**Outer diameter, D (m)**	**Thickness, t (m)**	**Moment of inertia, I_p (m^4)**	**Elastic modulus, E_p(kN/m^2)**	**Yielding strength (kN/m^2)**
Pile	21.3	0.61	0.0095	8.08×10^{-4}	2.02×10^{8}	2.41×10^{5}

Table 3-10. Calculated sand properties of the remaining soils

Soil depth measured from mudline before scour(m)	ΔD_r (%)	ϕ_{int}' (deg)	ϕ_{sc}' (deg)	γ_{sc}' (kN/m^3)	D_{rsc} (%)	OCR
0-3		38.8				
4.5	1.3	41.4	43.5	10.34	88.7	3.01
6	0.9	40.7	41.7	10.35	89.1	2.01
9	0.5	39.6	40.3	10.37	89.5	1.50
15	0.3	38.3	38.7	10.37	89.7	1.25

3.3.4.2 Properties of the remaining sand after scour

An unloading index C_{ur} = 0.02 was selected (Lancelot et al. 2006), which was higher than the C_{ur} ranges of typical sands (Kulhawy and Mayne 1990), to demonstrate the effect of C_{ur} on the change of relative density of the sand.

Tables 3-9 and 3-10 show that the relative density and unit weight of the soil at different depths decreased by 1.4% and 0.6%, respectively, at the depth of 4.5 m (measured from the pre-scour mudline) after scour. However, the friction angle and *OCR* values increased after scour, especially at elevations close to the post-scour mudline. For instance, the friction angle and *OCR* values increased 5% and 200%, respectively, at the depth of 4.5 m (measured from the pre-scour mudline). At greater depths, however, the *OCR* of the sand approached 1.0 so that no changed happened for the unit weight, friction angle, and relative density. In Equation 3.44 , ΔD_r would become zero when the *OCR* decreases to 1.0. These results indicated that scour had a limited depth influencing the properties of the remaining soils. If the depth at which *OCR* = 1.0 is defined as the critical depth, d_{cr}, the properties of the remaining soils below this depth remain unchanged after scour. According to Equations 3.41, 3.44, and 3.46, the critical depth depends primarily on the depth of scour.

3.3.4.3 Ultimate soil resitance and modified p-y curve

Equation 3.34 was used to calculate the coefficient of lateral earth pressure at rest for the remaining sand after scour at four depths. The calculated K_{oc} was then inputted into Equations 3.48 and 3.49 to compute the ultimate soil resistance at the corresponding depths. Once the ultimate soil resistance was calculated, the procedure proposed by Reese et al. (1974) was

followed to generate a modified *p-y* curve. The modified *p-y* curve was then exported into the *LPILE* software to determine the response of the pile under a lateral load.

The modified *p-y* curves for the remaining soils after scour at four depths are presented in Figure 3-12. A comparison of the *p-y* curves before scour, modified after scour, and unmodified after scour at two depths (d_1 = 1.5 m and d_2 = 3 m) are presented in Figure 3-13. The figure indicates that the scour resulting from removal of S_d = 3 m soils around the pile foundation reduced the lateral soil resistance near the ground surface by approximately 50% at y = 25 mm. The modified *p-y* curve shows approximately 100% higher soil resistance than the unmodified *p-y* curve at y = 25 mm. This result demonstrates that the approach of simply removing the soil layer and keeping the properties of the remaining soils unchanged underestimated the lateral soil resistance to the pile foundation in sand affected by scour.

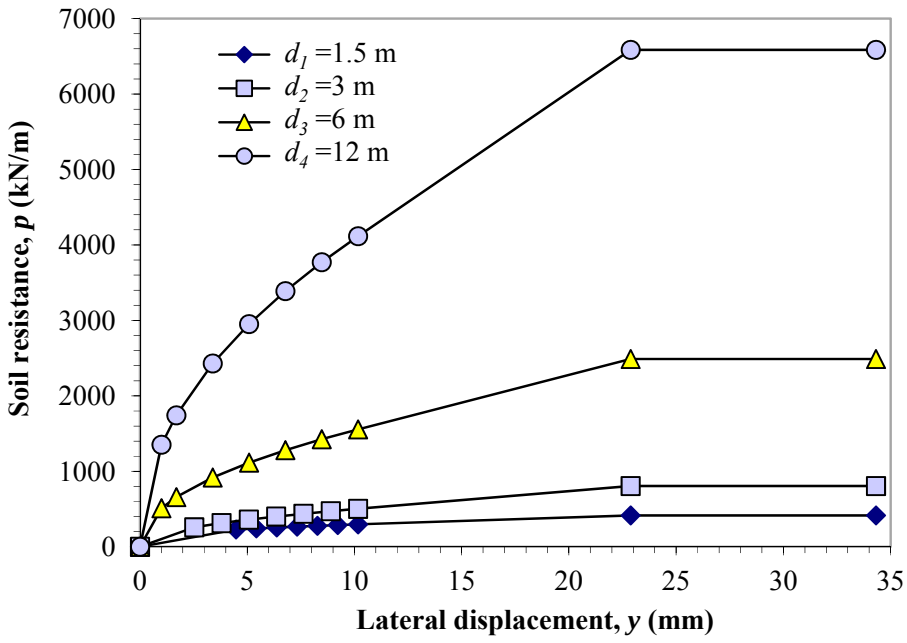

Figure 3-12. Modified *p-y* curves accounting for stress history of the remaining soils after scour, at varying scour depths

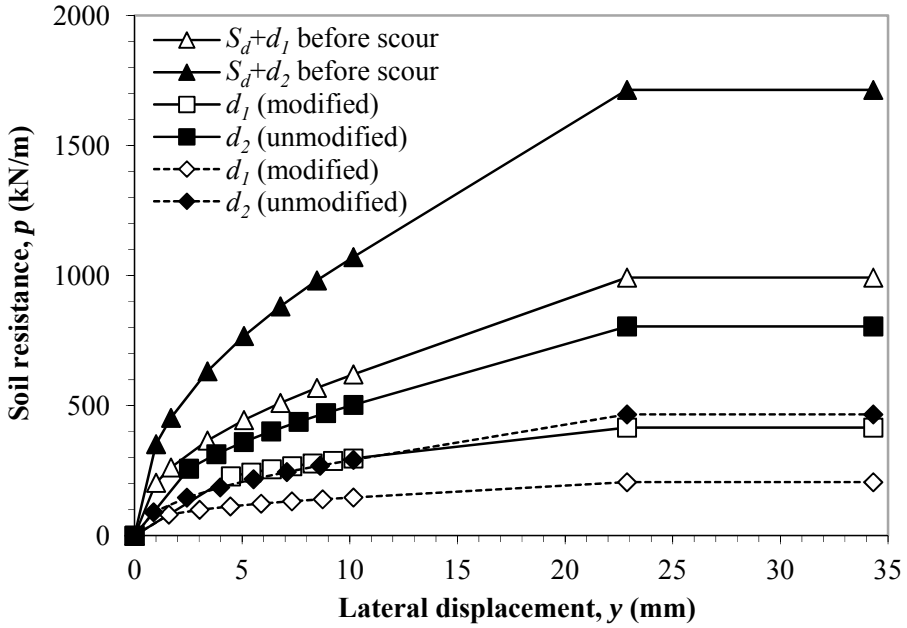

Figure 3-13. Comparison of *p-y* curves (d_1=1.5 m, d_2=3 m, and S_d=3 m)

3.3.4.4 Pile responses

The deflections of the pile at the ground line under various lateral loads were calculated using the computer software, *LPILE* and are presented in Figure 3-14. It is shown that the ground line deflection at the pre-scour mudline increased with an increase of the lateral load. The calculated deflections matched with the Mustang Island experimental data well for the pre-scour conditions. At the lateral load of 100 kN, the deflection of the pile, after scour, using the modified *p-y* curves for the remaining soils was approximately 5 times that at the pre-scour condition. After scour, the pile using the modified *p-y* curves had approximately 25% smaller lateral deflection than that using the unmodified *p-y* curves at the lateral load of 100 kN. The difference of the ground line deflections increased to 40 % at a higher lateral load of 150 kN. The results presented in Figure 3-14 further indicate that consideration of the effects of stress history of the remaining soils resulted in consideration of increased lateral support for the pile.

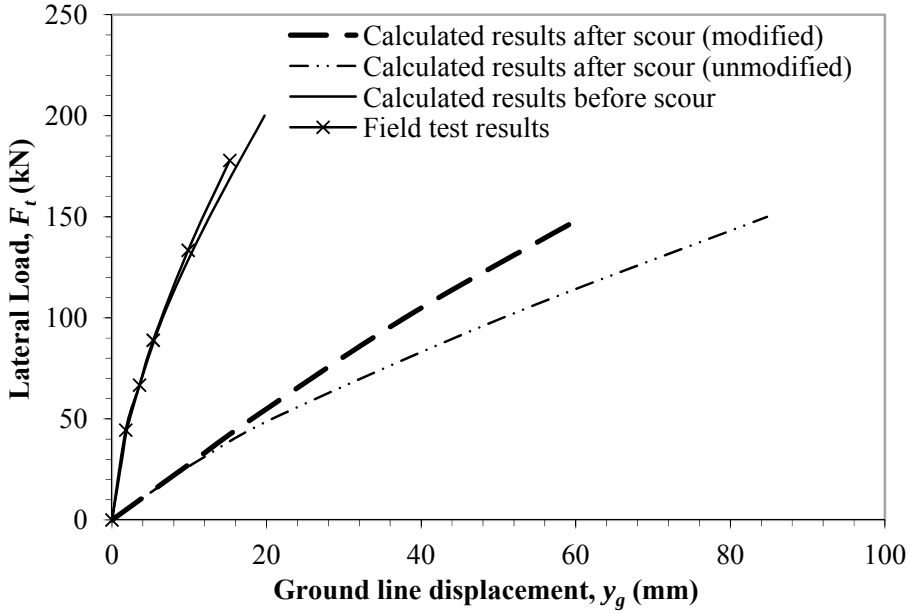

Figure 3-14. Ground line displacement under lateral loading

This study also investigated the mobilized soil reaction at different lateral loads. Figure 3-15 presents a comparison of the mobilized soil reaction of the remaining sand based on unmodified and modified *p-y* curves. This comparison shows that higher soil reaction was mobilized when the stress history of the remaining sand was considered. As a result, the mobilized depth for the soil reaction was lower when the stress history of the remaining sand was considered. Similarly, the pile responses, including bending moments and shear forces, were limited to a smaller depth of influence (presented in Figures 3-16 and 3-17) when the stress history of the remaining sand was considered. These results imply that during the design of laterally loaded piles under scour conditions, consideration of the stress history of the remaining sand may be effective in reducing the required pile length.

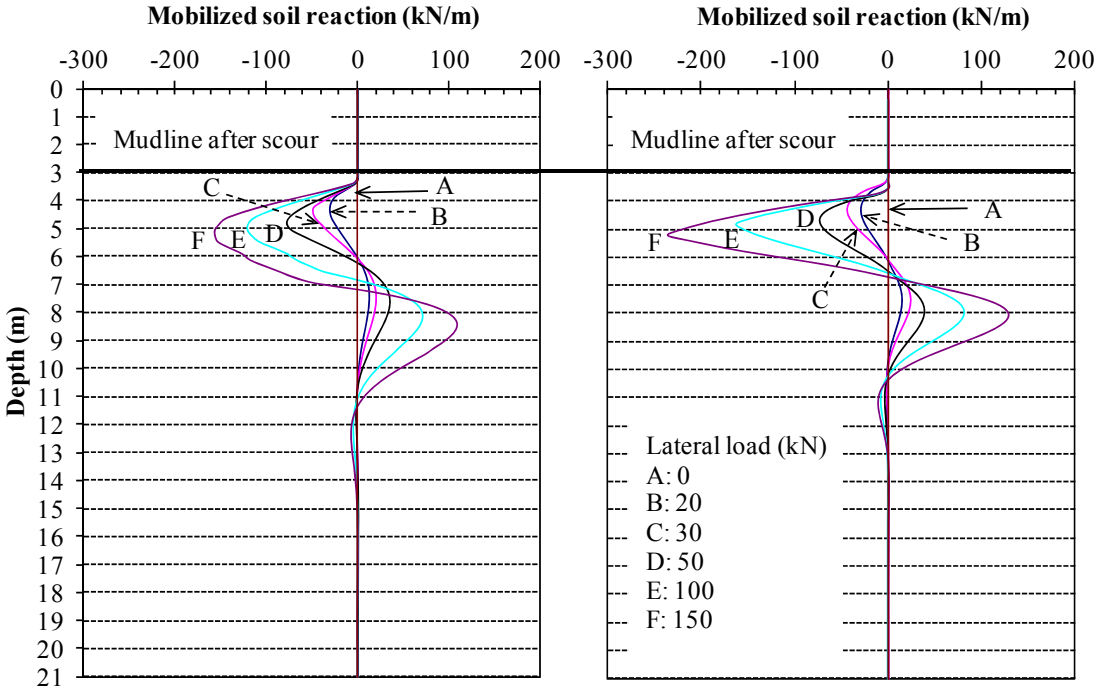

Figure 3-15. Mobilized soil reaction versus soil depth

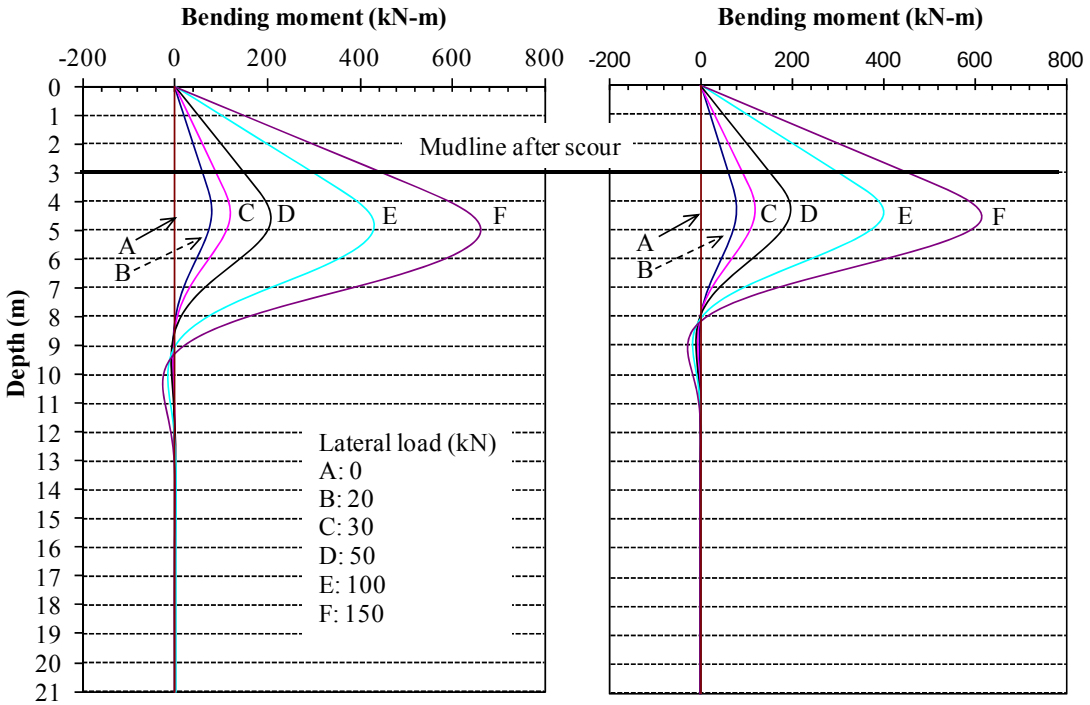

Figure 3-16. Bending moment versus soil depth

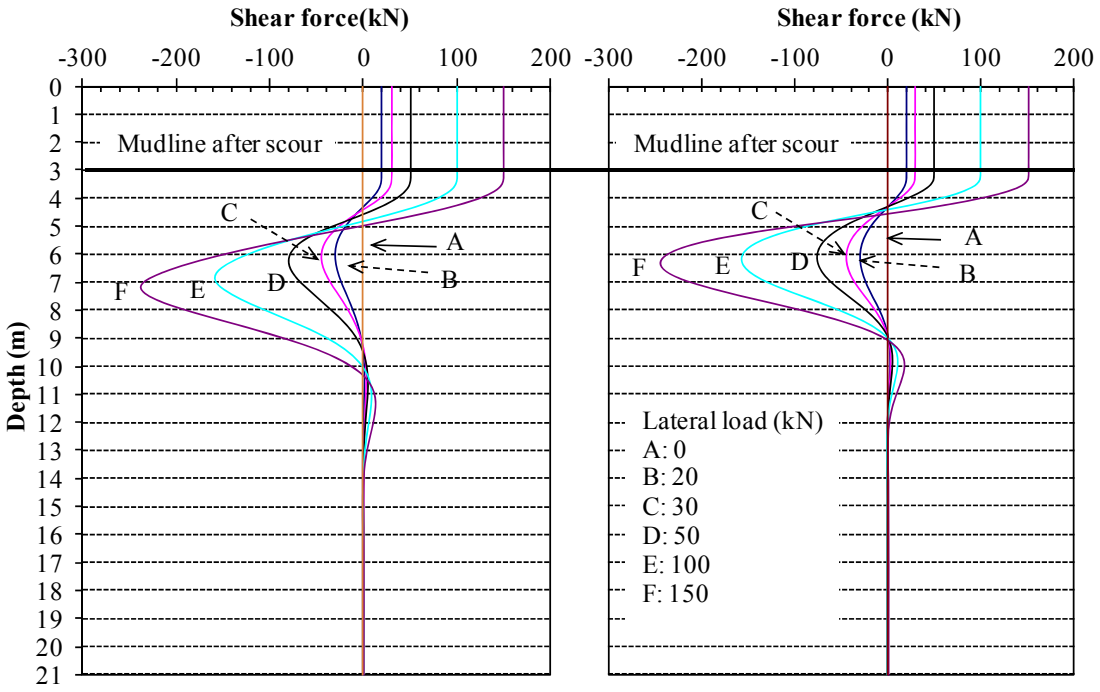

Figure 3-17. Shear forces versus soil depth

From the above analysis, scour tended to slightly reduce the relative density, and modulus of subgrade reaction of the remaining sand. However, scour was found to slightly increase the friction angle and considerably increase the overconsolidation ratio of the remaining sand, which has a greater effect on the behavior of laterally loaded piles than the other soil properties considered. Similar to that found in clay, change of effective unit weight by scour was insignificant and could be ignored too in the analysis.

Scour was found to significantly reduce the lateral resistance of sand, and thus tended to increase the lateral deflection of the pile head. However, consideration of the stress history of the remaining sand increased the lateral sand resistance and the mobilized soil reaction as compared with those same values found when ignoring the stress history. As a result, pile responses were limited to a smaller depth when the stress history of the remaining sand was considered. In other

words, consideration of stress history of the remaining sand may reduce the required pile length in terms of the design of laterally loaded piles.

3.4 Summary

Scour induced stress history of the remaining soils were considered in the analysis of laterally loaded piles. The conventional *p-y* curves were modified to consider the stress history effects. To accomplish the modifications, effective unit weight and undrained shear strength in clays were updated after scour; while in sands, soil parameters (i.e. effective unit weight and friction angle) were updated by the change of relative density, and change of lateral soil resistance to piles was associated with the stress history of sand. From the above analyses, conclusions can be drawn as follows:

(1) Ignoring stress history of soil led to a conservative analysis and design in sand but unconservative analysis and design in soft and stiff clays. However, stress history of clay due to scour had a limited effect on the response of laterally loaded pile. Stress history of sand, on the other hand, had a relatively significant effect on the response of laterally loaded piles.

(2) Change of effective unit weight due to scour was small and its effects on lateral behavior of piles were insignificant. Hence, scour induced change of effective unit weight could be ignored in the analysis of laterally loaded piles under scour conditions.

(3) Responses of laterally loaded piles due to stress history of clays resulted from the change of undrained shear strength although it was not remarkable; Responses of laterally loaded piles due to stress history of sand, in contrast, was attributed to the change of lateral soil stress which depended on overconsolidated ratios.

(4) As laterally loaded piles are more influenced by the soils at low depths, analysis using average values of soil parameters along the influence soil depth might not be conservative; instead, analysis using varying values of soil parameters along the soil depth was more reasonable and conservative.

CHAPTER 4

NUMERICAL STUDY OF LATERALLY LOADED PILES IN SOFT CLAY CONSIDERING SCOUR-HOLE DIMENSIONS

Scour, especially local scour, creates holes around bridge pile foundations. Scour-hole dimensions are often evaluated to estimate the quantities of backfill materials (e.g. riprap) needed for protecting agaist scour. However, during analysis and design of pile foundations under scour conditions, scour is typically treated as a total removal of soils to a presumed scour depth for simplificity without dealing with specific scour holes and their dimensions. In fact, ignoring dimensions of scour holes may result in a different solution from the reality because it ignores the effects of overburden stresses from the surrounding unscoured soils. The objective of this chapter is to evaluate effects of scour-hole dimensions on the behavior of laterally loaded piles. This evaluation was conducted using the 3D finite difference software *FLAC*^{3D}. The numerical model was first analyzed to assure reasonable inputs, and then calibrated with the full-scale test result available in the literature. Finally, a parametric study was conducted to investigate the effects of scour-hole dimensions (e.g. scour depth, scour width and scour-hole slope angle) on the behavior of laterally loaded piles. From the parametric analyses, numerical results were discussed in terms of lateral load versus pile-head displacement, lateral load capacity, *p*-*y* curves, and distributions of bending moment, shear force, and lateral displacement along the pile.

4.1 Preliminary Analysis of Finite Difference Model

A preliminary analysis of a finite difference model was performed for examining the efficiency and accuracy of the model by selecting proper input parameters and model geometry.

The model was first analyzed using the conditions in the full-scale test of a laterally loaded single pile in soft clay in Austin, Texas (Matlock 1970), which was detailed in Chapter 3.1.

4.1.1 Material parameters

The pile was modeled as an elastic medium which had Poisson's ratio of 0.3 and the pile dimensions were presented in Table 3-2. Besides, the test pile (pipe pile) was modeled as an equivalent solid pile having the same outside diameter of the test pile. As a result, the equivalent elastic modulus was used and calculated to be 6.15×10^7 kN/m^2 from the equation below,

$$E_{eq} = \frac{E_p I_p}{I_{eq}} = \frac{64 E_p I_p}{\pi D^2} \qquad 4.1$$

where E_{eq} = elastic modulus of the equivalent solid pile, kPa, and I_{eq} = inertia moment of the equivalent solid pile with the diameter equal to outside diameter of the test pipe pile, m^4.

The soft clay was simulated using the Mohr-Coulomb constitutive model. Its properties included total unit weight (γ = 20 kN/m^3), undrained shear strength (C_u = 32.3 kN/m^2), elastic modulus (E_s = 1600 kN/m^2), and Poisson's ratio (υ = 0.495).

4.1.2 Interface parameters

Interface between pile and soft clay was built to allow for their possible relative sliding or separation. The interface parameters included interface stiffnesses (normal and shear stiffness), cohesion, and friction angle as shown inTable 4-1. The cohesion at the interface, c, was obtained by multiplying undrained shear strength of the soil with adhesion factor, α, which was chosen

based on Tomlinson's study (Tomlinson 1957). Interface stiffnesses were determined based on a parametric study. It is evident from Figure 4-1 that when interface stiffnesses (k_n and k_s) were equal or greater than 5×10^5 kPa/m, the influence of the stiffnesses on the response of laterally loaded piles was neglectable. However, this value could not prevent the interpenetration because the calculated joint displacement was greater than 10% of the adjacent zone size (Itasca Consulting Group 2006). Hence, in this study, $k_n = k_s = 2\times10^7$ kPa/m was selected, which was sufficient to minimize the interpenetration between soil and pile elements. It should be pointed out that Figure 4-1 was plotted based on finite points of data, which were selected from the smoothed curve using the 3rd order polynomial regression in Figure 4-2. The oscillation of the lateral load versus pile-head displacement curve (F_t-y_t curve) was due to a large difference in the stiffness between the pile and soft clay. Thus, for the purpose of comparison and consistency, the smoothed F_t- y_t curves were used throughout this study.

Table 4-1. Interface parameters

Cohesion, c (kPa)	**Adhesion factor, α**	**Friction angle, ϕ' (°)**	**Normal stiffness, k_n (kPa/m)**	**Shear stiffness, k_s (kPa/m)**
32.3	0.9	0	5×10^4-2×10^7	5×10^4-2×10^7

4.1.3 Model analysis

Lateral loads were applied to the pile head under displacement controll. Displacement of the pile head was calculated from the velocity at the pile head in *FLAC*3D. To optimize numerical simulation, a servo-control function was facilitated by applying an average velocity of $5\text{x}10^{-8}$ m/s

and maintaining the unbalanced force within prescribed bounds. The velocity varied between $5x10^{-8}$ and $1x10^{-6}$ m/s depending on the unbalanced force between 10 and 50 N. The system was assumed to reach equilibrium when ratio of the out-of-balance force to the maximum unbalanced force was less or equal to $1x10^{-6}$. The applied lateral loads were calculated by summing up the horizontal soil resistance along the pile length. The soil resistance was composed of the horizontal component of shear and normal forces generated at the soil-pile interface. The *p-y* curves were generated by relating soil resistance per unit length of the pile to the lateral displacement of the pile at each depth monitored. The bending moment was determined by taking integral of normal stresses on the pile cross section multiplying the distance to neutral plane over the cross-sectional area while the shear force was obtained by taking integral of shear stresses over the cross-sectional area.

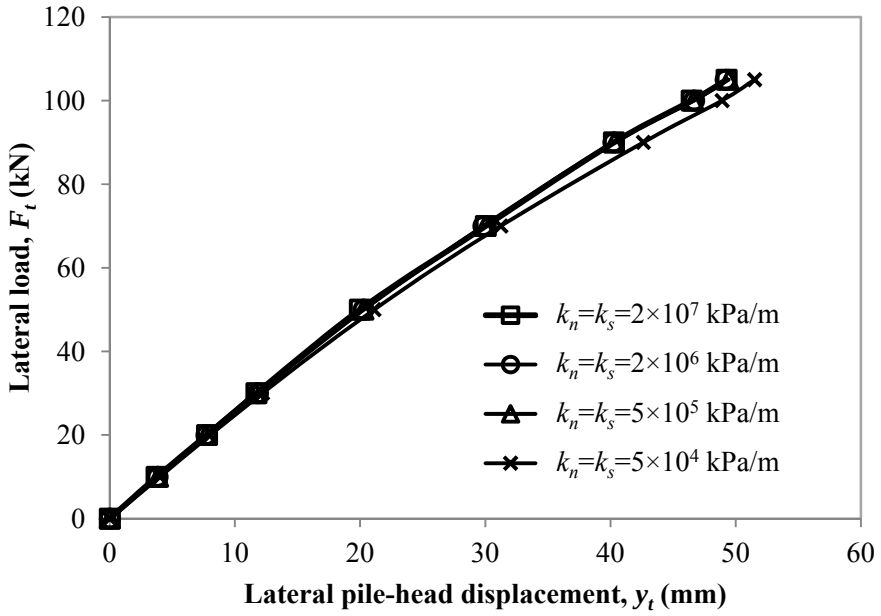

Figure 4-1. Effects of interface stiffnesses on the response of the laterally loaded pile

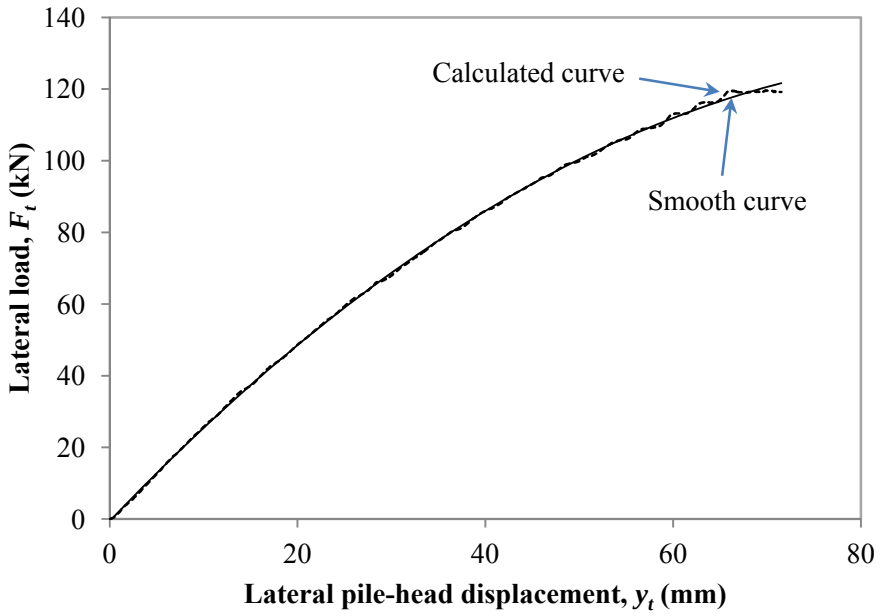

Figure 4-2. Calculated and smooth curves for the response of the laterally loaded pile

Only half of the cylindrical model was built to take advantage of its geometric symmetry, as illustrated in Figure 4-3. The model was fixed at the bottom against movement in *z* direction, fixed along its circumference in the horizontal directions (*x* and *y*), and on the symmetric plane in *y* direction.

The mesh density of the model decreased horizontally with the increase of the distance from the center of the pile to the edge of the model and decreased vertically with an increase of the distance from the mudline to the bottom of the model as presented in Figure 4-3. In the radial direction, the soil medium consists of 18 columns of elements with a minimum element size of 0.18 m and aspect ratio 1:1.15, while the pile was composed of six columns of elements with an equal element size. A total of 12 elements were arranged along the circumference of both the soil and the pile. In the vertical direction, the soil and pile were divided into three major layers: the first large layer consisted of 56 layers of elements with thickness of 0.107 m from ground surface

to 6 m deep; the second layer consisted of nine layers of elements with a minimum thickness of 0.107 m and aspect ratio 1:1.15 from 6 to 9 m deep; and the third layer consisted of a number of layers of 1 m thick elements from 9 m deep to the bottom of the model.

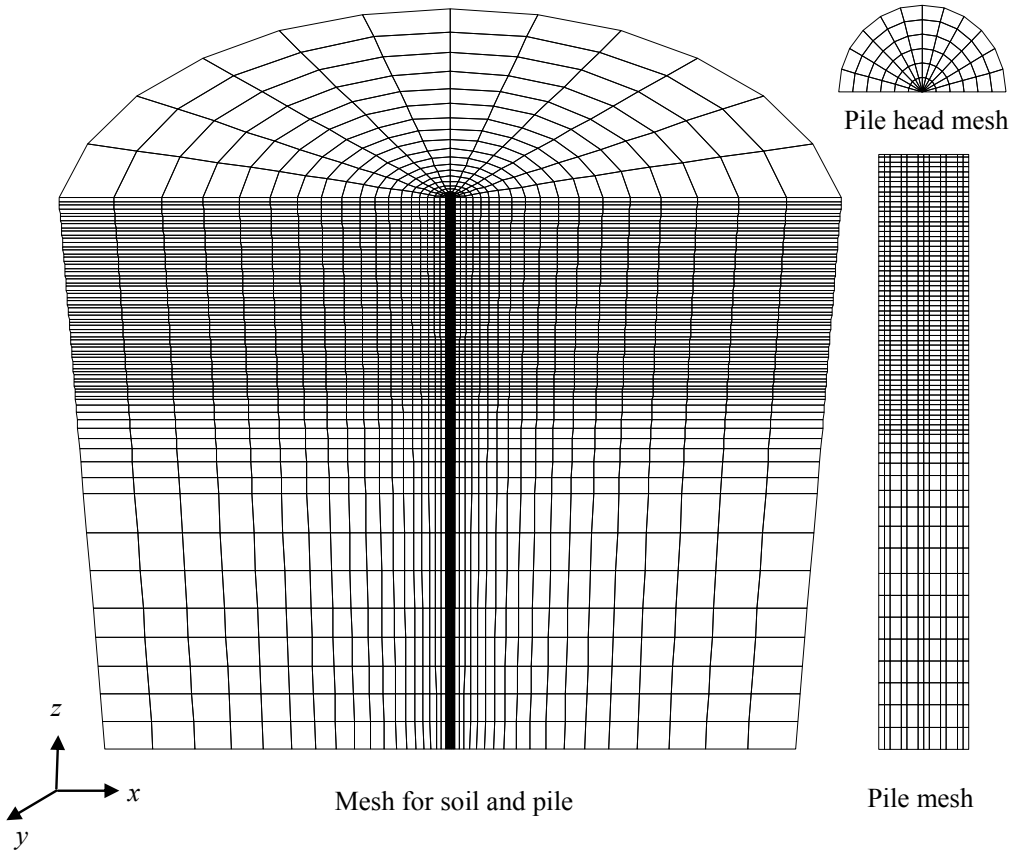

Figure 4-3. Model geometry and discretization

The effects of horizontal and vertical boundaries on the response of laterally loaded piles were evaluated, and the result in terms of lateral load versus pile-head displacement was compared in Figures 4-4 and 4-5. It is clear from the figures that the horizontal boundary at the distance of 40 *D* (*D* is the diameter of the pile) from the center of the pile and vertical boundary at

the distance of 0.4 L (L is the length of the pile) below the tip of the pile had minimal effect on the numerical result.

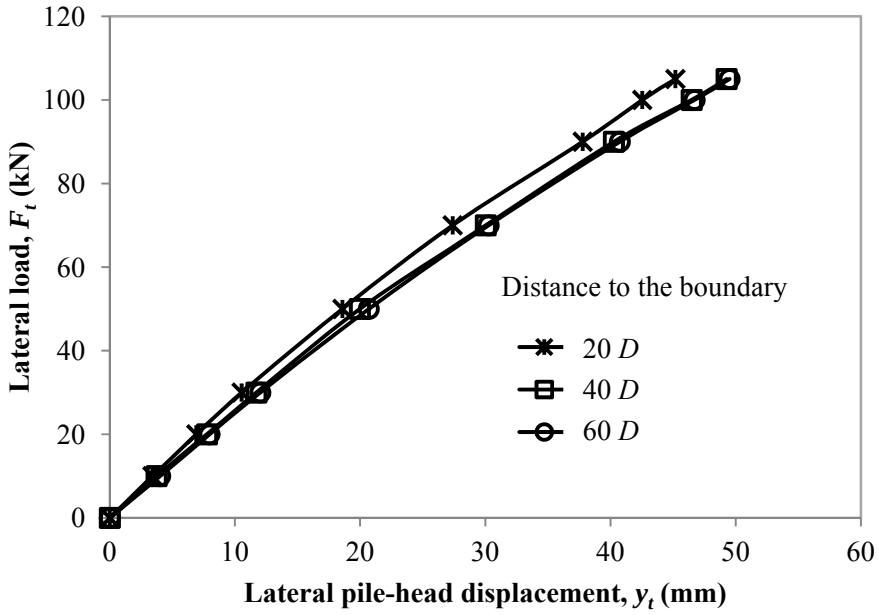

Figure 4-4. Effects of horizontal boundary on the response of the laterally loaded pile

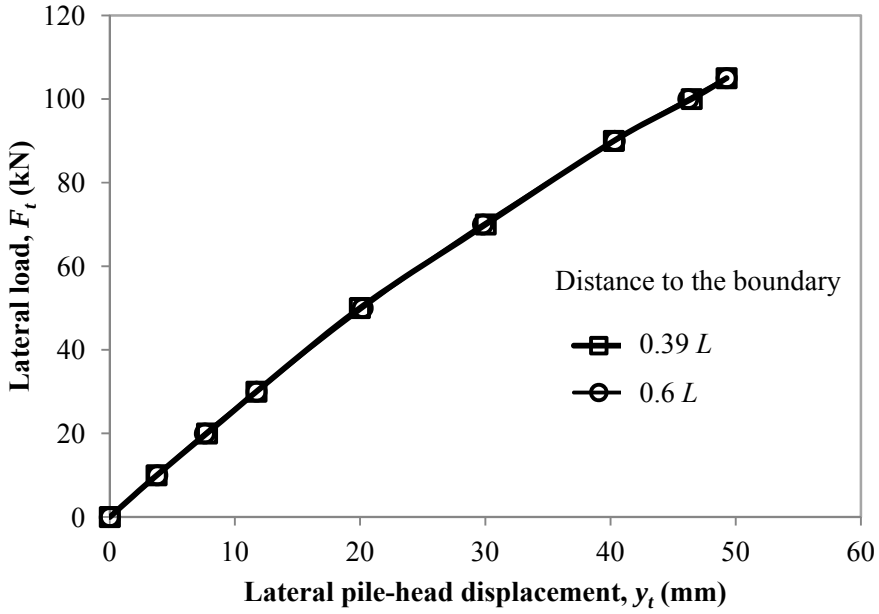

Figure 4-5. Effects of vertical boundary on the response of the laterally loaded pile

4.2 Model Calibration

Due to anisotropy and secondary structures of clays, the measured soil strength needs to be corrected before used in the analysis and design (Kulhawy and Mayne 1990). Based on the corrected soil strength, the 3D finite difference model in the foregoing preliminary analysis was further calibrated with the measured results from the full-scale test in Lake Austin, Texas (Matlock 1970). Figure 4-6 presents the F_t-y_t curves calculated by the 3D Finite Difference Analysis (FDA) and from Matlock's *p-y* method (Matlock 1970), which were compared with the measured ones from the field test. Figure 4-6 includes three cases of FDA: FDA_1, FDA_2, and FDA_3 which had different undrained shear strength (C_u), mesh densities, and soil constitutive models, as summarized in Table 4-2. The FDA_1 and FDA_2 had the C_u reduced by 72% from the original measured value, 32.3 kPa, which was within the range of the reduction documented

by Bjerrum (1972). The C_u in FDA_3 used the uncorrected value (the measured, 32.3 kPa). The elastic modulus of the soils was chosen to be $70C_u$ (FDA_1 and FDA_2) and $50C_u$ (FDA_3), which was within the range of 15 to $95C_u$, as reported by Poulos (1971). The FDA_2 case had 2520 and 6516 elements for modeling pile and soil respectively and used the Mohr-Coulomb (M-C) constitutive model for the inner soil zone (within a distance of 20 *D* from the center) but the elastic model to the outer zone (in the range of 20-40 *D* from the center), as shown in Figure 4-7. In contrast, FDA_1 and FDA_3 cases discretized the pile and the soil into 2,520 and 17,316 elements respectively and used the Mohr-Coulomb model all over the soil zone.

Table 4-2. Cases for finite difference analyses

Case	Elastic modulus of soil, E_s	Undrained shear strength of soil, C_u (kPa)	Number of elements	Constitutive model
FDA_1	$70C_u$	23	19,836	M-C
FDA_2	$70C_u$	23	9,036	Elastic and M-C
FDA_3	$50C_u$	32.3	19,836	M-C

The numerical analyses showed that the FDA_2 case significantly improved the computation efficiency as compared with the FDA_1 and FDA_3. For example, in a 64-bit workstation computer with eight Intel 2.53 GHz processors and 12.0 GB RAM, FDA_2 and FDA_3 required 4.8 hours to complete the analysis but FDA_1 and FDA_3 case took 7.5 and 6.1 hours that were 56% and 27% more than the FDA_2 case did. Despite the substantially short computation time, the FDA_2 case produced almost the same result as FDA_1 case and was also compared well with the measured (Figure 4-6). FDA_3 case led to smaller lateral pile-head

displacement at a high load level than the field test, indicating the undrained shear strength (C_u = 32.3 kN/m^2) used in the analysis was too high. Figure 4-6 also shows that at the low loading level, Matlock's *p-y* method resulted in much smaller lateral pile-head displacements than the field test. This is due to the characteristics of the Matlock's *p-y* curve that has relatively high soil stiffness.

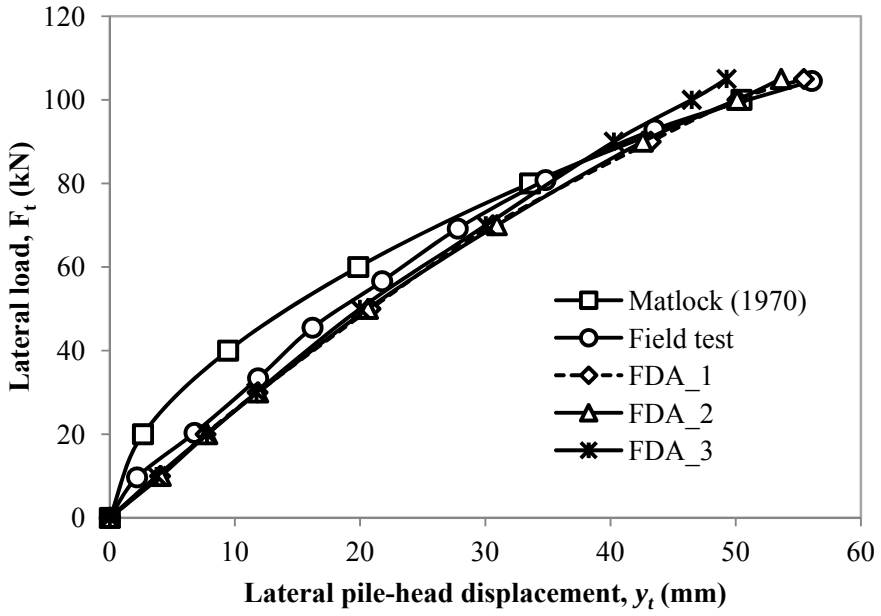

Figure 4-6. Comparison of calculated and measured lateral pile-head displacement

Due to the favorable results of the FDA_2 case, the computed maximum bending moment, distribution of bending moment, shear force, and lateral displacement of the pile in the FDA_2 case were compared with those from *LPILE* based on Matlock's *p-y* method and the field test. Hereafter, the FDA_2 case is referred to *FLAC*^{3D}. The maximum bending moments of the pile at different loading levels are plotted in Figure 4-8. The maximum bending moment calculated by *FLAC*^{3D} was nearly 20% less than the measured. Coincidentally, Dodds (2005) also found both the lateral displacement at pile head and bending moment of the pile could not

simultaneously agree the results measured in the field test, and in most of cases the computed bending moments were smaller than the measured. However, this minor inconsistence of bending moment with the measured would not influence the comparison of laterally loaded pile responses under scour conditions by considering and ignoring the scour-hole dimensions because each analysis inherently involved similar extent of inconsistence which can be canceled out during the comparison.

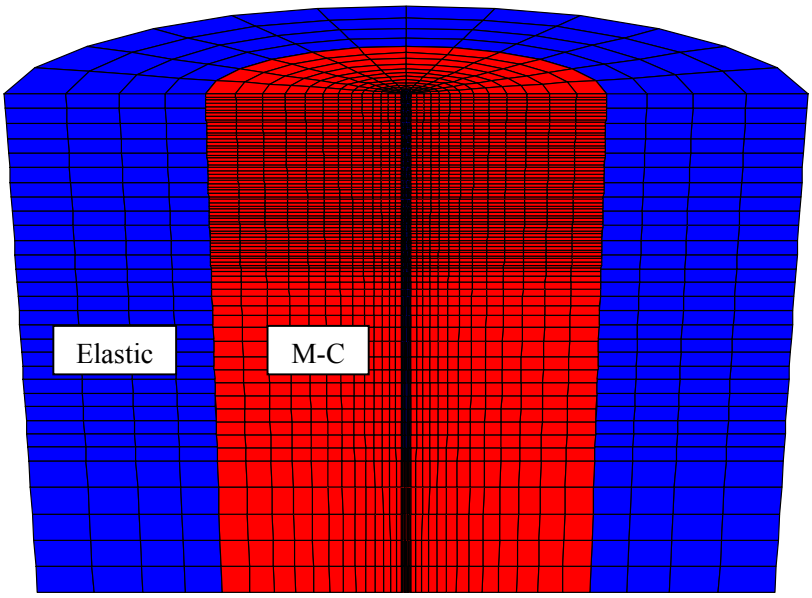

Figure 4-7. The soil model with two constitutive model zones

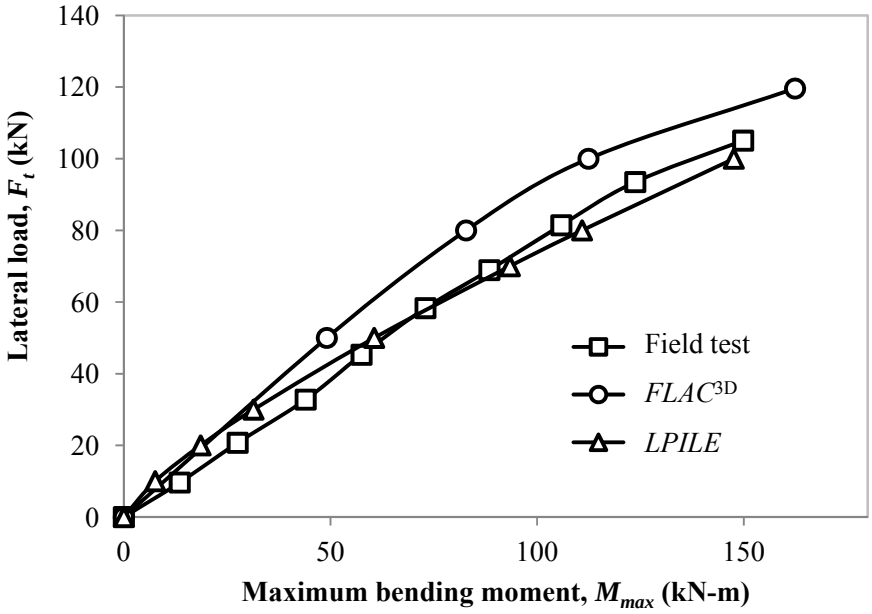

Figure 4-8. Comparison of the measured and calculated maximum bending moment of the pile

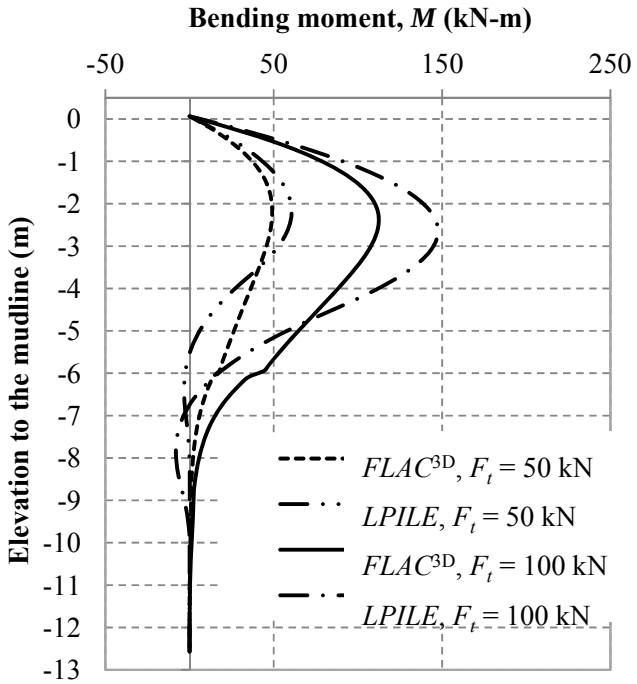

Figure 4-9. Comparison of calculated bending moment of the pile by *FLAC*^{3D} and *LPILE*

The calculated *p-y* curves by *FLAC*^{3D} at depths (e.g. 0.3, 1, 1.3, and 2.0 *D*, *D* is the diameter of the pile) from the mudline were compared with the curves from *LPILE* in Figure 4-10. The *p-y* curves from *FLAC*^{3D} appeared somewhat discontinuity which might be due to the considerable difference of stiffness between the soft clay and the pile. The curves were also approximately smoothed in the later scour analysis. The comparison in Figure 4-10 indicates that the *p-y* curves from *LPILE* had a higher initial stiffness response but mostly had lower ultimate soil resistance than those from *FLAC*^{3D}.

Figure 4-11 shows *FLAC*^{3D} and *LPILE* obtained similar distributions of shear forces at shallow depths but much different distributions at greater depths. The difference of the lateral pile displacement (Figure 4-12) from *FLAC*^{3D} and *LPILE* decreased when the lateral load increased from 50 to 100 kN. Since at a high lateral load, the soils around the pile mobilized their strength at the shallow depth, the lateral pile displacement was mainly controlled by the shear strength of the soils. In contrast, at a low load or at great soil depths, the lateral pile displacement was primarily influenced by soil stiffness. As a result, the *p-y* curves from *LPILE* had stiff response at small loads due to the high soil stiffness. This result is consistent to that found in Figure 4-6.

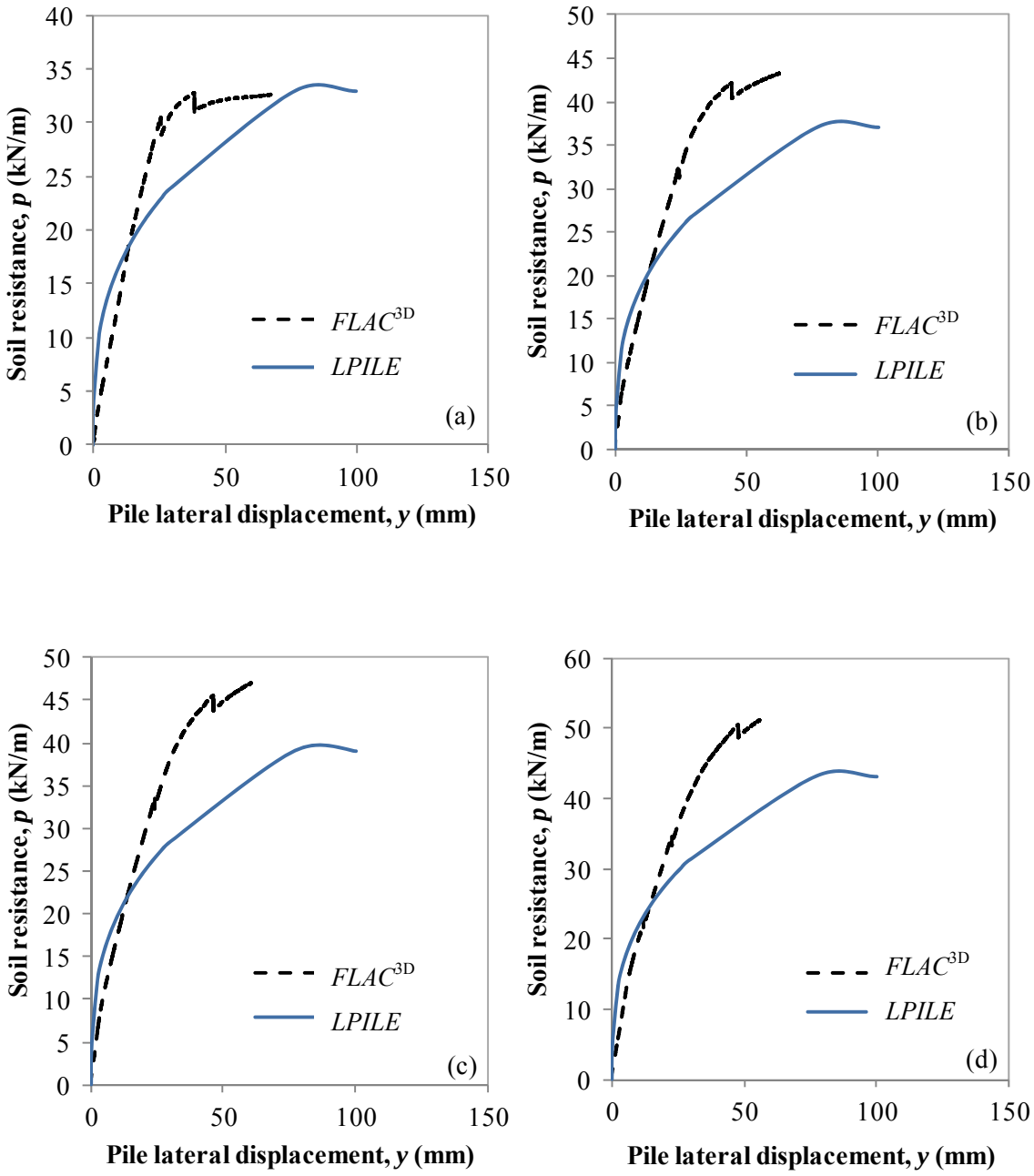

Figure 4-10. The *p-y* curves calculated by *FLAC*^{3D} and *LPILE* at depths of: (a) 0.3 *D*; (b) 1 *D*; (c) 1.3 *D*; (d) 2 *D*

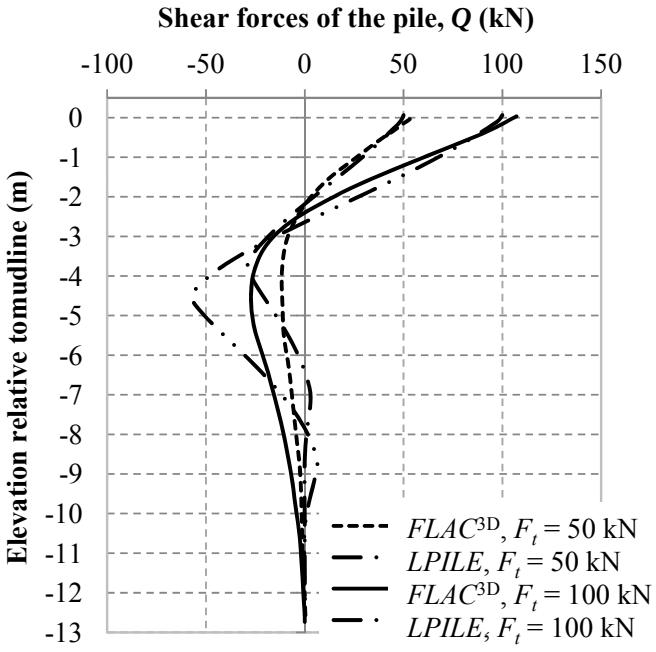

Figure 4-11. Comparison of shear force distributions of the pile calculated by *FLAC*^{3D} and *LPILE*

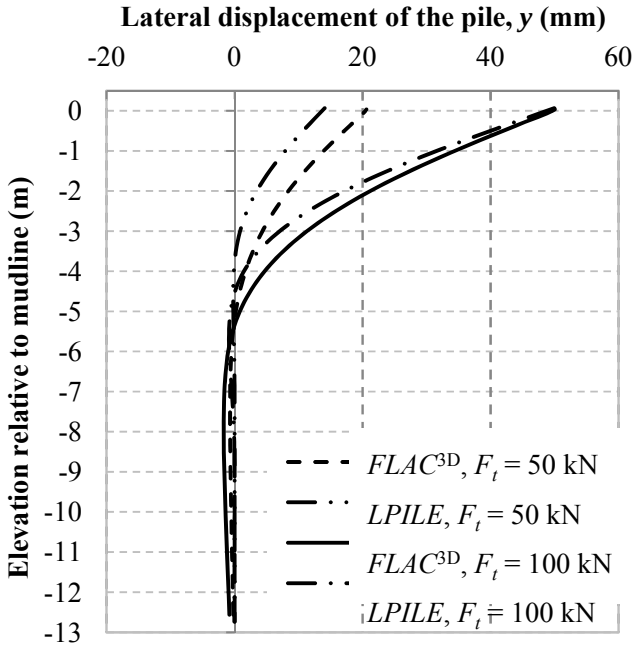

Figure 4-12. Comparison of the lateral displacement profiles of the pile calculated by *FLAC*^{3D} and *LPILE*

4.3 Effects of Scour-Hole Dimensions

Based on the forgoing analyses, the effects of scour-hole dimensions on laterally loaded pile behavior are presented in this section. This investigation was based on the model configuration as described in FDA_2 and the input parameters of soil and interface as presented in Tables 4-3 and 4-4. As illustrated previously, the pile was modeled as an equivalent solid pile with an equivalent elastic modulus of 6.15×10^7 kN/m^2, Poisson's ratio of 0.3, and the pile dimensions tabulated in Table 3-2.

Table 4-3. Soil parameters

United weight, γ (kN/m^3)	Undrained shear strength, C_u (kPa)	Friction angle, ϕ (^{o})	Poisson's ratio, υ	Elastic modulus, E_s (MPa)
20	23	0	0.495	1.6

Table 4-4. Interface parameters

Cohesion, c (kPa)	Adhesion factor, α	Friction angle, ϕ_i' (^{o})	Normal stiffness, k_n (kPa/m)	Shear stiffness, k_s (kPa/m)
23	1	0	2×10^7	2×10^7

During the modeling, the system was first brought to equilibrium before scour took place; next, the scour hole was excavated, and then the system was brought to equilibrium again; finally, the velocity control was used to apply a lateral load to the pile head

To investigate the effects of scour-hole dimensions on the behavior of the laterally loaded pile, various scour depths, widths, and scour-hole slope angles were considered and the calculated results were interpreted in terms of pile-head response (F_t-y_t curves), the p-y curves, and distributions of bending moment, shear forces, and lateral displacement. For simplicity, only circular geometry of scour hole was considered, but top and bottom widths of the scour hole varied, as presented in Figure 4-13. The pre-scour and post-scour mudline represented the ground line before and after scour respectively as illustrated in the figure. The scour width, S_w, is referred to the width measured from the pile periphery to the scour-hole slope toe. The scour depth, S_d, is the distance between pre-scour and post-scour mudline, and scour-hole slope angle, θ (called slope angle for short herein), was defined as the angle formed between the scour-hole slope and the post-scour mudline. The soil depth, d, representing the elevation with respect to the post-scour mudline is used for the comparison of the p-y curves.

4.3.1 Effects of scour depth

To investigate the effects of scour depth on the lateral pile behavior, four scour depths (i.e. 1, 3, 6, and 8D) were selected in the analysis. The slope angle remained constant at 40˚. In this series of analyses, the scour width was either zero or infinite; the infinite scour width means a total removal of the scoured soil layer and thus scour-hole dimensions are ignored. The computation results are presented in terms of lateral pile-head displacement, allowable lateral load, p-y curves, and profiles of bending moment, shear force, and lateral displacement along the pile.

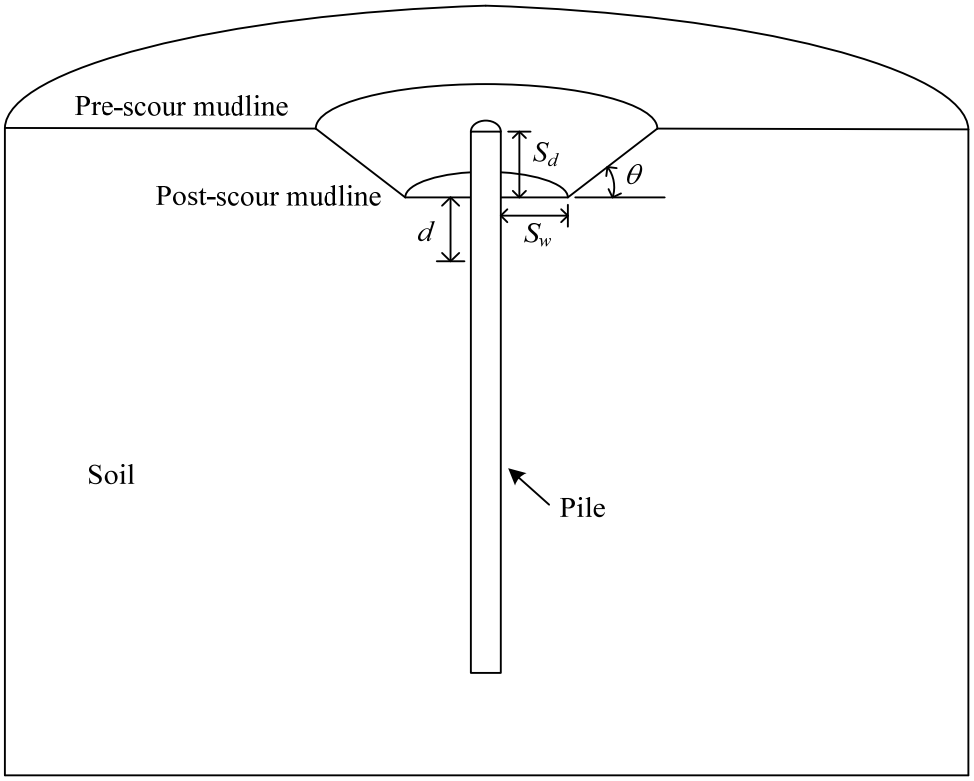

Figure 4-13. Measure of scour-hole dimensions in the *FLAC*^{3D} model

4.3.1.1 Lateral pile-head displacement

Lateral pile-head displacement at different scour depths (from 0 to 8*D*) and two scour widths (i.e. zero and infinite) was computed at different loading levels, such as 20, 30, and 50 kN. The numerical results are summarized in Figures 4-14 and 4-15 and show that as the scour depth increased, the lateral pile-head displacement increased nonlinearly; the nonlinearity became significant with an increase of the applied lateral load at the pile head. At F_t = 30 kN, when the scour depth increased from 0 to 6 *D*, the lateral displacement at the pile head increased by

approximately 2.6 and 3.2 times for S_w = 0 and S_w = ∞ respectively; However, At F_t = 50 kN, the increase of the lateral displacement became 2.8 and 3.5 times respectively.

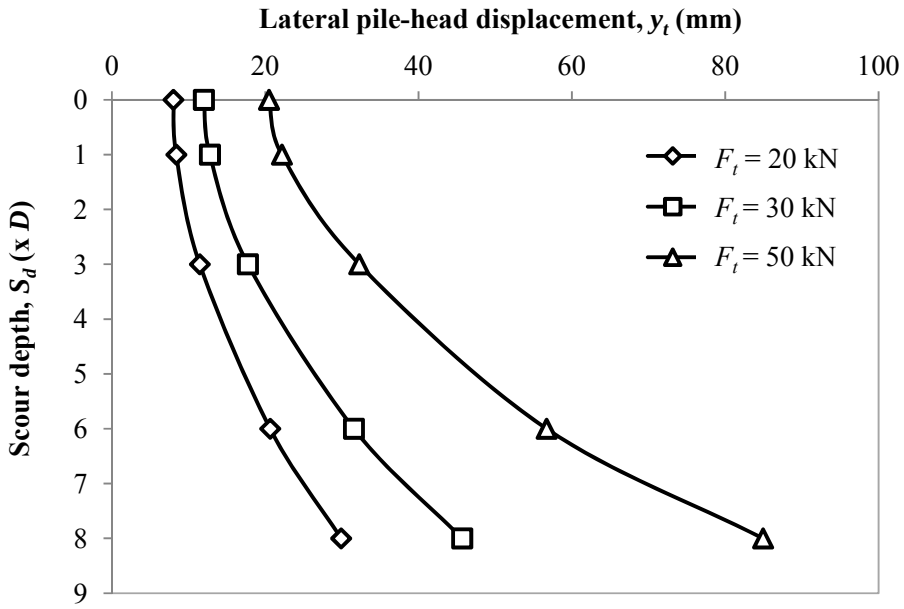

Figure 4-14. Lateral pile-head displacement versus scour depths (S_w =0)

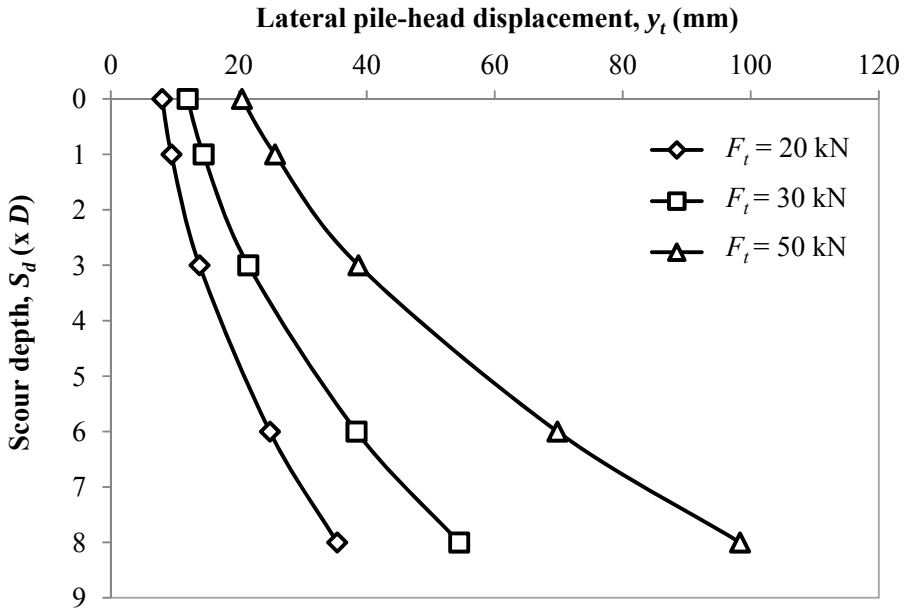

Figure 4-15. Lateral pile-head displacement versus scour depths (S_w =∞)

The lateral load versus lateral displacements at the pile head (i.e., the F_t-y_t curves) at different scour depths, such as S_d = 0, 1, 3, 6, and 8D, were investigated and are summarized in Figures 4-16 and 4-17. The numerical results show that increasing the scour depth reduced the lateral load at the same lateral displacement of the pile head. For example, at the lateral pile-head displacement of 40 mm, when scour depth increased from 0 to 6 D, the applied lateral load needed at the pile head decreased by 2.2 times for S_w = 0 and 3.9 times for S_w = ∞. The numerical results from also suggest that the degree of the nonlinearity of F_t-y_t curve decreased with the increased scour depth, especially for S_w = ∞. This phenomenon is because at a larger scour depth, the pile-head behavior was influenced more by the elastic pile behavior than by elastic-plastic soil behavior, indicating sufficiently strong pile above the post-scour mudline was necessarily used to transfer the lateral load at the pile top to the lower surrounding soil.

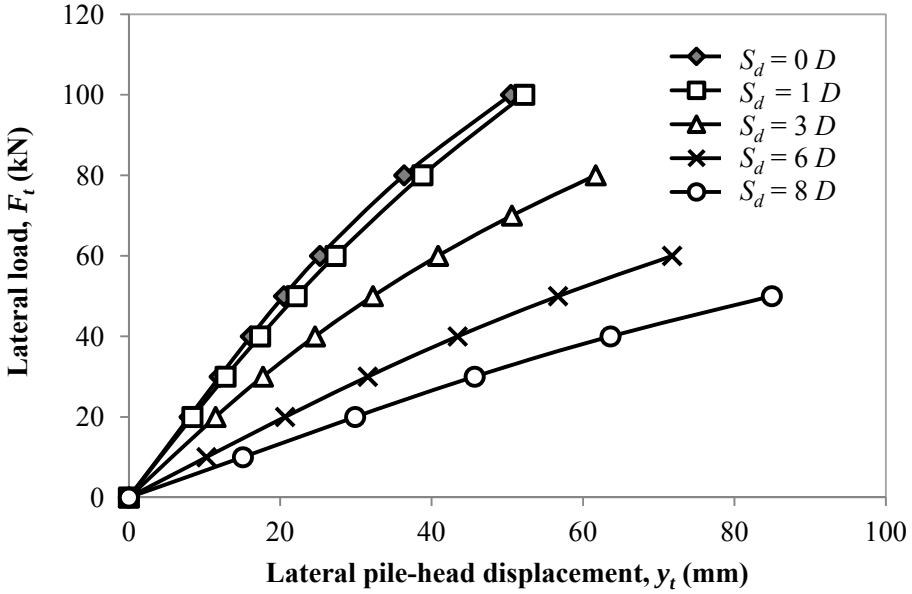

Figure 4-16. Lateral loads versus lateral pile-head displacement (S_w =0)

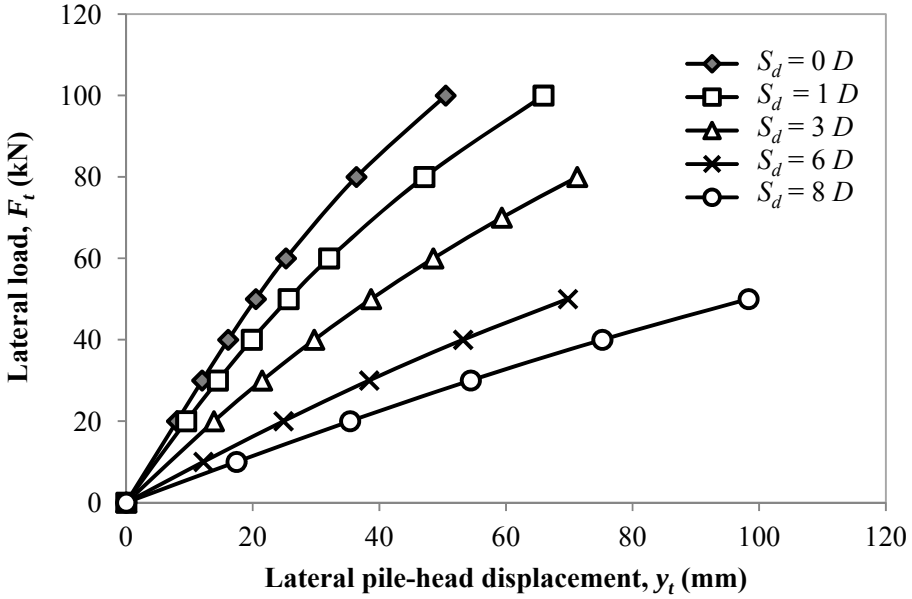

Figure 4-17. Lateral loads versus lateral pile-head displacement (S_w = ∞)

4.3.1.2 Allowable lateral load capacity

The allowable lateral load, F_{tmax}, is referred to the applied lateral load causing the pile to reach the allowable bending moment. The allowable bending moment was calculated to be 116 kN-m by taking a factor of safety of 2 from the yielding bending moment, M_y (Table 3-2). From this perspective of view, the allowable lateral load also represented the allowable lateral load capacity of the pile. The corresponding lateral displacement at the pile head, y_{tmax}, is called allowable lateral pile-head displacement. Figure 4-18 presents the F_{tmax} values calculated at different scour depths, which decreased with an increased of the scour depth. For example, the F_{tmax} value dropped approximately by 50% when the scour depth increased from 0 to 6 D. The figure also indicates the scour width had a limited effect on the allowable bending moment. Figure 4-19 provides the y_{tmax} values at different scour depths, which ranged from 16% to 20% D for $S_w = 0$ and 16% to 23% D for $S_w = \infty$. Furthermore, the figure also shows scour significantly increased the allowable lateral pile-head displacement, and the effects of the scour width (i.e. $S_w = 0$ and $S_w = \infty$) on the displacement was more evident at a greater scour depth.

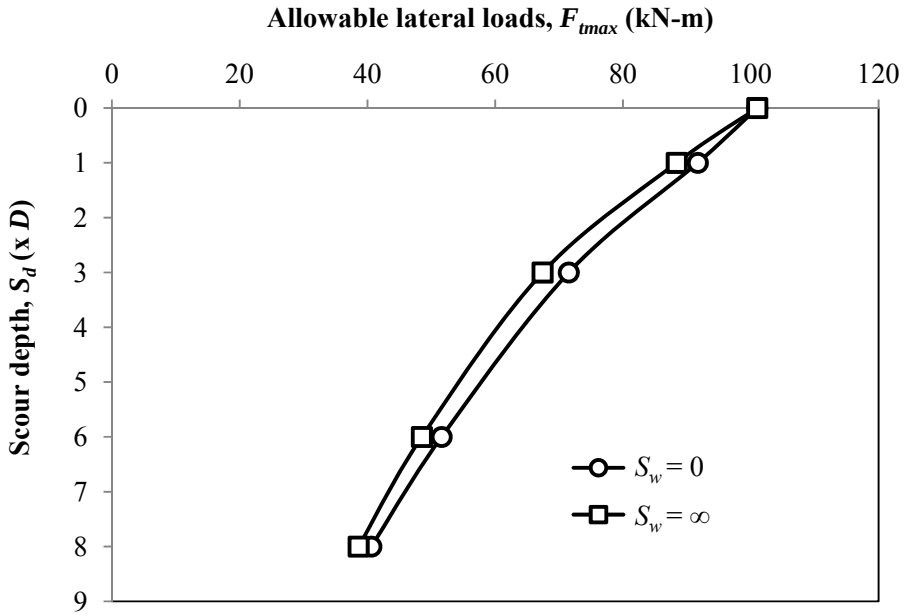

Figure 4-18. Allowable lateral loads on the pile at various scour depths

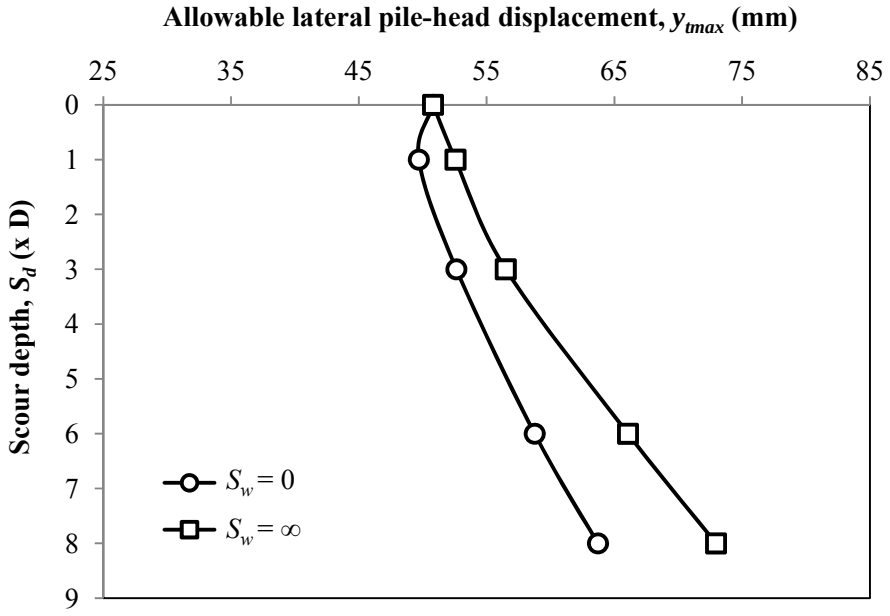

Figure 4-19. Allowable lateral pile-head displacement at various scour depths

4.3.1.3 The p-y curves

A series of *p-y* curves at two soil depths (i.e. d = 0.3 D and d = 1 D) below post-scour mudlines were computed at the zero scour width and various scour depths. The computed results were smoothened using the third order polynomial regression as presented in Figures 4-20 and 4-21. The analysis with a shallower soil depth (d = 0.3 D) captured a complete *p-y* curve as compared with a relatively deeper soil depth (d = 1 D) because the lateral displacement mobilized the soil resistance more at the shallower depth than that at the deeper location. The soil-pile stiffness defined by the initial linear slope of the *p-y* curve decreased substantially when the scour depth increased from 0 to 3 D, but remained almost unchanged from 3 to 8 D. The ultimate soil resistance decreased significantly when the scour depth increased from 0 to 6 D, and then remained almost unchanged after the scour depth exceeded 6 D.

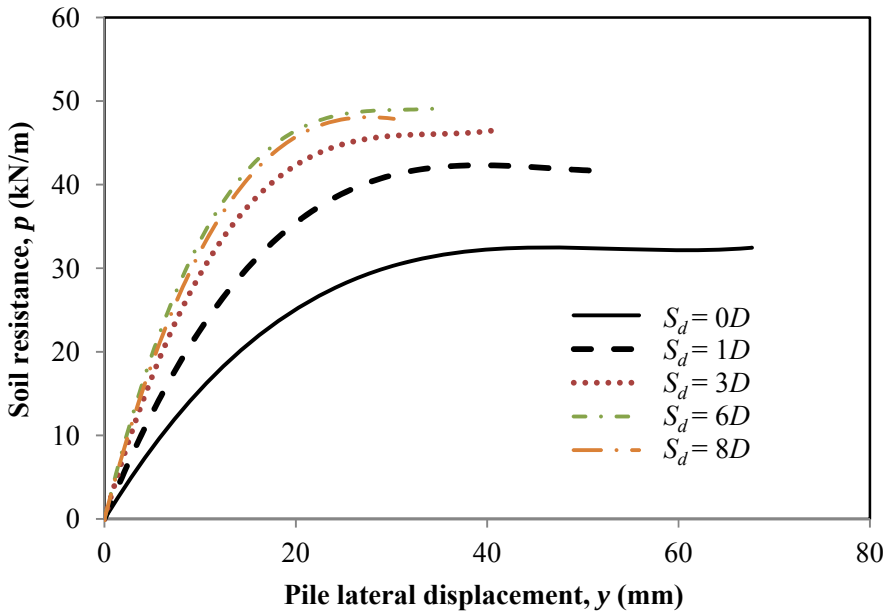

Figure 4-20. The *p-y* curves at the soil depth, d = 0.3 D and S_w = 0

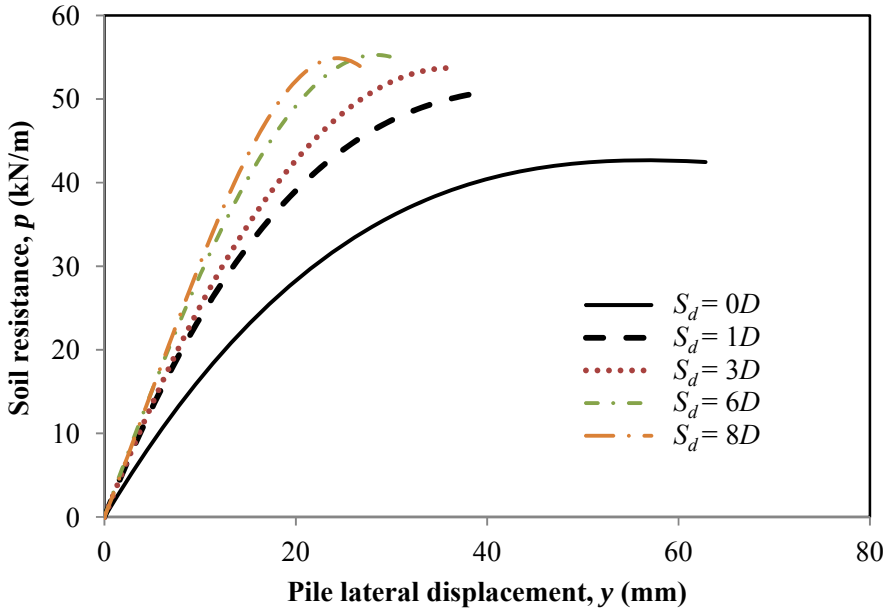

Figure 4-21. The *p-y* curves at the soil depth, d = 1 D and S_w = 0

4.3.1.4 Profiles of bending moment, shear force, and lateral displacement along the pile

The profiles of bending moment, shear force, and lateral displacement along the pile are presented in Figures 4-22 and 4-23, which show flexural behavior. From the pre-scour mudline, locations of the maximum bending moment and the negative maximum shear force moved downward with an increase of the scour depth. However, from post-scour mudline, the maximum bending moment shifted its location upward with an increase of the scour depth. For example, when the scour depth increased from 0 to 6 D, the elevation relative to the post-scour mudline rapidly decreased from 6.5 to 3.2 D, which can be calculated by subtracting the distance of the maximum bending moment to pre-scour mudline by the scour depth.

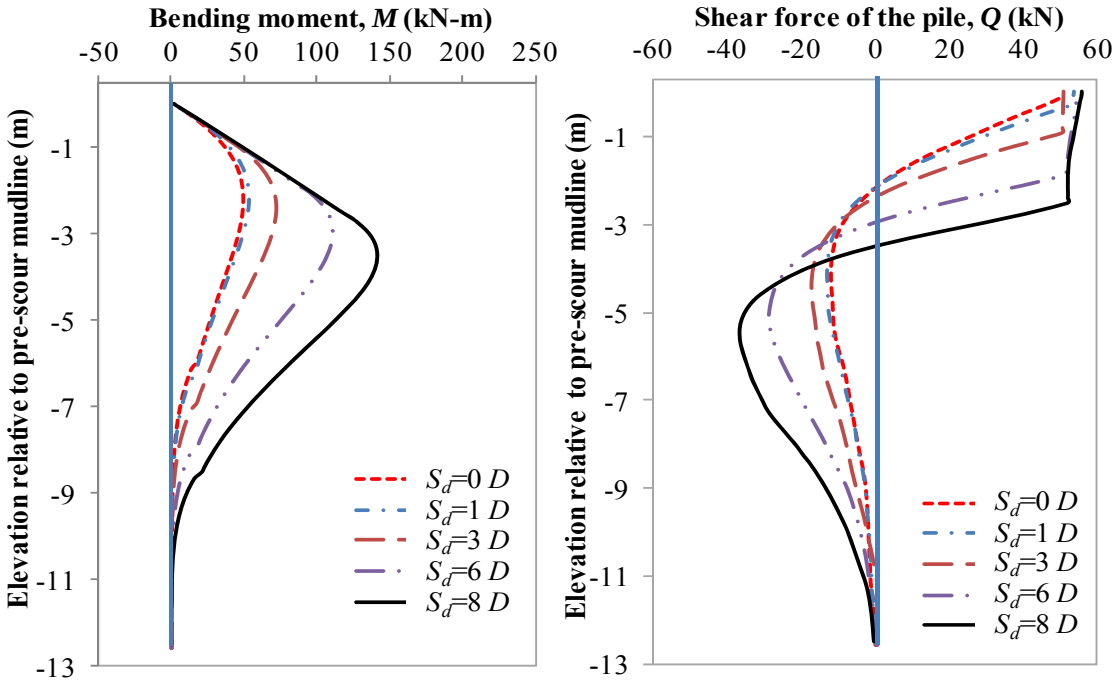

Figure 4-22. Profiles of bending moment and shear force (F_t = 50 kN and S_w =0)

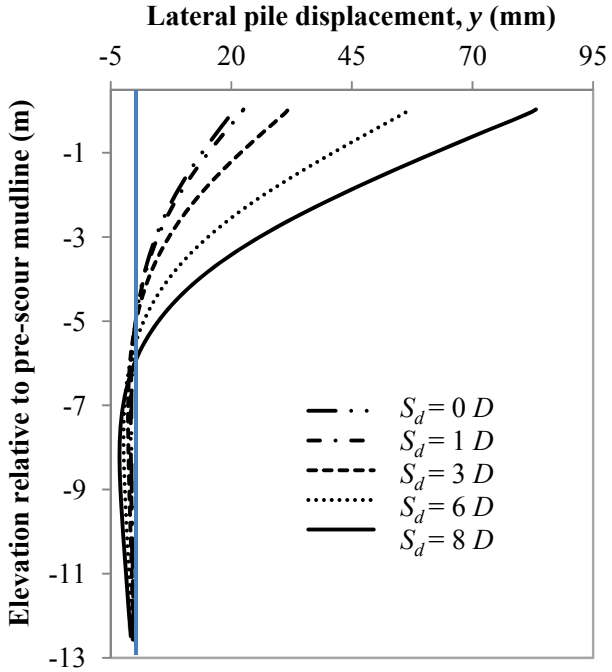

Figure 4-23. Profiles of pile lateral displacement (F_t = 50 kN and S_w =0)

4.3.2 Effects of scour width

Scour widths ranging from 0, 1 *D*, 3 *D*, 6 *D*, 8 *D*, to ∞ were investigated in this study. The effects of the scour width on the behavior of the laterally loaded pile were evaluated by the computed lateral pile-head displacements, allowable lateral load, the *p-y* curves, and profiles of bending moment, shear force, and lateral displacement. Two scour depths (i.e. 1 and 3 *D*) were considered during each investigation.

4.3.2.1 Lateral pile-head displacement

The lateral displacement at the pile head, as shown Figures 4-24 and 4-25, increased slightly with an increase of the scour width and the lateral applied load, but remained constant when the scour width exceeded 8 *D*. In order to clearly explain the effects of the scour width, an influence width is introduced herein, which is defined as the scour width when its effects on laterally loaded pile behavior can be neglected. As a result, the influence width is 8 *D* based on the result of the lateral pile-head displacement. Figures 4-24 and 4-25 shows the effects of scour width on the lateral pile-head displacement became increasingly evident as the scour depth increased. For example, under F_t = 80 kN, an increase of S_w from 0 to 8 *D* increased the y_t value by 8 mm for S_d = 1 *D* and by 10 mm for S_d = 3 *D*.

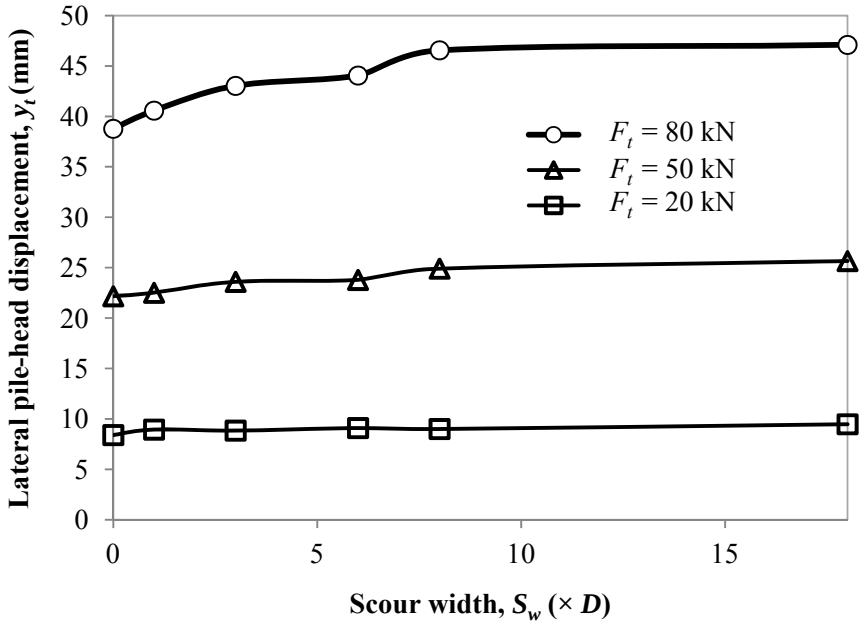

Figure 4-24. Lateral pile-head displacement versus scour widths (S_d = 1 D)

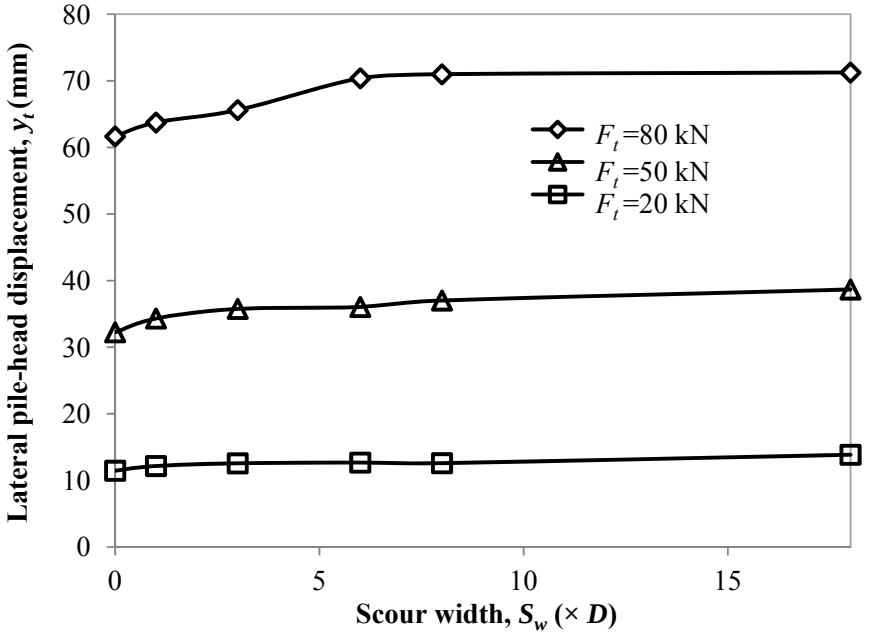

Figure 4-25. Lateral pile-head displacement versus scour widths (S_d = 3 D)

4.3.2.2 Allowable lateral load capacity

The allowable lateral load which was determined as described in the section of 4.3.1 is presented as a function of the scour width in Figure 4-26. The allowable lateral load slightly decreased with increased scour width. Similarly, the influence width was found to be 8 *D* after which the maximum lateral load remained constant.

As the allowable lateral load varied insignificantly with the scour width, the corresponding allowable displacement also shows a minor change with the scour width. For example, the allowable lateral displacement changed with scour width from 50 to 52 mm for S_d = 1 *D*, and from 52 to 56 mm for S_d = 3 *D*.

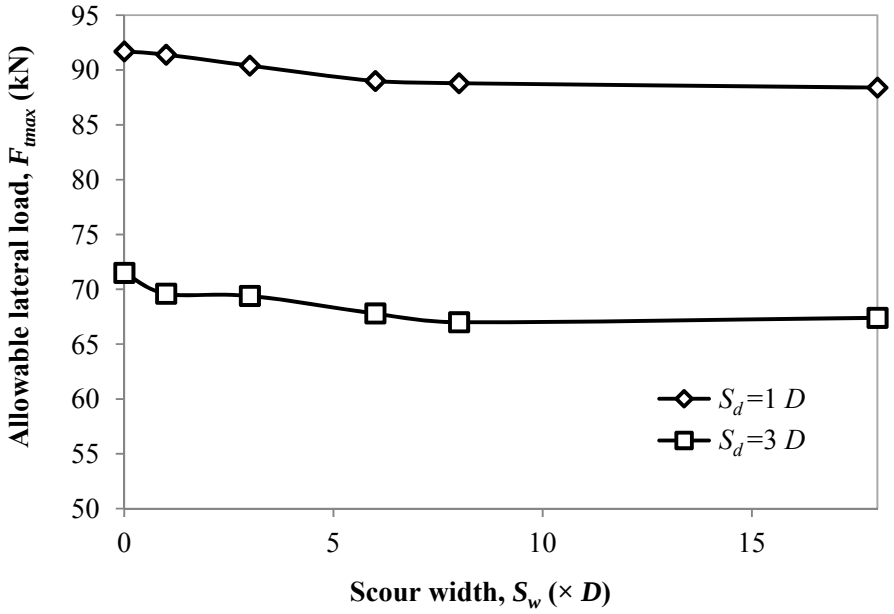

Figure 4-26. Lateral pile-head displacement versus scour widths

4.3.2.3 The p-y curves

The calculated *p-y* curves corresponding to depths of 0.3 and 1 *D* at the scour depth of 1 and 3 *D* are shown in Figures 4-27 to 4-30. It is shown that an increase of the scour width reduced the stiffness and ultimate soil resistance rapidly to constant values after the scour width reached 3 *D*. This influence width is different from that (i.e., 8 *D*) from the previous discussion. The soils at the shallow depth fully mobilized their resistance in the *p-y* curve while the soils at the deep depth only partially mobilized their strength. The laterally loaded pile response depends not only on the soils at the shallow depth but also on the soils at the deep depth. Therefore, the influence width obtained in this analysis may not be representative.

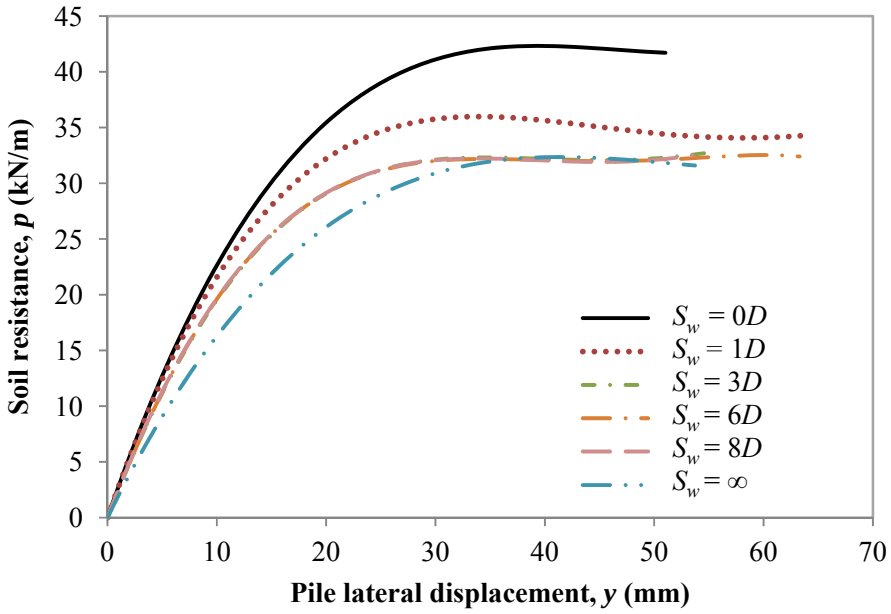

Figure 4-27. The *p-y* curves at soil depth, $d = 0.3\ D$ ($S_d = 1\ D$)

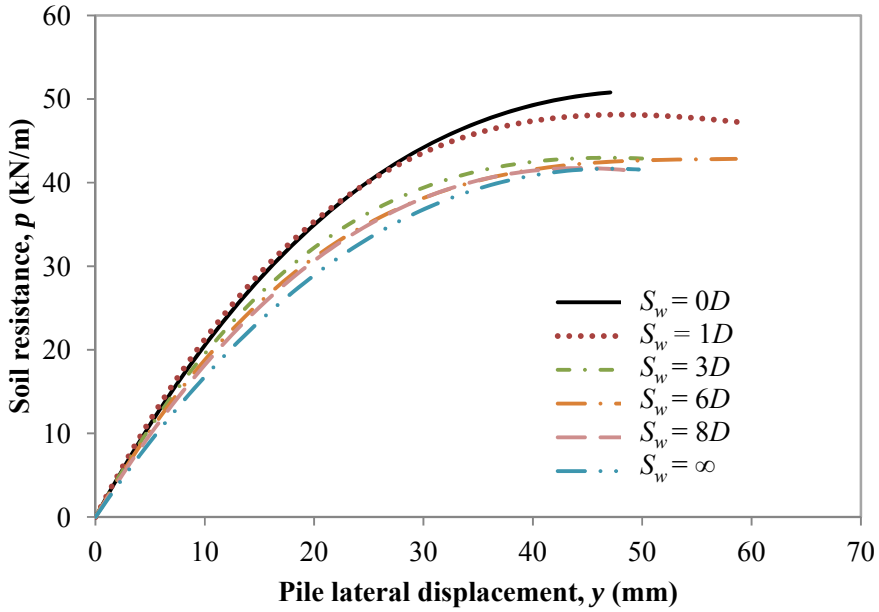

Figure 4-28. The *p-y* curves at soil depth, $d = 1\ D$ ($S_d = 1\ D$)

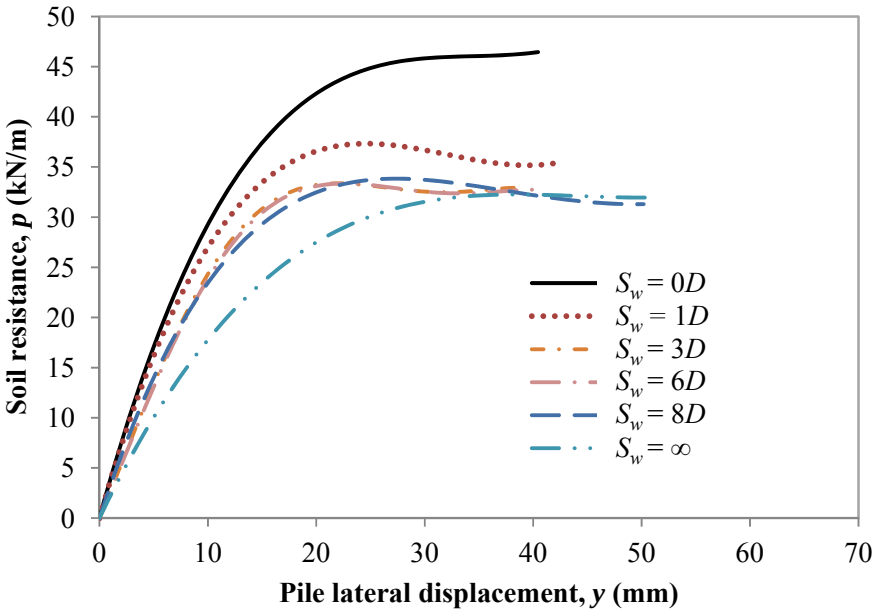

Figure 4-29. The *p-y* curves at soil depth, $d = 0.3\ D$ ($S_d = 3\ D$)

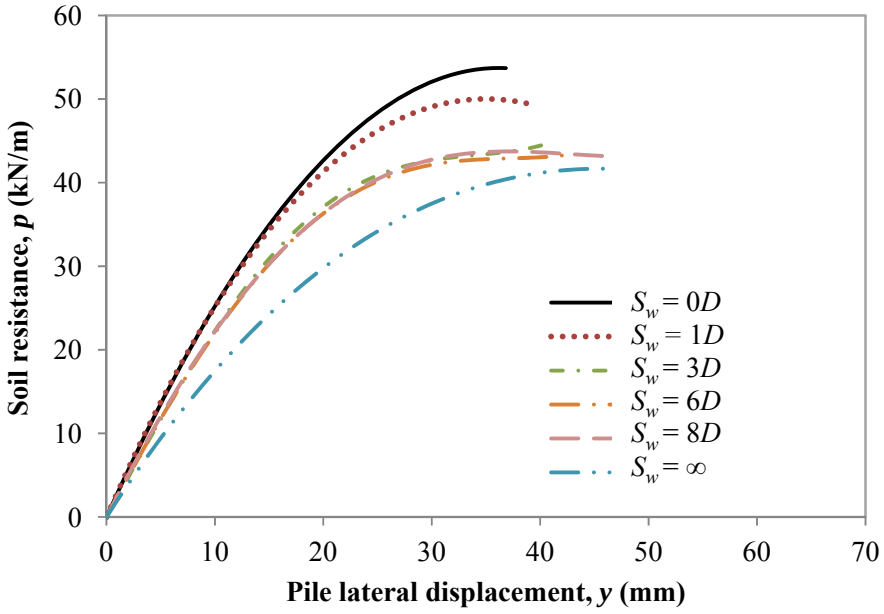

Figure 4-30. The *p-y* curves at soil depth, $d = 1\ D$ ($S_d = 3\ D$)

4.3.2.3 Profiles of bending moment, shear force, and lateral displacement

The calculated profiles of the bending moment, shear force, and lateral displacement at different scour widths are almost identical in terms of their magnitude and shape. This result is especially true for the cases with small scour depths. At large scour depths as shown in Figure 4-31 as an illustration, the influence of the scour width on the bending moment became more obvious but was still limited. The location of the maximum bending moment relative to the pre-scour mudline remained almost the same with an increase of the scour width.

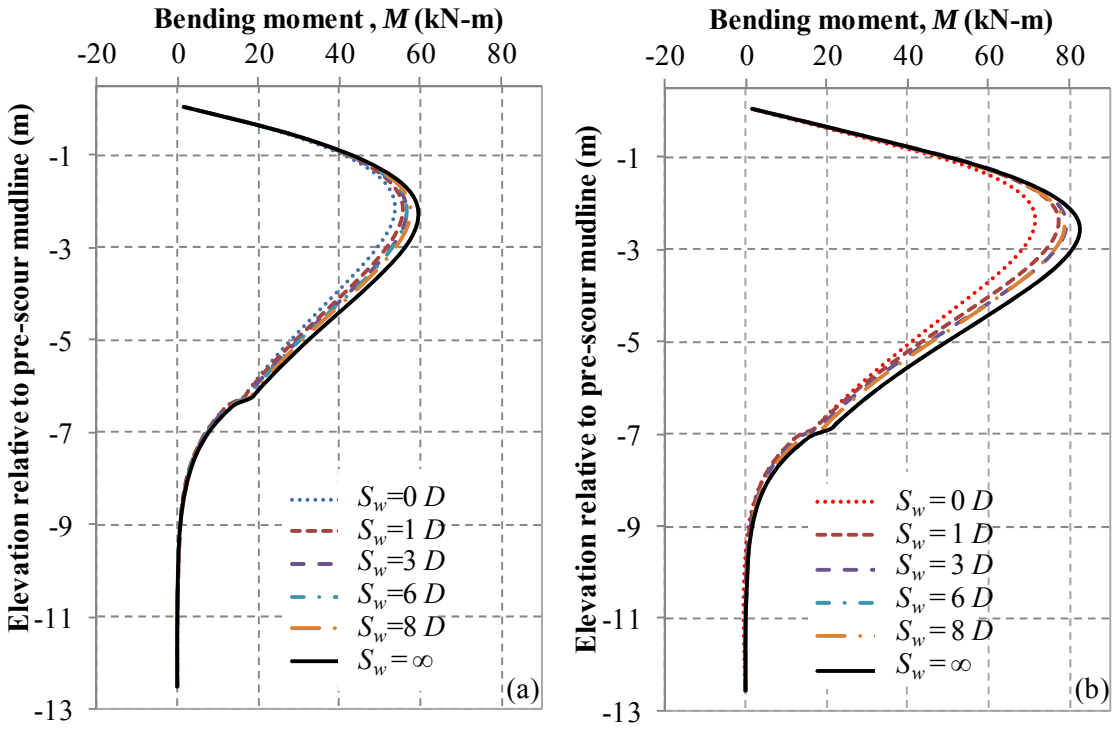

Figure 4-31. The profiles of bending moment under F_t = 50 kN: (a) S_d = 1 D and (b) S_d = 3 D

4.3.3 Effect of scour-hole slope angle

The scour holes with the slope angles ranging from 0˚, 10˚, 20˚, 40˚ to 60˚ were modeled at the scour depth of 3D and the scour width of 0. The effects of the slope angle on the lateral pile-head displacement, allowable lateral load, and the *p*-*y* curves were investigated.

4.3.3.1 Lateral pile-head displacement

Figure 4-32 shows that the lateral load decreased with the slope angle at the same lateral pile head displacement.

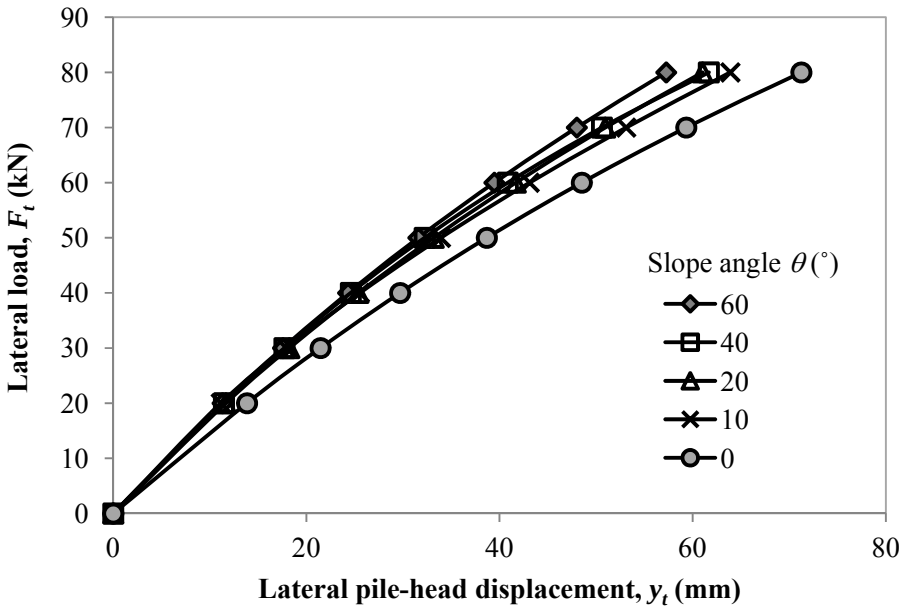

Figure 4-32. Lateral load versus displacement at the pile head for S_d =3 D and S_w = 0

The influence of the slope angle on the lateral displacement can be expressed by a relative difference parameter, R_d, which is defined below:

$$R_d = \frac{y_t(0) - y_t(\theta)}{y_t(0)} \times 100\% \qquad 4.2$$

where, $y_t(\theta)$ = lateral pile-head displacement for the slope angle equal to θ, m; $y_t(0)$ = lateral pile-head displacement for slope angle equal to 0˚, m. Figure 4-33 presents the relative difference of the lateral displacement at the pile head, R_d, versus the slope angle, which shows the maximum difference over 18% at F_t = 50 kN. However, the difference of the lateral displacement for the slope angle between 10˚ and 60˚ was not that significant.

The result of R_d at F_t = 50 kN showed that the most difference could be over 18% by considering slope angle. However, the difference of the displacement for the slope angle between 10˚ and 60˚ was not significant.

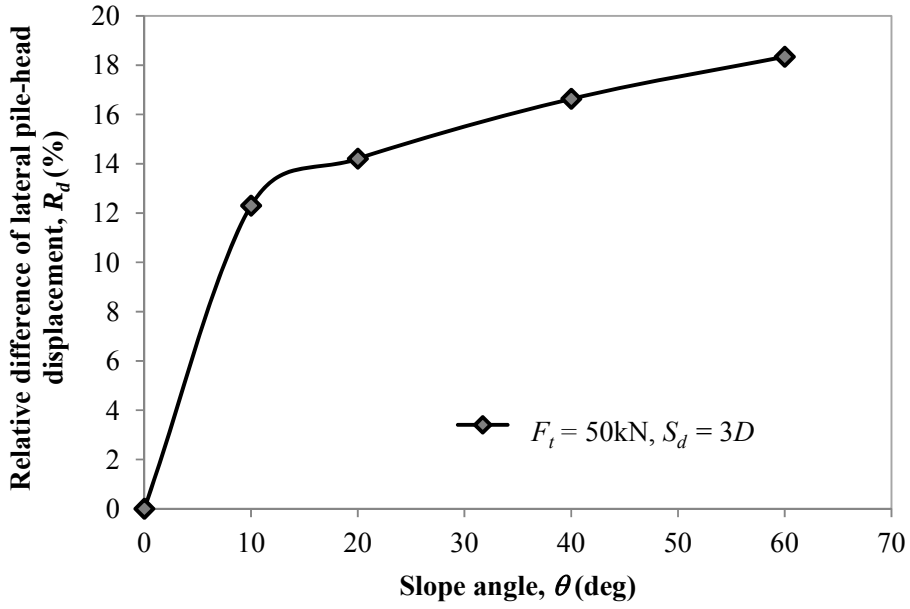

Figure 4-33. Effect of the slope angle on the relative difference of the lateral pile-head displacement (S_w = 0)

4.3.3.2 Allowable lateral load capacity

The effects of the slope angle on the allowable lateral load and allowable pile-head displacement are presented in Figure 4-34. Although there are some variations in the result, the allowable lateral load generally increased with the slope angle while the allowable lateral pile head displacement generally decreased with the slope angle. However, the variation for either F_{tmax} or y_{tmax} was approximately within 10%.

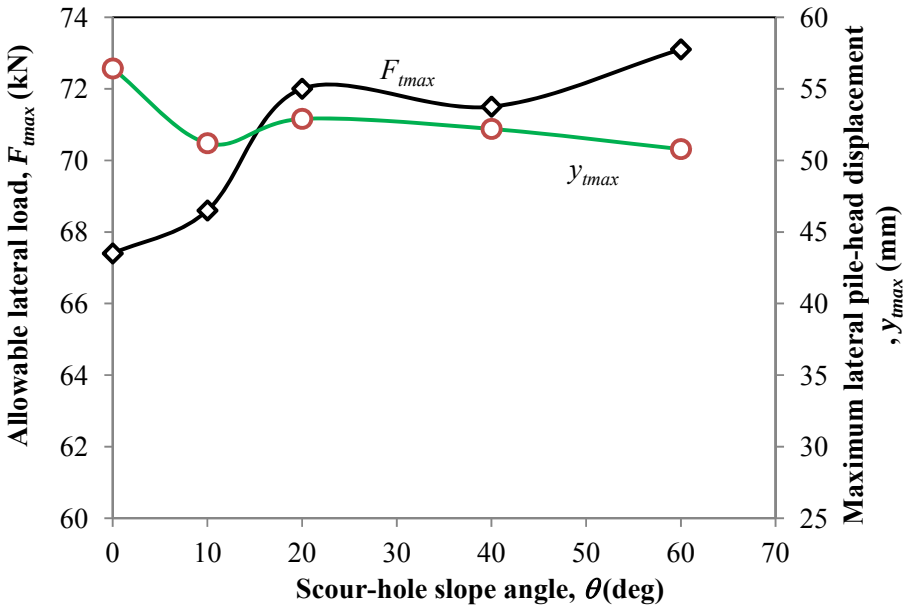

Figure 4-34. Maximum lateral load and displacement at pile head (S_d = 3 D and S_w = 0)

4.3.3.3 The p-y curves

The *p-y* curves at two shallow depths (i.e. d = 0.3 and 1 D) are depicted in Figures 4-35 and 4-36. The numerical results show that the differences in the *p-y* stiffness values for the cases with the slope angles larger than 0˚ are small. The ultimate soil resistance, however, shows an obvious difference with the slope angle, i.e., as the slope angle increased, the ultimate soil resistance increased greatly. For example, when the slope angle increased from 10˚ to 60˚, the ultimate soil resistance at d = 0.3 D increased by over 40%. The change of the slope angle would change the level of the overburden stress thus affecting some of the behavior of laterally loaded piles.

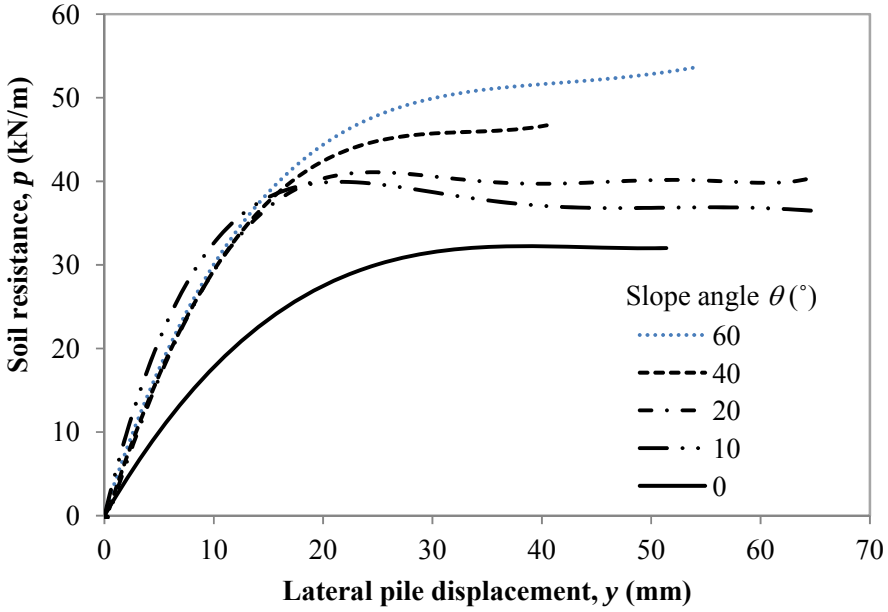

Figure 4-35. The *p-y* curve at soil depth, $d = 0.3\ D$ ($S_d = 3\ D$ and $S_w = 0$)

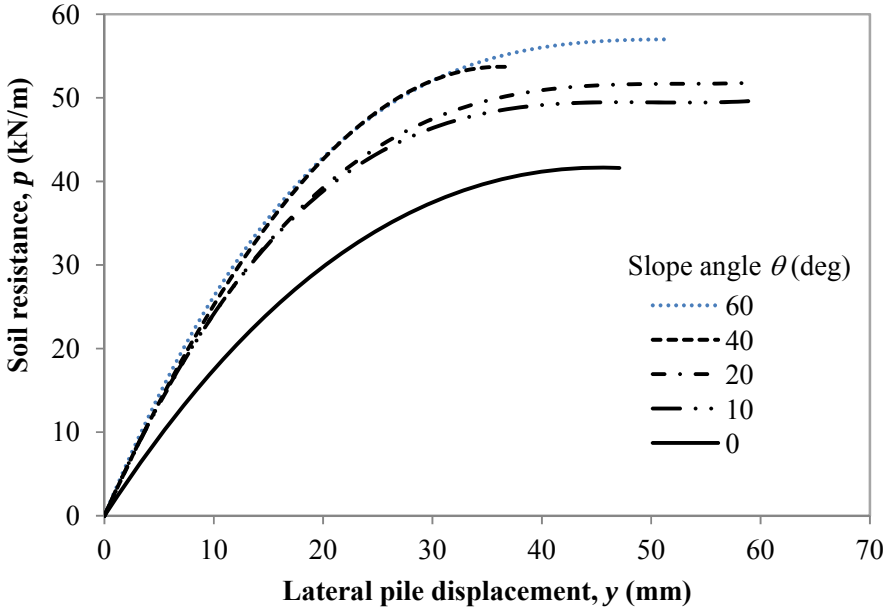

Figure 4-36. The *p-y* curve at soil depth, $d = 1\ D$ ($S_d = 3\ D$ and $S_w = 0$)

4.4 Summary

The effects of the scour-hole dimensions on the behavior of laterally loaded single piles in soft clay were investigated using the 3D finite difference method in *FLAC*^{3D}. Three key influence factors including scour depth, scour width, and slope angle were considered. Before this parametric study, the 3D finite difference model was pre-analyzed and calibrated to ensure the correctness and accuracy of the model. The following conclusions can be made based on the above analyses.

(1) Based on the 3D modeling of the Lake Austin test (Matlock 1970), the boundary effects were minimized when the horizontal distance from the pile periphery exceeded 40 *D* (*D* is the pile diameter) and the vertical distance from the pile tip to the model bottom was 40% *L* (*L* is the pile length). Sufficient densities of pile and soil meshes were necessary to achieve satisfactory results; otherwise, coarser meshes could lead to stiff responses of piles subjected to lateral loading.

(2) For undrained soft clay, laterally loaded pile behavior was not sensitive to the change of the interface stiffness. Anisotropy and secondary structure of the soft clay were considered by using 72% of the measured undrained shear strength (Vane Shear). The ratio of elastic modulus to undrained shear strength was 50.

(3) The scour depth influenced the laterally-loaded pile behavior more significantly than the scour width and slope angle; the lateral displacement at the pile head decreased nonlinearly with the scour depth, especially at the high loading level. At large scour depths, the laterally loaded pile behavior was primarily dependent on the pile stiffness because the pile above the post-scour mudline transferred the applied lateral load from the pile head to the lower surrounding soils. The pile lateral load capacity decreased substantially with an increase of the scour depth; the reduction of the pile

capacity could reach 50% when the scour depth increased from 0 to 6 *D*. The corresponding allowable displacement at the pile head ranged from 16% to 23% *D* and increased with the scour depth. The scour depth significantly influenced the pile *p-y* curve, but its influence gradually decreased with an increase of the scour depth. Under the same applied lateral load, the maximum bending moment and negative maximum shear force increased rapidly with an increase of the scour depth. The elevation of the maximum bending moment at a certain applied load moved away from the pre-scour mudline but shifted toward the post-scour mudline when the scour depth was increased.

(4) The lateral pile-head displacement increased with an increase of the scour width, but the lateral load capacity slightly decreased with the scour width. The effects of the scour width on both results were also dependent on the loading level. An influence scour width was found at 8 *D* beyond which the effects of the scour width on the laterally loaded pile behavior were negligent. At shallow soil depths (i.e. $d \leq 1$ *D*), the ultimate soil resistance decreased with the scour width and remained constant after the scour width reached 3 *D*.

(5) The laterally loaded pile behavior was also influenced by the scour-hole slope angle. With an increase of the slope angle, the lateral pile-head displacement decreased, with the most reduction of the displacement by 18% for the slope angle between 0˚ and 60˚. The slope angle had a limited effect on the pile lateral load capacity, with the most increase by only 8% for the slope angle from 0˚ to 60˚. Moreover, an increase of the slope angle significantly reduced the ultimate soil resistance but limitedly changed the *p-y* stiffness.

CHAPTER 5

NUMERICAL STUDY OF LATERALLY LOADED BRIDGE PILES IN SANDS CONSIDERING SCOUR-HOLE DIMENSIONS

Following the analysis on laterally load piles in clays in Chapter 4, this chapter is to address the effects of scour-hole dimensions on the behavior of laterally loaded piles in sands. Similar to the previous analysis, the 3D finite difference model was first pre-analyzed to ensure proper geometric boundaries and mesh densities. Next, the model was calibrated by the field test to warrant a proper selection of soil and pile parameters. Finally, the calibrated model was "scoured" to form a scour hole around a single pile in sands. The scour-hole dimensions include scour depth, scour width, and scour-hole slope angle. The calculated results are expressed in terms of lateral pile-head displacement, maximum applied lateral load, *p-y* curve, and profiles of bending moment, shear force, and lateral displacement. By analyzing the numerical results, the effects of the scour-hole dimensions on laterally loaded pile behavior are evaluated.

5.1 Preliminary Analysis of Finite Difference Model

A preliminary analysis of the finite difference model was performed to ensure an efficient and accurate numerical analysis by selecting proper interface parameters and model geometry. The pile lateral-load test in Mustang Island, Texas (Cox et al. 1974) was employed herein for the preliminary analysis and later calibration of the finite difference model.

5.1.1 Material parameters

The test employed the pipe pile that had parameters as summarized in Table 5-1. The pile was simulated in the model as a non-yielding elastic material. To facilitate the modeling, the

hollow pile was equivalent to the solid pile that had the same flexural stiffness, *EI* and diameter, *D* as the hollow pile had. The elastic modulus of the equivalent solid pile, E_{eq}, was computed by Equation 3.31 to be 2.4×10^7 kN/m^2 that was lower than the original modulus, E_p (Table 5-1). The lower equivalent modulus helped reduce the difference of stiffness between pile and soil, thus improving the numerical stability for the model.

Table 5-1. Pile parameters

Length, *L*(m)	**Outer diameter, *D* (m)**	**Moment of inertia, I_p (m^4)**	**Poisson's ratio, υ**	**Elastic modulus, E_p(kN/m^2)**	**Yielding bending moment, M_y (kN-m)**
21.3	0.61	8.08×10^{-4}	0.3	2.02×10^8	640

The soil was a uniformly-graded fine sand, which was simulated as a linearly elastic-perfectly plastic material with the Mohr-Coulomb failure criterion. The effective stress analysis was used in a drained condition that is commonly encountered in sands. The elastic modulus of a drained material is typically assumed to vary with a confining stress and was calculated herein using the equation suggested by Janbu (1963):

$$E_s = E_o \left(\frac{\sigma_3}{p_a} \right)^n \qquad 5.1$$

where E_s = elastic modulus of the soil, kPa, p_a = atmospheric pressure, kPa, equal to 100 kPa, σ_3= minimum principal stress, and n= the exponent factor.

The soil parameters are tabulated in Table 5-2 where the effective unit weight and friction angle were obtained directly from the measurement; a typical value was assumed for Poisson's ratio; the reference modulus and exponent were chosen based on Mitchell and Gardner's study (Mitchell and Gardner 1971), which had similar gradation (poorly graded) and friction angle (30˚-40˚) of sand.

Table 5-2. Soil parameters

Effective united weight, γ (kN/m^3)	Friction angle, ϕ' (^{o})	Poisson's ratio, υ	Reference modulus, E_o (MPa)	Exponent, n
10.4	39	0.3	120	0.5

5.1.2 Interface parameters

The soil-pile interface included the parameters of cohesion, friction angle, normal stiffness, and shear stiffness. The cohesion was assumed to be zero for the interaction between sand and pile. The friction angle at the interface was estimated to be 0.5-0.7 ϕ', as suggested by Kulhawy et al. (1983) and Kulhawy (1991). The interface stiffness as stated previously was determined by the parametric analysis and different friction angles and interface stiffness values were used as listed in Table 5-3. Figure 5-1 shows that the interface friction angle had some effects on the pile behavior; however, the interface stiffness almost had no effect on the pile response as shown in Figure 5-2. Note that the ground line displacement, y_g, denotes the lateral displacement of the pile at the location of the ground line. A small interface stiffness may result in the interpenetration of two sides of the interface while a high stiffness may increase the computation time and lead to the difficulty of convergence. Hence, a proper value for the

interface stiffness should be selected. Figure 5-2 shows that 2×10^7 kPa/m can be representative interface stiffness where normal and shear stiffnesses are often assumed to be the same due to the simplicity and high magnitude of the interface stiffnesses required to prevent interpenetration. Moreover, the joint displacement at the interface was calculated to be less than 10% of the adjacent zone size, which minimized the interpenetration of two sides of the interface. The interface friction angle can be determined through the calibration with the field test results, which will be discussed later.

Table 5-3. Interface parameters

Cohesion, c (kPa)	**Friction angle, ϕ_i' (^{o})**	**Normal stiffness, k_n (kPa/m)**	**Shear stiffness, k_s (kPa/m)**
0	0.5×39	1×10^6	1×10^6
0	0.5×39	2×10^7	2×10^7
0	0.5×39	1×10^8	1×10^8
0	0.6×39	2×10^7	2×10^7
0	0.7×39	1×10^7	1×10^7

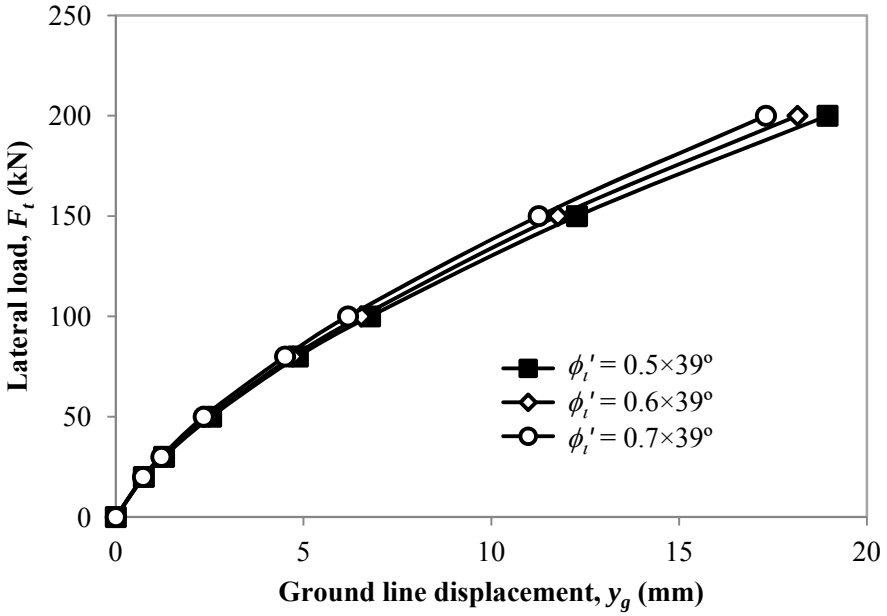

Figure 5-1. Effects of interface friction angle on the ground line displacement of the pile

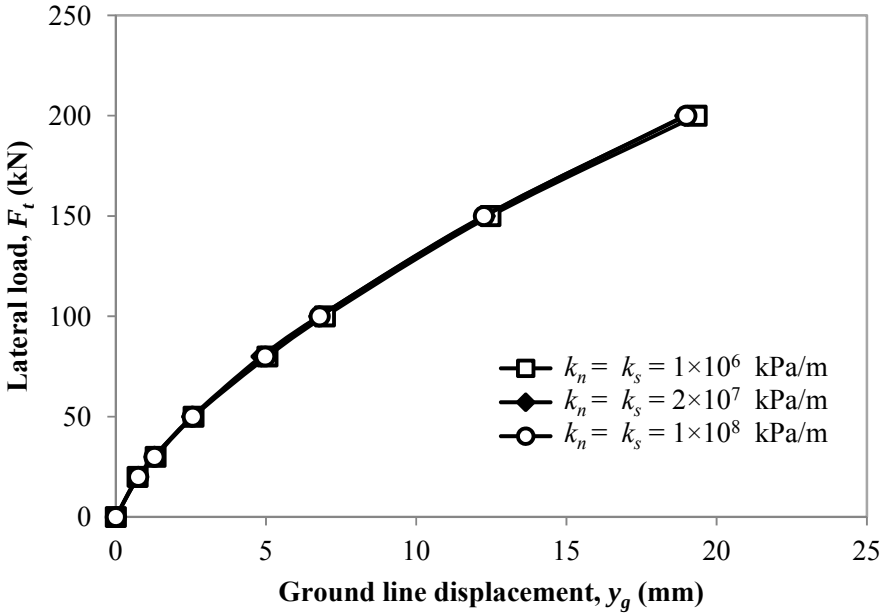

Figure 5-2. Effects of interface stiffness on the ground line displacement of the pile

5.1.3 Model analysis

Due to the symmetry of the model, half of the model was built, as illustrated in Figure 5-3. The model discretization followed the rule that coarse elements were assigned to the zones with small deformation. In the radial direction, the soil was built up of 17 columns of elements with the minimum width of 0.18 m and the aspect ratio of 1:1.15 while the pile was composed of three columns of elements with the equal element width. A total of 12 elements were arranged along the circumference of both soil and pile. In the vertical direction, the soil and pile were divided into three zones: the first zone consisted of 60 layers of elements with the thickness of 0.12 m from the top to 6 m below, followed by nine layers of elements with the aspect ratio of 1:1.15 from the bottom of the first zone to 3 m below, and ended at the last zone with a number of layers of 1 m thick elements.

The radial boundary of the model was located at 24 D from the pile periphery, which was proven adequate to minimize the boundary effects Dodds (2005) and was also verified in the author's model. The vertical boundary from the pile tip to the bottom of the mode should be: 0.38 L according to Dodds (2005) but 0.6 to 0.7 L as suggested by Trochnis et al. (1988). To capture a better vertical boundary, a parametric analysis on the lateral pile-head response was conducted. The numerical results, as presented in Figure 5-4, clearly show that the vertical boundaries at 0.24, 0.38, and 0.6 L below the pile tip resulted in the same lateral pile-head response; hence, the distance of 0.24 L from the pile tip to the model bottom was sufficient and used in this study.

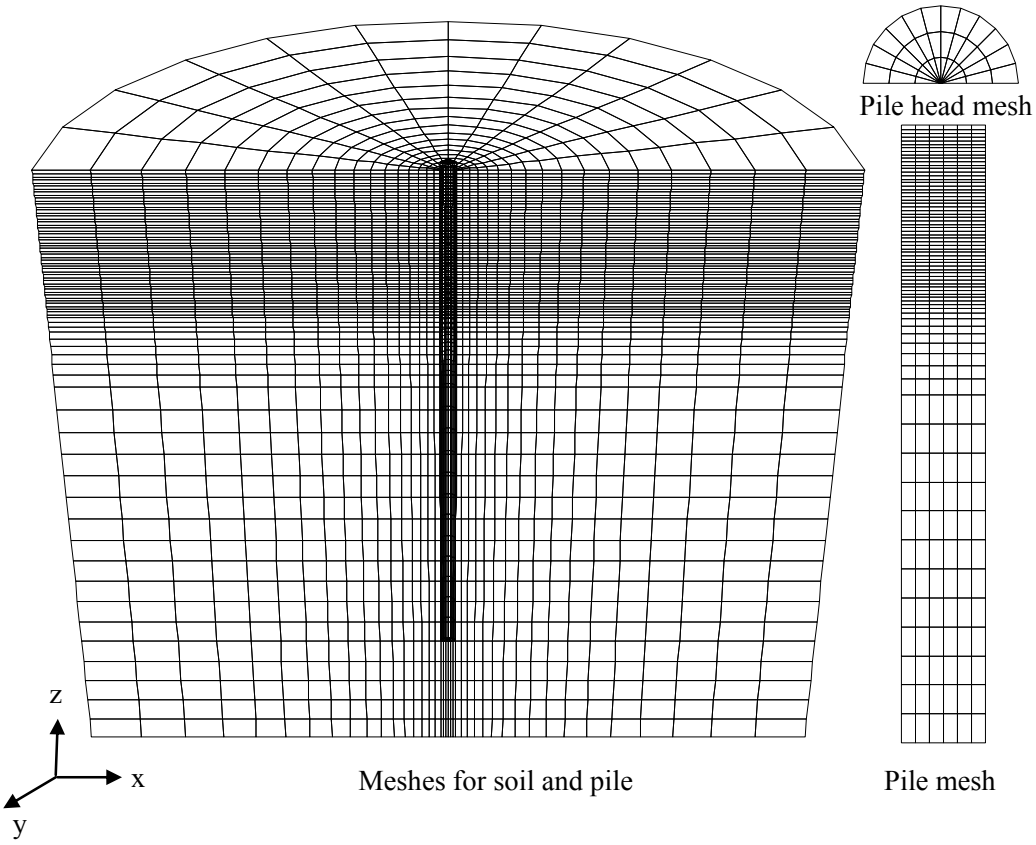

Figure 5-3. Model geometry and discretization

Velocity-control loading was used to apply the lateral load at the pile head. The servo-control function was also used, which sustained an average velocity of $5x10^{-7}$ m/s with a range within $5x10^{-8}$ m/s and $1x10^{-6}$ m/s based on the prescribed unbalanced force bounds (10 and 50N). The model was assumed to reach the equilibrium when the unbalance force was equal or smaller than $1x10^{-6}$ of the maximum unbalance force.

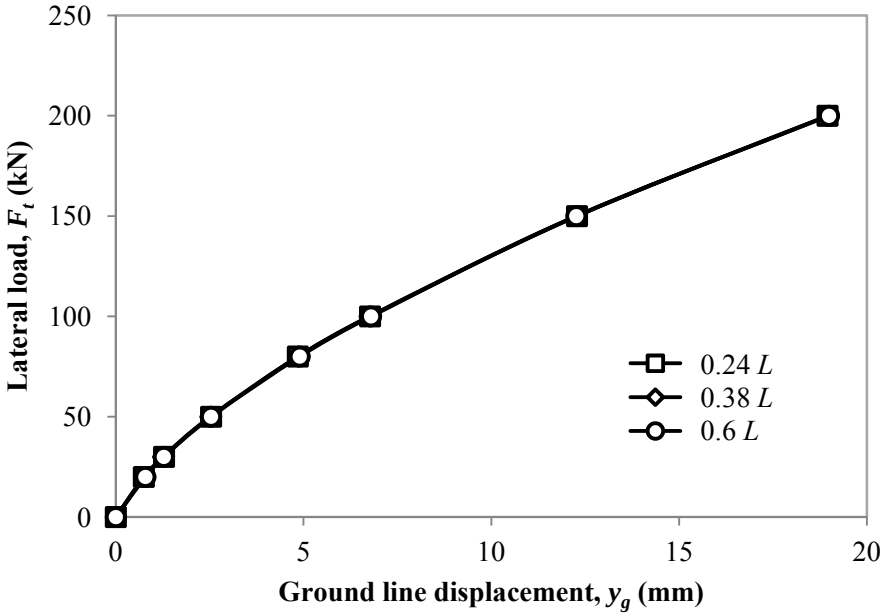

Figure 5-4. Effects of the vertical boundary below the pile tip on the lateral pile-head response

5.2 Model Calibration

Based on the preliminary analysis, the finite difference model was further calibrated with the results from the field test in Mustang, Texas (Cox et al. 1974). To calibrate the model, only the friction angle at the interface needed to be clarified. By comparing the result of F_t-y_g curves, the interface friction angle of 20˚ (0.5ϕ') resulted in a favorable result with the measured from the field test, as shown in Figure 5-5. Hence, the interface friction angle of 20˚was used. In the figure, the result from *LPILE* using the *p*-*y* curves proposed by Reese et al. (Reese et al. 1974) is also compared well the measured.

Unlike the numerical results for the pile in soft clay, the *FLAC*^{3D} simulation in sand generally produced favorable results as compared with the measured or the *LPILE* calculated as

presented in Figures 5-6, 5-7, and 5-8. In fact, the difference of the stiffness between pile and sand was smaller than that between pile and soft clay, which might partly contribute to a better simulation of the pile in sand. Moreover, the elastic modulus of the sand varied with the confined stress rather than had the constant value used in soft clay. The stress-dependent modulus might reflect the field condition better and thus gave a better comparative result with the measured.

However, there is much difference in the *p-y* curves from the *FLAC*^{3D} and *LPILE* based on Reese et al. (1974) where the initial p-y stiffness were similar but the ultimate soil resistance was considerably different.

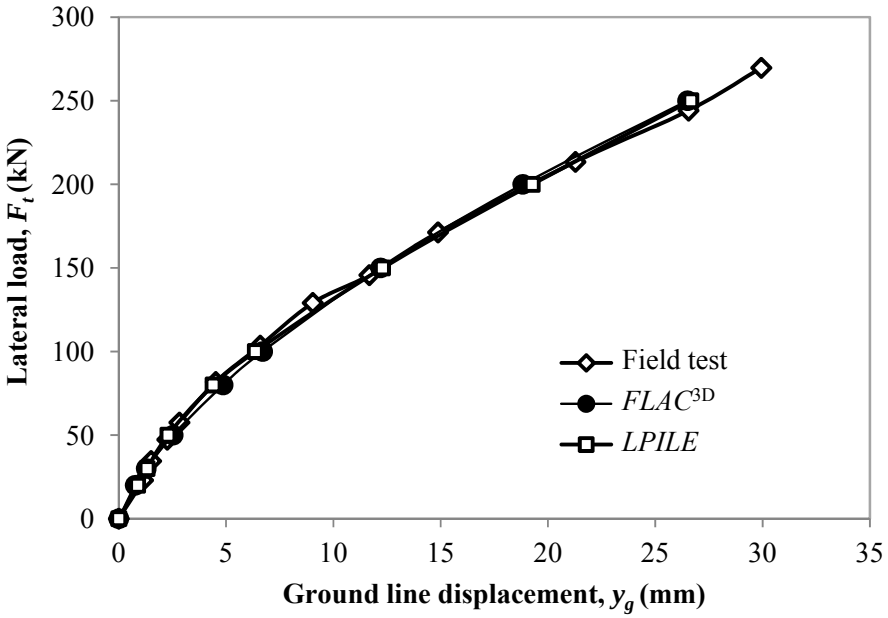

Figure 5-5. Comparison of experimental and calculated ground line displacement

In general, the numerical model was calibrated with the measured F_t-y_g curve from the field test. In addition, the computed maximum bending moment by *FLAC*^{3D} was compared well

with the measured. Hence, the calibrated numerical model was used in the further research on the effects of scour-hole dimensions.

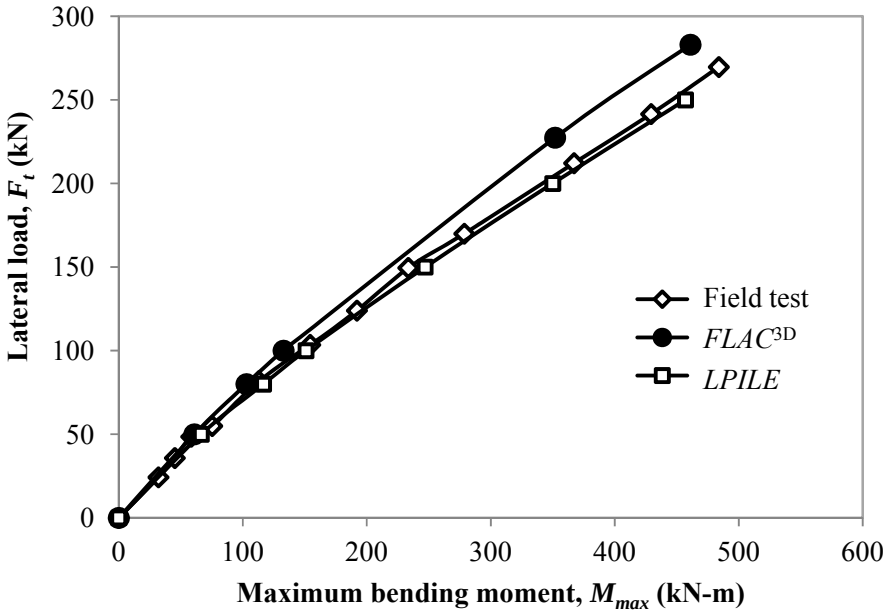

Figure 5-6. Comparison of measured and calculated maximum bending moments

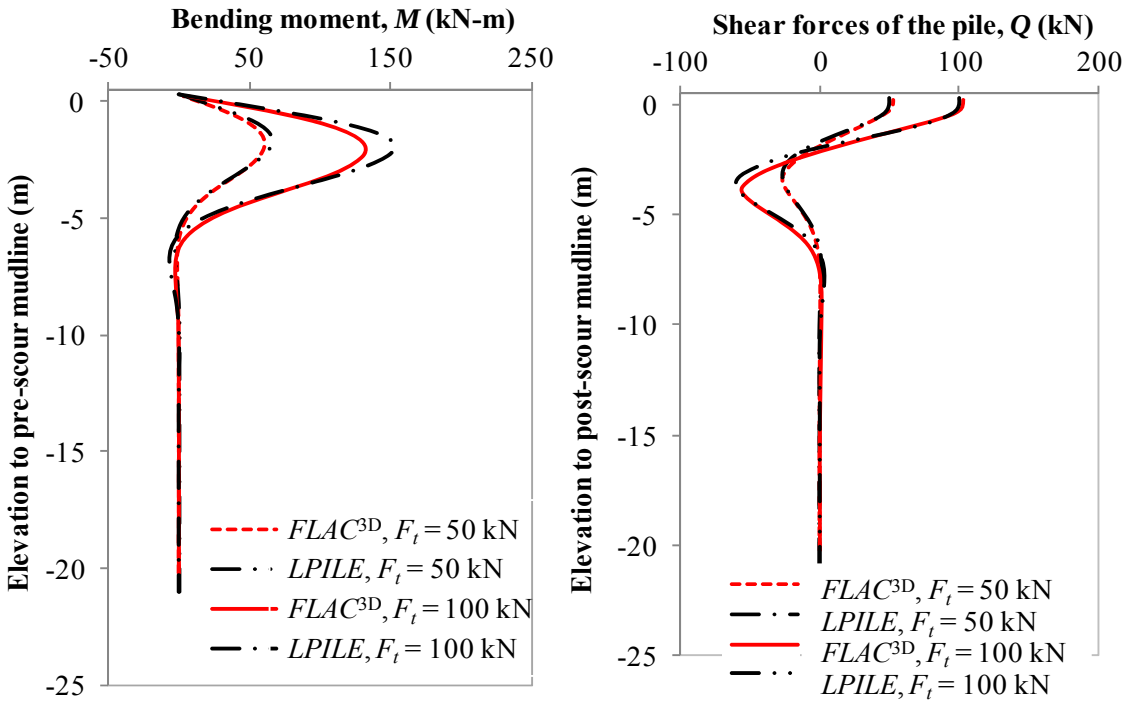

Figure 5-7. Profiles of bending moment and shear force

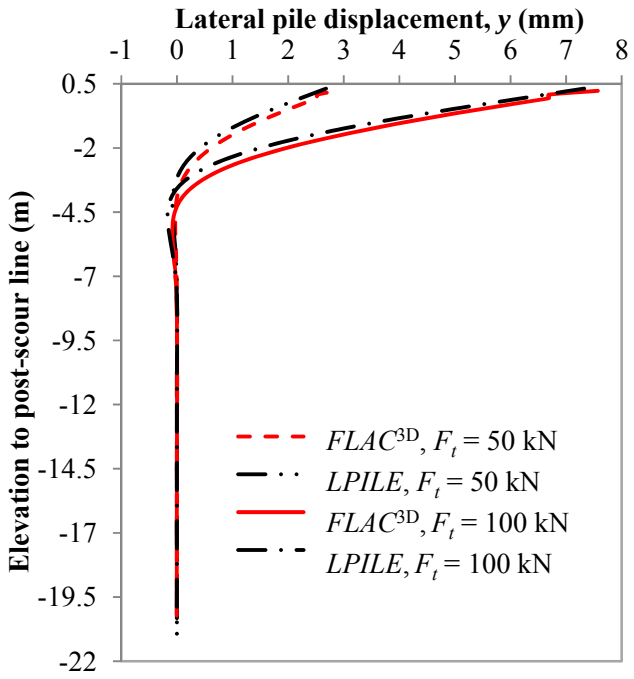

Figure 5-8. Profiles of lateral pile displacement

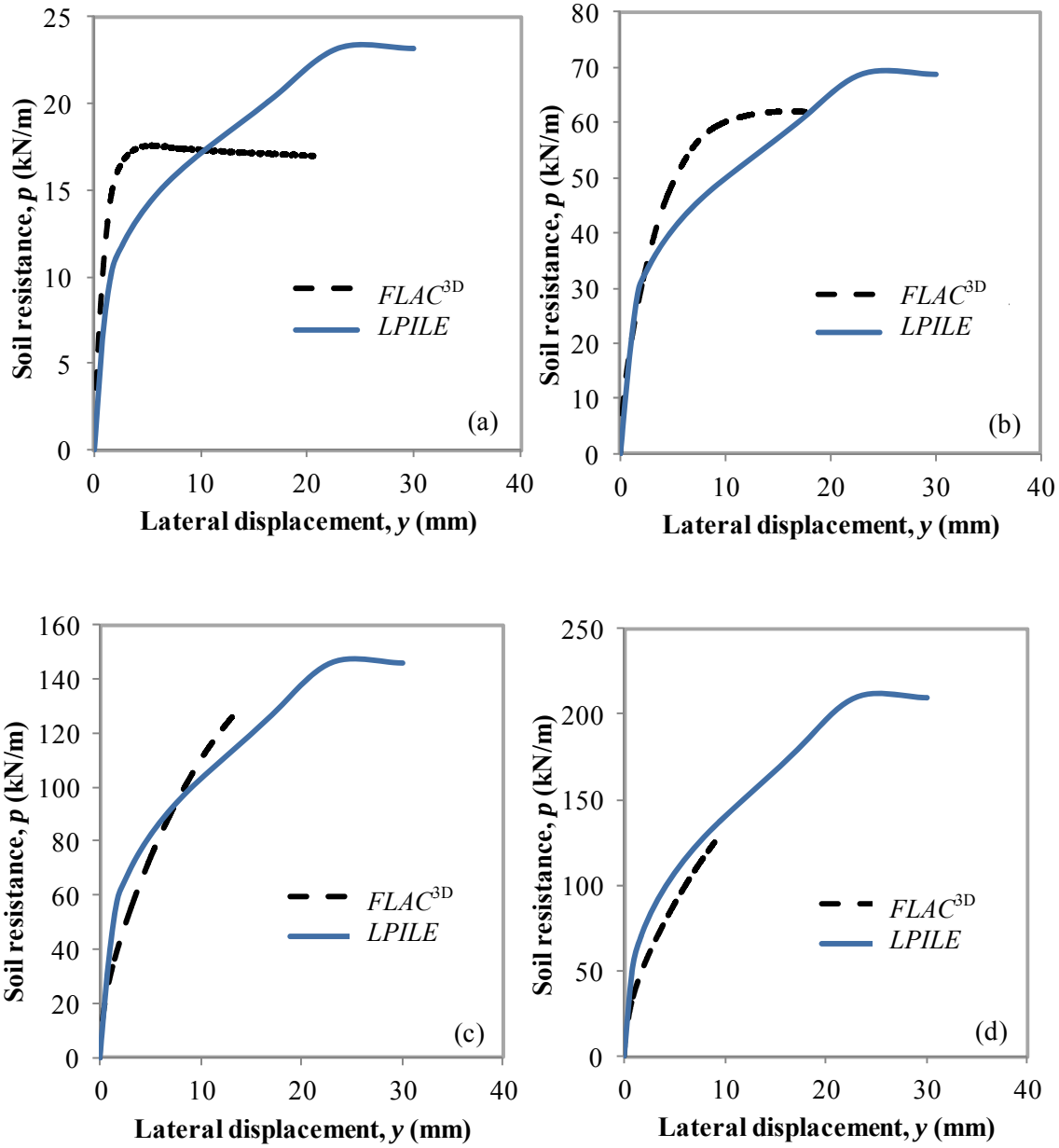

Figure 5-9. Comparison of the calculated *p-y* curves by *FLAC*^{3D} and *LPILE* at various depths: (a) 0.4 *D*; (b) 1 *D*; (c) 2 *D*; (d) 3 *D*

5.3 Effects of Scour-Hole Dimensions

During the modeling, the system was first brought to equilibrium before scour took place. Next, the scour hole was excavated, and then the system was brought to equilibrium again. During this process, the elastic modulus of soil was updated after the confining stress was calculated. Finally, the displacement velocity was applied to the pile head to investigate the laterally-loaded pile behavior at different scour-hole dimensions.

As described similarly for the pile in soft clay, the scour hole was modeled as a circular hole with a varying diameter at the scour depth, as shown in Figure 4-13. Three key influence factors, the scour depth (S_d), scour width (S_w), and scour-hole slope angle (θ), were investigated on their effects on laterally-loaded pile behavior. The numerical results include the relationships of lateral load versus ground line displacement (F_t-y_g curve), maximum lateral load (F_{tmax}) versus ground line displacement (y_{gmax}), *p*-*y* curve, and profiles of bending moment, shear force, and lateral dispalcement. Note that to be consistent, the ground line displacement, y_g, under the scour conditions are referred to the lateral displacement of the pile at the location of the pre-scour mudline.

5.3.1 Effects of scour depth

Five scour depths (i.e. S_d = 0, 1, 3, 6, and 8*D*) and two scour widths (i.e. S_w = 0 and ∞) at the scour-hole slope angle of 39˚ were investigated to evaluate the scour depth effects. Two extreme scour widths were considered to check whether the scour width affects the effects of the scour depth on laterally-loaded pile behavior. The slope angle was selected at its maximum value in order to highlight the effectss from the scour depth and width. The effects of slope angle on the laterally-loaded pile behavior would be discussed in the later section.

5.3.1.1 Lateral load versus ground line displacement

The ground line displacement, as shown in Figures 5-10 and 5-11, increased nonlinearly with an increase of the scour depth. At S_w = 0, the ground line displacement increased slightly with the scour depth increased from 0 to 1 D, but the increase of the displacement was significant when the scour depth was greater than 1 D. The nonlinearity of the ground line displacement with the scour depth was enhanced at a high loading level. In other words, at a great scour depth, an increase of the lateral load significantly increased the ground line displacement.

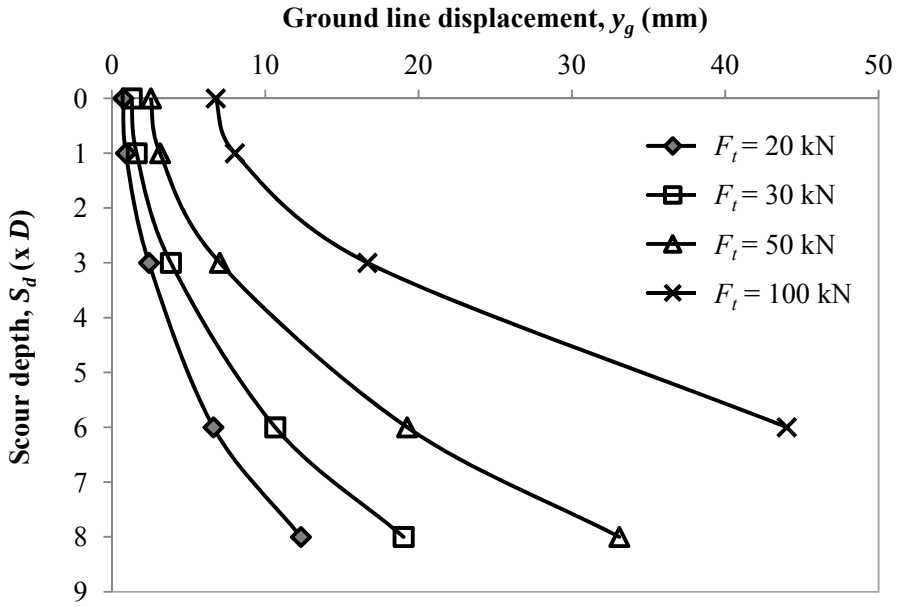

Figure 5-10. Effects of sour depth on ground line displacement (S_w = 0)

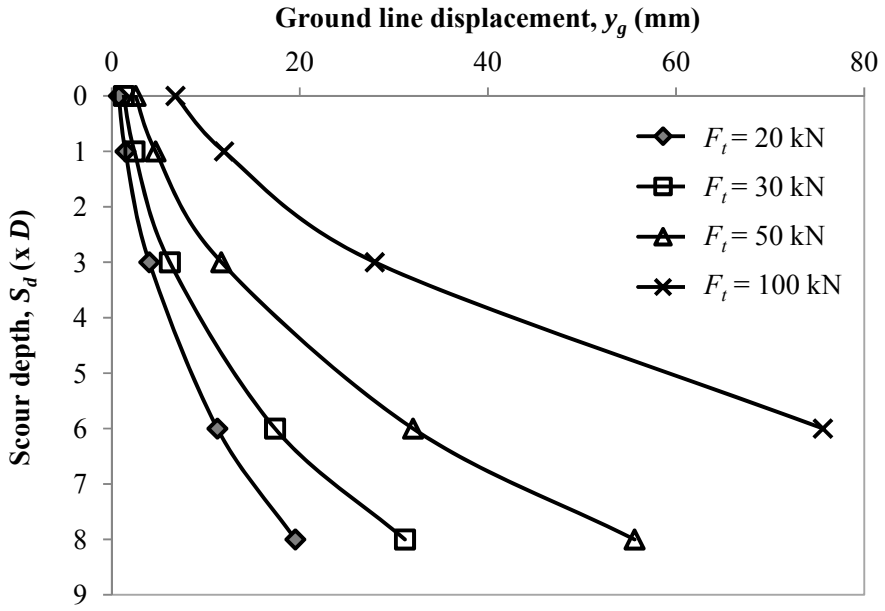

Figure 5-11. Effects of scour depth on ground line displacement ($S_w = \infty$)

The F_t-y_g curves calculated at S_w = 0 and ∞ are plotted in Figures 5-12 and 5-13, which show close relationships at scour depths of 0 and 1 D. At larger scour depths, the F_t-y_g curves had more elastic behavior. This result is similar to that for piles in the soft clay, i.e., the overall pile behavior at a large scour depth was more dependent on the pile properties than on the sand properties.

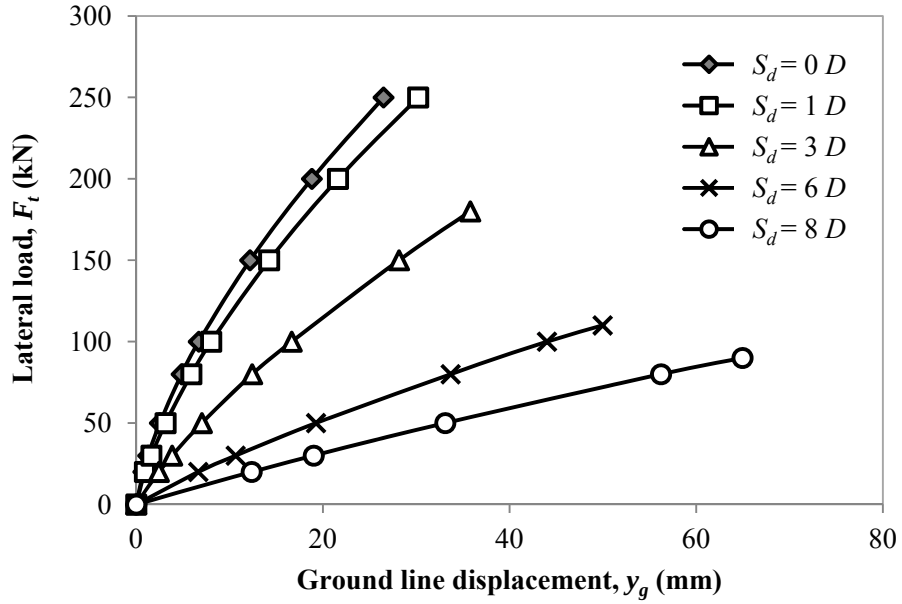

Figure 5-12. Lateral load versus ground line displacement (S_w = 0)

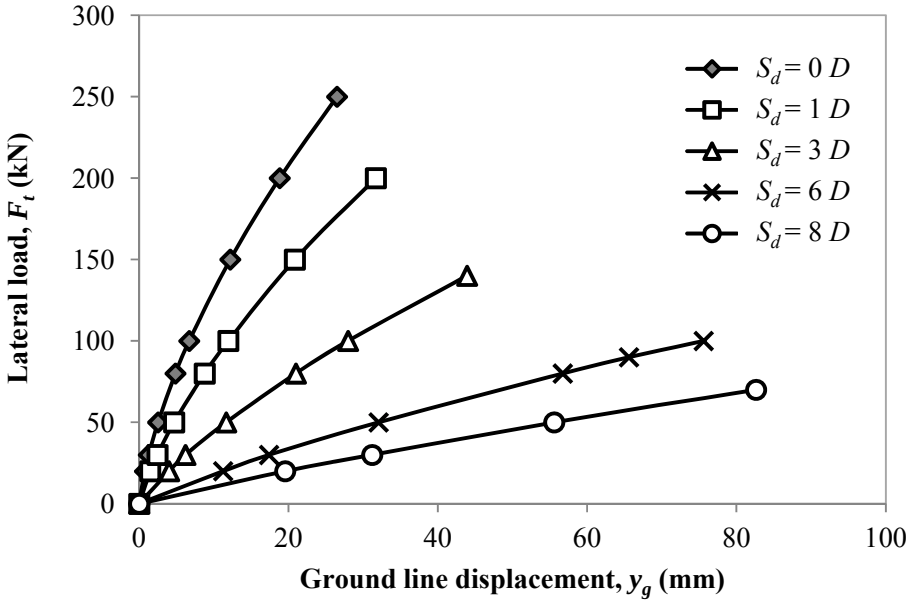

Figure 5-13. Lateral load versus ground line displacement (S_w = ∞)

5.3.1.2 Allowable lateral load capacity

The allowable lateral load or lateral load capacity was determined based on the allowable bending moment of 427 kN-m. This value was estimated by taking a factor of safety of 1.5 (Reese and Van Impe 2001) from the yielding bending moment, M_y, at which the extreme fibers yielded. The ground line displacement corresponding to the maximum lateral load is termed as allowable ground line displacement.

The allowable lateral load, as presented in Figure 5-14, decreased significantly with the scour depth; for example, the decrease of the allowable lateral load by increasing S_d = 0 to 6 D was as high as 66%. However, the reduction rate slowed down at a higher scour depth. This result indicates that the lateral pile capacity changed more significantly at the shallow scour depths than at greater scour depths. The case with a scour hole at S_w = 0 had the higher lateral load capacity than that with a scour hole at S_w = ∞; however, the difference in the lateral load capacity at each scour depth remained almost the same. In contrast, the difference in the allowable ground line displacement increased with the scour depth. The allowable ground line displacement was between 5% to 14% D at S_w = 0 and 5% to 10.3% D at S_w = ∞. Note the above displacement ranges are only applicable to the dense sand with a friction angle of 39˚.

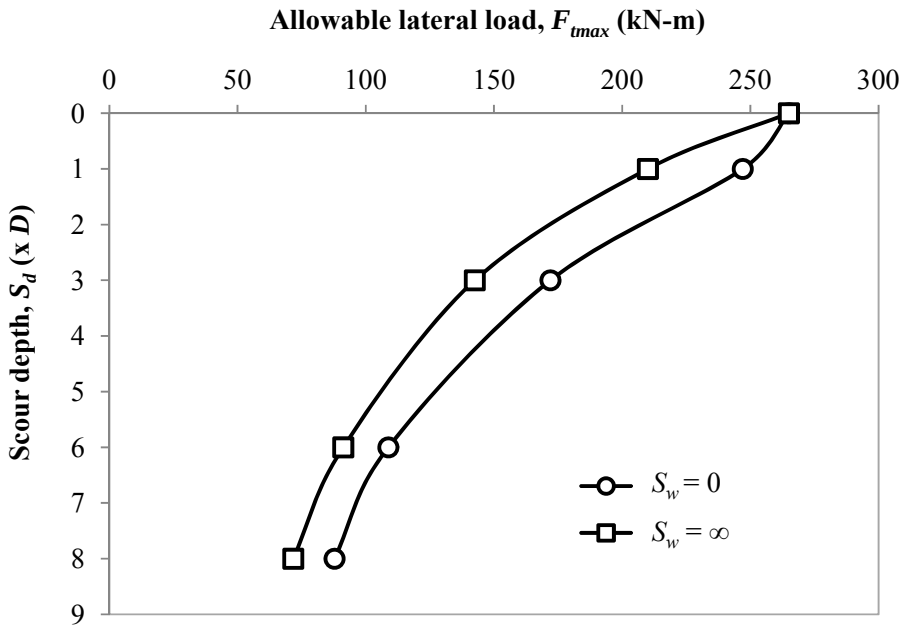

Figure 5-14. Allowable lateral load versus scour depth

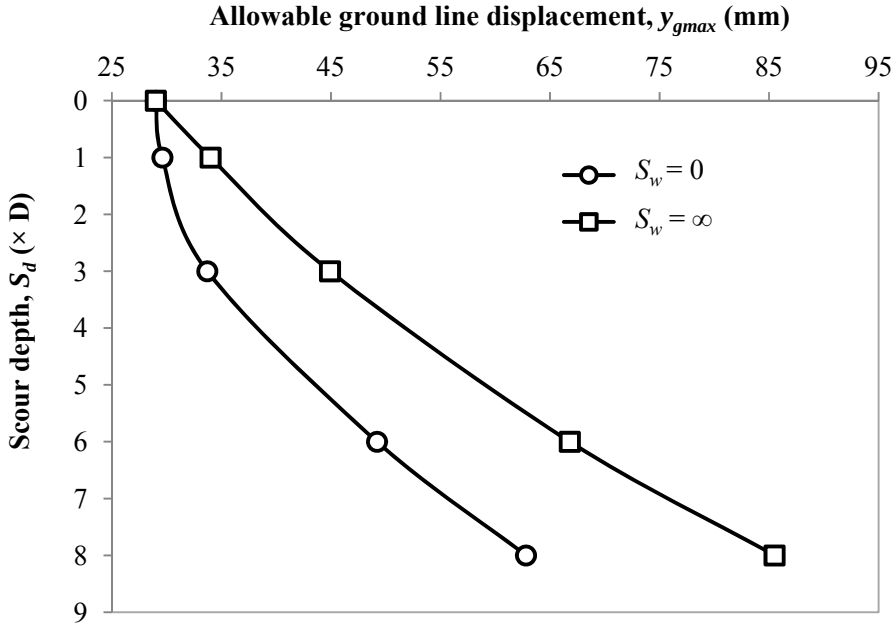

Figure 5-15. Allowable ground line displacement versus scour depth

5.3.1.3 The p-y curves

The *p-y* curves at the shallow soil depth (d = 0.4 D) were fully developed as shown in Figure 5-16. Note that the results were computed for the case with the zero scour width and the slope angle of 39º. The soil depth, d, is defined as the depth below the post-scour mudline. Figure 5-16 demonstrates both the stiffness (i.e, the initial slope of the *p-y* curve) and the ultimate soil resistance increased considerably with an increase of the scour depth. For example, with an increase of the scour depth from 0 to 6 D, the ultimate soil resistance increased by more than seven times. However, the influence from the scour depth gradually decreased as the scour depth was further increased. This result clearly demonstrates that the consideration of the scour-hole dimensions increased the soil resistance to the pile.

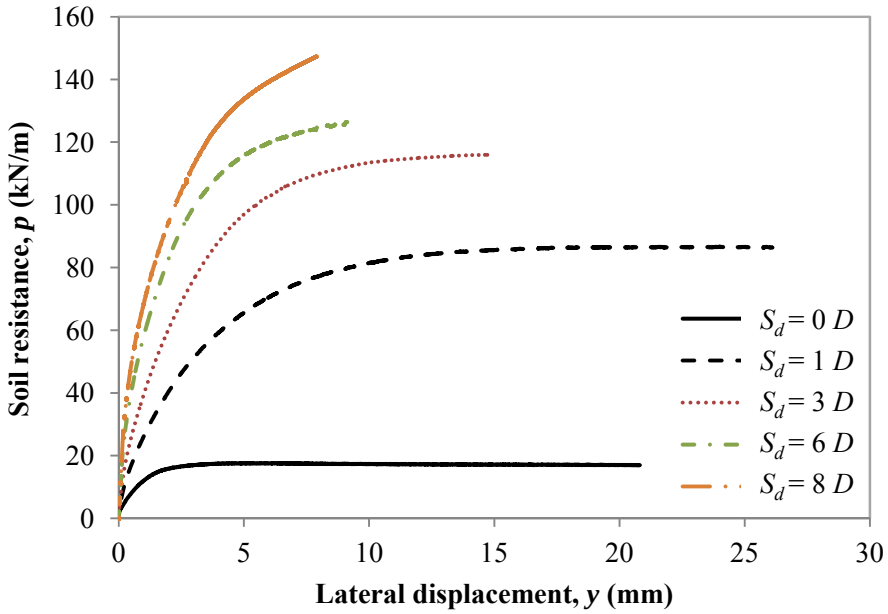

Figure 5-16. The *p-y* curves at the soil depth, d = 0.4 D (S_w = 0 and θ = 39°)

Figure 5-17 shows the *p-y* curves at the soil depth of d = 1 D. The ultimate soil resistance was not fully mobilized, especially at large scour depths. It is also shown that and the *p-y* stiffness increased with an increase of the scour depth.

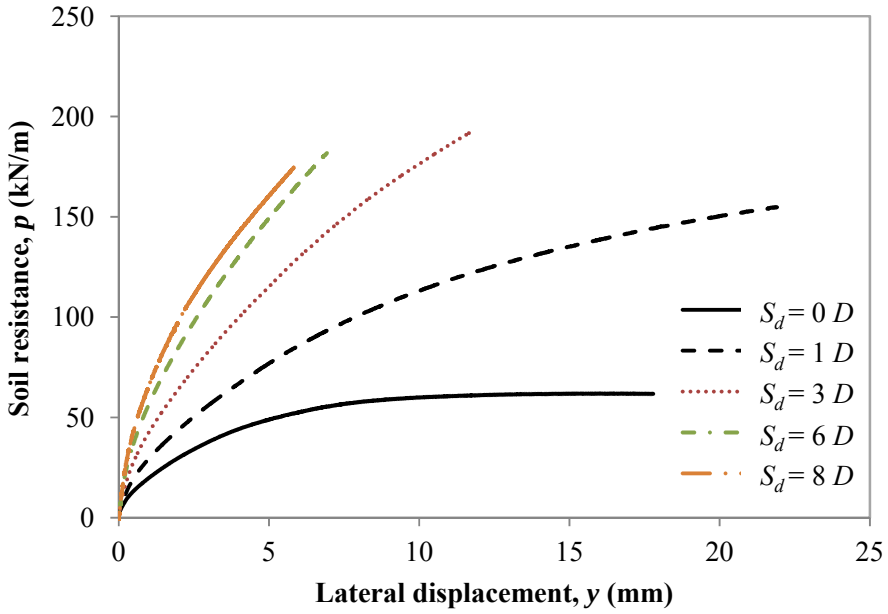

Figure 5-17. The *p-y* curves at soil depth, d = 1 D (S_w = 0 and θ = 39°)

5.3.1.4 Profiles of bending moment, shear force, and lateral displacement

Figures 5-18 and 5-19 present the profiles of bending moment, shear force, and lateral displacement of the pile at the applied lateral load of 50 kN. The numerical results indicate the flexible behavior of the pile with a significant amount of pile length unresponsive to the lateral loading.

The numerical result of the bending moment shows that the location of the maximum bending moment in reference to the pre-scour mudline moved down as the scour depth increased

as shown in Figure 5-18. However, its location relative to the post-scour mudline moved up as the scour depth increased. For example, the distances of the location of the maximum bending moment to the pre-scour mudline were 3.0, 3.1, 4.3, 6.9, and 8.7 D at S_d = 0, 1, 3, 6, and 8 D; however, the distances to the post-scour mudline became 3.0, 2.1, 1.3, 0.9, and 0.7 D at S_d = 0, 1, 3, 6, and 8 D.

Figure 5-18 shows the profiles of the shear force in the pile. After the scour depth exceeded 3 D, the absolute value of the minimum shear force was even higher than the applied lateral load of 50 kN. There was no such phenomenon observed for the pile in soft clay in Figure 4-22. Hence, this phenomenon may only occur in relatively strong soils and at a relatively large scour depth. A further investigation is needed to clarify the above explanation considering sand with different stiffness and strength values. In addition, the excessive negative shear force necessitates the shear design of the pile in dense sands under an excessive scour.

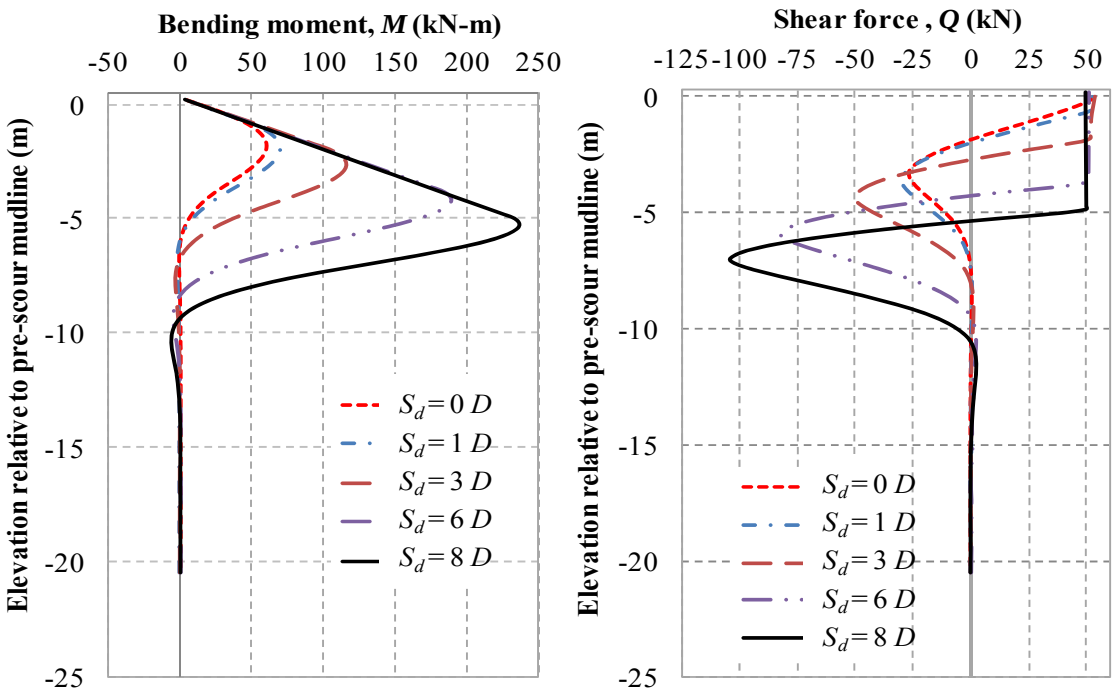

Figure 5-18. Profiles of bending moment and shear force (F_t = 50 kN and S_w = 0)

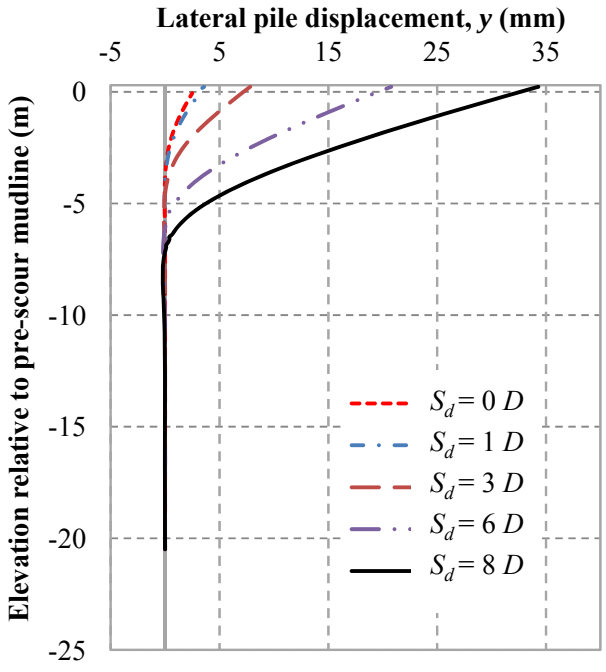

Figure 5-19. Profiles of lateral pile displacement (F_t = 50 kN and S_w = 0)

5.3.2 Effects of scour width

To investigate the effects of the scour width on the laterally loaded pile behavior, seven scour widths (i.e. S_w = 0, 0.5 D, 1 D, 3 D, 6 D, 8 D, and ∞) were considered in the numerical simulation. Note the infinite scour width indicates totally removing the scoured soil layer (i.e. ignoring the scour hole). Three scour depths (i.e., S_d = 1, 3, and 6 D) and one slope angle (i.e., 39˚) were considered in the numerical analysis.

5.3.2.1 Ground line displacement

Figure 5-20 presents the ground line displacements of the pile at different scour widths and at the scour depth of 3 D. It is shown that the ground line displacement increased significantly with an increase of the scour width, especially at the high loading level. A substantial increase of the ground line displacement was observed at the scour width ranging from 0 to 3 D, and the increase became less after the scour width was larger than 3 D. After the scour width exceeded 8 D, the ground line displacement remained almost constant. Thus, the influence width was determined to be 8 D at the condition of S_d = 3 D.

The relative difference of ground line displacement due to scour width, R_d, was defined herein to clarify the effects of scour width as below,

$$R_d = \frac{y_g(\infty) - y_g(S_w)}{y_g(\infty)} \times 100\% \qquad 5.2$$

where, $y_g(S_w)$ = ground line displacement for the scour width equal to S_w, m; $y_g(\infty)$ = ground line displacement when ignoring scour hole or S_w = ∞, m.

Figures 5-21 and 5-22 show that the relative difference in the ground line displacements by considering and ignoring the scour-hole dimensions was as high as 40%. This relative difference, R_d, decreased with an increase of the scour width. At the influence width, the R_d approached to 0 and the influence of the scour width vanished. However, $R_d = 0$ was not always reached. When the criterion of R_d not greater than 5% was used to estimate the influence width, the influence width varied with the scour depth but was independent of the loading level. For example, at $F_t = 50$ kN, the influence width was 6, 8, and 12 D when the scour depth reached 1, 3, and 6 D. However, at $F_t = 100$ kN, the influence widths almost remained the same as those at $F_t = 50$ kN.

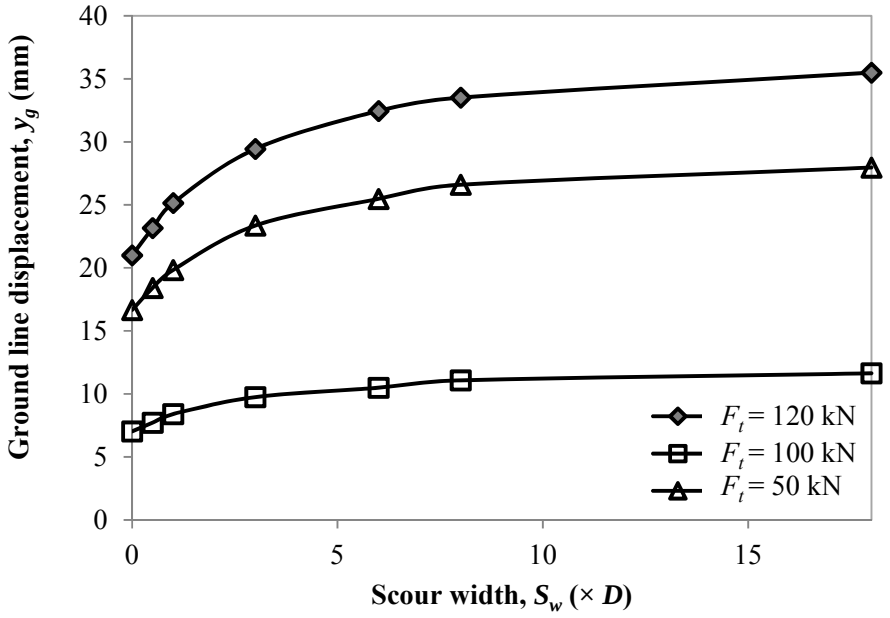

Figure 5-20. Ground line displacements under various scour widths (S_d =3 D)

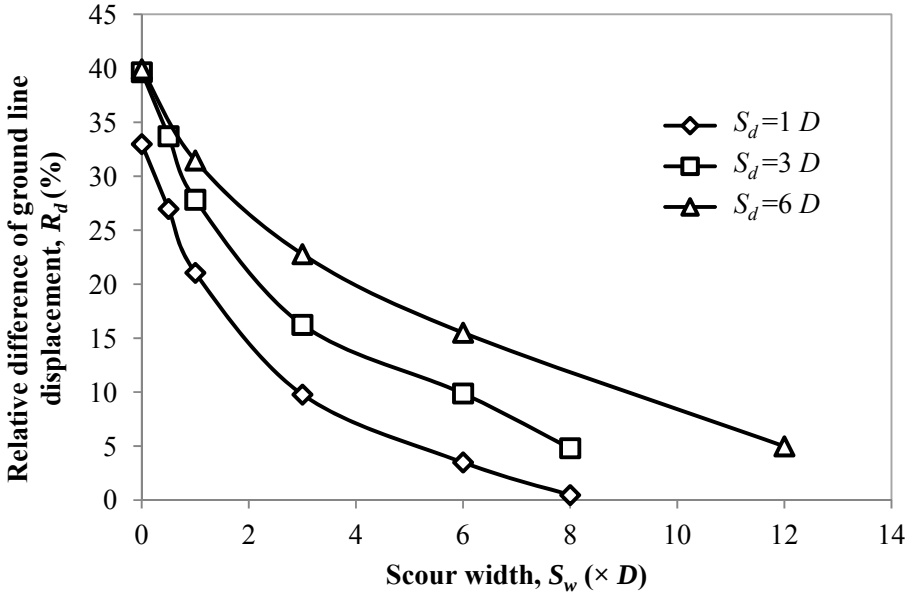

Figure 5-21. Relative difference of the ground line displacement versus the scour width (F_t =50 kN)

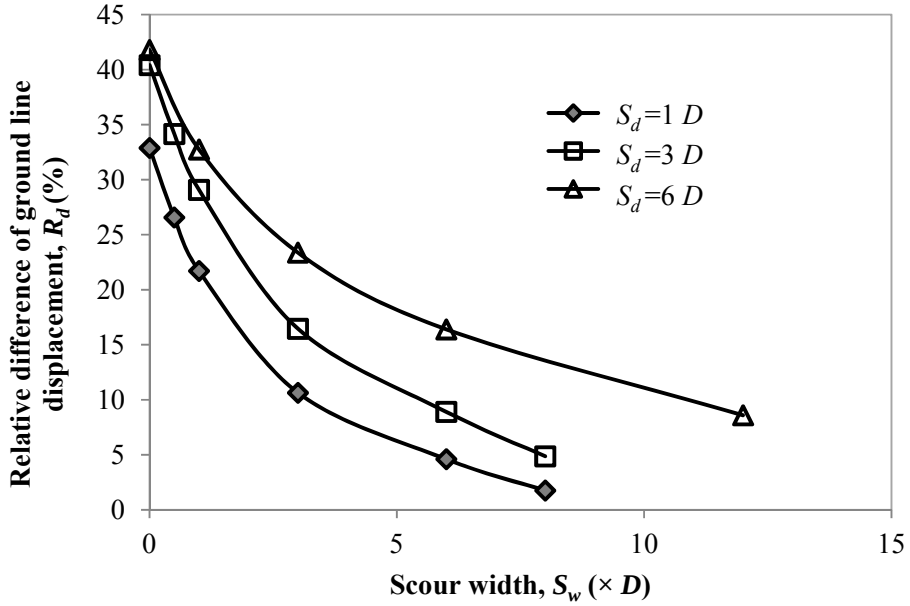

Figure 5-22. Relative difference of the ground line displacement versus the scour width (F_t = 100 kN)

5.3.2.2 Allowable lateral load capacity

Figure 5-23 shows that the allowable lateral load decreased with the scour width. The change of the allowable lateral load due to the scour width was more obvious at a small scour depth than that at a large scour depth. For example, at S_d = 6 D, the maximum change of F_{tmax} was 17.6 kN while at S_d = 1 D, the maximum change increased to 37 kN. This result is because a large scour depth led to the pile more sensitive to the change of the loading level. In addition, the F_{tmax} was almost constant after the scour width exceeded 3 D, which was much smaller than the influence width found in the analysis of the ground line displacement.

The allowable ground line displacement increased with the scour width, as shown in Figure 5-24, and the increase became more noticeable when the scour depth increased. The effects of the scour width on the allowable ground line displacement became negligent when the scour width reached 6, 8, and 12 D at the scour depths of 1, 3, and 6 D respectively.

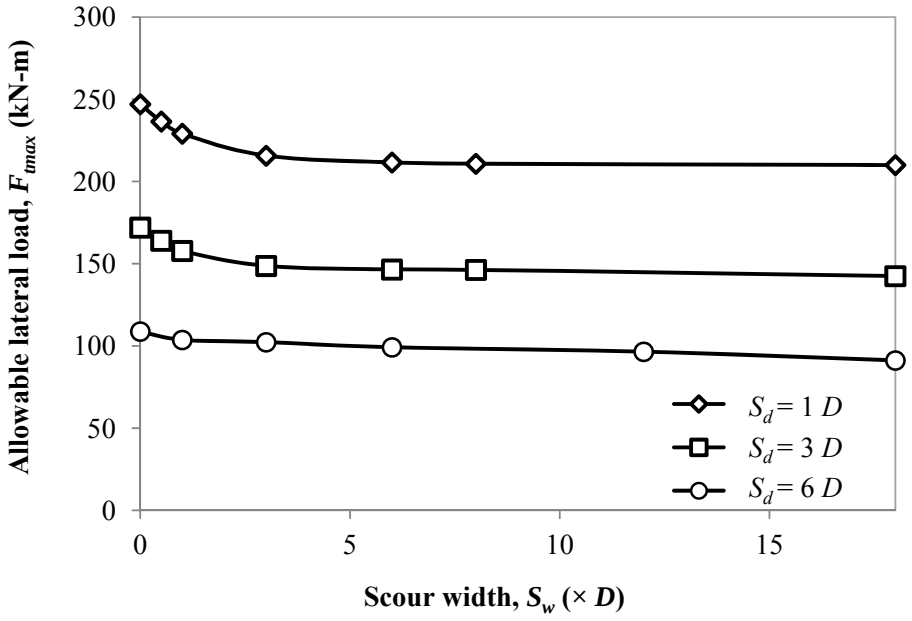

Figure 5-23. Allowable lateral load versus scour width

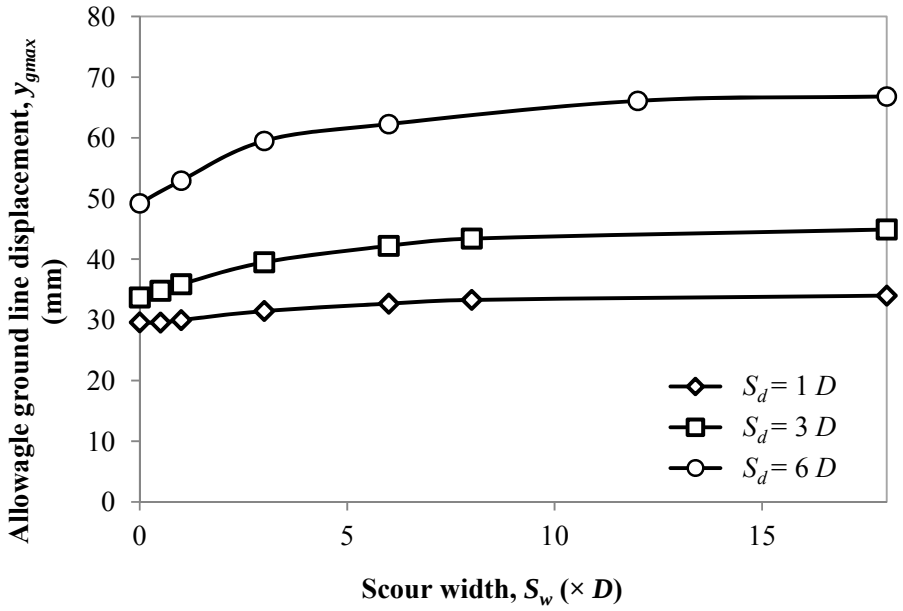

Figure 5-24. Allowable ground line displacement versus scour width

5.3.2.3 The p-y curves

Figures 5-25, 5-26, and 5-27 show the *p-y* curves generated at the soil depths of 0.4, 1, and 2 *D*, respectively. It is shown that the reduction of the scour width would significantly increase both the *p-y* stiffness and ultimate soil resistance. Therefore, it is beneficial to consider the scour width (i.e., an increase of the lateral soil resistance). However, the effect of the scour width on the *p-y* curve at different soil depth varied. For example, at d = 0.4 D, a considerable difference in the *p-y* curves was found at the scour widths between 0 and 3 D; at d = 1 D, a considerable difference was observed at the scour widths between 0.5 and 6 D; at d = 2 D, it was

found at the scour widths between 1 and 8 *D*. This finding provides a clue that each scour width has its influence range of soil depths.

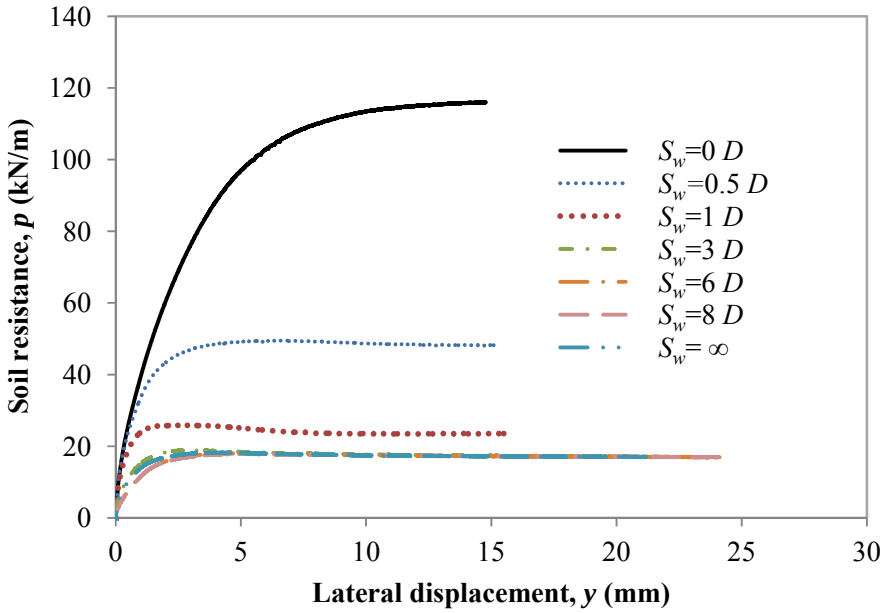

Figure 5-25. Effects of the scour depth on the *p*-*y* curve at soil depth, $d = 0.4\ D$ ($S_d = 3\ D$ and $\theta = 39^\circ$)

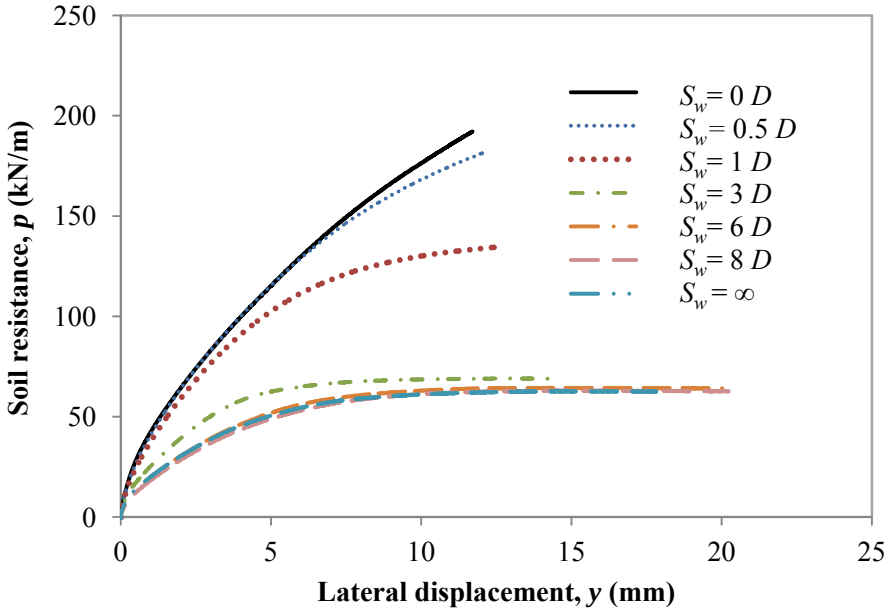

Figure 5-26. Effects of the scour depth on the *p-y* curve at soil depth, d = 1 D (S_d = 3 D and θ = 39°)

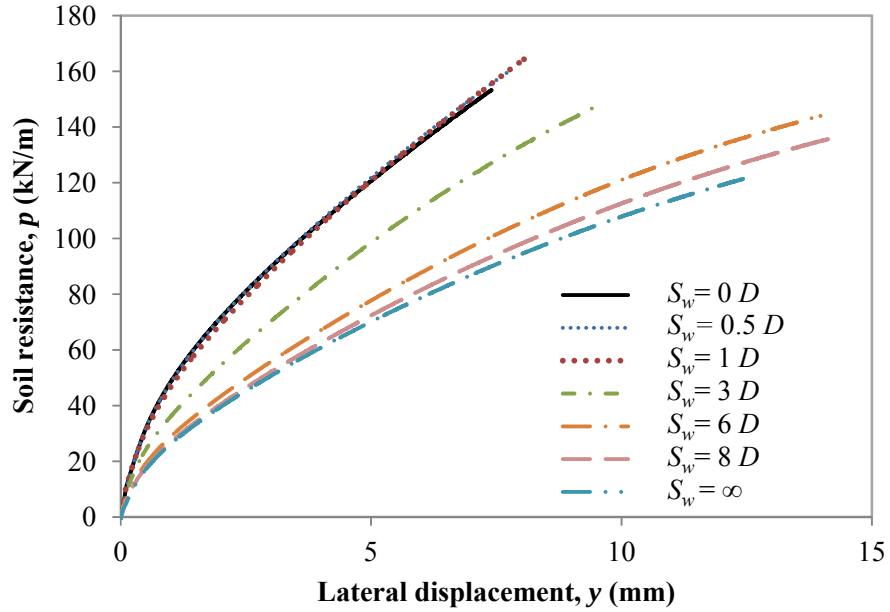

Figure 5-27. Effects of the scour depth on the *p-y* curve at soil depth, d = 2 D (S_d = 3 D and θ = 39°)

5.3.2.4 Profiles of bending moment, shear force, and lateral displacement

As compared with the profiles in soft clay, the profiles of bending moment, shear force, and lateral displacement were more considerably influenced by the scour width. Figure 5-28 shows the profiles of the bending moment and shear force at the scour depth of 3 *D* under the lateral load of 100 kN. It is evident that at the same scour depth, an increase of the scour width moved the profiles of the bending moment and shear force gradually downward to greater depths. At the scour depth of 3 *D*, the maximum bending moment shifted its location from -2.85 to -3.45 m (in reference to the pre-scour mudline) when the scour width was increased from zero to infinite. At the same time, the negative maximum shear force moved from -4.77 to -5.85m. At a greater scour depth, the shift of the locations was increased. For example, at the scour depth of 6 *D*, even though not presented herein, the location of the maximum bending moment and negative maximum shear force moved down from -4.32 to -5.04 m and from -6.36 to -7.68 m respectively. Moreover, with an increase of the scour width, the maximum bending moment increased, while the negative maximum shear force was generally unchanged. In general, the consideration of the scour width increased the resistance of the pile to scour by reducing the bending moment and the influence to the greater depth. The greater scour depth was, the more it was benefited.

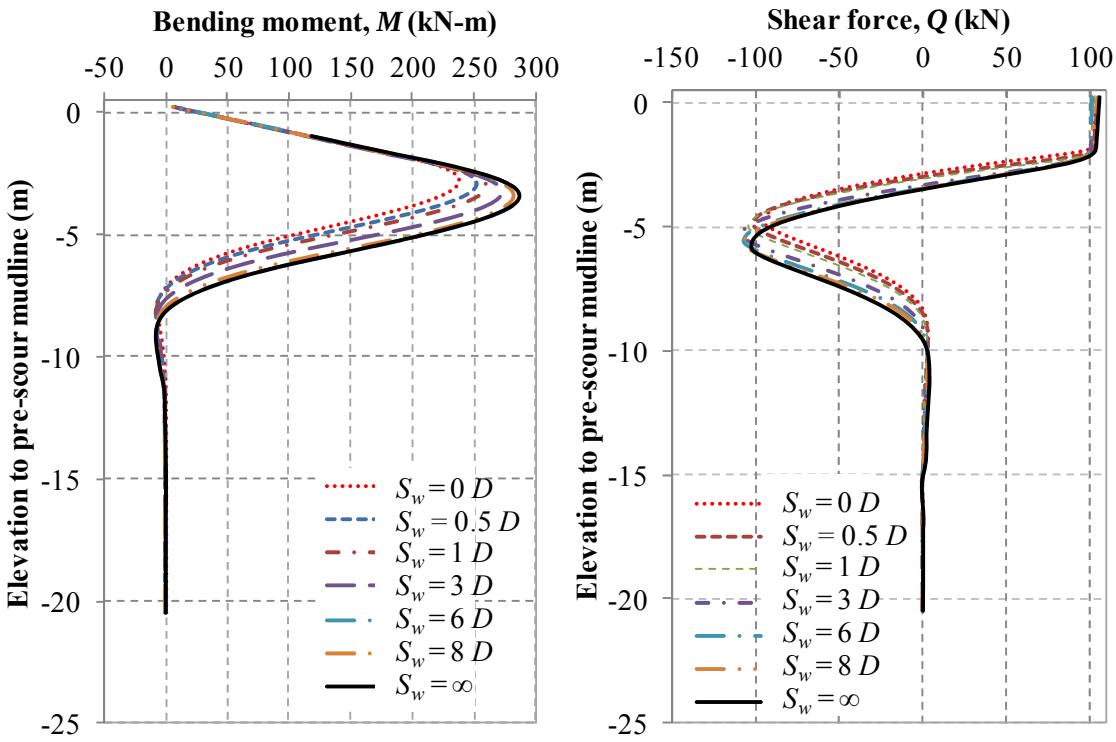

Figure 5-28. Profiles of bending moment and shear force at different scour widths (F_t=100 kN and S_d=3 D)

5.3.3 Effects of scour-hole slope angle

In the previous analyses, the slope angle was set at the friction angle of the sand (i.e. ϕ' =39˚), which is the maximum angle at which the scour-hole slope could maintain. In this section, six slope angles (i.e. $\theta = \phi'$, 0.9 ϕ', 0.8 ϕ', 0.6 ϕ', 0.3 ϕ', and 0) were selected to evaluate the effects of the slope angle on laterally loaded pile behavior. One scour depth (i.e. S_d = 3 D) and two scour widths (i.e. S_w = 0 and 3 D) were chosen in this numerical simulation.

5.3.3.1 Lateral load versus ground line displacement

The lateral load versus ground line displacement curves (F_t -y_g curves) at various slope angles are presented in Figures 5-29 and 5-30. As the slope angle decreased, the F_t -y_g curve approached to the curve without the scour hole effects (i.e., $\theta = 0^{\circ}$). The slope angle between 1 and 0.8 ϕ' had an insignificant effect on the F_t -y_g curve. Moreover, the effects of the slope angle on the change of the F_t -y_g curve decreased as the scour width increased as compared in Figures 5-29 and 5-30. A closer investigation of the ground line displacement versus slope angle in Figure 5-31 clearly reveals the following findings: the maximum decrease of the ground line displacement due to the slope angle was 36% at $S_w = 0$ or 11% at $S_w = 3\ D$.

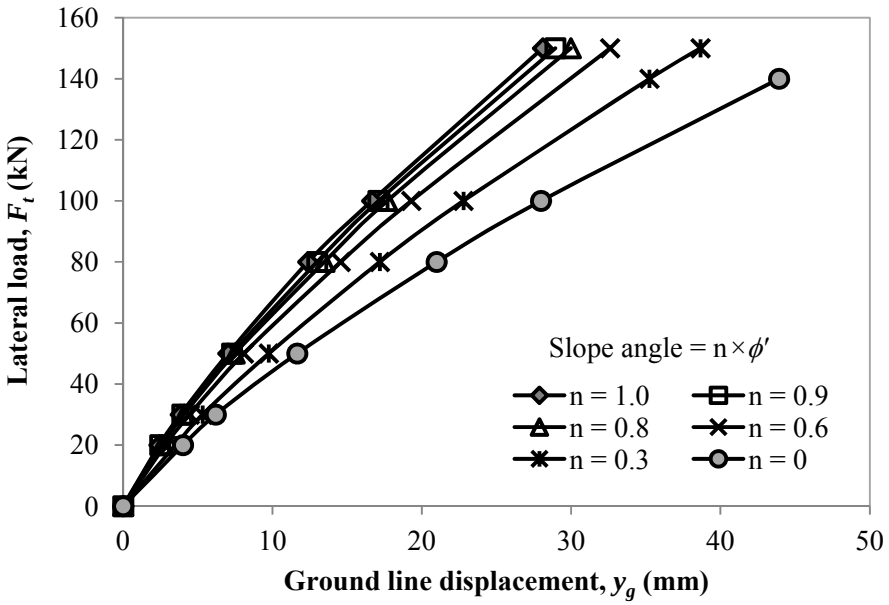

Figure 5-29. Lateral load versus ground line displacement at different scour-hole slope angles ($S_d = 3\ D$ and $S_w = 0$)

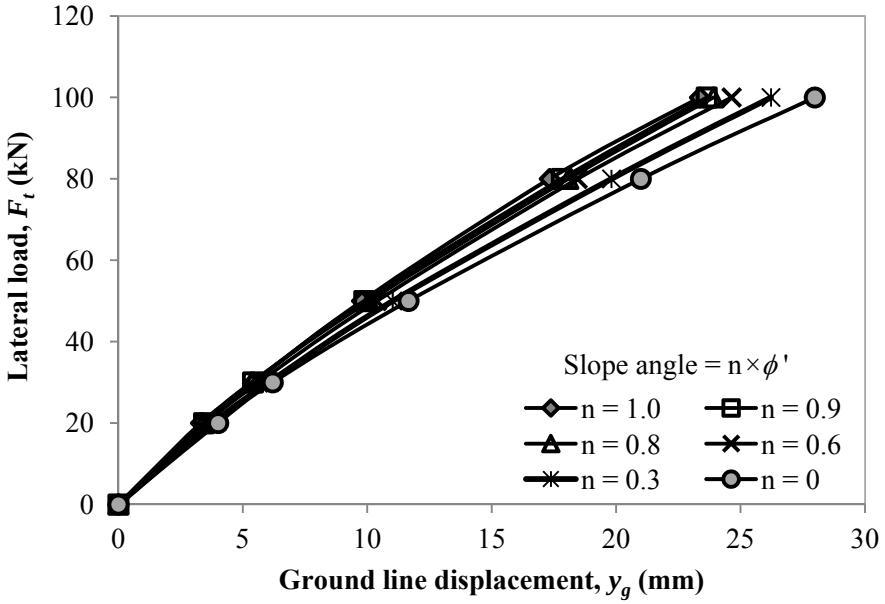

Figure 5-30. Lateral load versus ground line displacement with different scour-hole slope angle (S_d = 3 D and S_w = 3 D)

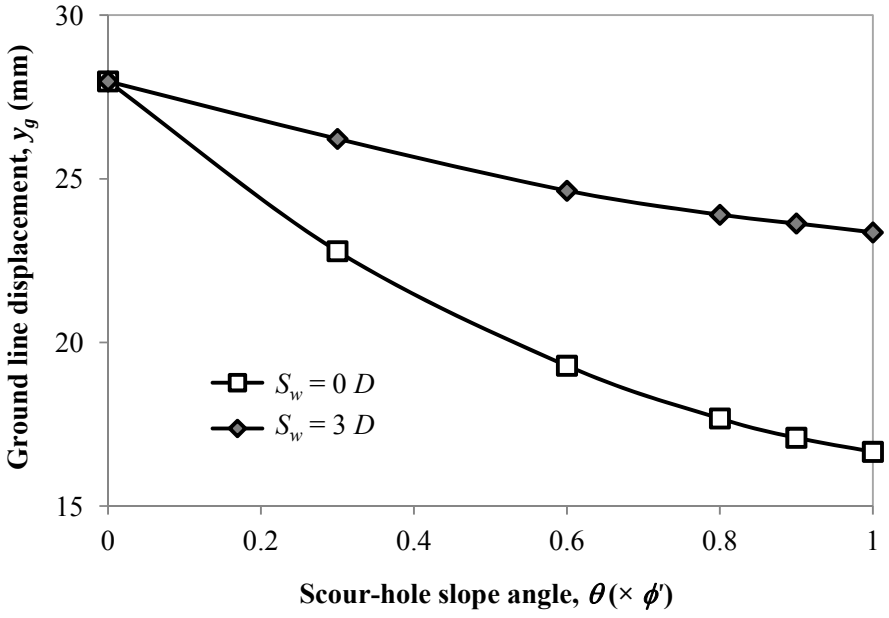

Figure 5-31. Ground line displacement versus scour-hole slope angle (S_d = 3 D and F_t = 100 kN)

5.3.3.2 Allowable lateral load capacity

Figure 5-32 shows that the lateral load capacity of the pile increased with an increase of the slope angle, but the allowable ground line displacement decreased gradually with the slope angle. The maximum increase of the lateral load capacity was 21% while the maximum decrease of the ground line displacement was 25%. In other words, the consideration of the slope angle effects increased the lateral load capacity of the pile. This result can be explained as the overburden stress induced by the remaining soils above the post-scour mudline contributed to the soil resistance to the pile. The slope at a larger angle around the pile applied a higher overburden stress and thus increasing the soil resistance. The increased soil resistance led to the increase of pile lateral load capacity.

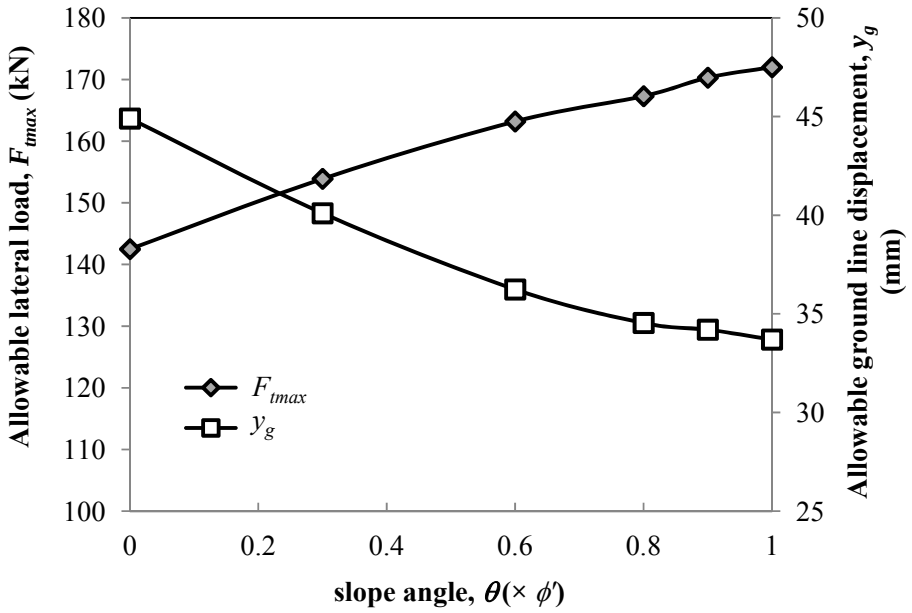

Figure 5-32. Allowable lateral load and ground line displacement versus scour-hole slope angle (S_d = 3 D and S_w = 0)

5.3.3.3 The p-y curves

Figures 5-33 and 5-34 show the *p-y* curves at different slope angles. It is shown that the slope angle had a significant effect on the soil resistance with the maximum increase of the ultimate soil resistance by more than six times at $d = 0.4\ D$. The slope angle also increased the *p-y* stiffness; however, its effect was less significant at the slope angle between 0.8 and 1 ϕ' than that at other slope angles (i.e. $\theta = 0.8\ \phi'$ *to* 0).

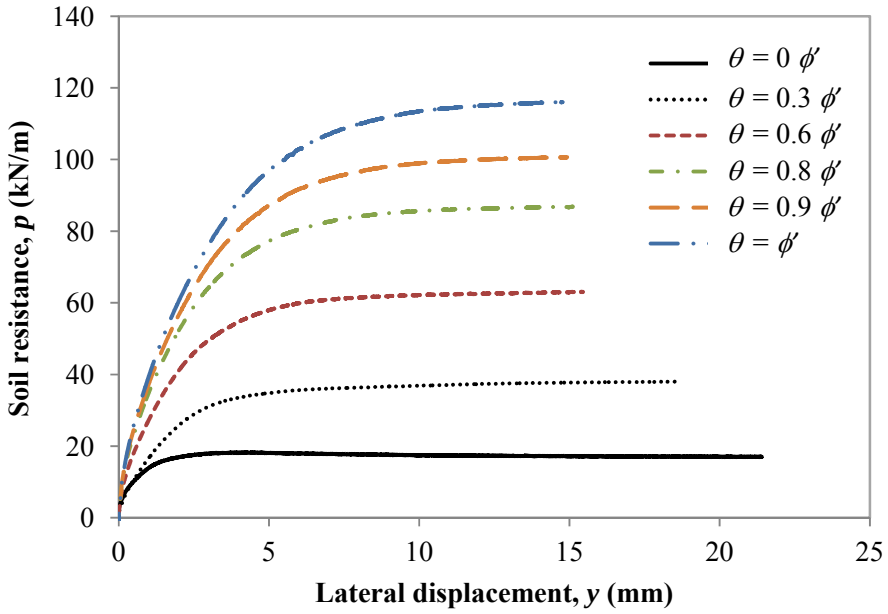

Figure 5-33. The *p-y* curves at soil depth, $d = 0.4\ D$ at various scour-hole slope angles ($S_d = 3\ D$ and $S_w = 0$)

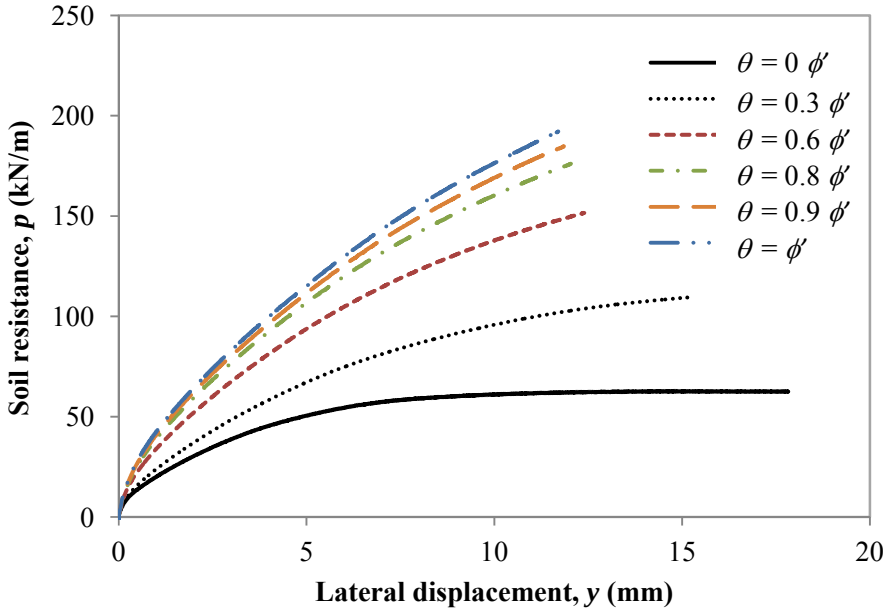

Figure 5-34. The *p*-*y* curves at soil depth, $d = 1\ D$ at various scour-hole slope angles ($S_d = 3\ D$ and $S_w = 0$)

5.4 Summary

Scour-hole dimensions were investigated in the 3D finite difference method incorporated in *FLAC*^{3D} was adopted to investigate the effects of scour-hole dimensions on the behavior of the laterally loaded single pile in sands. Three key influence factors including scour depth, scour width, and scour-hole slope angle were considered. Before the parametric study, the 3D finite difference model was pre-analyzed and calibrated to ensure the accuracy of the model. The following conclusions can be made from this study:

(1) For the 3D finite difference model based on the pile lateral load test in Mustang, Texas (Reese et al. 1974), the boundary effects were eliminated when the horizontal distance from the pile periphery was greater than 24 *D* (*D* is the diameter of the pile)

and the vertical distance from the pile tip to the bottom of the mode was 0.24 L (L is the length of the pile).

(2) The numerical results were more sensitive to the interface strength than the interface stiffness. The model with the interface friction angle of 0.5ϕ' (ϕ' is the effective friction angle of sand) resulted in a favorable comparison with the measured. The stress-dependent elastic modulus was successfully used for sands to describe the effects of the scour-hole dimensions on the change of the soil properties.

(3) The scour depth influenced the laterally-loaded pile behavior more significantly than the scour width and slope angle. The ground line displacement decreased nonlinearly with the scour depth, which was more remarkable at a high loading level. At a large scour depth, the laterally-loaded pile behavior in sand was primarily dependent on the behavior of the pile material itself. A strong pile section above the post-scour mudline was needed to transfer the applied lateral load from the pile head to the lower surrounding soils. The allowable lateral load capacity decreased substantially with the scour depth and the rate of the decrease was reduced with an increase of the scour depth. The reduction in the lateral load capacity reached 66% when the scour depth was increased from 0 to 6 D. The allowable ground line displacement was increased between 5% and 14% D with the scour depth. The p-y curve was significantly influenced by the scour depth, but the degree of influence gradually decreased with an increase of the scour depth. Under the same applied lateral load, the maximum bending moment and negative maximum shear force increased rapidly with an increase of the scour depth. When the scour depth increased, the elevation of the maximum bending moment at a certain applied load moved away from the pre-scour mudline but shifted toward the post-scour mudline. Moreover, when the scour depth was greater than 3 D, the negative maximum shear force even exceeded the

applied lateral load, which raised the concerns of potential shear failure under extreme scour events.

(4) The ground line displacement increased significantly with an increase of the scour width and the maximum increase of the displacement was as high as 40%. The influence of the scour width depended more on the scour depth than the loading level. At the scour depths of 1, 3, and 6 *D*, the influence scour widths were 6, 8, and 12 *D,* respectively.

(5) The scour-hole slope angle also affected the laterally-loaded pile behavior. With an increase of the slope angle, the ground line displacement decreased, with the maximum decrease of 36%. However, the effects of the slope angle became less as the scour width increased. The slope angle increased the allowable lateral load capacity of the pile, with the maximum increase of 21%.

CHAPTER 6

SIMPLIFIED METHODS FOR ANALYZING LATERALLY LOADED PILES CONSIDERING SCOUR-HOLE DIMENSIONS

Three-dimensional finite difference modeling provides comprehensive insights into the effects of scour-hole dimensions on the behavior of laterally loaded piles. However, it has some drawbacks such as computation inefficiency and operation complexity. Due to these limitations, 3D numerical modeling has not been widely used to analyze or design laterally loaded piles in practice. Instead, the one-dimensional *p-y* curve method is well accepted in practice because it is easy to use and has been well developed based on full-scale experimental data. Unfortunately, the conventional *p-y* curve method has not been developed to address the problems pertaining to scour-hole dimensions. To this end, a simplified method that is capable of considering the effects of scour-hole dimensions is needed for analyzing laterally loaded piles in scour events. In this study, a simplified method was developed based on the conventional *p-y* curves (e.g. Matlock's soft clay and Reese's sand) by modifying them to accommodate the effects of the scour-hole dimensions. In this chapter, the solutions of the simplified method are first derived; then the derived solutions are verified with the results that are obtained from the 3D finite difference modeling; finally, discussion is made on the simplified method considering the contributions of remaining overburden soils. The simplified solutions cover the laterally loaded piles in soft clay and sand.

6.1 The Simplified Method for Laterally Loaded Piles in Soft Clay

In the *p-y* curve method, it is essential to solve for the equations of a beam in the Winkler foundation for a laterally-loaded pile. As stated in Chapter 1, the laterally loaded pile is described by a governing equation of the beam (Equation 2.10) and the Winkler foundation is represented

by a series of nonlinear springs which are described by families of *p-y* curves (Figure 2-9). For soft clay, Matlock's *p-y* curves (Matlock 1970) as illustrated in Equations 3.1 to 3.4 have been widely used in practice. However, as discussed in Chapter 4.2, the Matlock's *p-y* curves resulted in much higher soil stiffness than the reality because the *p-y* curves do not introduce a reasonable coefficient of subgrade reaction. As a result, this *p-y* curve method often yields much smaller displacement than the experiment, for example, as shown in Figure 4-6. In the next section, a simplified approach is developed by modifying Matlock's *p-y* curve method to accommodate the effects of the scour-hole dimensions, such as scour depth, scour width, and scour-hole slope angle.

6.1.1 Derivation of the simplified method

The basic concept for deriving the simplified solution is to seek an equivalent failure wedge that has the same ultimate soil resistance as the failure wedge considering the scour-hole dimensions, as shown in Figure 6-1. With the equivalent ultimate soil resistance, the soil depth, *Z*, of the equivalent failure wedge as shown in right part of the figure is computed. By substituting *Z* for the *z* in Equation 3.3, Matlock's *p-y* curve is updated to be able to consider the effects of the scour-hole dimensions.

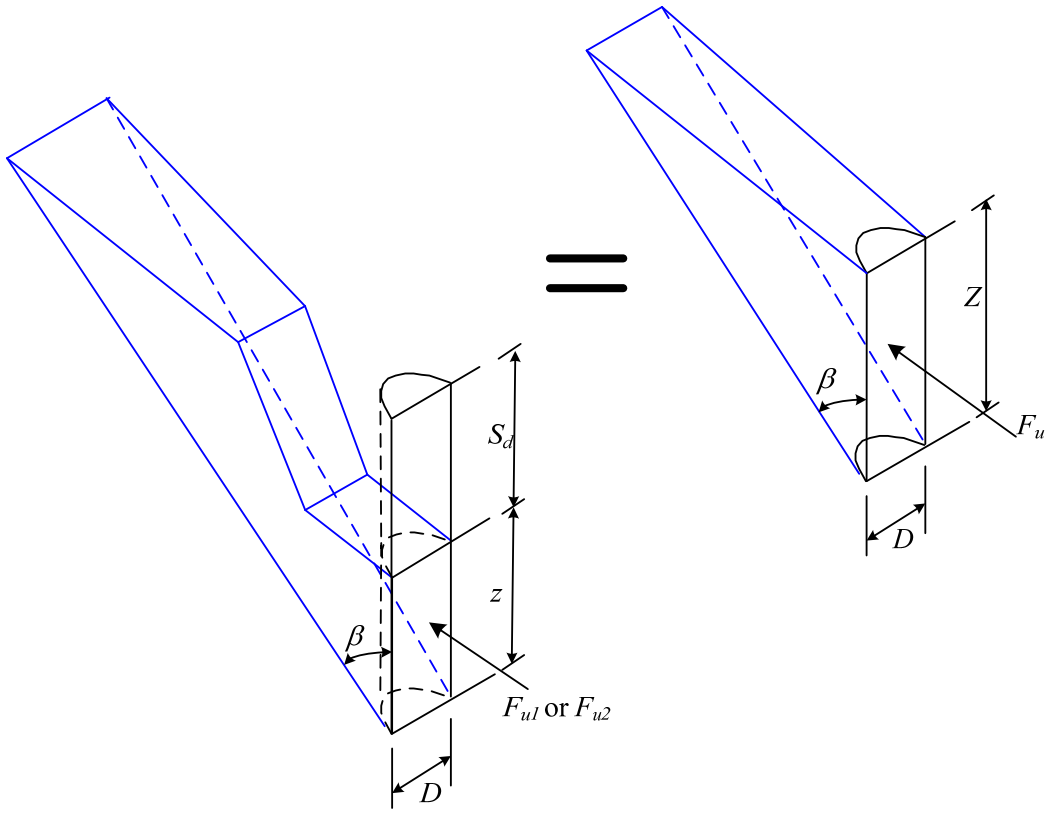

Figure 6-1. Failure wedges for the ultimate soil resistance of the pile in clay with scour-hole dimensions

The above process assumes the scour-hole dimensions only have an effect on the ultimate soil resistance near the ground surface but not at a great depth. This assumption is reasonable because laterally loaded piles are mainly influenced by the soils at the shallow depth and the plane undrained failure at a deep location is not influenced by overburden stress. Additionally, the scour-hole slope surface that the failure wedge encompasses is assumed to be planar (Figure 6-1) instead of the envisioned curved shape in the 3D finite difference model (Figure 4-13). Since the scour hole that the wedge failure contains is rather smaller than the whole scour hole, plus the planar slope surface of the scour hole differs slightly from the curved slope surface in terms of overburden stress, the errors caused by the second assumption are expected to be

negligible. It should be pointed out that although Matlock's *p-y* curve is not rigorously developed based on the wedge failure mode, its empirical equation of the ultimate soil resistance for the upper zone (Equation 3.3) corresponds to the one (Equation 3.25) established on the wedge failure model (Reese et al. 1975). For example, both equations contain the soil resistance from the surface and geometrical restraint and the overburden stress (Matlock 1970), only slightly differing in the value of some factors. It is believed that the additional soil resistance due to the remaining overburden soils above the post-scour mudline derived in the wedge model (the left one in Figure 6-1) is equal to the increase of the soil resistance in Matlock's *p-y* curve. As a result, the equivalent failure wedge concept is used to modify Matlock's *p-y* curve to consider the effects of scour-hole dimensions. For the equivalent failure wedge without scour hole (right one in Figure 6-1), the ultimate soil resistance force can be determined by (Reese et al. 1975):

$$F_u = \frac{1}{2}\gamma' DZ^2 + 2C_u DZ + \sqrt{2}C_u Z^2 \qquad 6.1$$

where D = width or diameter of the pile, m; Z = equivalent soil depth measured from the ground surface of the equivalent wedge, m; C_u = undrained shear strength, kPa; γ' = effective unit weight of the soil, kN/m^3.

Once the ultimate soil resistance, F_u, is known from Equation 6.1, the equivalent soil depth, Z, can be determined. The F_u value can be obtained from the ultimate soil resistance that is computed based on the failure wedge with the scour-hole dimensions, that is $F_u = F_{u1}$ or $F_u = F_{u2}$, as illustrated in Figure 6-1.

To determine the ultimate soil resistance (F_{u1} or F_{u2}), a detailed wedge failure mode from the side view, as presented in Figure 6-2, is proposed for the derivation. In the figure, z is the soil

depth at failure measured from the post-scour mudline, which also indicates the location of the failure plane. As anticipated, the ultimate soil resistance depends on the scour depth, scour width, and scour-hole slope angle. The figure indicates that the value is also influenced by the soil depth at failure, z, and slope failure angle.

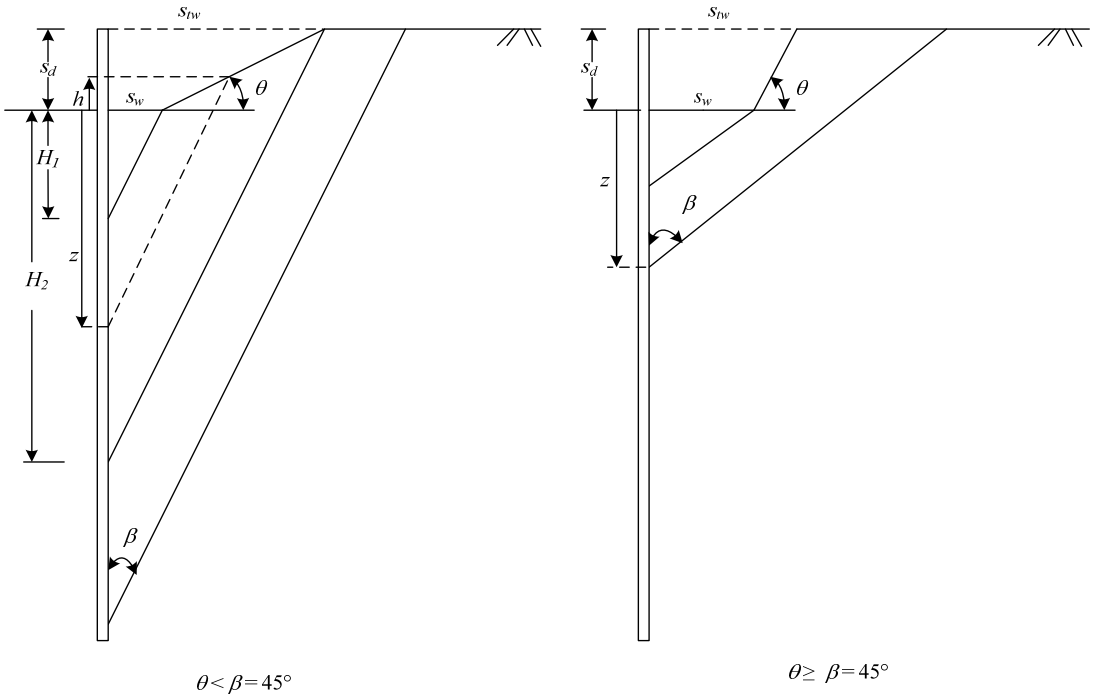

Figure 6-2. Side view of the wedge failure mode for the ultimate soil resistance of the pile in clay

For fully saturated and undrained clays, the failure slope angle is 90˚-β where β is 45˚. The solution varies according to the relative difference between the scour-hole slope angle (θ) and the slope failure angle. For $\theta < 90˚\text{-}\beta$, the failure plane passes through the scour-hole slope when z is between H_1 and H_2; however, for $\theta \geq 90˚\text{-}\beta$, the failure plane will never be able to cross the scour-hole slope surface. From Figure 6-2, H_1 and H_2 can be derived to be S_w and S_w+S_d/D_1 where S_w and S_d are scour width and depth, and D_1 is given by

$$D_1 = \frac{\tan\theta}{1-\tan\theta} \tag{6.2}$$

For $\theta < 90^\circ - \beta = 45^\circ$, the ultimate soil resistance can be determined as follows:

$$0 < z \le H_1 \qquad F_u = F_{u0} \tag{6.3}$$

$$H_1 < z \le H_2 \qquad F_u = F_{u1} \tag{6.4}$$

$$z > H_2 \qquad F_u = F_{u2} \tag{6.5}$$

For $\theta \ge 90^\circ - \beta = 45^\circ$, the ultimate soil resistance can be determined as follows:

$$0 < z \le H_1 \qquad F_u = F_{u0} \tag{6.6}$$

$$z > H_1 \qquad F_u = F_{u2} \tag{6.7}$$

In Equations 6.3 to 6.7, F_{u0}, F_{u1}, and F_{u2} are given by:

$$F_{u0} = \frac{1}{2}\gamma' D z^2 + 2C_u D z + \sqrt{2} C_u z^2 \tag{6.8}$$

$$\begin{aligned} F_{u1} &= \frac{1}{2}\gamma' D\left[z^2 + D_1 (z - S_w)^2\right] \\ &+ 2C_u D\left[z + (z - S_w) D_1\right] + \sqrt{2} C_u \left[z^2 + D_1 (z - S_w)^2\right] \end{aligned} \tag{6.9}$$

$$F_{u2} = \frac{1}{2}\gamma' D\left[(z+S_d)^2 - (2S_w + S_d / \tan\theta)S_d\right] + 2C_u D(z+S_d) + \sqrt{2}C_u\left[(z+S_d)^2 - (2S_w + S_d / \tan\theta)S_d\right] \quad 6.10$$

Note that for $z < H_1$, the ultimate soil resistance, F_{u0}, is determined at soil depth, z, based on the wedge failure mode without a scour hole. By comparing Equation 6.1 with 6.8, it can be determined that the equivalent soil depth, Z, should be equal to z. For $H_1 < z < H_2$, the failure plane intersects the scour-hole slope surface at the line situated h above the post-scour mudline (Figure 6-2), in which h is calculated in Equation 6.11; the ultimate soil resistance is calculated using Equation 6.9. By equating Equation 6.9 to 6.1, it is expected that the value of Z falls between z and z + h, and can be determined by adding a reduction factor to h as shown in Equation 6.12. For z > H_2, the failure plane falls behind the scour-hole slope, and the ultimate soil resistance is calculated using Equation 6.10; similarly, the Z value is expected to fall between z and z + S_d and can be determined in Equation 6.13. The above calculation is for the case with θ < 45˚. For the case with $\theta \geq 45$˚, the Z value is equal to z when $z \leq S_w$; however, the Z value is obtained from Equation 6.13 when $z > S_w$.

$$h = (z - S_w)D_1 \quad 6.11$$

$$Z = z + f_{sd}h \quad 6.12$$

where f_{sd} = a reduction factor for h and S_d , and $0 \leq f_{sd} < 1$

$$Z = z + f_{sd} S_d \qquad 6.13$$

The reduction factor f_{sd} accounts for the situation that the remaining overburden soils above the post-scour mudline (termed as the remaining overburden soils for short) can be equivalent to a certain thickness of soil layer (i.e. $f_{sd}h$ or $f_{sd}S_d$) on top of the post-scour ground surface. The value of f_{sd} can be determined by substituting Equations 6.12 and 6.13 into Equation 6.1, and then using one of Equations 6.3 to 6.7 based on the location of failure plane (z).

In general, the simplified approach is developed by seeking the equivalent soil depth at failure, Z that develops the same ultimate soil resistance with the soil depth, z, at which the wedge with the scour-hole dimensions fails. By applying updated soil depth, Z, to the equations 3.1 to 3.4 (i.e. substituting Z for z), the conventional Matlock's *p-y* curve is then modified to account for effects of the scour-hole dimensions.

6.1.2 Verification of the simplified method

The simplified method is verified against the numerical results from the 3D finite difference analysis of the pile in soft clay as presented in Chapter 4. The procedure of the simplified method would be easily added to *LPILE* if the *LPILE* source codes were allowed for such a modification; otherwise, the modified *p-y* curves have to be generated in spreadsheet or other tools based on the foregoing descriptions and then input into the *LPILE*. However, this process would be rather troublesome and time-consuming because large amounts of *p-y* data need to be manually input to *LPILE*. A program so-called Soil Spring Module (*SSM*) was written using Visual Basic 2010 Express, which can generate *p-y* curves and converts them into nonlinear

soil springs. The *SSM* is seamlessly linked to structural code, *STAAD.Pro* where the structure model with soil supports can be analyzed. The *SSM* plus *STAAD Pro* (called *SSM* for short) possess the same analysis capacity and can produce similar results as *LPILE* does. Development of *SSM* will be presented in details in Chapter 7.

To compare with the results of 3D finite difference analysis, the current analysis also employed the conditions of the Lake Austin test and the scour-hole dimensions. The required parameters for *SSM* are the same as those for *LPILE*, including pile parameters (Table 3-2) and soil parameters (using C_u, γ', and ε_{50} in Table 3-1). A variety of scour depths, scour widths, and scour-hole slope angles as investigated in $FLAC^{3D}$ were also analyzed using the simplified method. For the purpose of verification, only the lateral load versus pile-head displacement curves (F_t-y_t curves) were compared.

6.1.2.1 Effects of scour depth

Four scour depths (i.e. 1, 3, 6, and 8 D) were investigated using the simplified method when scour-hole slope angle was 40˚ and scour width was 0 and ∞. As abovementioned, the *SSM* produces a slightly larger lateral displacement than the *LPILE*, as shown in Figure 6-3. To be consistent, the results from *SSM* were corrected with *LPILE* as follows: a correction factor, R_c, was first determined by dividing the lateral pile-head displacement (y_t) from *SSM* to that from *LPILE* at the same lateral load when the scour-hole dimensions (i.e. S_w= ∞) were ignored; lateral pile-head displacement that was calculated in *SSM* when scour-hole dimensions were considered, was corrected by dividing it by the R_c.

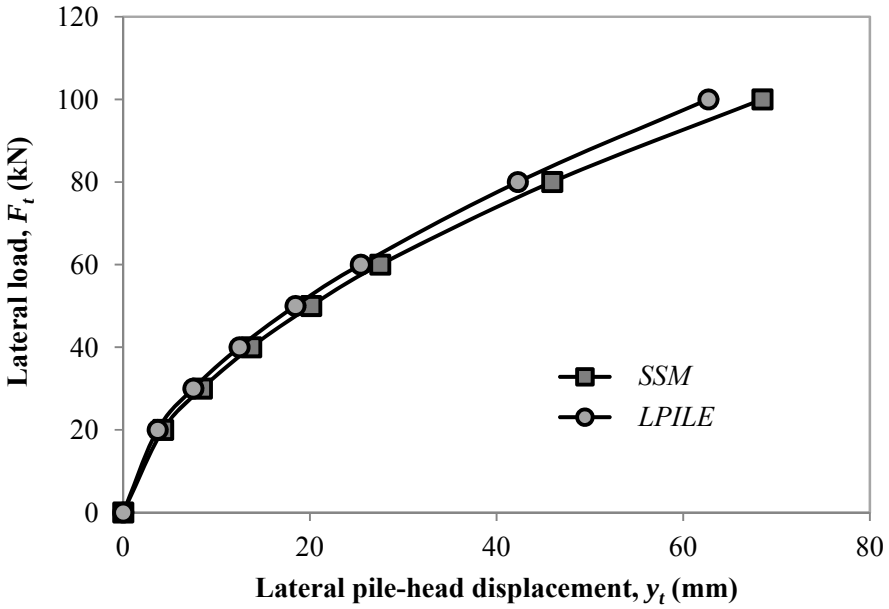

Figure 6-3. Lateral load versus pile-head displacement (S_d = 1 D and S_w= ∞)

The lateral pile-head displacement results from *SSM* presented below are corrected ones. The lateral load versus pile-head displacement curves at different scour depths are presented in Figure 6-4. The simplified method incorporated in *SSM* resulted in smaller displacements (in dash lines) than *FLAC*^{3D} (in solid lines) at lower loading levels. This discrepancy is expected as discussed in Chapter 4, i.e., Matlock's *p-y* curve has higher soil stiffness in the hyperbolic nature. However, at higher loading levels, the results from the simplified method are compared well with those from the 3D finite difference method. In general, the results of the simplified method are expected to be improved once the *p-y* curves for the soft clay are improved.

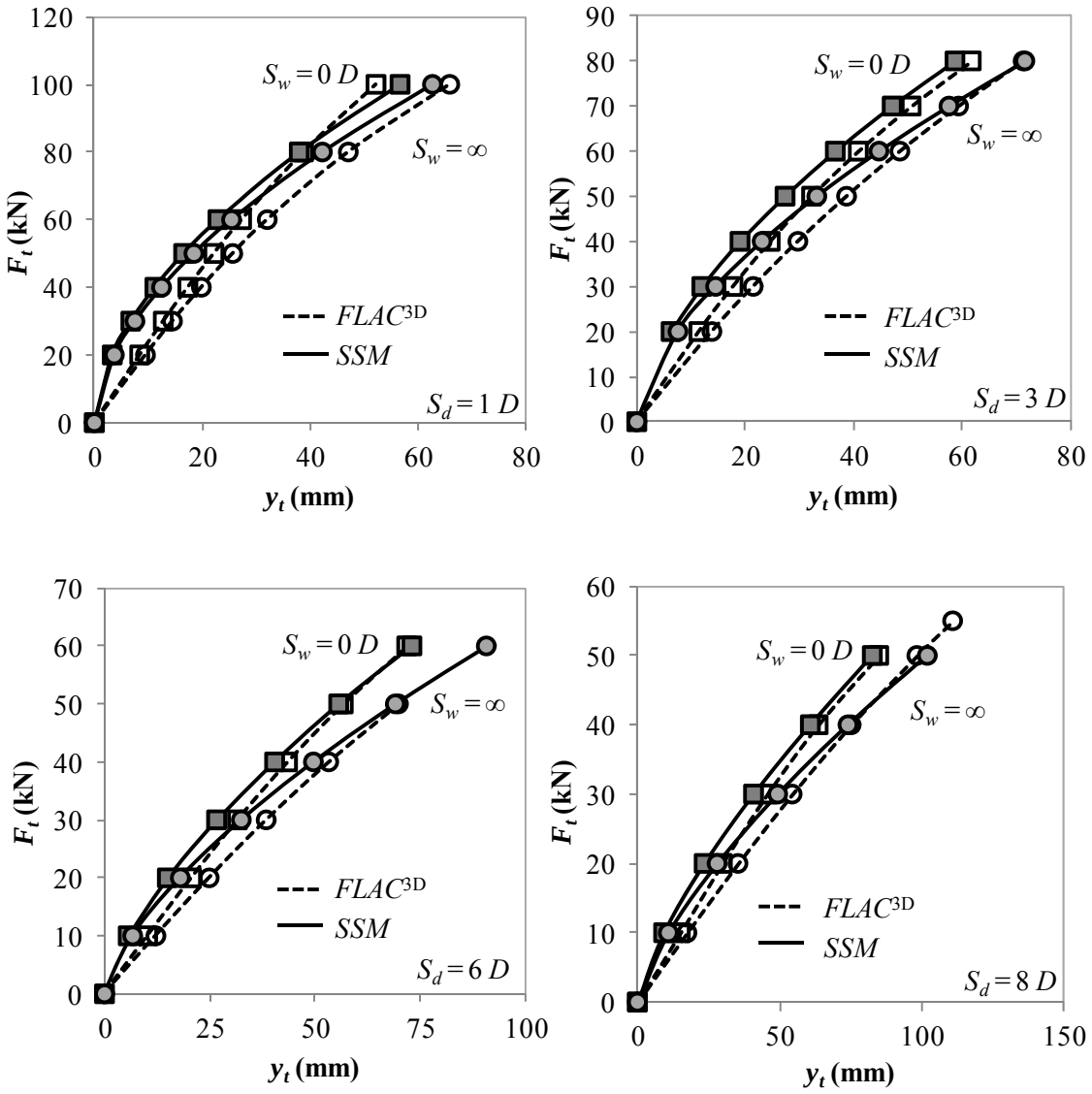

Figure 6-4. Lateral load (F_t) versus pile-head displacement (y_t) at different scour depths (θ =40˚)

To minimize the inherent limitations of Matlock's *p-y* curves, the simplified method could be compared with the 3D finite difference method by focusing on the relative difference of the F_t-y_t curves at different scour widths. Figure 6-4 shows that when the scour width was changed from 0 to ∞, the resulted increase in the lateral pile-head displacement in *SSM* was similar to that in $FLAC^{3D}$. In other words, if the simplified method and the 3D finite difference

method had the similar F_t-y_t curves at S_w=∞, they could generate similar results at S_w=0. From this perspective, the simplified method produced reasonable results that accounted for the effects of the scour-hole depth.

6.1.2.2 Effects of scour width

The effects of the scour width on the lateral pile-head displacement were evaluated using both the simplified method and the 3D finite difference method. The results presented in Figure 6-5 were based on the scour depth of 3 D and the scour-hole slope angle of 40˚. Similarly, at a lower load, the simplified method resulted in a smaller lateral pile-head displacements than the 3D finite difference method; at a higher loading level (e.g. F_t = 80 kN), the simplified method yielded similar results as the 3D finite difference method. Furthermore, the simplified method produced the similar lateral pile-head displacement versus scour width curve as the 3D finite difference method.

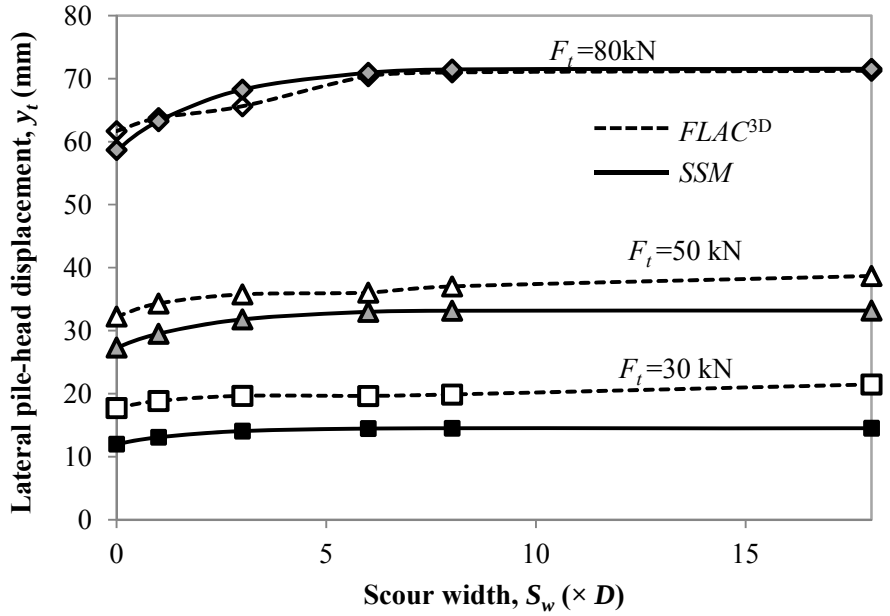

Figure 6-5. Lateral pile-head displacement versus scour width (S_d = 3 D and θ=40˚)

6.1.2.3 Effects of scour-hole slope angle

Figure 6-6 shows the F_t - y_t curves calculated by the simplified method and the 3D finite difference method when the scour-hole slope angle was from 10˚ to 60˚. In general, both methods produced similar results. As compared above, the simplified method and the 3D finite difference method produced the similar results. The simplified method proposed for single piles in soft clay can account for the effects of the scour-hole dimensions including the scour depth, the scour width, and the scour-hole slope angle. Since the simplified method was developed based on the equivalent wedge failure mode, it can also be applied to any *p-y* curves that are developed from the wedge failure concept.

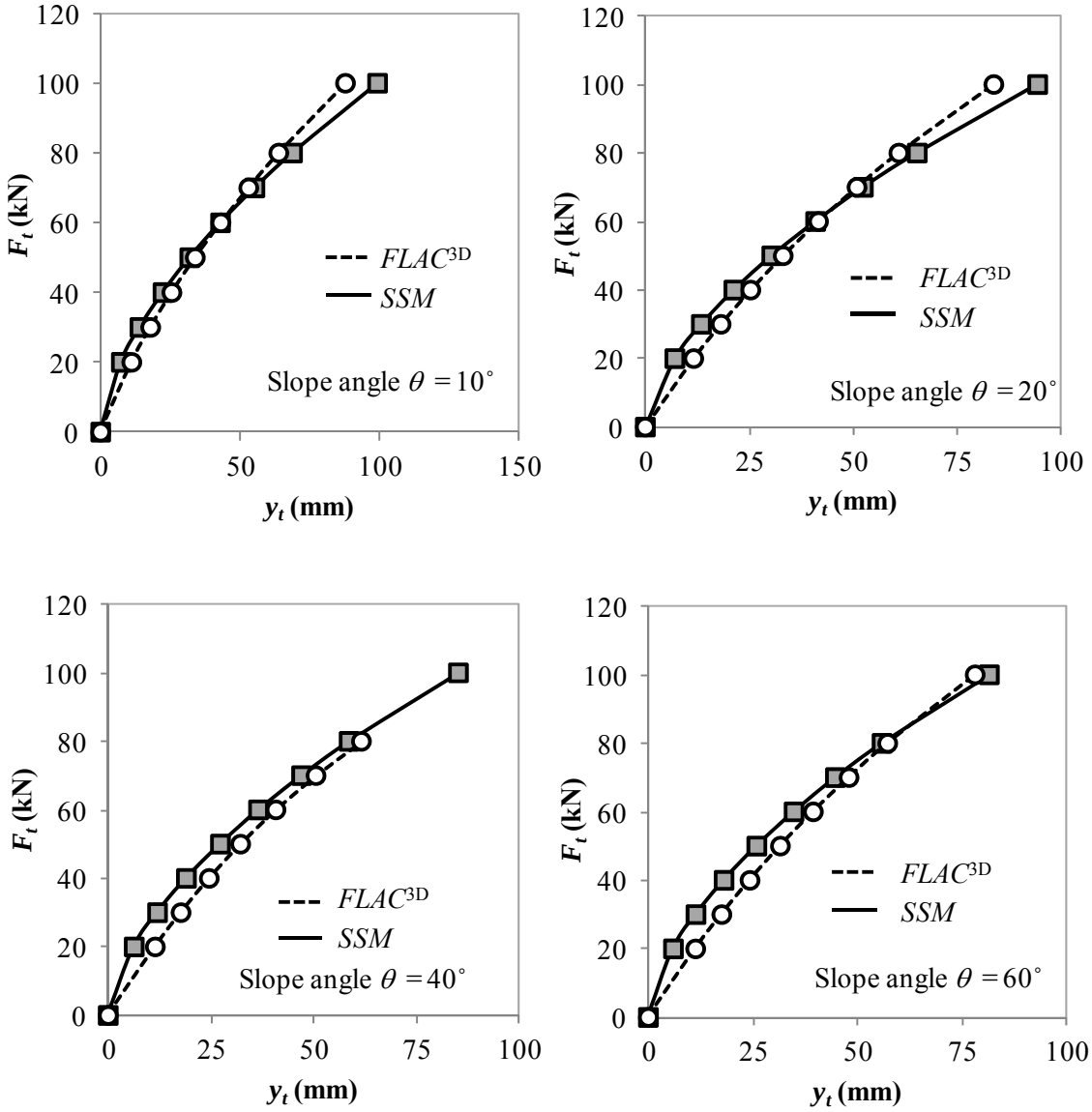

Figure 6-6. Lateral load (F_t) versus pile-head displacement (y_t) curves under different scour-hole slope angles (S_d = 3 D and S_w = 0)

6.1.3 Discussion of the simplified solution

The simplified method was also used to examine the reduction factor, f_{sd}, ratio of the increase of ultimate soil resistance by considering the effects of scour-hole dimensions, R_p, and the *p-y* curves. R_p is defined as ratio of the increase of the ultimate soil resistance per pile length by considering the effects of scour-hole dimensions as compared with that without any scour-hole effects as follows:

$$R_p = \frac{(p_u)_m - (p_u)_u}{(p_u)_u} \qquad 6.14$$

where $(p_u)_u$ = ultimate soil resistance per pile length without any scour-hole effects, kN/m; $(p_u)_m$ = ultimate soil resistance per pile length considering the scour-hole effects, kN/m.

The f_{sd}, R_p, and *p-y* curves are analyzed for the effects of the scour-hole dimensions including the scour depth, scour width, and scour-hole slope angle. Note the soil depth, *d*, is the distance measured from the post-scour mudline as defined in Chapter 4.

Figures 6-7 to Figure 6-9 show that f_{sd} generally increased with the soil depth. However, depending on the soil depth at which the failure plane passed through the scour-hole slope surface, f_{sd}, could decrease and then increase with the soil depth. For example, when both surfaces intersected, the f_{sd} decreased with the soil depth, while when there was no intersection of the surfaces, the f_{sd} increased with the soil depth. As a result, when the scour-hole slope was smaller than the slope failure angle (45˚) (Figure 6-9) or the scour depth was large (Figure 6-7), f_{sd} first decreased and then increased with the soil depth. Furthermore, these figures show that f_{sd} approached to one with an increase of the soil depth. This result indicates that the effects of the

scour-hole dimensions could be ignored during the analysis of laterally loaded piles in soft soil when the soil depth was well below the post-scour mudline.

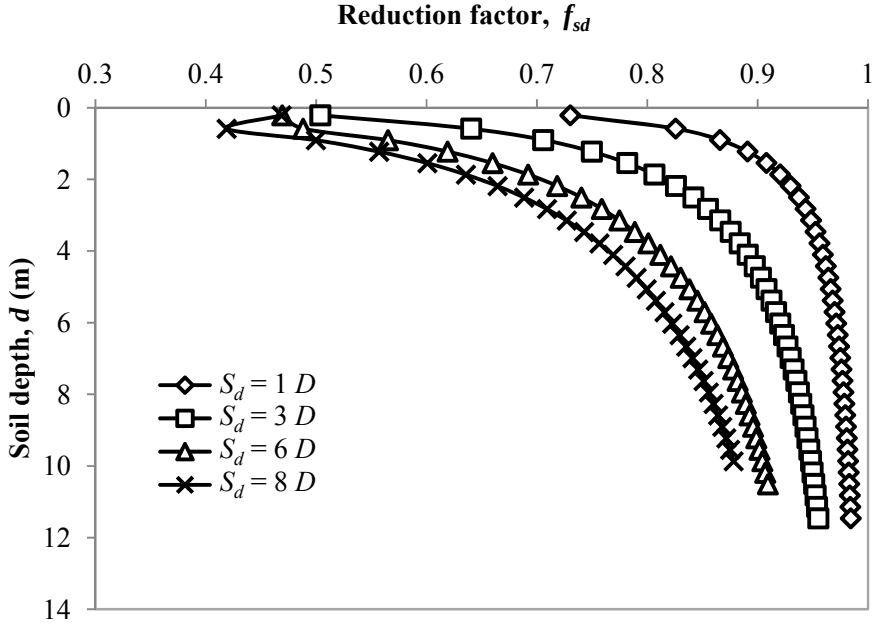

Figure 6-7. Reduction factors at different scour depths (S_w = 0 and θ = 40˚)

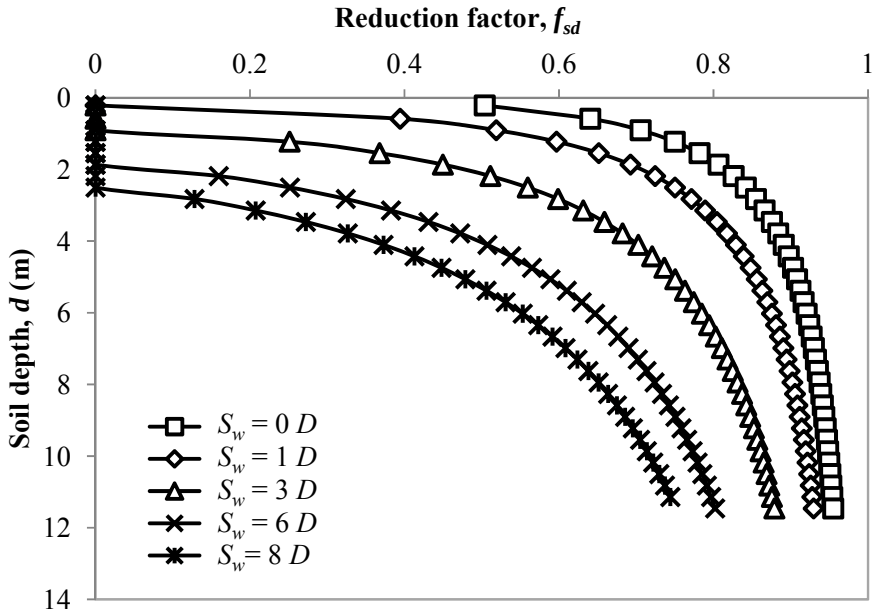

Figure 6-8. Reduction factors at different scour widths (S_d = 3 D and θ = 40˚)

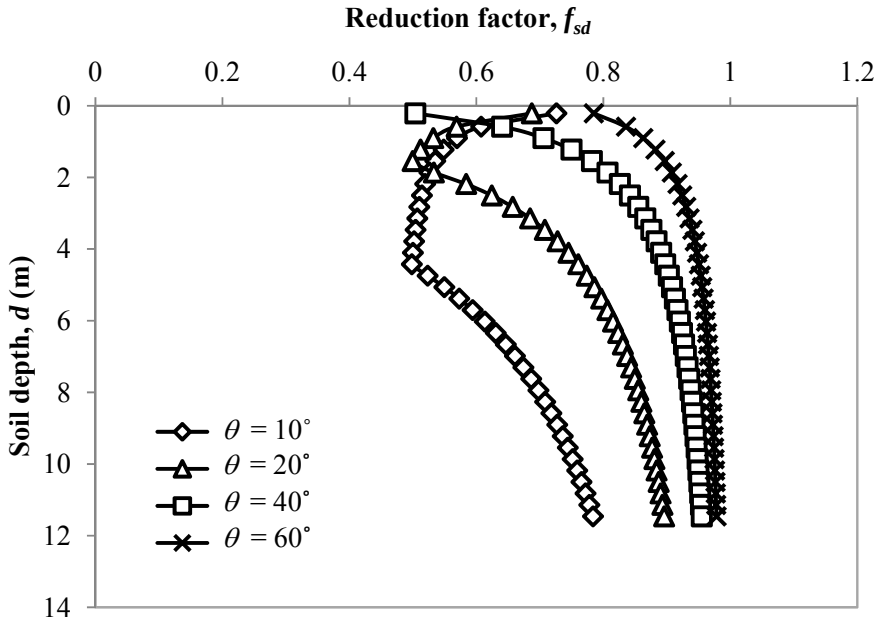

Figure 6-9. Reduction factors at different scour-hole slope angles (S_d = 3 D and S_w = 0)

The reduction factor, f_{sd}, only considered the extent that the remaining overburden soils could be equivalent to a soil layer above the post-scour mudline, but it could not directly indicate how much the remaining overburden soils contributed to the ultimate soil resistance. To this end, ratio of the increase of ultimate soil resistance, R_p, was introduced to examine the benefit of considering the effects of the scour-hole dimensions, as defined in Equation 6.14. Figures 6-10 to 6-12 show that the increase of ultimate soil resistance was limited to certain soil depths, i.e. from the post-scour mudline to 10 D deep. It is clear that the increase of scour depth and slope angle and the decrease of scour width significantly contributed to the increase of the lateral soil resistance to the pile. For example, at the scour depth of 8 D, the ultimate soil resistance increased by 50% by considering the scour-hole effects as presented in Figure 6-10. R_p increased rapidly with an increase of the soil depth, then decreased slowly, and finally decreased dramatically to zero. R_p became zero at a certain soil depth (i.e. d = 3.2 m) because at that location the ultimate soil resistance was controlled by the plane failure rather than the wedge failure. In Figure 6-11, as the scour width increased, the benefit to the soil resistance by considering the effects of the scour-hole dimensions decreased considerably as observed for S_w = 8 D. The location of the maximum R_p shifted downward from the post-scour ground surface when the scour width was increased, but moved upward to the surface when the scour-hole slope angle increased (Figure 6-12).

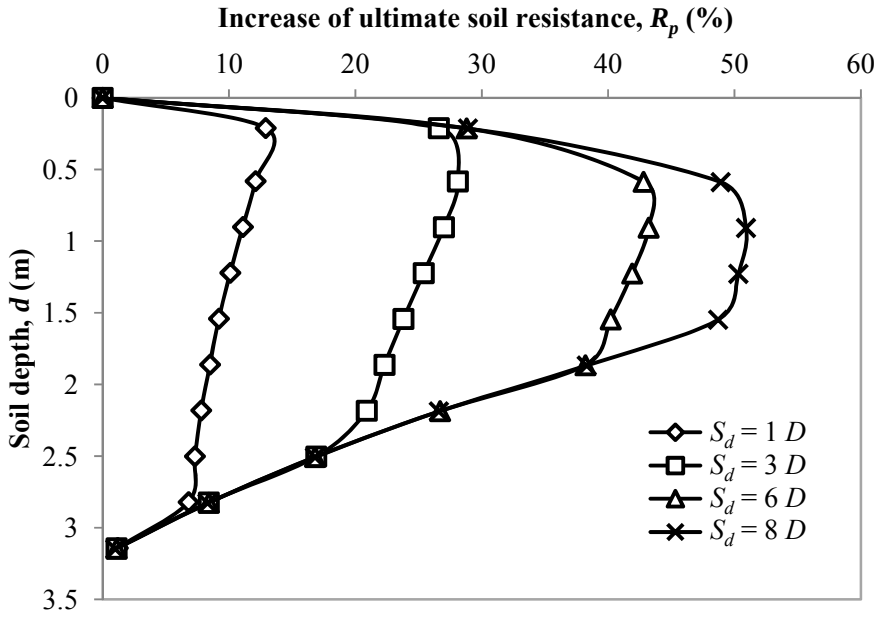

Figure 6-10. Increase of ultimate soil resistance at different scour depths (S_w = 0 and θ = 40˚)

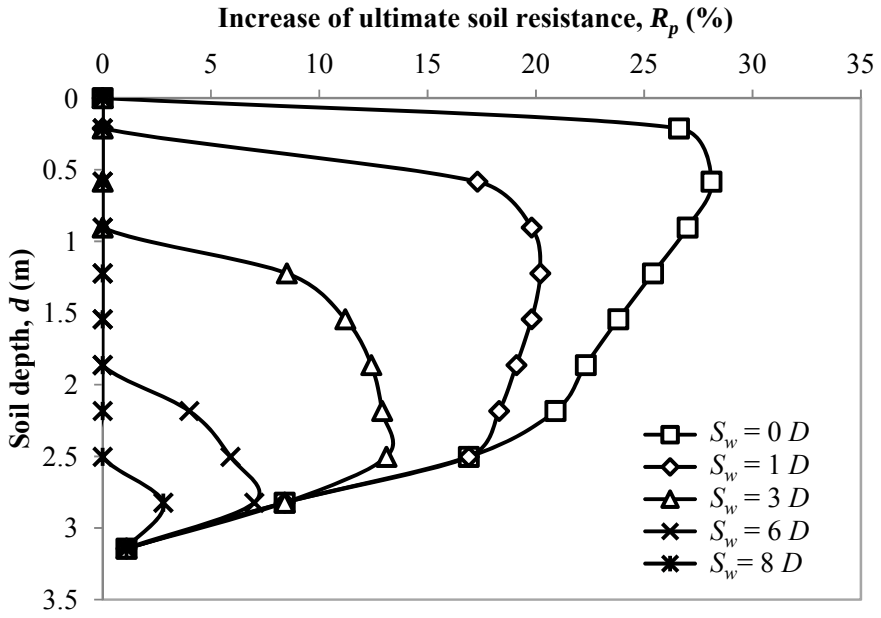

Figure 6-11. Increase of ultimate soil resistance at different scour widths (S_d = 3 D and θ = 40˚)

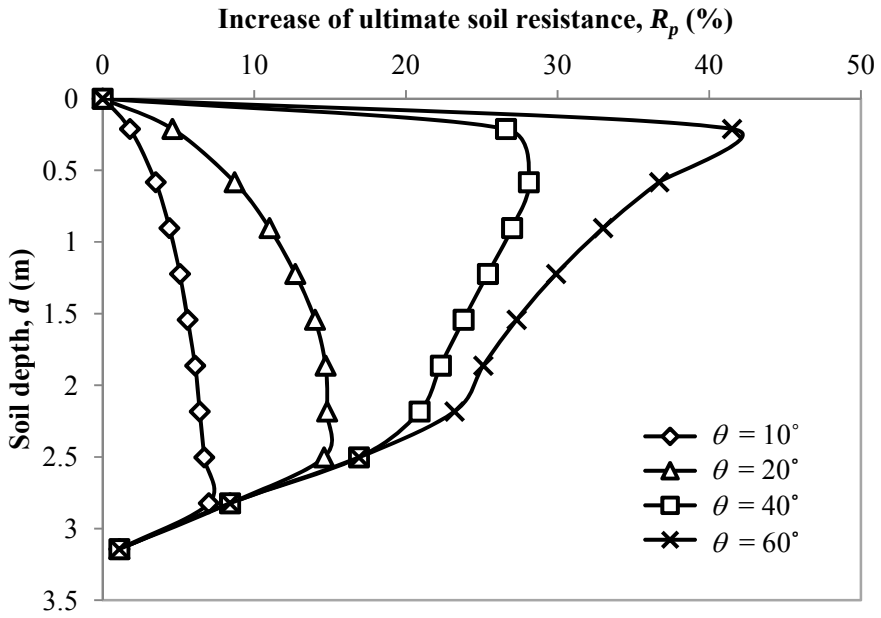

Figure 6-12. Increase of ultimate soil resistance at different scour-hole slope angles (S_d = 3 D and S_w = 0)

Figures 6-13 to 6-15 present the *p-y* curves at the shallow soil depth (i.e. d = 0.9 m). The simplified method clearly shows the increase of the soil resistance by considering the effects of the scour-hole dimensions. As expected, the soil stiffness was overestimated due to the hyperbolic nature of Matlock's *p-y* curve. In Figure 6-14, when the scour width exceeded 3 D, the *p-y* curves remained unchanged. This phenomenon was also observed in the numerical results from $FLAC^{3D}$ (Chapter 4). Likewise, this influence width is not representative from this analysis. By revisiting Figure 6-5, the lateral pile-head response clearly showed the influence width that was generally at 8 D. In addition, though not presented here, the soils at the deeper locations (> 0.9 m) had dissimilar *p-y* curves at the scour widths of 3, 6, and 8 D.

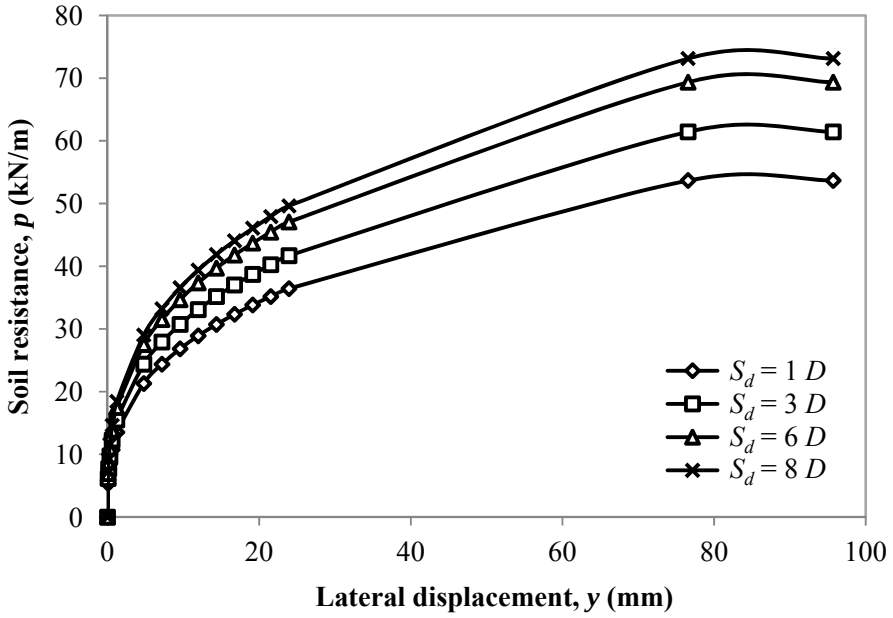

Figure 6-13. The *p-y* curves at d = 0.9 m for different scour depths (S_w = 0 and θ = 40°)

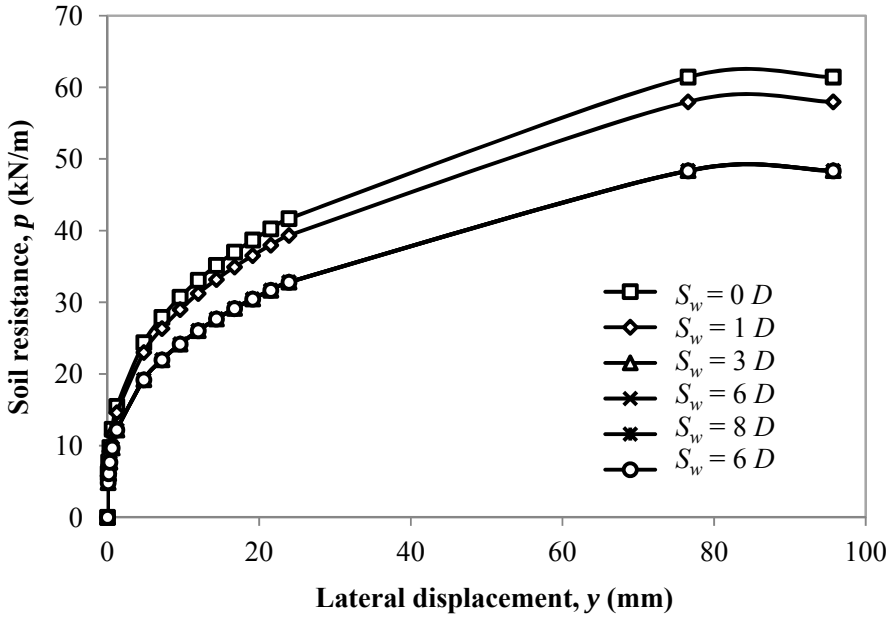

Figure 6-14. The *p-y* curves at d = 0.9 m for different scour widths (S_d = 3 D and θ = 40°)

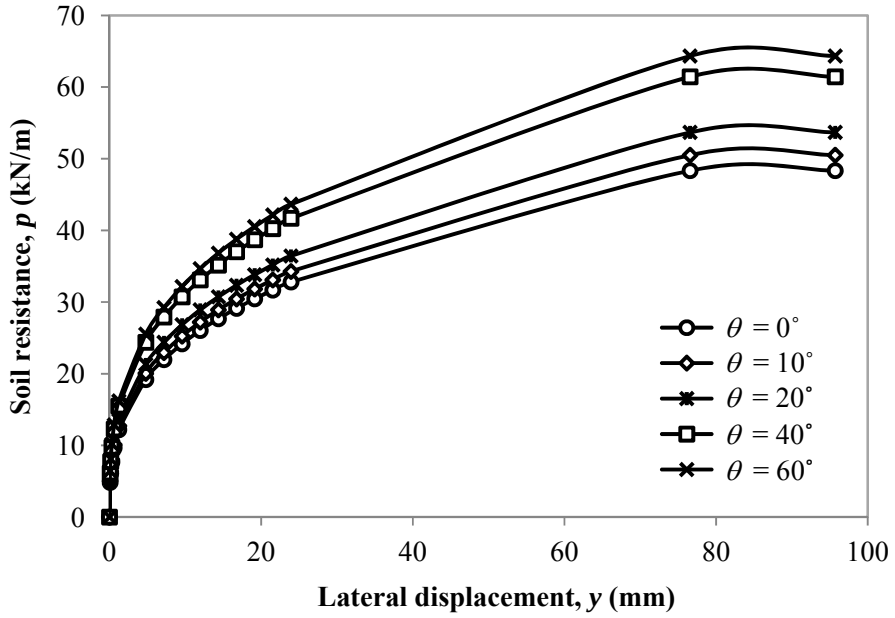

Figure 6-15. The *p-y* curves at d = 0.9 m for different scour-hole slope angles (S_d = 3 D and S_w = 0)

6.2 The Simplified Method for Laterally Loaded Piles in Sands

The commonly used *p-y* curves that were proposed by Reese et al. (1974) are adopted herein to develop the simplified method for the laterally loaded pile in sand. Similar to the method for soft clay, the developed simplified method for sand is based on the wedge failure concept, and thus it is also applied to any *p-y* curves that are developed based on the wedge failure mode.

6.2.1 Derivation of the simplified method

The equivalent wedge without a scour hole is established by seeking its ultimate soil resistance equivalent to that developed in the failure wedge with a scour hole, as illustrated in

Figure 6-16. The simplified method is then developed when the equivalent soil depth, *Z*, is found and input to Equations 3.48 and 3.49 to modify the Reese's *p-y* curves. The following two assumptions are made in the derivation: (1) the effects of the remaining overburden soils on the ultimate soil resistance at soil depths well below ground surface is considered where the soil depths well below ground surface define the soil plain failure; and (2) the possible errors caused by the use of planar surface of the scour-hole slope rather than curved surface are minimal. The first assumption was made considering stress-dependent behavior of sands. The plane failure for sands at soil depths well below ground surface is influenced by the overburden stress; therefore, the remaining overburden soils need to be considered although this effect on the laterally loaded pile behavior may be limited.

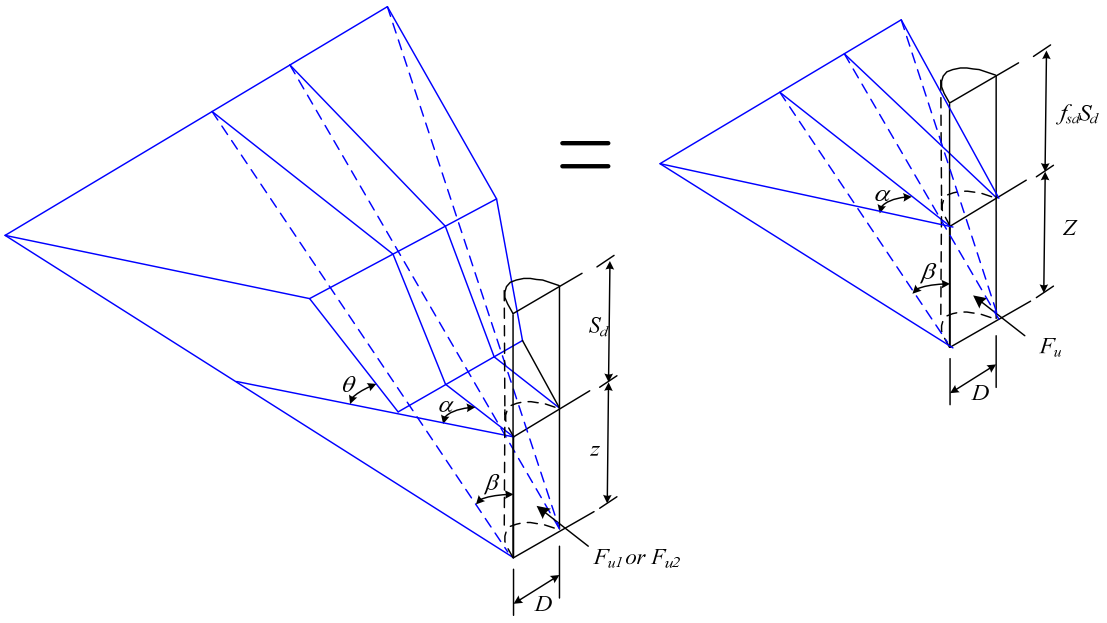

Figure 6-16. Failure modes for the ultimate soil resistance of the pile in sand with scour-hole dimensions

For the equivalent failure wedge without a scour hole (right one in Figure 6-16), the ultimate soil resistance can be determined by (Reese et al. 1974):

$$F_u = \frac{\gamma' K_o \tan\beta Z^3}{3\cos\alpha}\left[\cos\alpha\sin\beta\tan\phi' - \sin\alpha + \frac{\tan\phi'\cos\beta}{\tan(\beta-\phi')}\right] + \frac{\gamma' Z^2}{\tan(\beta-\phi')}\left(\frac{D\tan\beta}{2} + \frac{Z\tan^2\beta\tan\alpha}{3}\right) - K_a\frac{\gamma' DZ^2}{2} \quad 6.15$$

where F_u = ultimate soil resistance, kN; Z = equivalent soil depth, m; ϕ' = effective friction angle of sand; β = passive failure angle, using $45^\circ+\phi'/2$; α = angle defining the shape of the wedge, typically $\phi'/2$; K_o = coefficient of lateral earth pressure at rest, equal to 0.4; and K_a = coefficient of active lateral earth pressure, equal to $\tan^2(45^\circ - \phi'/2)$.

For the wedge with a scour hole, the ultimate soil resistance can be determined according to the location of the slope failure plane as presented in Figure 6-17.

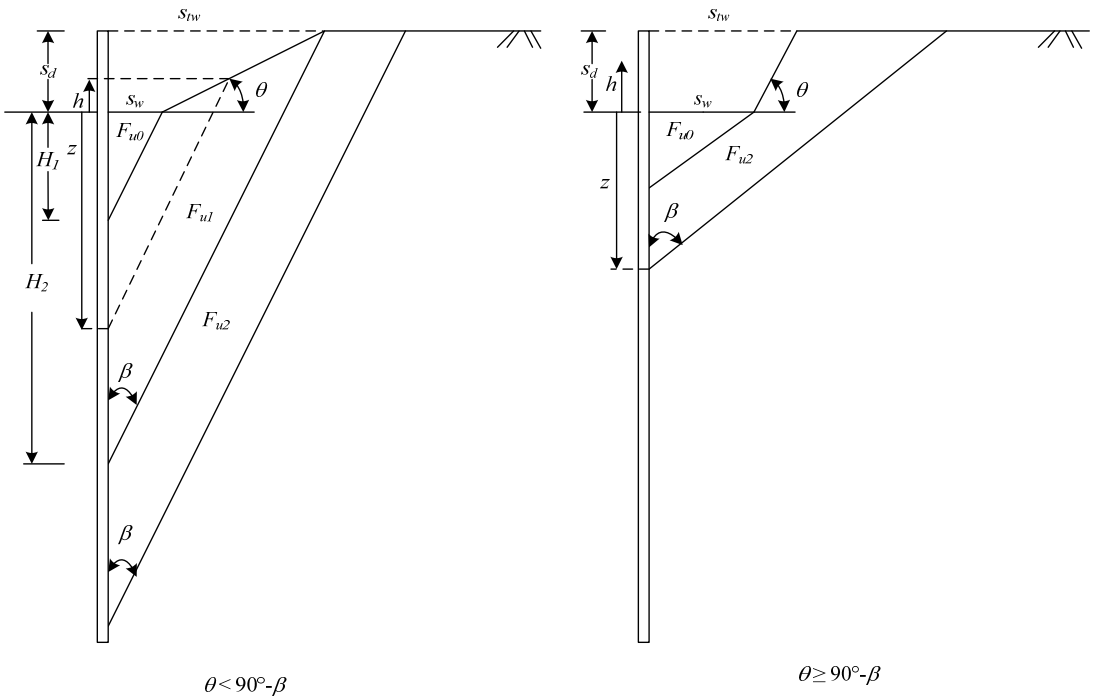

Figure 6-17. Side view of the wedge model for the ultimate soil resistance of the pile in sand

For $\theta < 90^{\circ}$-β, the slope failure plane passes through the scour-hole slope when z is between H_1 and H_2; however, for $\theta \geq 90^{\circ}$-β, the slope failure plane will never cross the scour-hole slope surface. From Figure 6-17, H_1 and H_2 can be derived as follows:

$$H_1 = \frac{S_w}{\tan\beta} \tag{6.16}$$

$$H_1 = \frac{S_w}{\tan\beta} + \frac{S_d}{D_1} \tag{6.17}$$

where D_1 is given by

$$D_1 = \frac{\tan\beta\tan\theta}{1-\tan\beta\tan\theta} \tag{6.18}$$

For $\theta < 90^\circ\text{-}\beta$, the ultimate soil resistance can be determined in Equations 6.3 to 6.5, while for $\theta \geq 90^\circ\text{-}\beta$, it can be determined in Equations 6.6 and 6.7, with F_{u0}, F_{u1}`, and F_{u2} given by

$$F_{u0} = \frac{\gamma' K_o \tan\beta z^3}{3\cos\alpha}\left[\cos\alpha\sin\beta\tan\phi' - \sin\alpha + \frac{\tan\phi'\cos\beta}{\tan(\beta-\phi')}\right] + \frac{\gamma' z^2}{\tan(\beta-\phi')}\left(\frac{D\tan\beta}{2} + \frac{z\tan^2\beta\tan\alpha}{3}\right) - K_a\frac{\gamma' D z^2}{2} \tag{6.19}$$

$$F_{u1} = \frac{\gamma' K_o \tan\beta}{3\cos\alpha}\left\{\begin{array}{l}\left[z^3 + 3D_1(z^3 - z^2 B/\tan\beta) + 2D_1^2(z - S_w/\tan\beta)^3\right] \\ \times\left[\cos\alpha\sin\beta\tan\phi - \sin\alpha + \frac{\tan\phi\cos\beta}{\tan(\beta-\phi)}\right]\end{array}\right\}$$

$$+\frac{1}{\tan(\beta-\phi)}\left\{\begin{array}{l}\frac{\gamma'(1-\tan\beta\tan\theta)\tan\beta}{6}\left\{\begin{array}{l}3D[z(1+D_1) - S_w D_1/\tan\beta]^2 \\ +2\tan\beta\tan\alpha[z(1+D_1) - S_w D_1/\tan\beta]^3\end{array}\right\} \\ +\frac{\gamma' {S_w}^2\tan\theta}{6}\left(3D + 2S_w\tan\alpha\right)\end{array}\right\} \tag{6.20}$$

$$-K_a\frac{\gamma' D z^2}{2}$$

$$F_{u2} = \frac{\gamma' K_o}{3\cos\alpha}\left\{\begin{array}{l}\left[(z+S_d)^3\tan\beta - 3(S_w + \frac{S_d}{\tan\theta})S_d{}^2 + 2\frac{S_d{}^3}{\tan\theta}\right] \\ \times\left[\cos\alpha\sin\beta\tan\phi' - \sin\alpha + \frac{\tan\phi'\cos\beta}{\tan(\beta-\phi')}\right]\end{array}\right\}$$
$$+\frac{1}{\tan(\beta-\phi)}\left\{\begin{array}{l}\frac{\gamma'(z+S_d)^2\tan\beta}{6}\left[3D + 2(z+S_d)\tan\beta\tan\alpha\right] \\ -\gamma'\frac{(S_w\tan\theta + S_d)^2}{\tan\theta}\left[\frac{D}{2} + \frac{1}{3}(S_w + \frac{S_d}{\tan\theta})\tan\alpha\right] \\ +\gamma' S_w{}^2\tan\theta\left(\frac{D}{2} + \frac{S_w\tan\alpha}{3}\right)\end{array}\right\} \qquad 6.21$$
$$-K_a\gamma' D\frac{(z+S_d)^2 - S_d{}^2}{2}$$

In Equations 6.19 to 6.21, K_a is given by

$$K_a = \cos\theta\frac{\cos\theta - \sqrt{\cos^2\theta - \cos^2\phi'}}{\cos\theta + \sqrt{\cos^2\theta - \cos^2\phi'}} \qquad 6.22$$

For $H_1 < d < H_2$, the θ is the scour-hole slope angle;for other conditions, θ is set to zero.

By equating both the ultimate soil resistances from the wedges with and without scour hole, the equivalent soil depth, Z can be determined. The determined Z is substituted for z in Equations 3.48 and 3.49, and then the conventional Reese's *p-y* curves are modified to account for the scour-hole effects in sand. It is clear that the simplified method modifies only the ultimate soil resistance, p_u, not the soil stiffness, k_{py}. In fact, the selection of k_{py}, as suggested by Reese et al. (1974), is roughly based on the relative density of sand. By employing the similar approach in Chapter 3 (i.e., the change of sand relative density is dependent on the state of overburden stress),

the relative density of the sand after scour can be solved. However, the empirical correlation between k_{py} and relative density involves a large range of values as presented in Table 3-8. The change of the relative density due to scour may not induce the change of k_{py}. As a result, the derivation here ignores the effects of the remaining overburden soil on the soil stiffness.

The reduction factor, f_{sd}, in developing the equivalent thickness of soil layer from the remaining overburden soils is also calculated by Equations 6.12 and 6.13, but the h is different from that in soft clay and can be determined by:

$$h = (z - S_w / \tan\beta) D_1 \qquad 6.23$$

6.2.2 Verification of the simplified method

The simplified method was verified with the numerical results of the 3D finite difference analysis in sands as presented in Chapter 5. The *SSM* was used to include the simplified solution for analyzing the effects of the scour-hole dimensions. The required parameters for *SSM* were the same as those for *LPILE*, including the pile parameters (Table 3-9) and the soil parameters such as $\phi' = 39^\circ$, $\gamma' = 10.4$ kN/m^3, and $K_{py} = 34$ MN/m^3. The key influence factors including the scour depths, scour widths, and scour-hole slope angles were investigated. For the purpose of verification, only the lateral load versus pile-head displacement curves (F_t-y_t curves) were compared. The *SSM* results were also corrected based on the results from *LPILE* as described in Chapter 6.1.2.

6.2.2.1 Effects of scour depth

Figure 6-18 shows that at four scour depths, the simplified method (*SSM*) produced the F_t-y_g curves consistent with those from the 3D finite difference analysis ($FLAC^{3D}$).

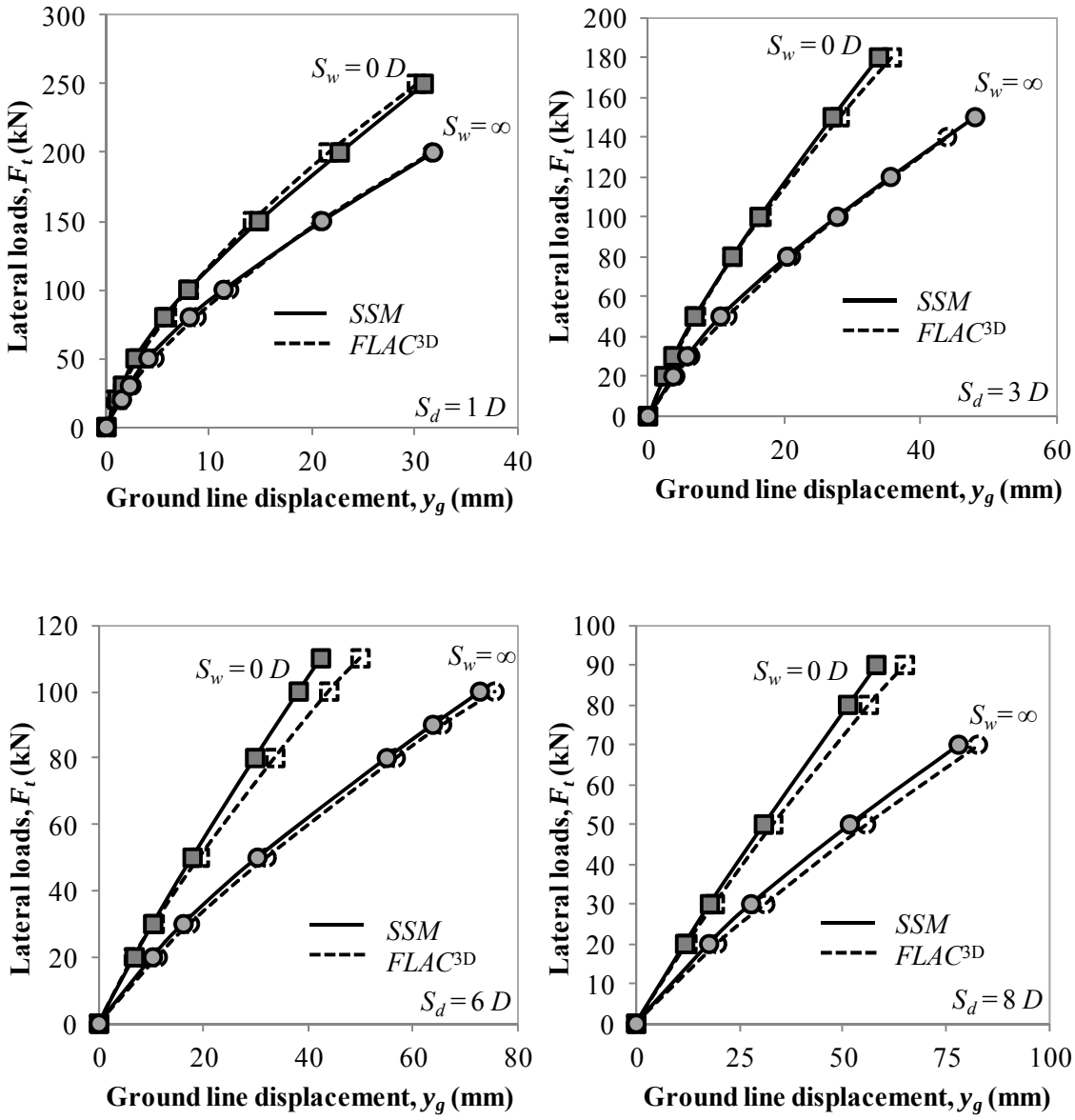

Figure 6-18. Lateral load (F_t) versus pile-head displacement (y_t) curves at different scour depths ($\theta = 39^\circ$)

6.2.2.2 Effects of scour width

Figure 6-19 presents the effects of the scour width on the ground line displacement. It is shown that the simplified method obtained the similar results as *FLAC*^{3D}.

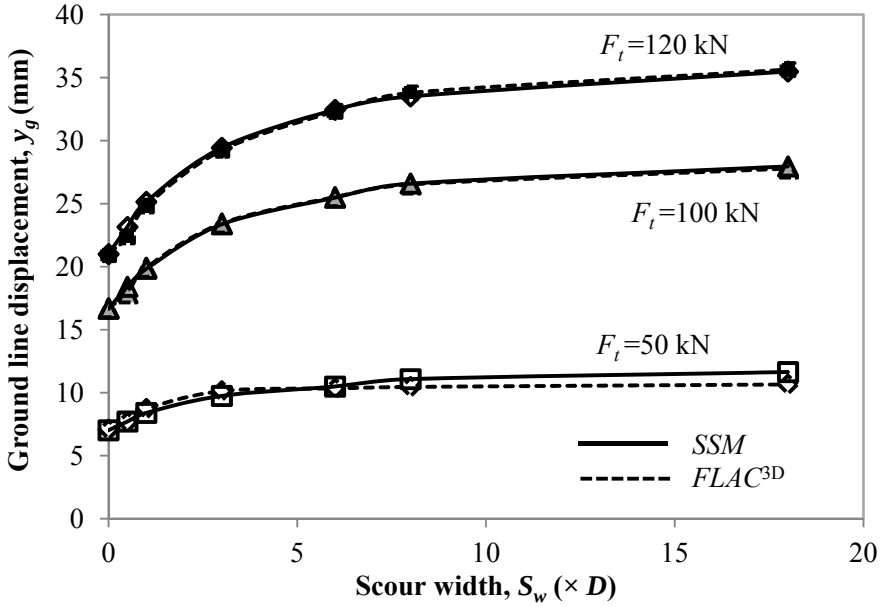

Figure 6-19. Lateral pile-head displacement versus scour width (S_d = 3 D and θ = 39°)

6.2.2.3 Effects of scour-hole slope angle

Figures 6-20 and 6-21 show the effects of the scour-hole slope angle on the lateral pile response at two scour widths (i.e. S_w = 0 and 3 D) using the simplified method and *FLAC*^{3D}. At the scour width of 0, the simplified method resulted in a similar F_t-y_g relationship as *FLAC*^{3D}. It is shown that the increase of the scour-hole slope angle increased the pile resistance to lateral loading. At a larger scour width (e.g. S_w = 3 D), the results from these two methods matched well.

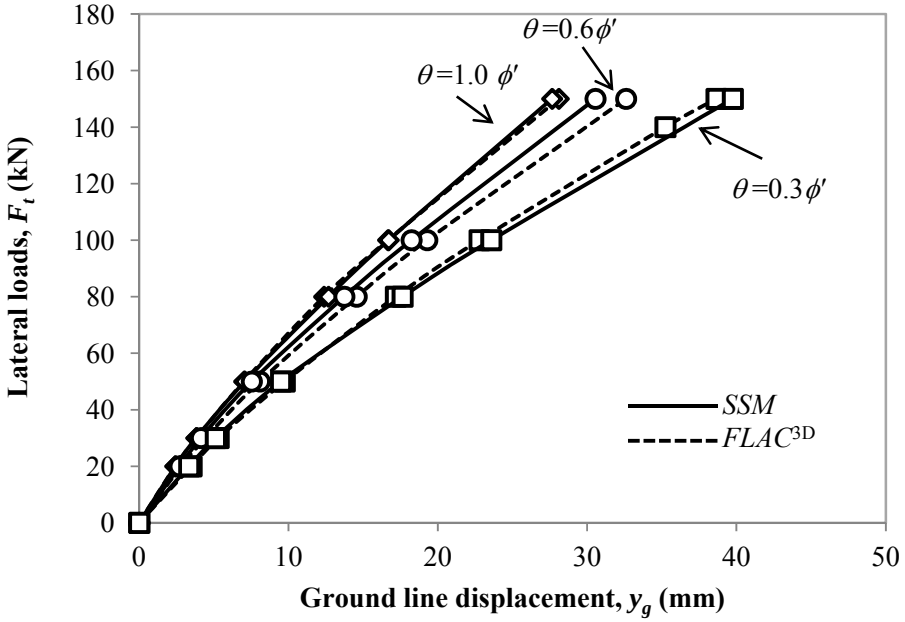

Figure 6-20. Lateral load (F_t) versus pile-head displacement (y_t) curves under different scour-hole slope angles (S_d = 3 D and S_w = 0)

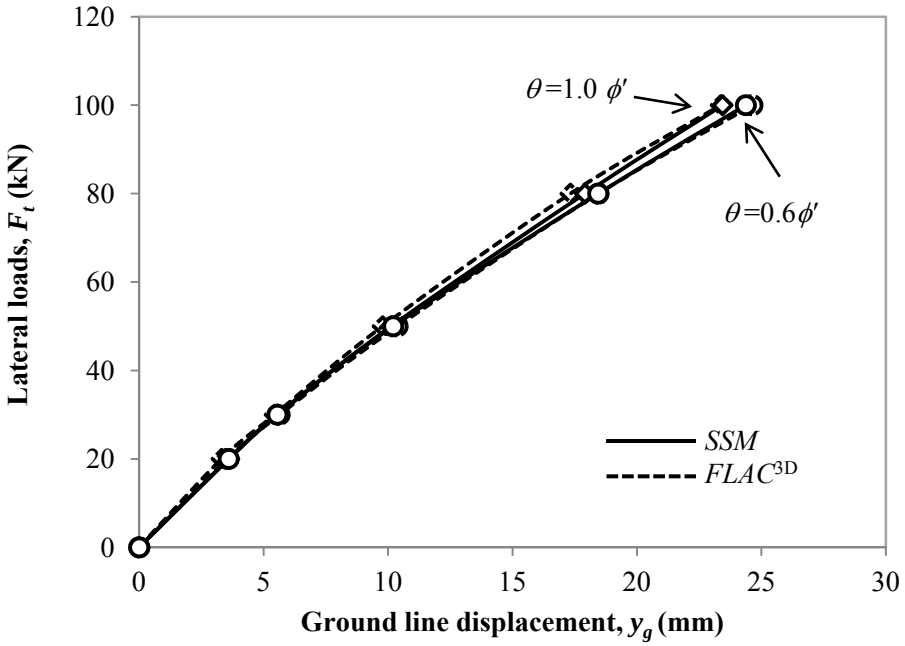

Figure 6-21. Lateral load (F_t) versus pile-head displacement (y_t) curves under different scour-hole slope angles (S_d = 3 D and S_w = 3 D)

6.2.3 Discussion on the simplified method

The simplified method was also used to calculate the reduction factor, f_{sd}, ratio of the increase of ultimate soil resistance by considering the scour-hole dimensions, R_p, and the *p-y* curves. The effects of the scour depth, scour width, and scour-hole slope angle on f_{sd}, R_p, and the *p-y* curve were also investigated.

Figures 6-22 and 6-24 show that f_{sd} generally increased with the soil depth, and the scour depth, and the scour-hole slope angle but decreased with the scour width. In Figure 6-22, an increase of the scour depth increased f_{sd} up to one at a great soil depth. This result is different from that obtained for the pile in soft clay (Figure 6-7). This discrepancy may be caused by the different shapes of wedges used in sands and clays. Furthermore, f_{sd} close to one at the great soil depth indicates the insignificant effects of the remaining overburden soils on the soil behavior at the deep location. In Figure 6-24, f_{sd} increased with the soil depth but in two stages for $\theta=0.3\phi'$. The first-stage increase of f_{sd} with the soil depth occurred at the soil depths where the slope failure plane intersected with the scour-hole slope surface while the second-stage increase occurred under the condition where the slope failure plane fell behind the scour-hole slope surface. At the scour-hole slope angle, $\theta = \phi'$ (=39˚), the slope failure plane at an angle of 25.5˚ (= 90˚-β) would never cross the scour-hole slope surface. As a result, there was no two-stage increase occurring at $\theta = \phi'$.

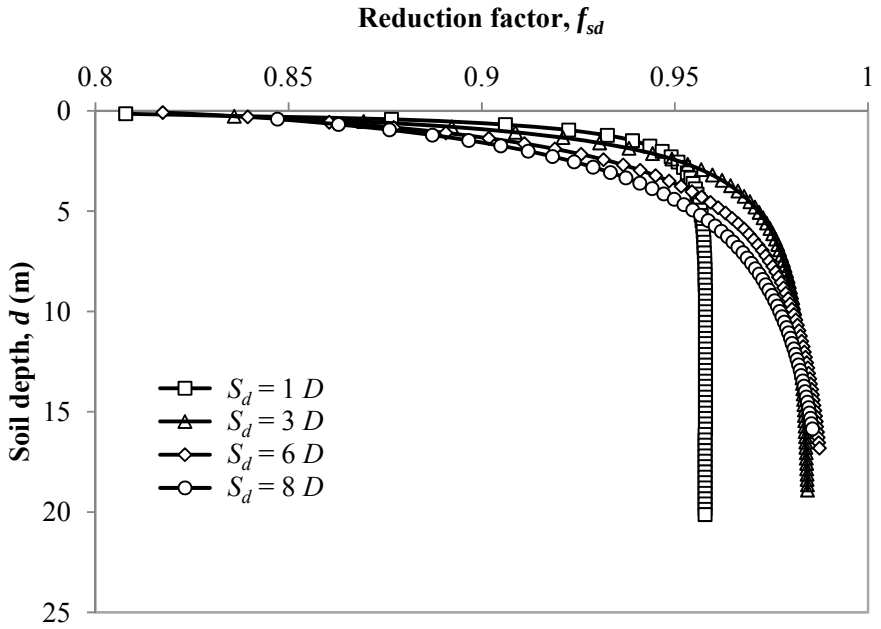

Figure 6-22. Reduction factors developed at different scour depths (S_w = 0 and θ = 39°)

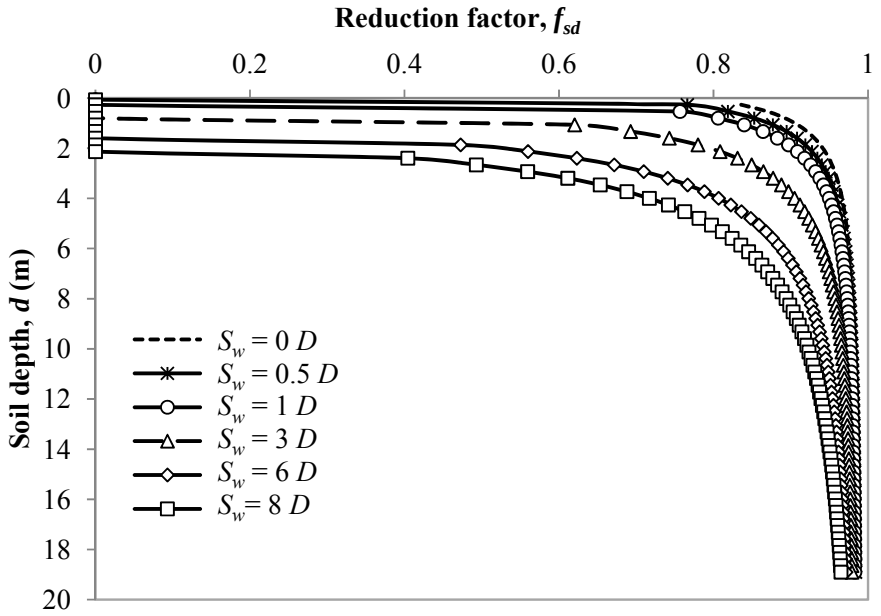

Figure 6-23. Reduction factors at different scour widths (S_d = 3 D and θ = 39°)

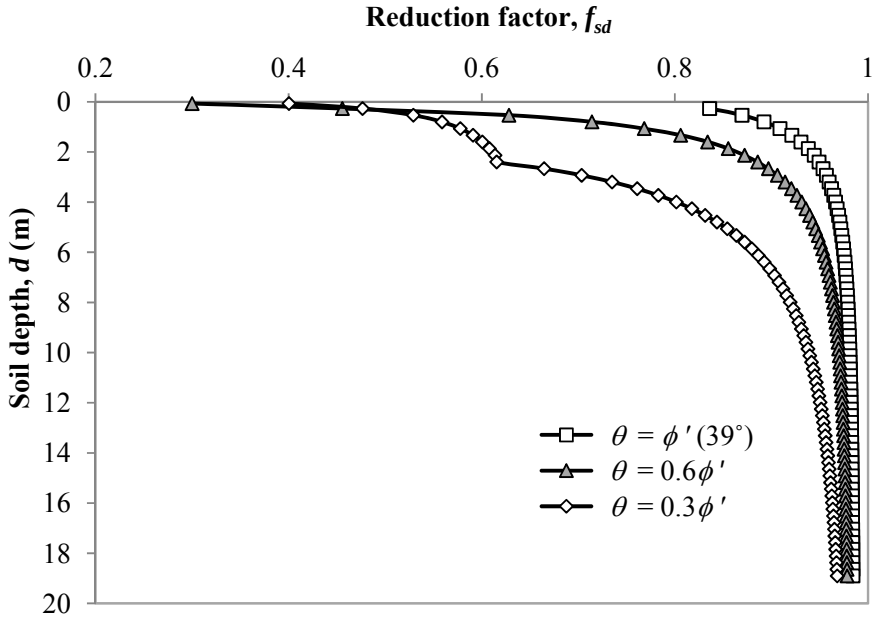

Figure 6-24. Reduction factors at different scour-hole slope angles (S_d = 3 D and S_w = 0)

Ratio of the increases of ultimate soil resistance, R_p, is presented in Figures 6-25 to 6-27. It is shown that R_p rapidly decreased with an increase of the soil depth. Different from soft clay, the dense sand had a significant improvement of the ultimate soil resistance by considering the scour-hole effects with the maximum increase over 50 times (Figure 6-25). Figure 6-26 shows that an increase of the scour width greatly reduced the benefit of the remaining overburden soils to the soil resistance. As abovementioned, the case of $\theta = \phi'$ (=39°) having no intersection between the slope failure plane and the scour-hole slope surface resulted in the continuous decrease of R_p with the soil depth. However, for the cases with the surface intersection, such as θ = 0.3 or 0.6ϕ', R_p first increased and then decreased with the soil depth, as presented in Figure 6-27.

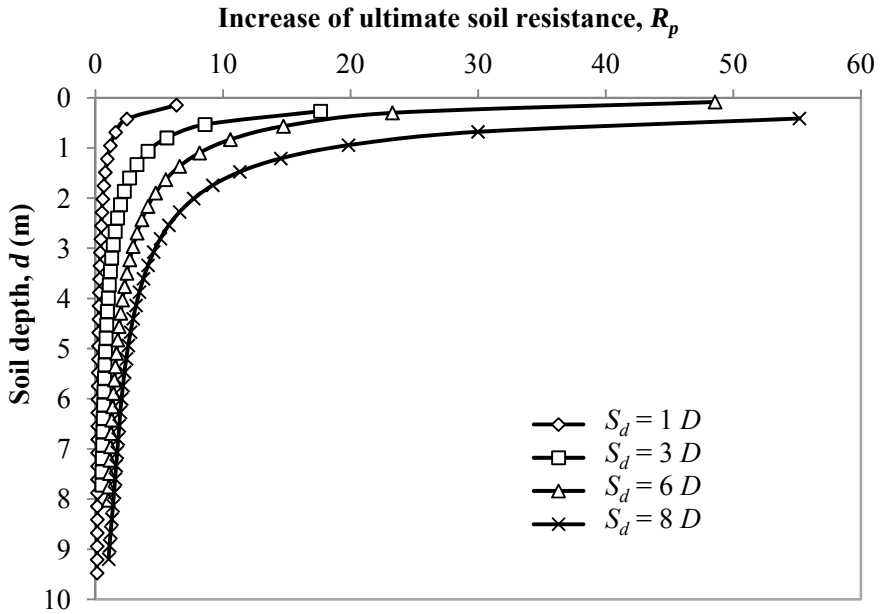

Figure 6-25. Increase of ultimate soil resistance at different scour depths (S_w = 0 and θ = 39˚)

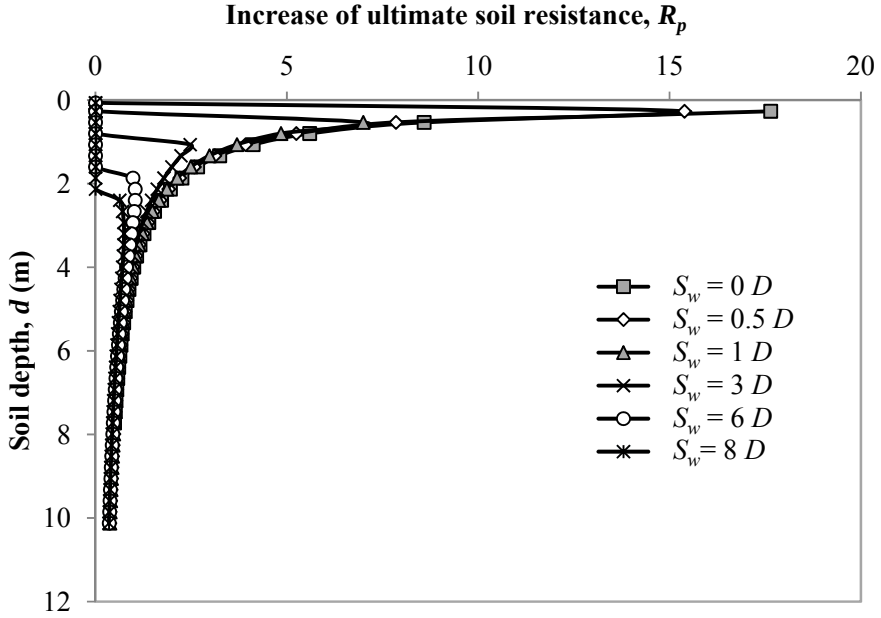

Figure 6-26. Increase of ultimate soil resistance at different scour widths (S_d = 3 D and θ = 39˚)

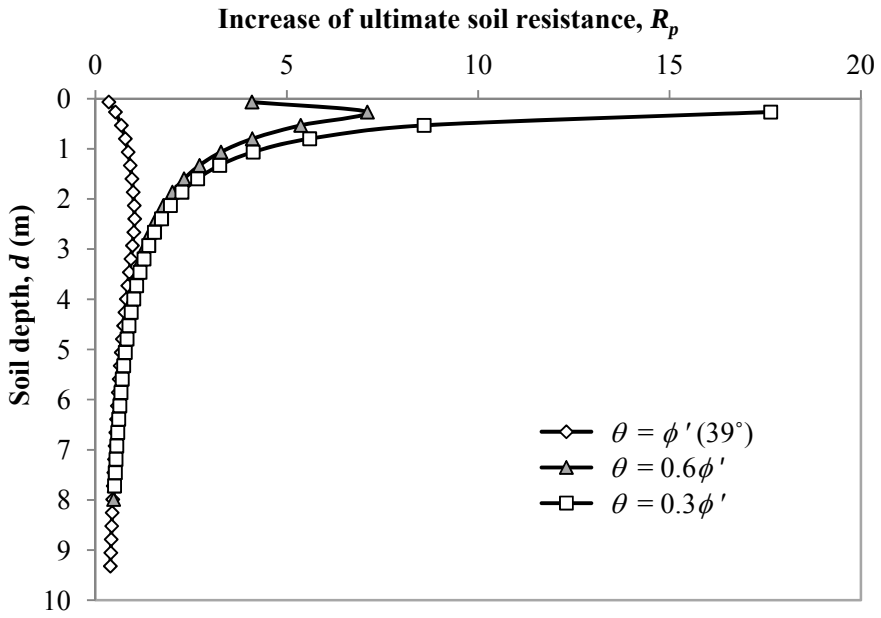

Figure 6-27. Increase of ultimate soil resistance at different scour-hole slope angles (S_d = 3 D and S_w = 0)

The *p-y* curves at the shallow soil depth (i.e. d = 1 m) are presented in Figures 6-28 to 6-30. The simplified method clearly shows the benefits of the remaining overburden stress to the increase of the soil resistance by considering the effects of scour-hole dimensions. These figures also show that the scour depth contributed to the increase of soil resistance more than the scour width and scour-hole slope angle. However, the benefits from the scour width and scour-hole slope angle were still significant with the maximum increase by more than two times. In Figure 6-29, when the scour width exceeded 6 D, the *p-y* curves remained unchanged. By revisiting Figure 6-19, the lateral pile-head response clearly shows the influence width at 8 D.

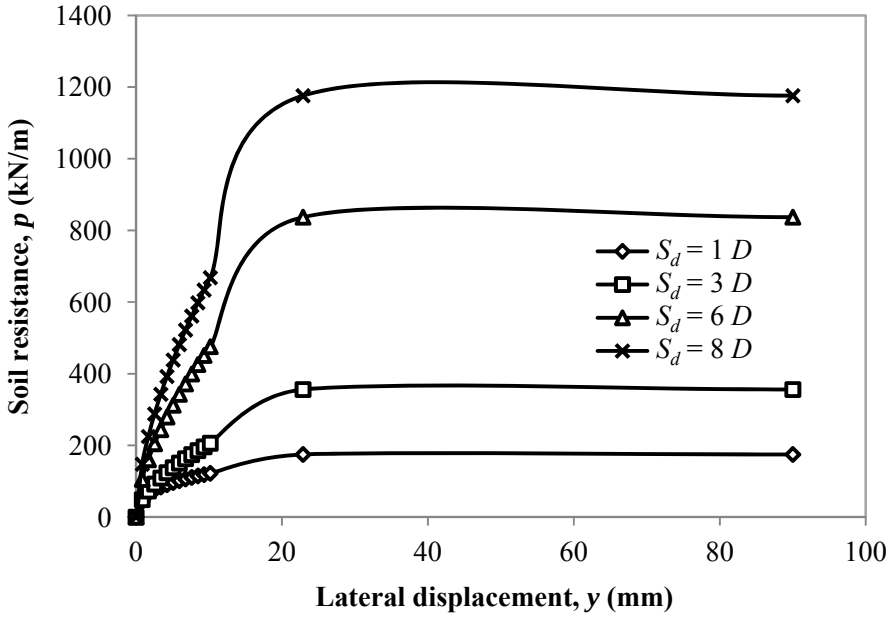

Figure 6-28. The *p-y* curves at d = 1.0 m for different scour depths (S_w = 0 and θ = 39°)

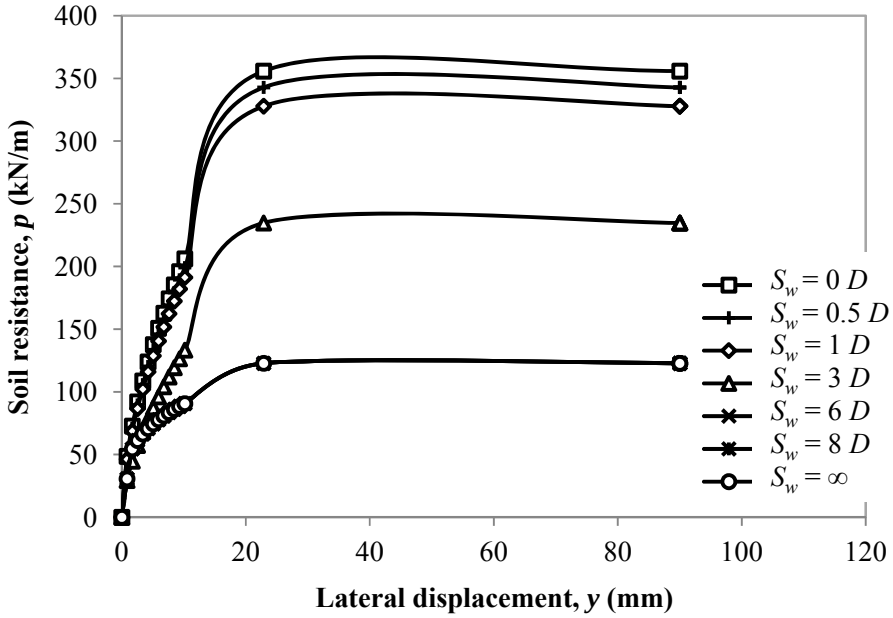

Figure 6-29. The *p-y* curves at d = 1.0 m for different scour widths (S_d = 3 D and θ = 39°)

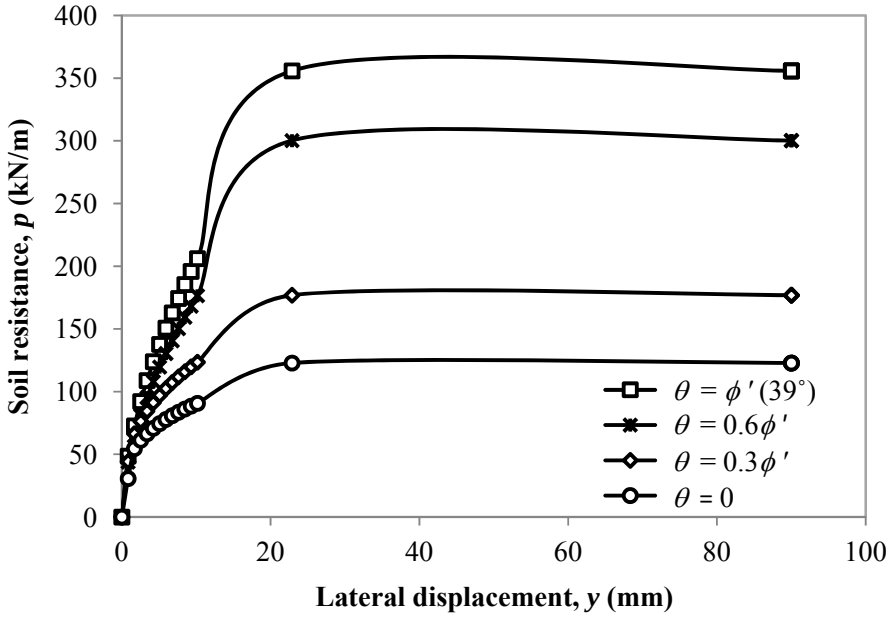

Figure 6-30. The *p-y* curves at *d* = 1.0 m for different scour-hole slope angles (S_d = 3 *D* and S_w = 0)

6.3 Summary

The one-dimensional simplified methods were developed for analyzing the effects of scour-hole dimensions on the pile behavior under lateral loading. The simplified methods were obtained by modifying the *p-y* curves based on the wedge failure to account for the effects of the scour-hole dimensions. The equivalent soil depth at failure, *Z*, was calculated based on the equivalent ultimate soil resistance between the wedge failure modes with and without a scour hole. The modified *p-y* curves were obatined by substituting the new soil depth, *Z*, for the original soil depth, *z*, during the computation of the *p-y* curve. The simplified methods were developed herein for piles in soft clay and sand and they can be applied to any *p-y* curves that have been developed based on the wedge failure concept.

It was assumed that the remaining overburden soils had no effect on the soil resistance of soft clay well below the ground surface, but had an effect on the soil resistance of sand well below the ground surface. The effects of the remaining overburden stress on the soil stiffness were neglected for both soft clay and sand. The possible errors caused by the assumed planar surface of the scour-hole slope that the wedge failure encompassed were considered to be negligible.

The simplified methods for soft clay and sand were verified with the results of 3D finite difference analysis as discussed in Chapters 4 and 5, including the lateral load versus pile head or ground line displacements at different scour depths, scour widths, and scour-hole slope angles. Once the original *p-y* curves were similar to those from the 3D finite difference analysis, the simplified methods could produce the similar results with the 3D analysis.

In the soft clay, the remaining overburden stress increased the ultimate soil resistance but to the limited soil depth. As compared with the soft clay, the remaining overburden stress of the dense sand significantly increased the ultimate soil resistance by the maximum over 50 times.

CHAPTER 7

LATERAL BEHAVIOR OF PILE-SUPPORTED BRIDGES UNDER SCOUR CONDITIONS

In the preceding chapters, scour effects on laterally loaded piles have been analyzed by considering stress history of soils and scour-hole dimensions. This chapter focuses on the analysis of an entire bridge under scour conditions, which requires consideration of reactions of soil, foundation, and bridge superstructure. As stated previously, the limitations of current bridge analysis or design are that bridge superstructure and foundation are considered separately. For example, the current structure softwares (e.g. STAAD and Risa) do not include sufficient soil analysis functions, especially for nonlinear soil behavior. Hence, it is necessary to consider the bridge as a whole system, especially for the bridge under scour impact. To achieve the integrated analysis, the Soil Spring Module (*SSM*) as stated shortly in Chapter 6 was developed and integrated with the structural analysis software, *STAAD.Pro*. With the seamless link between *SSM* and *STAAD.Pro*, the soil model (expressed as nonlinear soil springs) is successfully integrated to the structural model in which the integrated analysis is accomplished. With the integrated analysis program (i.e. *SSM* plus *STAAD.Pro*), an example study of the bridge in the State of Kansas is presented. In addition, theories for considering effects of stress history and scour-hole dimensions are attempted to add to the integrated analysis. However, only stress history effects are considered because the theory for scour-hole dimensions is developed only for laterally loaded single pile rather than for the pile group that appeared in the example bridge. Finally, lateral behavior of pile-supported bridge under different scour depths is evaluated with the integrated analysis program, and stress history effects on the computation results are also discussed.

7.1 Integrated Analysis Program for Analyzing Lateral Behavior of Bridges

The integrated analysis program simulates the entire bridge by integrating two components: the structure model and soil model. The structure model referred to the bridge structure including piles is constructed in *STAAD.Pro*, while the soil model is only concerned with soil behavior under lateral loading, and is generated in the Soil Spring Module, *SSM*. The integrated analysis program achieves the analysis through communication between *STAAD.Pro* and *SSM*. Figure 7-1 outlines the operation procedure for integrated analysis program: first, build structure model including bridge superstructure and foundation structures in *STAAD.Pro*; next, select a single pile or pile group in structure model, and then switch to *SSM* inputting soil parameters or scour depths, and assigning soil supports to the selected piles; finally, go back to *STAAD.Pro* where the structure model has included the soil model (i.e. nonlinear soil springs), and perform lateral analysis in *STAAD.Pro*. The example for this operation process is illustrated in Figure 7-2.

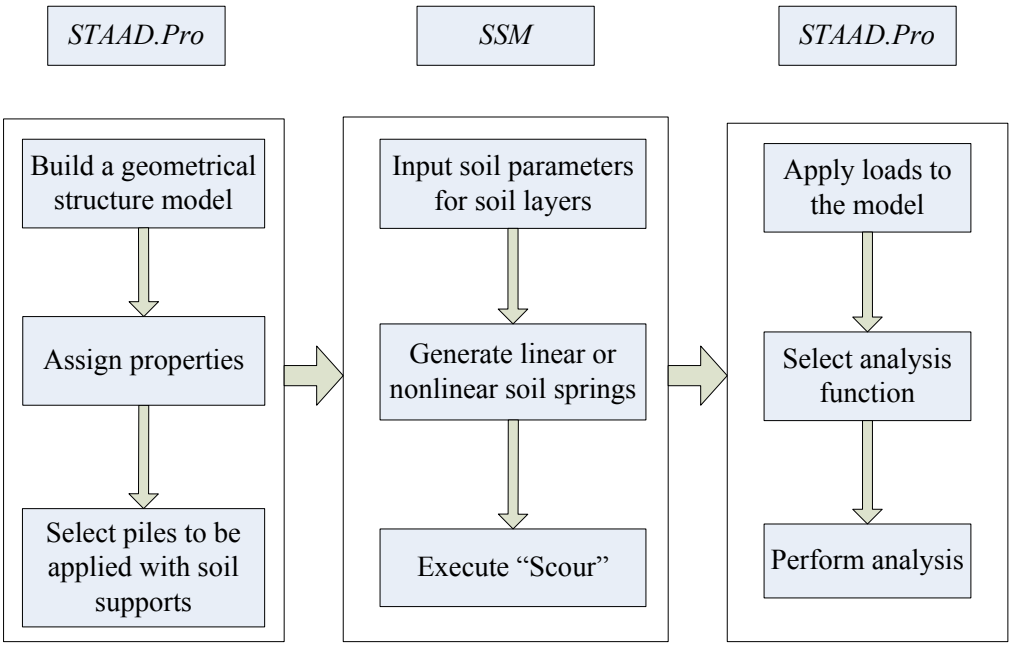

Figure 7-1. Operation procedure for integrated analysis program

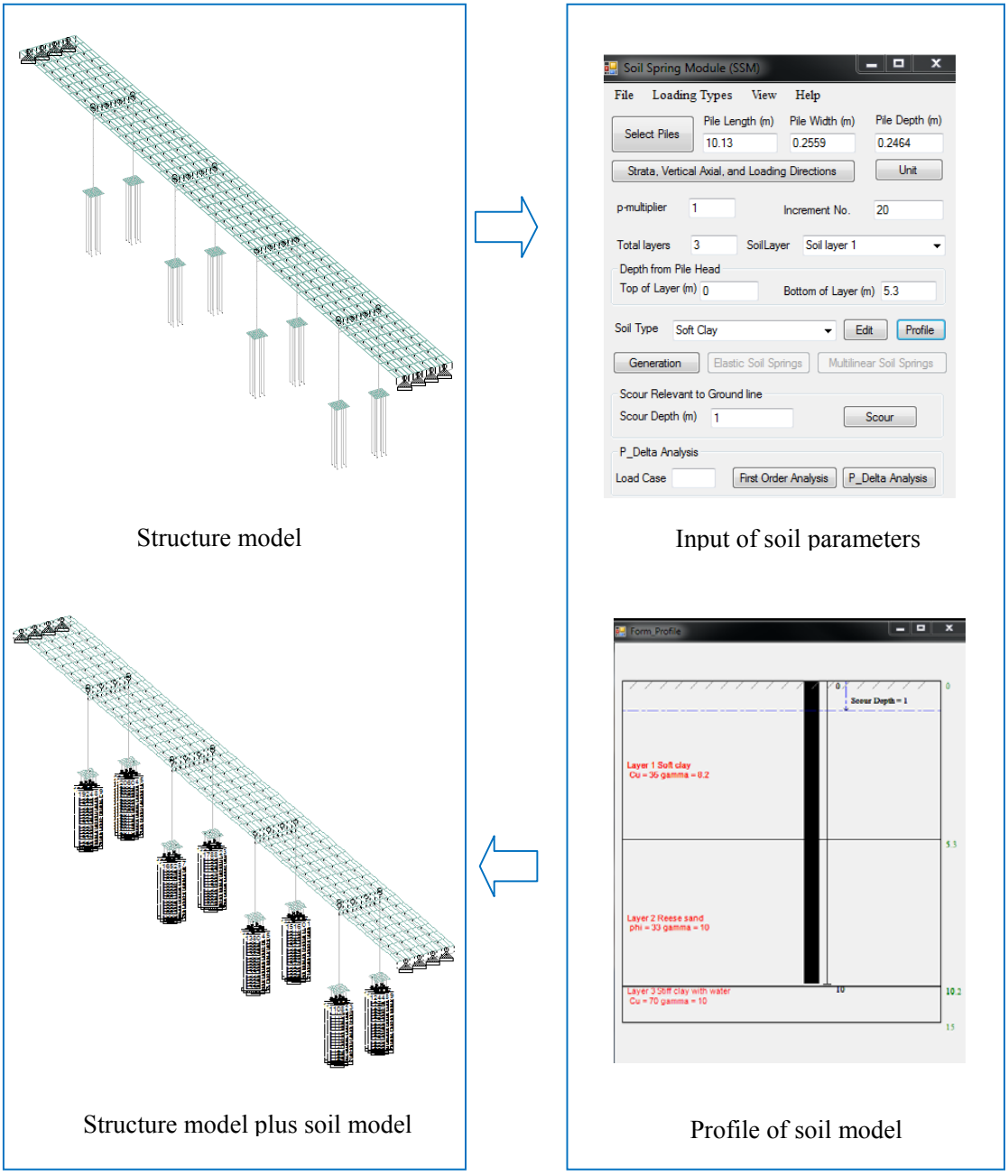

Figure 7-2. Illustration of running the integrated analysis program

The seamless link between *SSM* and *STAAD.Pro* was achieved by the *OpenStaad* function in *STAAD.Pro* that allows external programs (e.g. *SSM*) to access *STAAD.Pro*'s internal functions and routines as well as graphical commands. The Soil Spring Module (*SSM*) was programmed in Visual Basic 2010 Express to generate soil model that is described as a series of nonlinear Winkler springs derived from *p-y* curves. Figure 7-3 shows the flow chart for developing *SSM*, and more details can be referenced to the manual of *SSM* (Lin et al. 2012).

The *p-y* curves that are available in the literature or derived directly from the field test were approximated by multilinear lines at which each slope represents the stiffness, k_i, as shown in Figure 7-4. The multilinear spring is the product of k_i and length of pile element, L_i, and a series of the springs approximately represent nonlinear Winkler springs and act as soil supports to the piles in the structure model.

In total, the integrated analysis program fully harnesses the advantages that *STAAD.Pro* and *p-y* method have, but also their limitations. The integrated analysis program may be used to analyze a variety of structures (e.g. bridges, buildings, water tanks, and so on) that can be constructed in *STAAD. Pro,* and can access the design functions as well as powerful analysis engines provided by *STAAD.Pro*. Furthermore, by including the *p-y* method for modeling soil behavior, the integrated analysis program greatly improves its computation efficiency. However, the integrated analysis program is unable to perform p-delta analyses in nonlinear soil foundations because the p-delta analysis function in *STAAD.Pro* is not compatible with multilinear soil springs. In addition, it cannot analyze dynamic behavior of structures in soils described by the *p-y* curves because the curves cannot consider dynamic loading as encountered in earthquake and machine foundations.

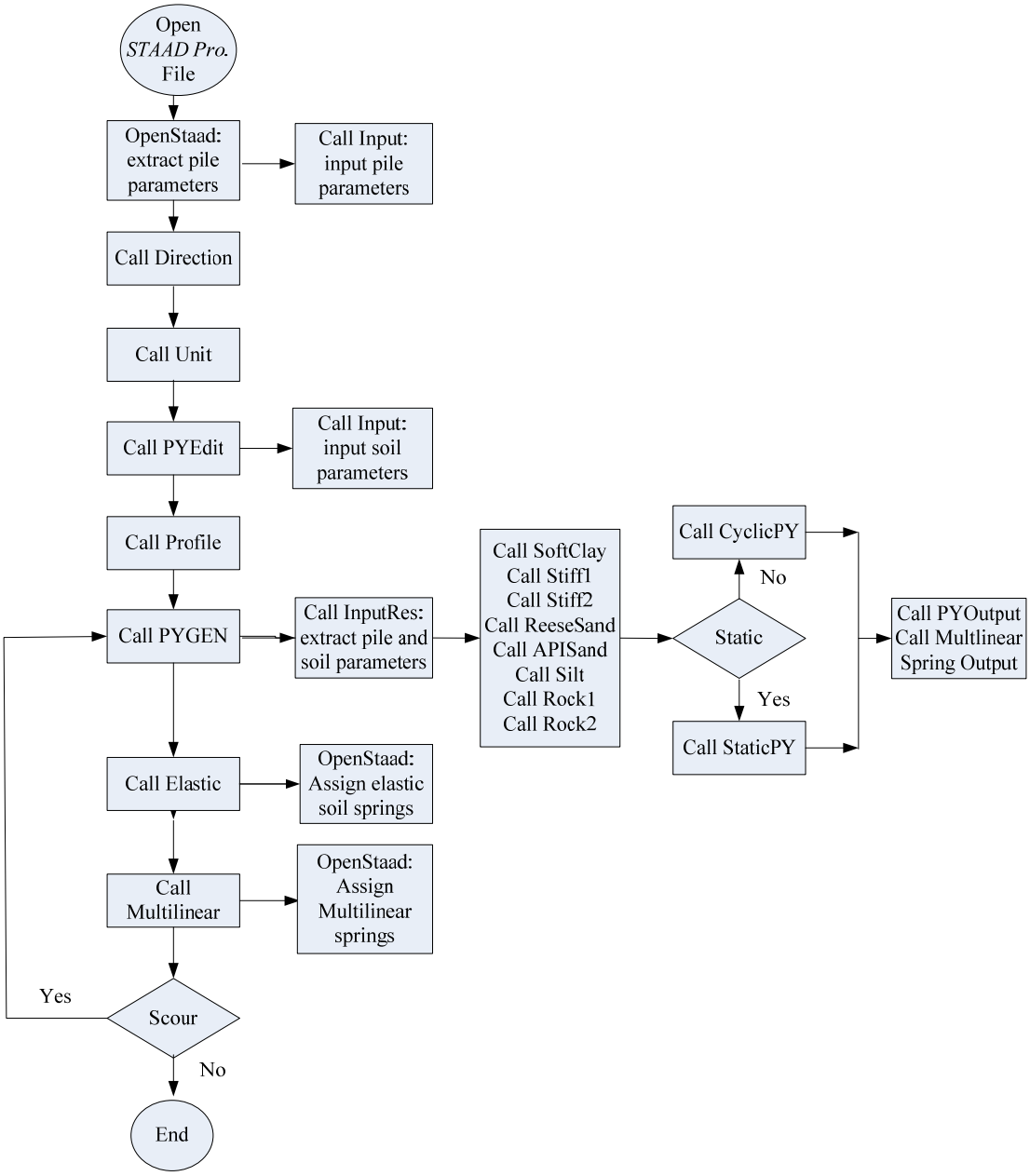

Figure 7-3. Flow chart for developing Soil Spring Module (*SSM*)

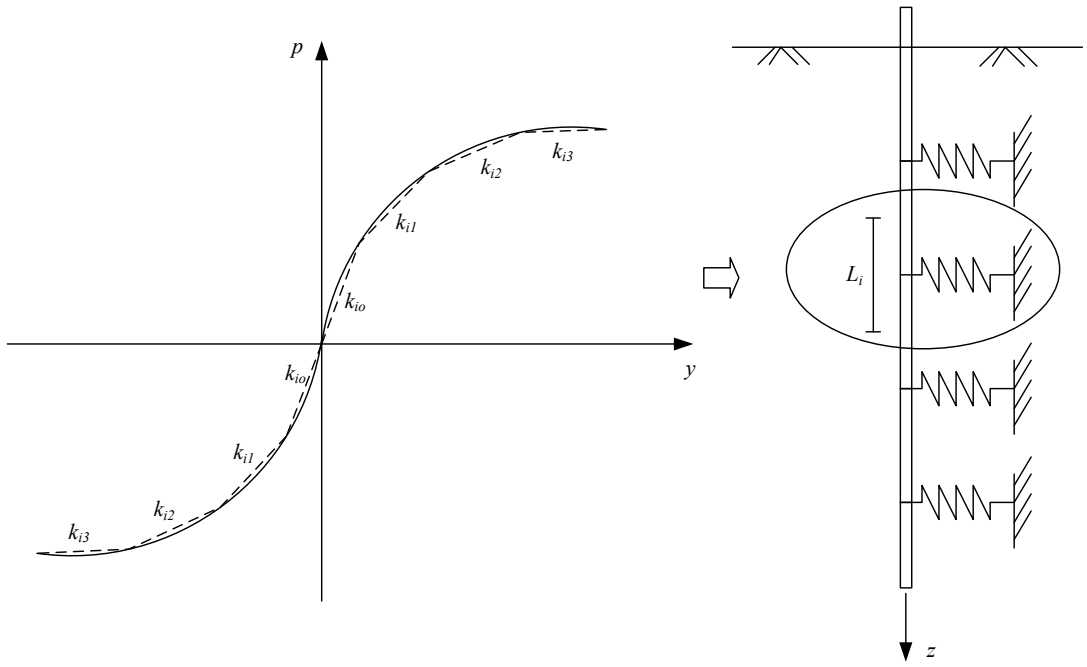

Figure 7-4. Approximation of multilinear stiffness to nonlinear *p-y* curves

7.1.1 Validation of the integrated analysis program

Validation of the integrated analysis program was conducted using two examples including laterally loaded single pile in soft clay and laterally loaded pile group in sand. As commonly-used commercial softwares *LPILE* and *FB-Multipier* have been verified satisfactorily with experimental data, the integrated analysis program was compared with them. Note that for convenience, the integrated analysis program has been referred to as *SSM* when comparing it to *LPILE* and *FB-Multipier*. In the analysis of laterally loaded single pile soft clay, *SSM* has been compared with *LPILE*; while in the case of laterally loaded pile group in sand, it was compared with *FB-Multipier*.

7.1.1.1 Laterally loaded single pile in soft clay

The test conducted at Lake Austin, Texas (Matlock 1970) was simulated herein for the comparison; pile parameters are given in Table 3-2 and soil parameters including C_u, γ', and ε_{50} are provided in Table 3-1. The lateral load was applied at 0.0635 m above the mud line, and the water table was kept above the mud line. Lateral pile-head displacement and maximum bending moment were compared as shown in Figures 7-5 and 7-6. The *SSM* developed slightly higher lateral pile-head displacement than *LPILE* but generated the maximum bending moment that matched well with that from *LPILE*. The different results for lateral pile-head displacement from *SSM* and *LPILE* were likely caused by the different *p-y* stiffnesses they used. For instance, *SSM* employs the multilinear secant stiffnesses (Figure 7-4), but *LPILE* uses the secant stiffnesses that are the slopes formed between the point on the *p-y* curve and the point of origin.

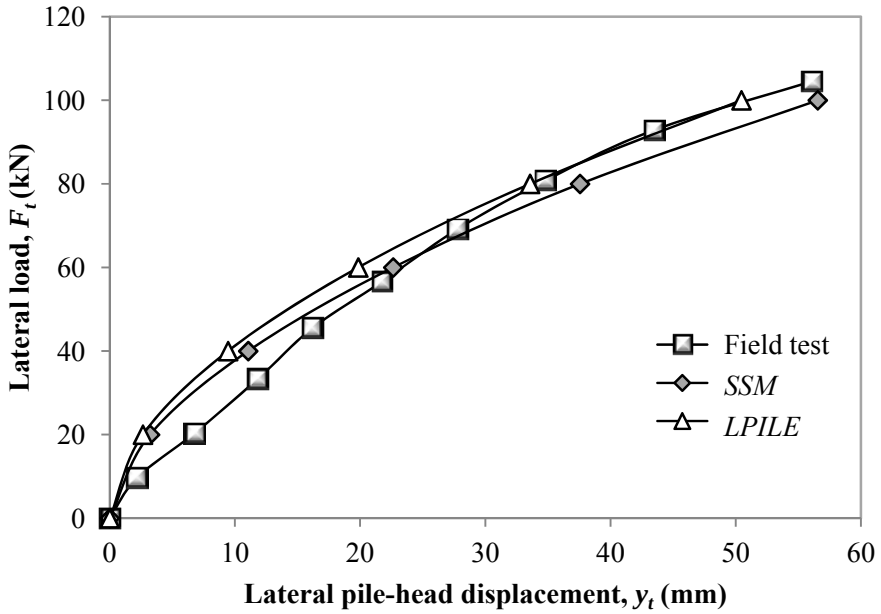

Figure 7-5. Comparison of lateral pile-head displacement from field test, *SSM* and *LPILE*

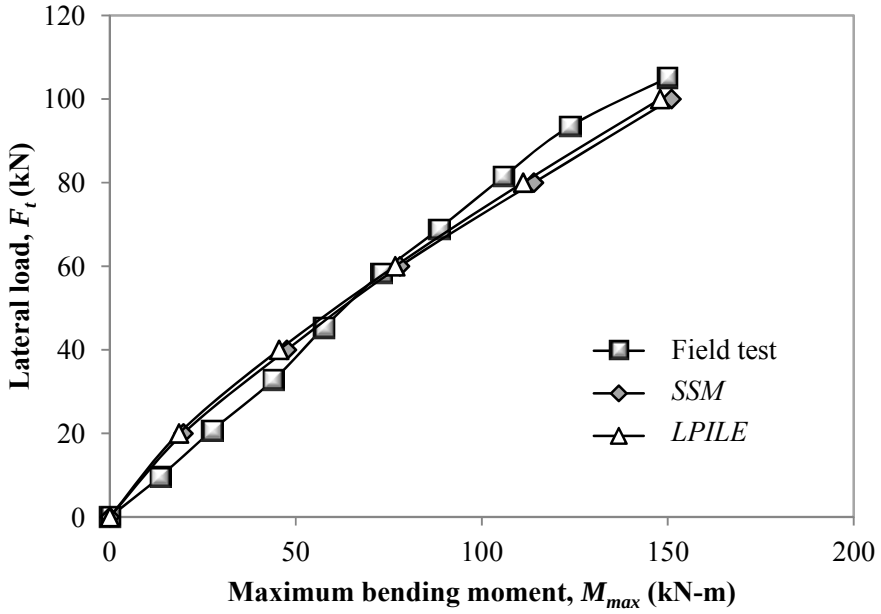

Figure 7-6. Comparison of the maximum bending moment from field test, *SSM* and *LPILE*

7.1.1.2 Laterally loaded pile group in sands

In this case, a 3x3 pipe pile group in sand under the lateral loading was analyzed. The pile and soil properties as used in the single pile test in Mustang Island (Cox et al. 1974) were used herein. However, the configuration of the pile group and the pile cap were assumed as follows: the center-to-center spacing of piles at the 3x3 pile group was three times the pile diameter and the pile cap only served to rigidly connect piles together and had dimensions of (thickness × length × width) 1 ×1.83 × 1.83 m. The parameters of piles are tabulated in Table 3-9, and the pile cap had an elastic modulus of 2.17×10^7 kN/m^2. The piles were embedded 0.5 m into the pile cap. The pile group model constructed in *STAAD.Pro* is shown in Figure 7-7. During the calculation, the group effects ere considered by using p-multiplier, f_m (Figure 2-11) as

suggested by Mokwa et al. (2000). The soil properties included friction angle (ϕ'), effective unit weight (γ'), and coefficient of subgrade reaction (K_{py}) where ϕ' = 39°, γ' = 10.4 kN/m^3, and K_{py} =34 MN/m^3.

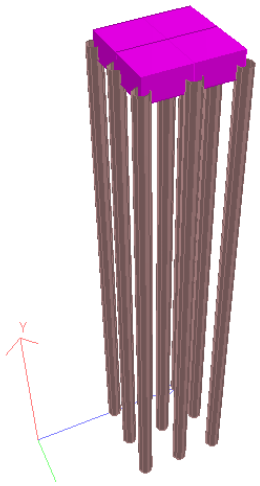

Figure 7-7. 3D view of the pile group model

The calculated results from *SSM* were then compared with those from *FB-Multipier* as presented in Figure 7-8. In the figure, if *FB-Multipier* employs the same f_m with *SSM*, i.e. 0.82, 0.68, and 0.58 for the leading to trailing piles as indicated in Figure 2-11, then the calculated lateral displacements of the pile cap from *FB-Multipier* (indicated by *FB-Multipier*_1 in Figure 7-8) *and SSM* can be seen to agree with each other very well. If using the default f_m provided by *FB-Multipier* which is 1.0, 0.3, and 0.3 respectively for leading to trailing piles, the calculated displacement as indicated by *FB-Multipier*_2 in Figure 7-8 is about 10-30% greater than that from *SSM*.

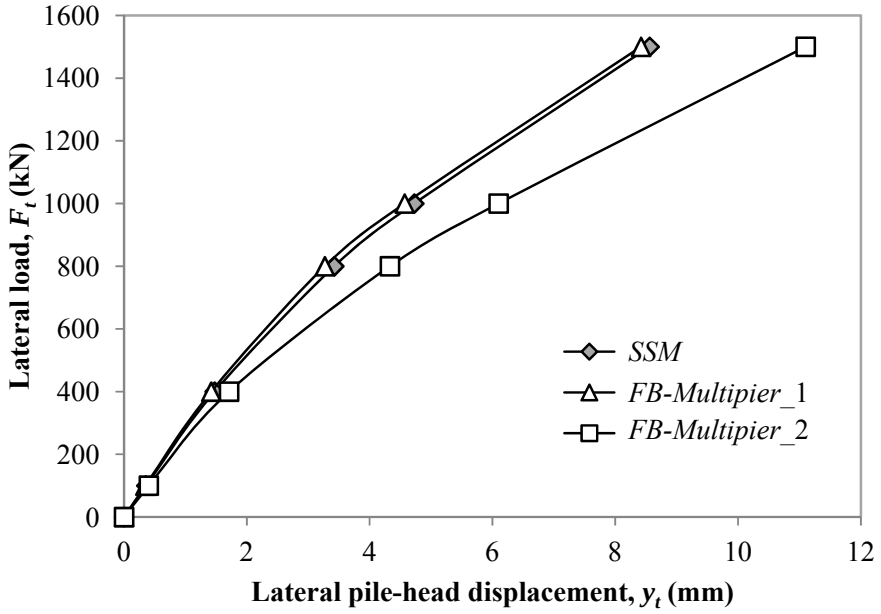

Figure 7-8. Comparison of lateral displacement of pile cap calculated from *SSM* and *FB-Multipier*

In general, the integrated analysis program developed satisfactory results such as lateral displacement of pile head or pile cap as well as maximum bending moment of piles as compared with *LPILE* and *FB-Multipier*. Therefore, it can be confidently used in the integrated analysis of lateral behavior of an entire bridge under scour conditions; this is presented in the following.

7.2 Evaluation of Bridge Lateral Behavior under Scour Conditions

Using the integrated analysis program, a case study was performed to investigate the bridge lateral behavior under scour conditions. Bridge 45 in the state of Kansas was used for the case study; different scour depths were investigated. Stress history effects were considered by comparing the calculated results with those obtained by ignoring stress history effects. The stress history effects as presented in Chapter 3 were considered only for homogenous soil. To be

consistent, the soil conditions in Bridge 45 that consist of layered soil were no longer used; instead, the homogenous soil such as soft clay (Lake Austin) and sand (Mustang Island) were used for the analysis.

7.2.1 Bridge description

Bridge 45 is situated in Jewell County, Kansas and carries State Highway K14 over a local creek. The five-span bridge was constructed in 1956 and has a total length of 112 m. Four W33x141 steel girders with the spacing of 2.3 m support the concrete bridge deck, as shown in Figure 7-9. Bridge 45 has eight concrete piers (four bents), and each pier is supported by a group of eight HP10x42 piles with average length of 10 m as shown in Figure 7-9. The pile cap has thickness of 1.1 m and length and width of 2.3 m. The pile cap is rigidly connected with the piles. The concrete materials in the model use elastic modulus of 2.17×10^7 kN/m^2, Poisson's ratio of 0.17, and unit weight of 24 kN/m^3.

As abovementioned, homogenous soil, i.e. soft clay at Lake Austin, Texas (Matlock 1970) or sand at Mustang island, Texas (Reese et al. 1974), was used for the study; properties of the soft clay (C_u, γ', and ε_{50}) are presented in Table 3-1 and the values for sand properties are ϕ' = 39°, γ' = 10.4 kN/m^3, and K_{py} =34 MN/m^3.

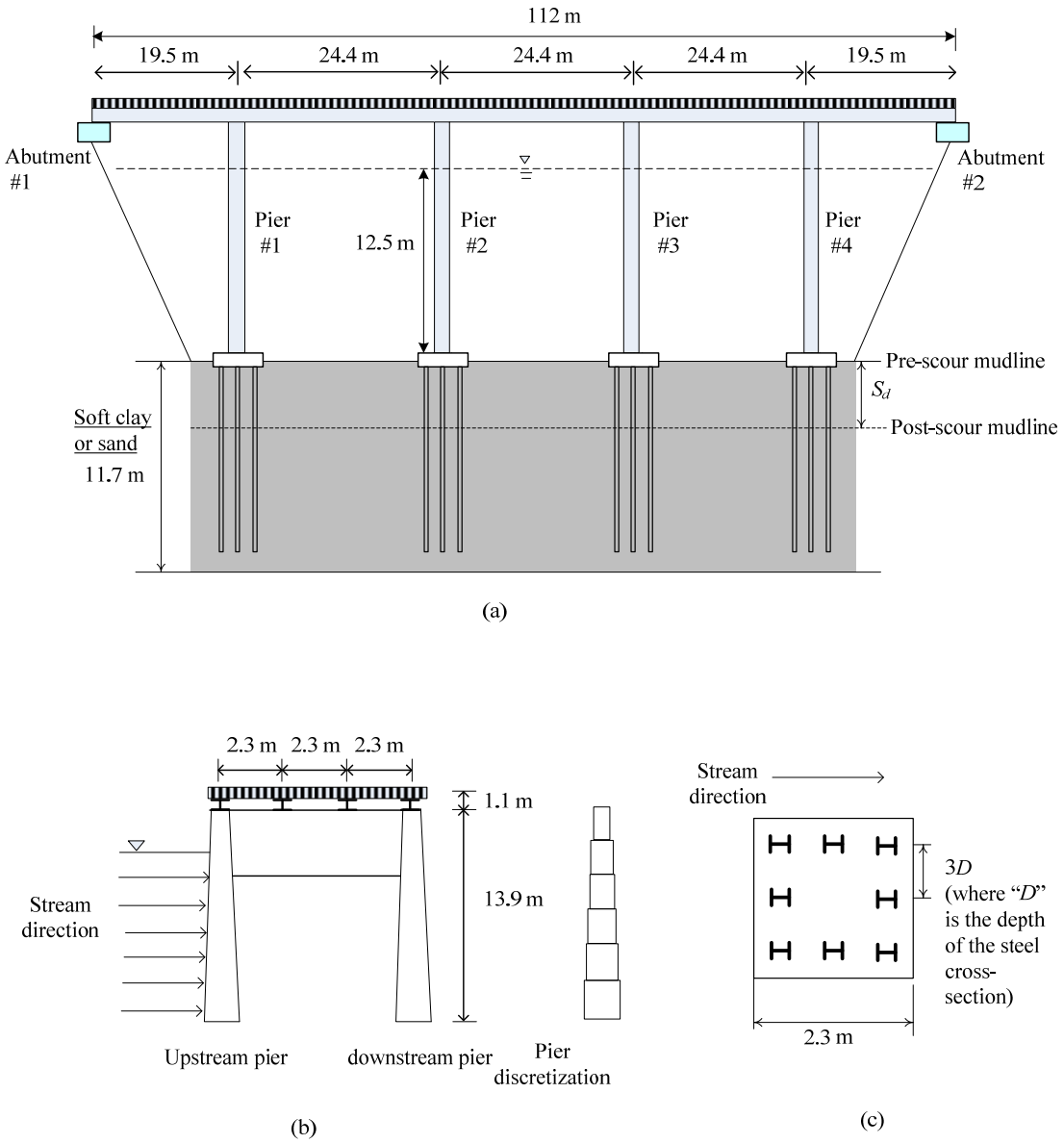

Figure 7-9. The entire bridge model in the integrated analysis program: (a) bridge configuration; (b) cross section of the bridge supersctructure; (c) cross section of the pile foundation.

7.2.2 Loading conditions

Loads considered in the analysis included flood loads with debris and wind loads, while vertical loads included self-weight of the bridge. All the applied loads were combined using load factors of 1.0 to reflect the actual behavior of the existing bridge system. The loads used in this case study represent one combination of lateral and gravity loads that a bridge would be likely to experience during a scour event.

Water loads were calculated using Equation 7.1 based on equation C3.7.3.1-1 from the 4th Edition AASHTO-LRFD Bridge Design Specifications (AASHTO 2007), provided here in metric units.

$$p = C_D \gamma V^2 \times 10^{-6} / 2 \qquad 7.1$$

where V = water velocity, m/sec; C_D = drag coefficient; γ = density of water, kg/m^3; p = water pressure MPa.

The design 100-year flood for the bridge was taken at the design elevation of 12.5 m above the base of piers. The design flood velocity used in the calculation was 3.66 m/sec. In addition to water loads, debris forces were calculated by multiplying the water pressure (Equation 7.1) by the area of debris accumulation at a pier based on Section C3.7.3.1 of the AASHTO-LRFD Bridge Design Specifications (AASHTO 2007). The dimension of debris-accumulation was simplified as an inverted triangle in which the width was taken as half the sum of adjacent span lengths, but not greater than 13.5 m, and the depth was taken as half the water depth, not greater than 3.0 m. Debris forces were applied only to the upstream piers of the bridge due to the relatively short distance between upstream and downstream piers (6.90 m) as compared with the

width of debris at a pier (13.7 m). Debris loads were applied to piers as concentrated loads, while water loads were applied as pressure to piers below the maximum depth of debris-accumulation.

Wind loads were calculated using Equations 7.2 and 7.3, which are based on Equations 3.8.1.2.1-1 and 3.8.1.1-1 from the 4th Edition AASHTO-LRFD Bridge Design Specifications (AASHTO 2007), provided here in metric units.

$$P_D = P_B \left(V_{DZ} / V_B \right)^2 \tag{7.2}$$

$$V_{DZ} = 2.5 V_o \left(V_{10} / V_B \right) \ln\left(Z / Z_o \right) \tag{7.3}$$

In Equations 7.2 and 7.3, P_D = wind pressure, MPa; P_B = base wind pressure, MPa; V_{DZ} = design wind velocity at design elevation, km/hr; V_B = base wind velocity, typically taken as 160 km/hr; Z = height of structure at which wind loads are calculated, mm; V_o = friction velocity, km/hr; V_{10} = wind velocity at 10,000 mm above low ground, km/hr; and Z_o = friction length of upstream fetch, mm.

Wind loads were calculated above the flood level and were applied as concentrated loads to bridge girders at the locations right above the piers. The concentrated wind loads were determined by multiplying the tributary area of the bridge deck and fascia girder normal to wind loads by the wind pressure calculated using Equation 7.2.

7.2.3 Integrated analysis

An entire bridge model was first built in *STAAD.Pro* 2007 as shown in "Structure model" of Figure 7-2. The abutments were supported using pin supports. The connections between girders and piers were assumed partially connected, for example, pin connections at Pier #3 and roller connections at other piers. The bridge piers, which are tapered, were discretized into columns with different sized cross-sections when modeled in *Staad.Pro* as depicted in Figure 7-2.

After the structure model was constructed, soil parameters were input in *SSM* and then the generated multilinear soil springs were assigned to the piles of the bridge. Finally, in *Staad.Pro*, the load combination was added to the bridge as described in Chapter 7.2.2 and the analysis of the bridge was performed. Two methods are available for considering scour depths in the analysis. One method is to repeat the above procedure but to change the elevation of initial ground line to that of the post-scour mudline; another one is to use the existing structure plus soil model but going back to *SSM* to assign the scour depths, and then running analysis again in *STAAD.Pro*. In this study, six scour depths from 0, 1, 2, 3, 4, to 5 m were designed to investigate scour effects on the lateral behavior of the bridge. To consider the stress history, the analysis procedure for soft clay and sand discussed in Chapter 3 were added to the code in the *SSM*. For soft clay, the varying C_u along the soil depth that was calculated after considering stress history of the remaining soils were used because it showed more significant effect on responses of laterally loaded piles than using averaging C_u as concluded from Chapter 3. Results were discussed, which included the maximum lateral displacement of bridge deck, pier, and pile cap, the maximum bending moment of pier and pile cap, and lateral and rotation stiffnesses of the pile foundations.

7.2.4 Results and discussion

Since two soil conditions were considered in the analysis, the results and discussion are presented separately for each soil type. The analysis for each soil includes results calculated both considering and ignoring stress history effects, where considering stress history effects were designated with the "M" and ignoring it with the "U" as appearing in the legend of the following figures.

7.2.4.1 Lateral behavior of the bridge in soft clay

Lateral displacement at the pile cap under Pier #2 (Figure 7-9) represented the maximum displacement among all the pile groups, and the result regarding the displacement versus scour depth is plotted in Figure 7-10. The lateral displacement of bridge deck and pier (also Pier #2) also represented the maximum values, and their relationships with scour depth are shown in Figure 7-11. Figure 7-10 shows the maximum lateral displacement at pile cap increased at an increasing rate with respect to scour depth. The pile cap under the upstream pier exerted a heavier lateral load (e.g. debris load) than its downstream counterpart, and therefore experienced larger lateral displacement, as observed in the figure. Furthermore, considering the stress history effects gave higher lateral displacement than ignoring it at each scour depth, with the greatest disparity being 8.6% (with respect to the displacement calculated by ignoring stress history effects).

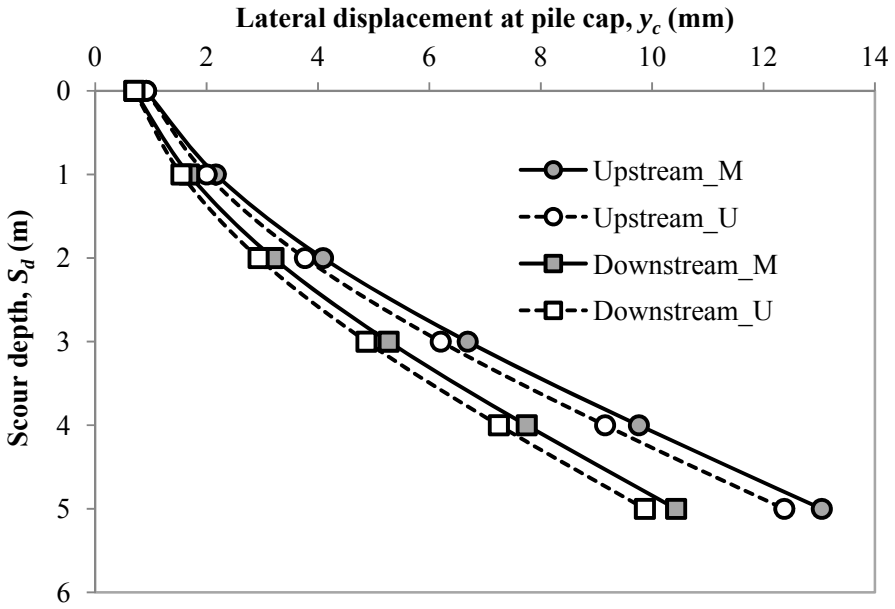

Figure 7-10. Lateral displacement at pile cap versus scour depth in soft clay

Figure 7-11 shows the maximum lateral displacement at superstructure (at the bridge deck and at the pier) increased almost linearly with scour depth, but the magnitude of the increase was limited. This result indicated that the bridge superstructure was less sensitive to scour than bridge pile foundations in terms of lateral displacement. Figure 7-11 also reflects that the upstream pier had higher lateral displacement than the downstream pier, and considering the stress history effects showed slightly higher lateral displacement at both the pier and the bridge deck than ignoring it.

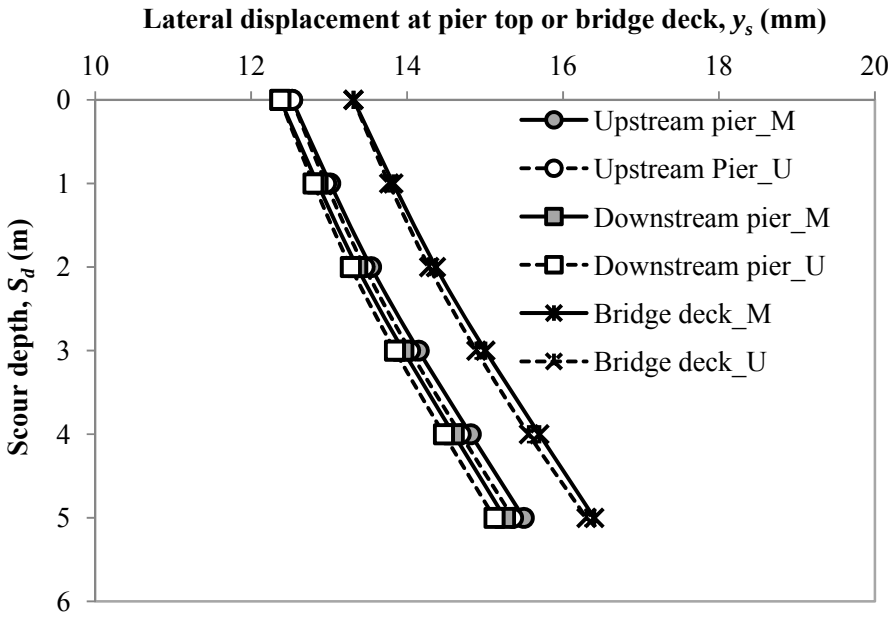

Figure 7-11. Maximum lateral displacement of superstructure versus scour depth in soft clay

The lateral forces exerted at the pile cap under Pier #2 and at Abutment #2 were recorded and presented in Figure 7-12. The results show that as scour proceeded, the lateral force gradually decreased at the pile cap but significantly increased at the abutment. Additionally, though not presented here, it was observed that piles also carried more shear forces as scour depth increased. The above results reflected as scour depth increased, abutment and piles shared more lateral forces, indicating more forces were transferred to the boundaries. Note that the current boundary for the abutment is pinned, and therefore the calculated lateral force at abutment would be higher than reality. But the results at abutment can still be seen as approximate results to reality due to enormously large lateral supports at abutments of the bridge. Additionally, Figure 7-12 shows lateral forces differed rarely in considering or ignoring stress history effects and the upstream pile cap carried higher lateral loads than the downstream one.

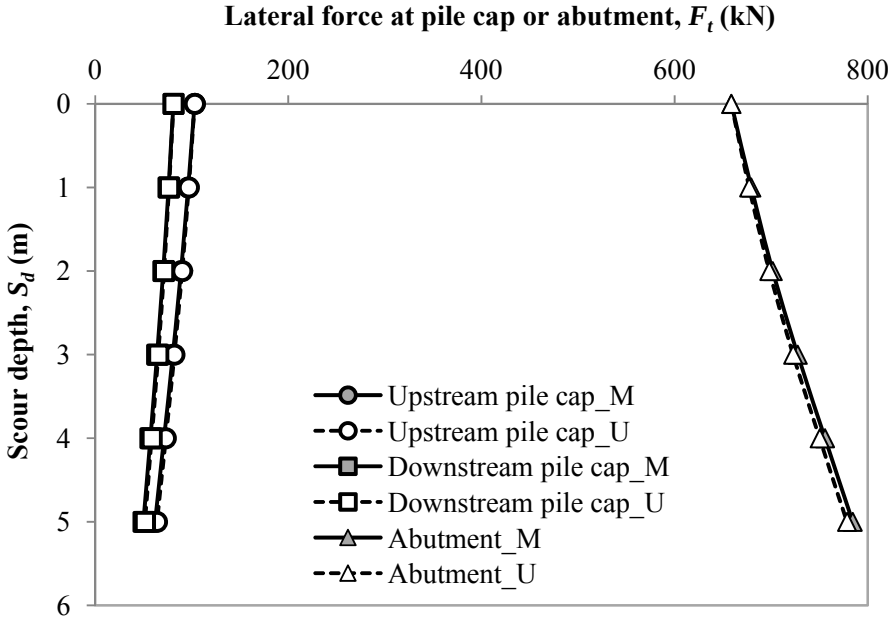

Figure 7-12. Lateral force at pile cap (under Pier #2) or Abutment #2 versus scour depth in soft clay

The bending moment at the pile cap (pier base) under Pier #2 and the maximum bending moment of the pier are shown in Figures 7-13 and 7-14 respectively. The results indicate that the bending moment showed a linear decrease with increased scour depth at the pile cap but showed a nonlinear decrease at the pier, and the former decreased more significantly than the latter. By comparing the distributions of bending moment of the entire bridge under different scour depths, it was found that decrease of the bending moment at the pile cap and pier with scour depth induced more of the bending moment carried by piles or abutments. The bending moment for upstream pile cap decreased more rapidly than that for downstream one; however, the decreasing rates of the maximum bending moment at pier for upstream and downstream were nearly the same. In addition, considering stress history effects resulted in marginally smaller bending moments than ignoring it; however the difference of bending moment at pile cap became more noticeable at higher scour depth. For example, the most difference (with respect to the bending

moment calculated by ignoring stress history effects) was approximately 16% for the pile cap but only 3% for the pier when scour depth was as large as 5 m.

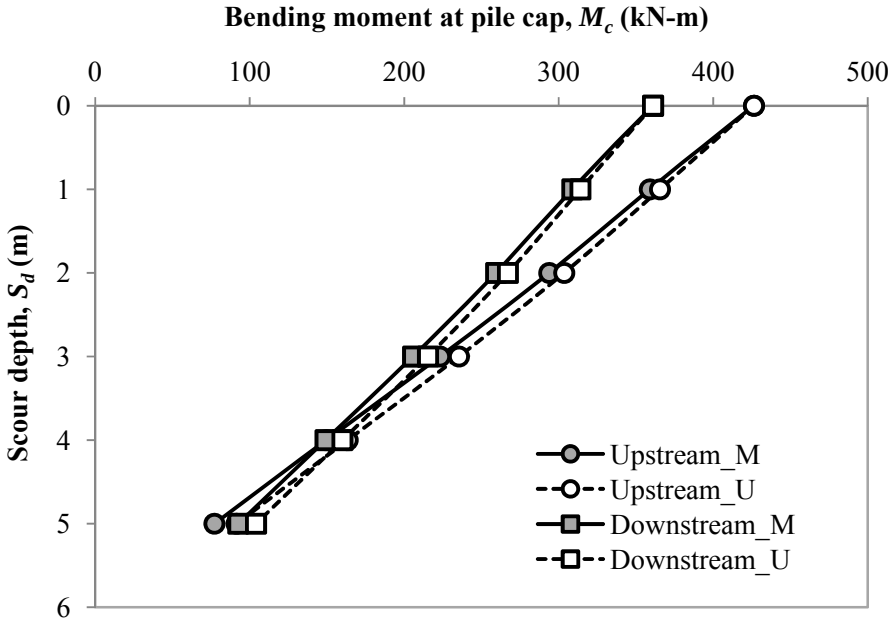

Figure 7-13. Bending moment at pile cap versus scour depth in soft clay

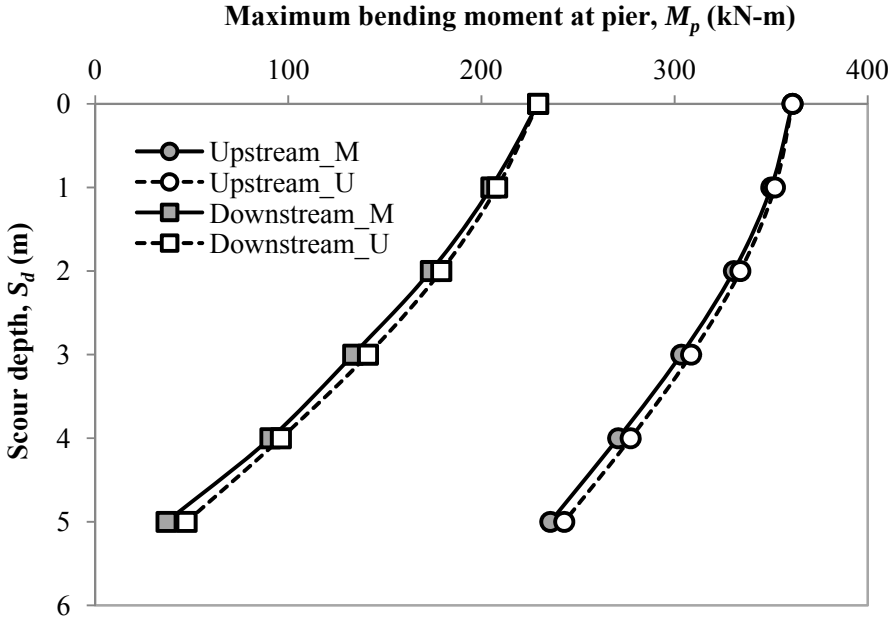

Figure 7-14. Maximum bending moment at pier versus scour depth in soft clay

The foundation stiffnesses in terms of lateral movement and rotation were determined respectively by dividing the lateral force or moment at pile cap (or pier base) by the corresponding displacement or rotation. The results are summarized in Figures 7-15 and 7-16. For the lateral stiffness, its magnitude ranged from 0 to 115 MN/m; for the rotation stiffness, the values were in the range of 2 to 8.5 MN-m/deg. The magnitude of both foundation stiffnesses indicated the extent that bridge foundations could provide lateral supports to the superstructure. The figures also showed both lateral and rotational stiffnesses decreased with increased scour depth, but the former decreased at a decreasing rate and the latter almost at an increasing rate with respect to scour depth. Moreover, both stiffnesses at upstream and downstream pile caps differed insignificantly. In general, scour significantly degraded the lateral foundation stiffnesses that support bridge superstructures, and thus posed the bridge susceptible to lateral loading induced by flood and debris.

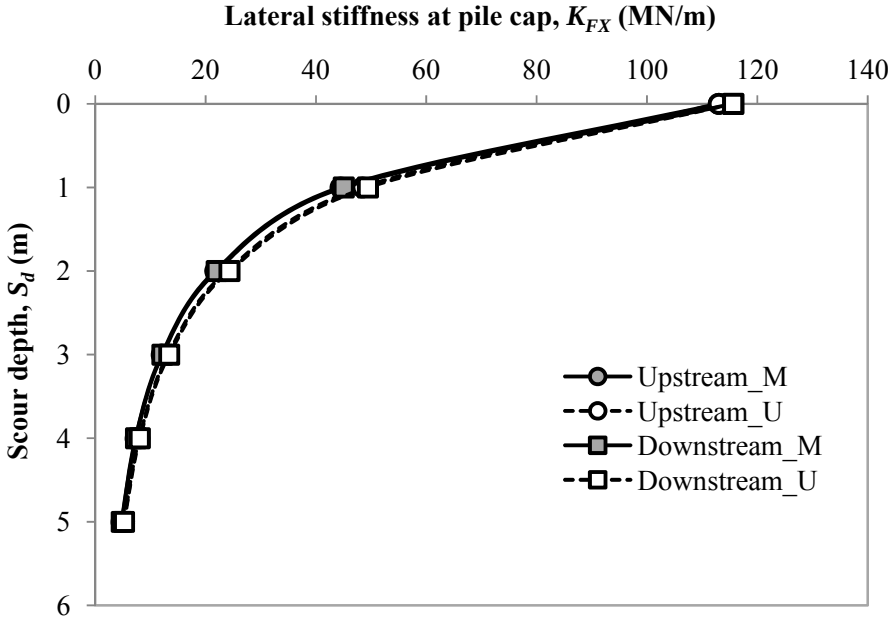

Figure 7-15. Lateral stiffness at pile cap versus scour depth in soft clay

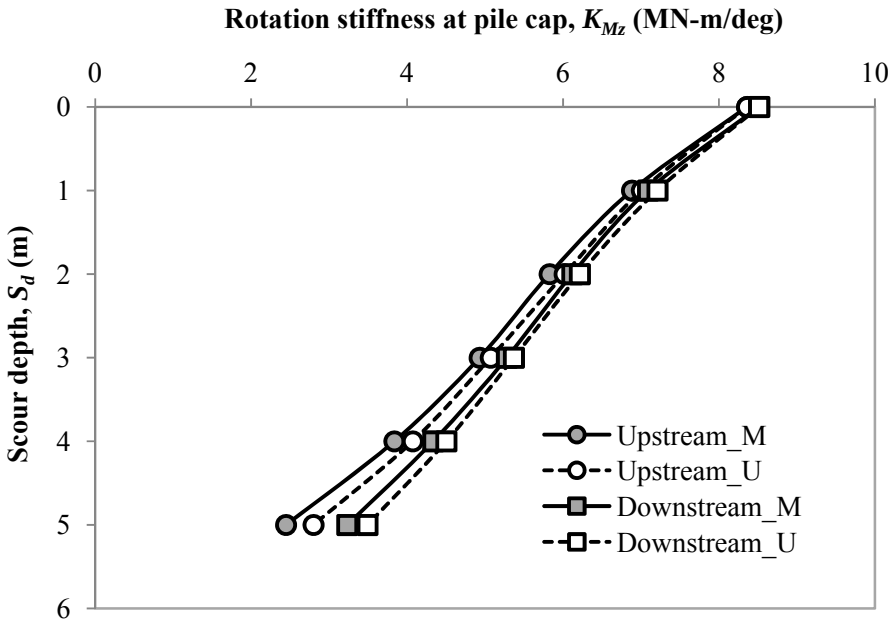

Figure 7-16. Rotation stiffness at pile cap versus scour depth in soft clay

7.2.4.2 Lateral bridge behavior in sands

Lateral behavior of the same bridge under the same loading conditions but in a different soil condition (i.e. Reese sand) was evaluated for scour depth at 0, 1, 2, 3, 4, and 5 m. Lateral displacements, forces, bending moments, and lateral foundation stiffnesses were evaluated at the pile cap, the same pile cap observed in soft clay (i.e. the one under Pier #2). The same pier and bridge deck locations were monitored for the maximum lateral displacement as was done in soft clay. Stress history effects were also included in the analyses.

Results are presented from Figures 7-17 to 7-23. The results in sands showed similar magnitude and changing trend with increased scour depth to those in soft clay. These similarities likely indicated that even though effect of different soils on a laterally loaded single pile with free head were significant as discussed in Chapter 3, the effects were fairly limited with regard to the lateral behavior of the whole bridge structure, especially for the boundary where abutment was fixed against lateral movement. This may be due to interactive effects within the bridge structural components; for example, the pile group had restraints from superstructure and the pile cap itself. Furthermore, the results also suggested that lateral responses of the pile cap were more sensitive to the change of scour depth than lateral responses of superstructure because soils had direct effects on pile group.

However, ignoring stress history effects in sands resulted in a conservative result, which was opposite to that found in soft clay. For example, considering stress history effects resulted in slightly smaller lateral displacement at pile cap than ignoring it as shown in Figure 7-17, with the most difference only 3% (with respected to the displacement by ignoring it). In contrast, the most difference of the displacement in soft clay could reach 8.6% (Figure 7-10). For another example, the bending moment of pile cap calculated by considering stress history effects was higher than that calculated by ignoring it as show Figure 7-20, and the most difference was 8% as opposed to

15.7% in soft clay. The more significant effects of stress history on the lateral response of pile cap observed in soft clay than in sand might be because the lateral load exerted on individual pile was significantly small (i.e. 10 to 20 kN). The relatively small lateral load could obtain more apparent results in soft clay than in strong sand, especially by using the varying C_u with soil depth in soft clay.

In general, considering and ignoring stress history effects in sand or soft clay created little difference of the result in terms of lateral behavior of the bridge, but the soft clay showed more noticeable stress history effects than sand. These results were inconsistent to the result discussed in Chapter 3. The reason could be explained by that interactive effects between superstructure and substructure (pile foundation) greatly limited soil effects and thus the stress history effects. Furthermore, the resulting small lateral force exerted individual pile led to the more significant stress history effect occurred in the soft (or weak) soil than in strong soils.

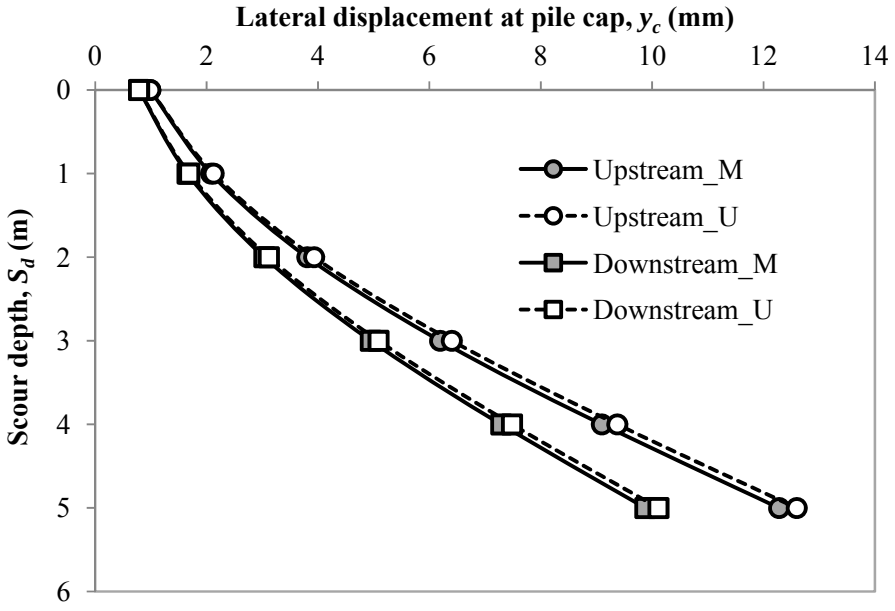

Figure 7-17. Lateral displacement at pile cap versus scour depth in sand

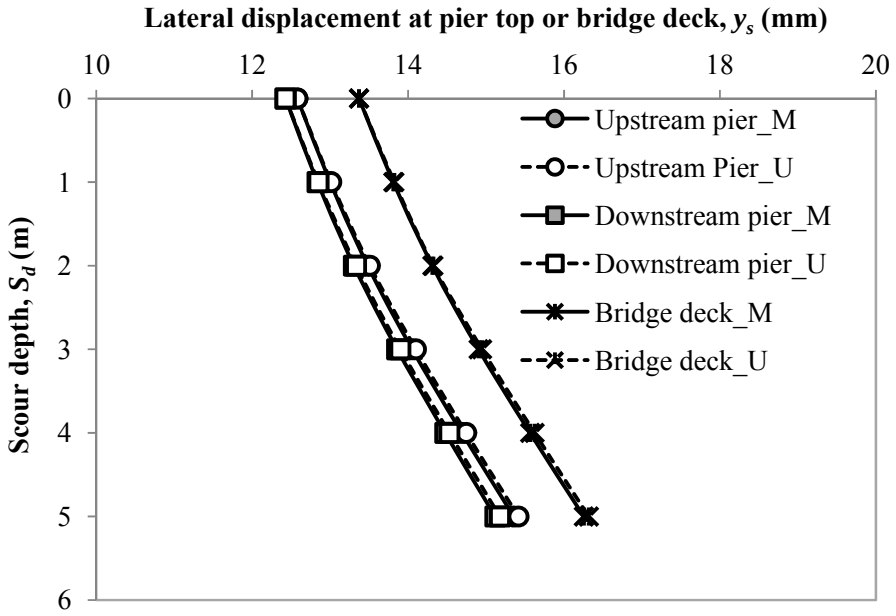

Figure 7-18. Maximum lateral displacement of superstructure versus scour depth in sand

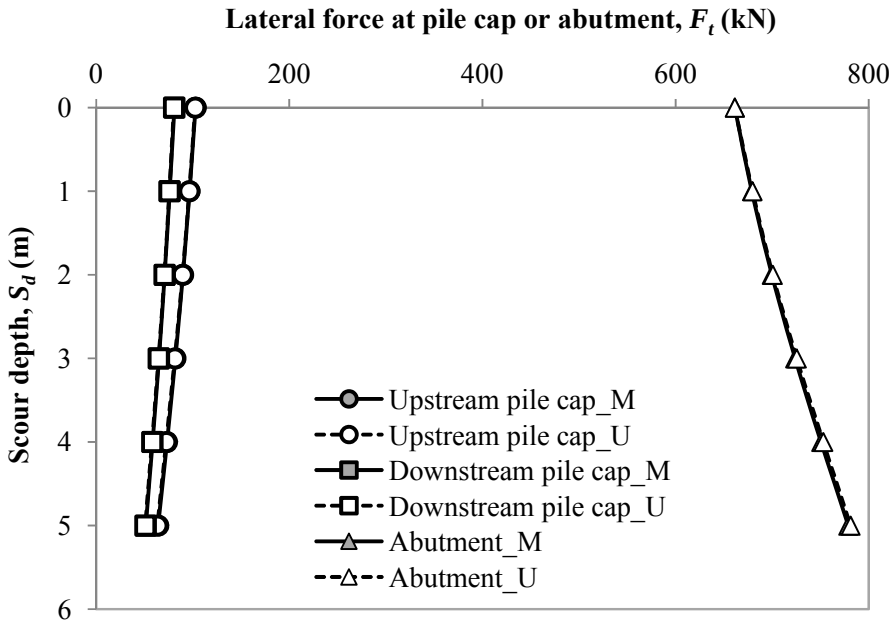

Figure 7-19. Lateral force at pile cap or abutment versus scour depth in sand

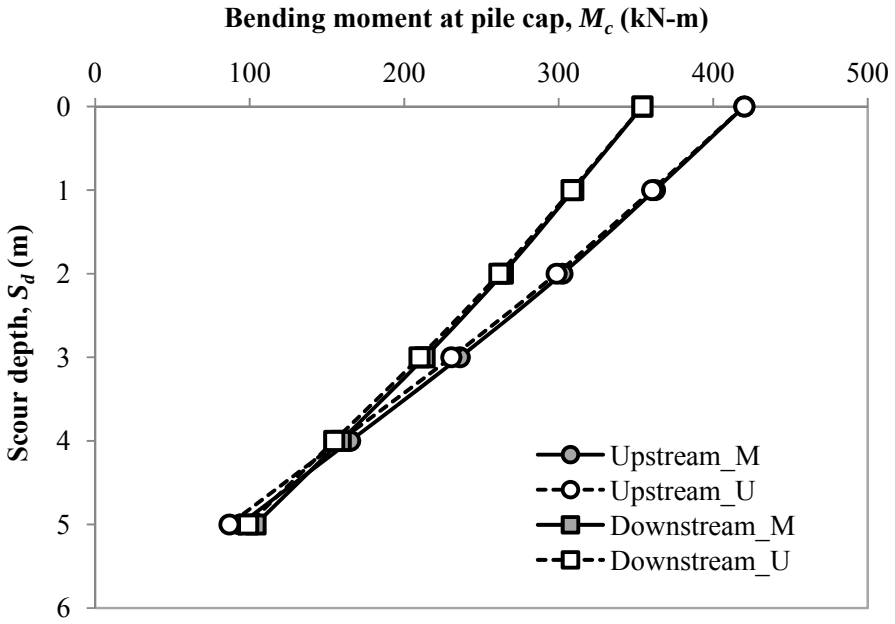

Figure 7-20. Maximum bending moment at pile cap versus scour depth in sand

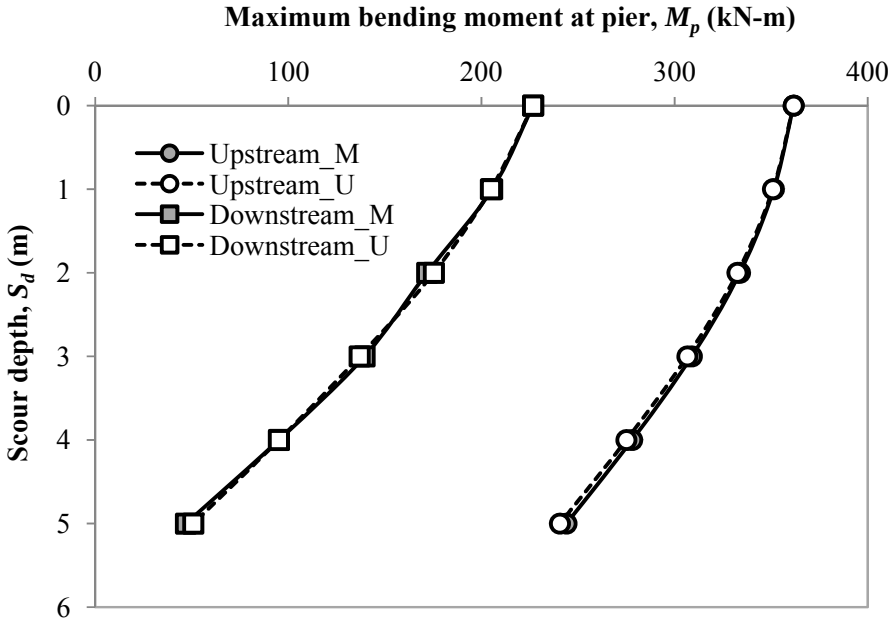

Figure 7-21. Maximum bending moment at pier versus scour depth in sand

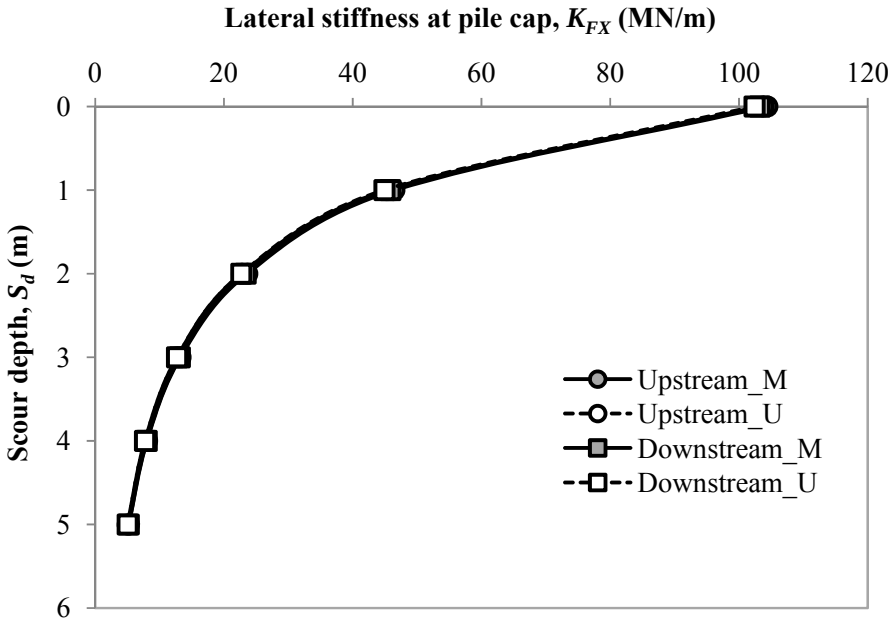

Figure 7-22. Lateral stiffness at pile cap versus scour depth in sand

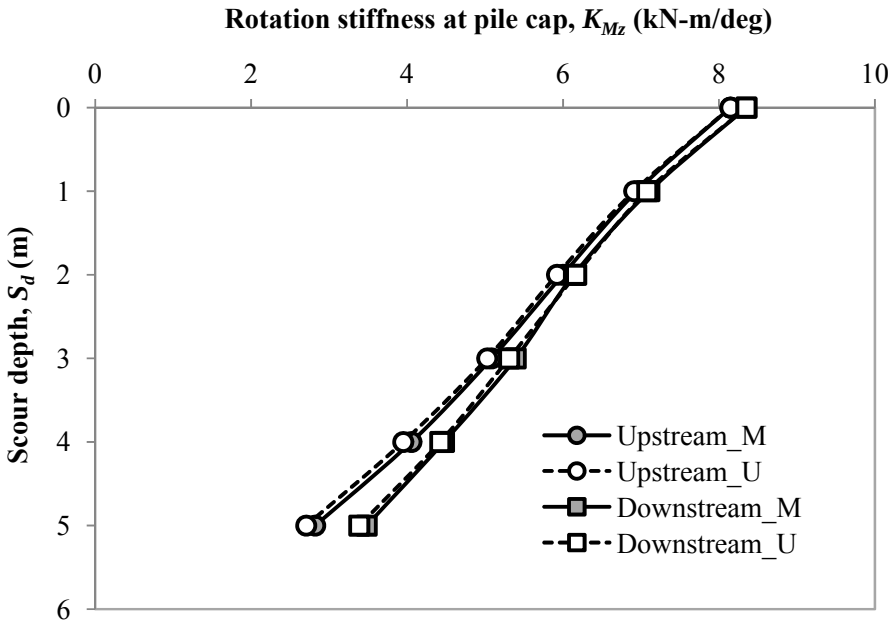

Figure 7-23. Rotation stiffness at pile cap versus scour depth in sand

7.3 Summary

To investigate lateral behavior of pile-supported bridges under scour conditions, the integrated analysis program was developed, which integrated the soil analysis and structural analysis. The soil analysis was achieved in the Soil Spring Module (*SSM*) that employed *p-y* methods to generate nonlinear soil springs for the structure model. In *STAAD.Pro*, the structure model was built and the integrated analysis was performed on the structure model incorporating the soil springs. The integrated analysis program fully harnessed the advantages as well as distadvantages of *STAAD.Pro* and *p-y* method; for example it had great computational efficiency and a wide range of applicability for different structures, but it was not feasible for p-delta analysis at nonlinear soil springs or dynamic analysis at dynamic loading as encountered in earthquake and machinery foundations.

The integrated analysis program was verified with *LPILE* for a laterally-loaded single pile in soft clay and *FB-Multipier* for a laterally-loaded pile group in sand, showing that the calculated results generally matched very well with those calculated in *LPILE* and *FB-Multipier*.

Using the integrated analysis program, an example study was conducted on Bridge 45 in the state of Kansas by assuming two homogenous soil conditions (i.e. soft clay and sand). Scour effects on the lateral responses of the bridge by considering and ignoring stress history of soils were investigated, and conclusions were drawn as follows:

(1) The interactive effects between superstructure and substructure were more decisive on the lateral bridge behavior than the soil effects (e.g. different soils); consequently, the soil stress history effects were limited on the lateral bridge behavior.

(2) Ignoring stress history effects resulted in an unconservative analysis in soft clay but a conservative analysis in sand as compared with considering it, and this result was more apparent when scour depth became larger.

(3) Lateral responses of pile cap were more sensitive to the change of scour depth than those of superstructures such as pier and bridge deck, which might explain why bridge pier top move upstream during the hinge failure as observed in case history studies in Chapter 2.

(4) With the progress of scour, less lateral loads and bending moments were carried by bridge structures such as pile cap and pier, but more were carried by boundaries such as abutment and piles (or soils).

(5) Lateral foundation stiffness was found to be between 0 to 115 kN/m and lateral rotation foundation stiffness was between 2 to 8.5 MN-m/deg for the case studies in soft clay and sand; both degraded significantly as scour depth increased, indicating the scour effects on bridge structure were in the manner of degrading foundation supports, thereby reducing lateral capacity of the bridge.

CHAPTER 8

CONCLUSIONS

This chapter summarizes the research work done in this study, the conclusions drawn based on the analytical and numerical results, and recommendations for future research.

8.1 Summary of Research Work

This research addressed lateral responses of pile-supported bridges under scour conditions. Chapter 1 defined the objective and scope of this research. Chapter 2 introduced the definition of scour and summarized the case studies of bridge failures due to scour. It also reviewed the research in the literature on the behavior of laterally loaded piles and bridges under scour conditions.

Scour affects bridge structures by changing soil behavior that changes the capacity of bridge foundations, thereby changing the behavior of the bridge structure. Therefore, this research was mostly focused on the scour effects of the change of the stress history of the remaining soils (Chapter 3) and the scour-hole dimensions (Chapters 4 to 6) on the behavior of laterally loaded single piles. The lateral behavior of an entire bridge under scour conditions was also evaluated using the integrated analysis program developed in Chapter 7.

In Chapter 3, the stress history effects in clays and sands due to scour were considered by modifying the conventional *p-y* curves. To accomplish this modification, the effective unit weight and undrained shear strength of clays were updated after scour; while in sands, the effective unit weight, friction angle, ultimate soil resistance were recalculated by considering the change of relative density or overconsolidation ratio (*OCR*) of the sand due to scour.

In Chapters 4 and 5, the scour-hole dimensions were considered in the 3D finite difference analysis of laterally loaded single piles in soft clay and sand. The 3D model was preliminarily analyzed and calibrated with the results of full-scale tests in field. Then the scour-hole dimensions including scour depth, scour width, and scour-hole slope angle were considered in the model to evaluate their effects on the behavior of laterally loaded single piles. Based on the numerical results in the 3D finite difference analysis, the 1D simplified methods considering the effects of scour-hole dimensions on the behavior of laterally loaded single piles in clay and sand were developed by modifying the *p-y* curves based on the wedge failure as discussed in Chapter 6.

Chapter 7 presented the development of the integrated analysis program for analyzing an entire bridge under scour conditions. By using the integrated analysis program, the scour effects on the lateral behavior of the bridge structure were evaluated, and the stress history effects on the behavior of the overall bridge system were also discussed.

8.2 Conclusions of Research

The following conclusions can be drawn from the analyses of the stress history and scour-hole dimension effects on the behavior of laterally loaded piles and the lateral behavior of the bridge under scour conditions:

(1) Ignoring the change of soil stress history by scour led to a conservative design of laterally loaded piles in sands but unconservative analysis and design in soft and stiff clays. The stress history effects became more significant when the scour depth was greater. The change of effective unit weight due to scour was small and its effects on the responses of laterally loaded piles were insignificant. The stress history effects on the responses of laterally loaded piles in clays were primarily the change of

undrained shear strength while that in sands was the change of lateral soil stress that depended on the overconsolidated ratio.

(2) The scour depth influenced the responses of laterally loaded piles more significantly than the scour width and scour-hole slope angle. The lateral displacement at the pile head increased at an increasing rate with the scour depth, which was more remarkable at a high loading level. In soft clays, the allowable lateral load capacity of the pile decreased substantially with the scour depth and the decrease could reach 50% when the scour depth increased from 0 to 6 *D* (*D* is the diameter of the pile). The lateral pile-head displacement increased with the increase of the scour width, but the lateral load capacity slightly decreased with the scour width. An influence scour width was found to be 8 *D*, beyond which the effects of the scour width on the behavior of laterally loaded piles were negligible. The elevation of the maximum bending moment at a certain applied load remained constant with respect to the pre-scour mudline but shifted toward the post-scour mudline when the scour depth increased. The behavior of laterally loaded piles was also influenced by the scour-hole slope angle. When the scour-hole slope angle was increased from 0˚ to 60˚, the lateral pile-head displacement decreased by 18% and the lateral load capacity increased by only 8%.

(3) In sands, the allowable lateral load capacity of the pile decreased substantially with the scour depth, but the reduction rate slowed down with an increase of the scour depth. The reduction in the allowable lateral load capacity could reach 66% when the scour depth increased from 0 to 6 *D*. When the scour depth was greater than 3 *D*, the negative maximum shear force even exceeded the applied lateral load. The ground line displacement increased significantly with the increase of the scour width, with the maximum increase up to 40%. The influence of the scour width depended more

on the scour depth than on the loading level. At the scour depths of 1, 3, and 6 *D*, the influence scour widths were 6, 8, and 12 *D* respectively. With the increase of the scour-hole slope angle (i.e. from 0 to ϕ'), the ground line displacement decreased with the maximum decrease by 36%, and the allowable lateral load capacity of the pile increased with its maximum increase by 21%.

(4) The simplified methods considering the effects of scour-hole dimensions on the behavior of piles in clay and sand were developed based on the wedge failure mode. These methods were verified with the numerical results of 3D finite difference analysis. Once the original *p-y* curves without scour were similar to those from the 3D finite difference analysis, the simplified methods considering scour effects produced the similar results as the 3D finite difference analysis.

(5) The integrated analysis program was verified with *LPILE* for the laterally loaded single pile in soft clay and *FB-Multipier* for the laterally loaded pile group in sand. The analysis of an entire bridge using the integrated analysis program showed that the interactive effects between superstructure and substructure were more important on the lateral behavior of the bridge than the soil effects (e.g. different soils). The lateral responses of the bridge substructure, such as pile caps, were more sensitive to the scour depth than those of the superstructures, such as the pier and the bridge deck. As scour progressed, less lateral loads and bending moments were carried by the bridge structures such as pile caps and piers, but more were carried by the boundaries, such as abutments and piles (or soils). Additionally, the lateral foundation stiffness was greatly degraded as the scour depth was increased.

8.3 Future Research

This research investigated the scour effects on lateral soil behavior, the behavior of laterally loaded piles, and the lateral behavior of an overall bridge system. Future research is needed to address the following issues:

(1) An advanced soil model needs to be employed in the 3D finite difference analysis to consider the effects of soil stress history. The results of this analysis can be used to verify the theories developed based on the *p-y* method in Chapter 3.

(2) The numerical analysis done in this study was only on the laterally-loaded single piles considering the soil stress history and the scour-hole dimensions. A further study is needed for the analysis of laterally loaded pile groups in the 3D finite difference model considering the stress history effects and the scour-hole dimensions.

(3) The simplified methods developed in this study can be used to analyze laterally-loaded single piles considering the effects of scour-hole dimensions. A further study is needed to improve these methods to analyze laterally-loaded pile groups considering the effects of scour-hole dimensions.

(4) Large-scale tests or full-scale field monitoring will be helpful for the verification of the integrated analysis program for pile-supported bridges under scour conditions.

(5) Analytical methods are also needed to evaluate the behavior of single piles and pile groups under vertical loading or a combination of vertical and lateral loading under scour conditions. The integrated analysis program can be improved by adding vertical (*t-z* curves) and torsional (*t-*θ curves) soil springs.

References

American Association of State Highway and Transportation Officials (AASHTO) (2007). *AASHTO LRFD Bridge Design Specifications*. 4th Ed., AASHTO, Washington, D.C.

Achmus, M., Kuo, Y. S., and Abdel-Rahman, K. (2010*)* "Numerical investigation of scour effect on lateral resistance of windfarm monopiles." *20th International Offshore and Polar Engineering Conference, ISOPE-2010,* International Society of Offshore and Polar Engineers, Beijing, China, 619-623.

Ahmadi, M. M., and Ahmari, S. (2009). "Finite-element modelling of laterally loaded piles in clay." *Proceedings of the Institution of Civil Engineers: Geotechnical Engineering*, 162, 151-163.

Avent, R. R., and Alawady, M. (2005). "Bridge scour and substructure deterioration: case study." *Journal of Bridge Engineering*, 10(3), 247-254.

Barker, R. M., and Puckett, J. A. (2007). *Design of Highway Bridges: An LRFD Approach*, John Wiley & Sons, Hoboken, N.J.

Bjerrum, L. (1972). "Embankments on soft grounds", *ASCE Proceedings of the Specialty Conference on Performance of Earth and Earth-Supported Structures*, 2, 1-54.

Bolton, M. D. (1986). "The strength and dilatancy of sands." *Geotechnique*, 36(1), 65-78.

Briaud, J. L., Chen, H. C., Li, Y., Nurtjahyo, P., and Wang, J. (2004). "Pier and contraction scour in cohesive soils." *NCHRP Report 516*, National cooperative highway research program, Transportation Research Board of The National Academies, Washington, D.C.

Briaud, J. L., Ting, F. C. K., Chen, H. C., Gudavalli, R., Perugu, S., and Wei, G. (1999). "SRICOS: Prediction of scour rate in cohesive soils at bridge piers." *Journal of Geotechnical and Geoenvironmental Engineering*, 125(4), 237-246.

Broms, B. B. (1964a). "Lateral resistance of piles in cohesive soils." *ASCE Journal of the Soil Mechanics and Foundations Division*, 90(SM2, Part 1), 27-63.

Broms, B. B. (1964b). "Lateral resistance of piles in cohesionless soils." *ASCE Journal of the Soil Mechanics and Foundations Division*, 90(SM3, Part 1), 123-156.

Brown, D. A., Morrison, C., and Reese, L. C. (1988). "Lateral load behavior of pile group in sand." *Journal of Geotechnical Engineering*, 114(11), 1261-1276.

Brown, D. A., and Shie, C. F. (1990). "Three dimensional finite element model of laterally loaded piles." *Computers and Geotechnics*, 10, 59-79.

Budhu, M. (2007). *Soil Mechanics and Foundations*, John Wiley & Sons, Inc., New York.

Budiman, J., and Ahn, K. (2005). "Effects of pile cap in single pile and lateral capacity of pile group." *Proceedings of the Geo-Frontiers 2005 Congress*, Austin, TX, 915-929.

Butch, G. K. "Scour-hole dimensions at selected bridge piers in New York." *North American Water and Environment Congress & Destructive Water*, ASCE, Anaheim, CA, 3043-3051.

Coduto, D. P. (2001). *Foundation Design: Principles and Practices*, Perason Hall, Inc., Roanoke, VA.

Cox, W. R., Reese, L. C., and Grubbs, B. R. (1974). "Field testing of laterally loaded piles in sand." *Proceedings of the Offshore Technology* Conference, Houston, TX, 2079.

Daniels, J., Hughes, D., Ramey, G. E., and Hughes, M. L. (2007). "Effects of bridge pile bent geometry and levels of scour and P loads on bent pushover loads in extreme flood/scour events." *Practice Periodical on Structural Design and Construction*, 12(2), 122-134.

Delphia, J. (2009). "Unpublished notes on determining the effects of scour on axial and lateral stability of foundation elements."

Diamantidis, D., and Arnesen, K. (1986). "Scour effects in piles structures-a sensitivity analysis." *Ocean Engineering*, 13,497-502.

Djoenaidi, W. J. (1985). "A compendium of soil properties and correlations." Master thesis, University of Sydney, Sydney, Australia.

Dodds, A. (2005). "A numerical study of pile behavior in large pile groups under lateral loading." Ph.D. Dissertation, University of Southern California, Los Angeles, CA.

Duncan, J. M., and Buchignani, A. L. (1976). "An engineering manual for settlement studies." *UCB/GT-76-01*, Department of Civil Engineering, University of California, Berkeley.

Foti, S., and Sabia, D. (2011). "Influence of foundation scour on the dynamic response of an existing bridge." *Journal of Bridge Engineering*, 16(2), 295-304.

Hau, K. W. (2003). "Application of a three-surface kinematic hardening model to the repeated loading of thinly surfaced pavements." Ph.D. Dissertation, University of Nottingham, Nottingham, UK.

Hetényi, M. (1946). *Beams on elastic foundation; theory with applications in the fields of civil and mechanical engineering*, The University of Michigan press, Ann Arbor, Michigan.

Hughes, D., Ramey, G. E., and Hughes, M. L. (2007a). "Effects of extreme scour and soil subgrade modulus on bridge pile bent buckling." *Practice Periodical on Structural Design and Construction*, 12(2), 96-108.

Hughes, D., Ramey, G. E., and Hughes, M. L. (2007b). "Bridge pile bent number of piles and X-bracing system: Impact on pushover capacity as scour increases." *Practice Periodical on Structural Design and Construction*, 12(2), 82-95.

Itasca Consulting Group (2006). Fast Lagrangian Analysis of Continua in 3 Dimensions *FLAC*^{3D} (version 3.1), Minneapolis, Minnesota.

Jackson, L. E., Thompson, P. L., and Richardson, E. V. (1991) Hatchie River and Schoharie Creek Bridge failures *Proceedings of the 1991 National Conference on Hydraulic Engineering,* ASCE, 202-208.

Jaky, J. (1944). "The coefficient of earth pressure at rest." *Journal of Society of Hungarian Architects and Engineers*, 355-358.

Janbu, N. (1963) "Soil compressibility as determined by oedometer and triaxial tests." *Proceedings of 3rd European Conference on Soil Mechanics and Foundation Engineering*, Wiesbaden, Germany, 19-25.

Kulhawy, F. (1991). "Drilled shaft foundations." *Foundation Engineering Handbook*, H. Fang, ed. Van Nostrand Reinhold, New York, 537-552.

Kulhawy, F., Trautmann, C., Beech, J., O'Rourke, T., McGuire, W., Wood, W., and Capano, C. (1983). "Transmission line structure foundations for uplift-compression loading." *Report EL-2870*, Electric Power Research Institute, Palo Alto,CA.

Kulhawy, F. H., and Mayne, P. W. (1990). "Manual on estimating soil properties for foundation design." *Report EL-6800*, Electric Power Research Institute, Palo Alto, CA.

Lagasse, P. F., Clopper, P. E., Zevenbergen, L. W., and Girard, L. W. (2007). "Countermeasures to protect bridge piers from scour." *NCHRP Report 593*, National cooperative highway research program, Transportation Research Board of The National Academies, Washington, D.C.

Lambe, T. W., and Whitman, R. V. (1969). *Soil Mechanics*, John Wiley and Sons, New York.

Lancelot, L., Shahrour, I., and Mahmoud, M. A. (2006). "Failure and dilatancy properties of sand at relatively low stresses." *Journal of Engineering Mechanics*, 132(12), 1396-1399.

Laursen, E. M. (1963). "Analysis of Relief Bridge scour." *Journal of the Hydraulic Division, ASCE*, 89(3), 93-118.

Lin, C., Bennett, C. R., Han, J., Parsons, R. L., and Parr, A. D. (2012). "Integrated analysis program, a program for analyzing lateral behavior of pile-supported structures under scour conditions." Prepared for Kansas Departmetn of Transportation.

Martin, G. R., and Chen, C. Y. (2005). "Response of piles due to lateral slope movement." *Computers & Structures*, 83(8-9), 588-598.

Matlock, H. (1970). "Correlation for design of laterally loaded piles in soft clay." *Proceedings of the II annual offshore technology* conference, Houston, TX, 277-594.

Mayne, P. W., and Kulhawy, F. H. (1982). "Ko-OCR relationship in soils." *Journal of the Geotechnical Engineering Division*, 108, 851-872.

McConnell, J. R., and Cann, M. (2010) "Assessment of bridge strength and stability under scour conditions." *Proceedings of ASCE SEI 2010 Structures Congress*, Orlando, FL, 121-132.

Melville, B. W. (1997). "Pier and abutment scour: integrated approach." *Journal of Hydraulic Engineering*, 123(2), 125-136.

Melville, B. W., and Coleman, S. E. (2000). *Bridge scour*, Water Resources Publications, LLC, Highlands Ranch, Colorado.

Mitchell, J. K., and Gardner, W. S. (1971). "Analysis of load- bearing fills over soft subsoils." *ASCE Journal of Soil Mechanics and Foundations Division*, 97, 1549-1571.

Mokwa, R. L., Duncan, J. M., and Charles, E. V. (2000). "Investigation of the resistance of pile caps and integral abutments to lateral loading." *FHWA/VTRC 00-CR4*, Virginia Transportation Research Council, Charlottesville, VA.

Muir Wood, D. (1990). *Soil Behaviour and Critical State Soil Mechanics*, Cambridge University Press, Cambridge, UK.

Ng, C. W. W., and Zhang, L. M. (2001). "Three-dimensional analysis of performance of laterally loaded sleeved piles in sloping ground." *Journal of Geotechnical and Geoenvironmental Engineering*, 127(6), 499-509.

National Transportation Safety Board (NTSB) (1990). "Highway accident report-collapse of the northbound U.S. route 51 bridge spans over the Hatchie River near Covington, Tennessee, April, 1989." Hydraulic, Erosion and Channel Stability Analysis of the Safety Board, Washington, D.C.

Poulos, H. G. (1971). "Behavior of laterally loaded piles: I-single piles." *ASCE Journal of the Soil Mechanics and Foundations Division*, 97(5), 711-731.

Ramey, G. E., Brown, D. A., Hughes, M. L., Hughes, D., and Daniels, J. (2007). "Screening tool to assess adequacy of bridge pile bents during extreme flood/scour events." *Practice Periodical on Structural Design and Construction*, 12(2), 109-121.

Raudkivi, A. J. (1986). "Functional trends of scour at bridge piers." *Journal of the Hydraulic Division, ASCE*, 112(1), 1-13.

Reese, L. C., Cox, W. R., and Koop, F. D. (1974) "Analysis of laterally loaded piles in sand." *Proceedings of the VI Annual Offshore Technology Conference*, Houston, TX, 473-485.

Reese, L. C., Cox, W. R., and Koop, F. D. (1975). "Field testing and analysis of laterally loaded piles on stiff clay." *Proceedings of the VII Annual Offshore Technology Conference*, Houston, TX, 473-485.

Reese, L. C., and Van Impe, W. F. (2001). *Single Piles and Pile Groups under Lateral Loading*, A.A. Balkema Publishers, Leiden, the Netherlands.

Richardson, E. V., and Abed, L. (1993). "Top width of pier scour holes in free and pressure flow." *Proceedings of the 1993 National Conference on Hydraulic Engineering. Part 1 (of 2)* ASCE, 911-915.

Richardson, E. V., and Davis, S. R. (2001). "Evaluating scour at bridges, 4 ed." *FHWA NHI 01-001 (HEC 18)*, Federal Highway Administration, Washington, D.C.

Sanjaya Kumar, V., Sharma, K. G., and Varadarajan, A. (2007). "Behaviour of a laterally loaded pile." *Proceedings of 10th International Symposium on Numerical Models in Geomechanics NUMOG 10*, Taylor and Francis/Balkema, 447-452.

Shen, H. W., Schneider, V. R., and Karaki, S. S. (1969). "Local scour around bridge piers." *Journal of the Hydraulic Division, ASCE*, 95(HY6), 1919-1940.

Storey, C., and Delatte, N. (2003). "Lessons from the collapse of the Schoharie Creek Bridge." *Proceedings of the Third Congress Forensic Engineering,* ASCE, San Diego, CA, 158-167.

Terzaghi, K., and Peck, R. B. (1948). *Soil Mechanics in Engineering Practice*, John Wiley and Sons, Inc., New York.

Terzaghi, K., Peck, R. B., and Mesri, G. (1996). *Soil Mechanics in Engineering Practice*, Wiley, New York.

Thompson, P. L. (1990). "April 1989 Hatchie River US-51 bridge failure." Transportation Research Board, 24-35.

Thornton-Tomasetti, P. C. (1987). "Overview report investigation of the New York State Thruway Schoharie Creek Bridge collapse." New York State Disaster Preparedness Commission.

Tomlinson, M. J. (1957). "The adhesion of piles driven in clay soils." *Proceedings of 5th Internation Conference, ISSMFE*, London, UK, 66-71.

Trochnis, A. M., Bielak, J., and Christiano, P. (1988). "A three-dimensional nonlinear study of piles leading to the development of a simplified model." *Report R-88-176*, Department of Civil Engineering, Carnegie Mellon University, Pittsburgh, PA.

Wakai, A., Gose, S., and Ugai, K. (1999). "3-D elasto-plastic finite element analyses of pile foundations subjected to lateral loading." *Journal of the Japanese Geotechnical Society: soils and foundation*, 39(1), 97-111

Wardhana, K., and Hadipriono, F. C. (2003). "Analysis of recent bridge failures in the United States." *Journal of Performance of Constructed Facilities*, 17, 144-150.

Wiss, J., Elstner Associates, Inc., and Mueser Rutledge Consulting Engineers (1987). "Collapse of Thruway Bridge at Schoharie Creek." Final Report Prepared for: New York State Thruway Authority.

Yang, J., and Mu, F. (2008). "Use of state-dependent strength in estimating end bearing capacity of piles in sand." *Journal of Geotechnical and Geoenvironmental Engineering*, 134(7), 1010-1014.

Zhang, L. M., Ng, C. W. W., and Lee, C. J. (2004). "Effects of slope and sleeving on the behavior of laterally loaded piles." *Soils and Foundations*, 44(4), 99-108.